

# **The ULK1 Complex In Autophagy Induction: Mandatory Or Negligible?**

Inaugural-Dissertation

zur Erlangung des Doktorgrades  
der Mathematisch-Naturwissenschaftlichen Fakultät  
der Heinrich-Heine-Universität Düsseldorf

vorgelegt von

**Nora Wallot-Hieke**  
aus Halle an der Saale

Düsseldorf, Juli 2017



aus dem Institut für Molekulare Medizin I  
der Heinrich-Heine-Universität Düsseldorf

Gedruckt mit der Genehmigung der  
Mathematisch-Naturwissenschaftlichen Fakultät der  
Heinrich-Heine-Universität Düsseldorf

Referent: Prof. Dr. Björn Stork

Korreferent: Prof. Dr. Dieter Willbold

Tag der mündlichen Prüfung: 15. September 2017



## **Eidesstattliche Erklärung**

Ich versichere an Eides Statt, dass die Dissertation von mir selbstständig und ohne unzulässige fremde Hilfe unter der Beachtung der „Grundsätze zur Sicherung guter wissenschaftlicher Praxis an der Heinrich-Heine-Universität Düsseldorf“ erstellt worden ist.

Düsseldorf, Juli 2017

---

Nora Wallot-Hieke



**Table of contents**

Acknowledgement.....	II
Abbreviations .....	III
1. Summary.....	1
2. Zusammenfassung .....	2
3. Introduction.....	3
3.1 Autophagy – recycle for a better life!.....	3
3.1.1 Autophagy regulation – pulling the trigger .....	6
3.2 The who is who in autophagy signalling.....	11
3.2.1 The ULK1 protein complex - a star is born.....	13
3.2.2 Upstream regulation of the ULK1 complex or: Why is life always that complicated? ...	17
3.2.3 Downstream signalling of the ULK1 complex: phosphorylation <sup>2</sup> .....	19
3.2.4 VPS34 lipid kinase complex: running down the PIPeline.....	20
3.2.5 The PI3P effector proteins: PImPing it up .....	23
3.2.6 Two ubiquitin-like protein complexes: tag me whole again .....	23
3.2.7 Autophagy receptors: trash is my major .....	26
3.2.8 The autolysosome: it all goes down in a bubble.....	28
3.2.9 The Autophagosomal membrane source – the essential question of life: Where am I coming from? .....	29
4. Summary of papers.....	31
4.1 Paper 1 .....	31
4.2 Paper 2 .....	33
4.3 Paper 3 .....	34
5. Discussion.....	35
6. References.....	40
7. Curriculum Vitae.....	52
8. Publications and conference contributions.....	54

## Acknowledgement

I would like to take this opportunity to thank everyone who supported me throughout the years of my PhD.

First of all I would like to thank Prof. Sebastian Wesselborg, who made my PhD at the Institute of Molecular Medicine possible, his valuable pieces of advice and his tireless readiness to discussion.

I would like to thank Prof. Dieter Willbold for taking over the duty of a second advisor and evaluating my dissertation.

A special thank goes to my PI Prof. Björn Stork, who supported me with his highly skilled guidance and advice throughout the course of my thesis. He taught me a lot about life, too and many of my talents have been revealed. I am a “Rückwärtspipettierer”, an exemplary representative of the Generation Y, and overall “almost” as good as the previous generations of PhDs. As he himself realises on a regular basis, it was just too good to leave!

I also want to thank Prof. Noboru Mizushima, who welcomed me at his lab in Tokyo, Japan, for a research visit, and taught me a lot about science, Japanese culture and tofu. In this context, I want to mention Noriko, who is the heart and soul of the Mizushima lab and who helped me to cope with the Japanese bureaucracy. Thank you Takeshi for your academic support and Hoshi for showing me Tokyo by night on the run!

Another thank you goes out to my colleagues, who made life so much more interesting. This is for us: #dawowirsindistvorne # Speerspitzedeserfolgs #makegenerationygreatagain

To Niklas and Sabine, thank you for the coffeeconnection! Sufficient supply with caffeine was a driving force while writing my thesis!

I want to thank my family and friends, especially Inga and Natasa, for always supporting me and taking me the way I am. To my mother, who is my role model: Thank you so much!

The best comes last: Thank you Tim for being you, for being with me and for marrying me. And for your cooking skills!

## Abbreviations

AMBRA1	activating molecule in beclin1-regulated autophagy
AMP	adenosine monophosphate
AMPK	AMP-activated protein kinase
APG	autophagy
ASK1	apoptosis signal-regulating kinase 1
ATF6	activation of transcription factor 6
ATG	autophagy-related
ATP	adenosine triphosphate
AUT	autophagy
BCL-2	B-cell lymphoma 2
BECN1	beclin1
BH-3	bcl-2 homology 3
BIF1	bax-interacting factor 1
BNIP3	BCL-2 interacting protein 3
BNIP3L	BNIP3 like
CARM1	coactivator-associated arginine methyltransferase 1
CBL1	calcineurin B-like protein 1
CMA	chaperone-mediated autophagy
CTD	C-terminal domain
CVT	cytoplasm-to-vacuole targeting
DEPTOR	DEP domain containing mTOR-interacting protein
DFCP1	double FYVE domain-containing protein 1
DLC1	dynein light chain 1
DNA	deoxyribonucleic acid
DUB	deubiquitinases
EIF2AK3	eukaryotic translation initiation factor 2- $\alpha$ kinase 3
4E-BP1	eukaryotic translation initiation factor 4E-binding protein 1
ER	endoplasmic reticulum

---

ERES	ER exit sites
ERGIC	ER-Golgi intermediate compartment
ERN1	ER to nucleus signalling 1
EXOC	exocyst complex component
FAK	focal adhesion kinase
FIP200	focal adhesion kinase-interacting protein of 200 kDa
FUNDC1	FUN14 domain containing 1
GABARAP	gamma-aminobutyric acid A receptor-associated protein
Galbi	galectin-8 binding region
GAP	GTPase-activating protein
GAPR1	Golgi-associated plant pathogenesis-related protein 1
GATOR	GTPase activating proteins toward Rags
GEF	guanine nucleotide exchange factor
GSA	glucose-induced selective autophagy
GSK3- $\beta$	glycogen synthase kinase 3 beta
GTP	guanosine triphosphate
HIF-1	hypoxia-inducible factor-1
hsc70	heat shock-cognate protein of 70 kDa
HSPA5	heat shock 70 kDa protein 5
IRE1	inositol-requiring enzyme 1
JNK1	c-Jun-N terminal kinase 1
kDa	kiloDalton
LAMP2	lysosome-associated protein 2
LAMTOR	lysosomal adapter of mTOR
LIR	LC3-interacting region
MAM	mitochondria associated ER membranes
(MAP1)LC3	(microtubule-associated protein 1) light chain 3
MDa	MegaDalton
MEF	murine embryonic fibroblast
MIM	MIT-interacting motif

---

MIT	microtubule interacting and transport
MLST8	mammalian lethal with SEC13 protein
mTORC1	mechanistic target of rapamycin complex 1
NBR1	neighbour of BRCA1 gene 1
NDP52	nuclear domain 10 protein 52
NEDD8	neural precursor cell expressed, developmentally down-regulated gene 8
NRBF2	nuclear receptor binding factor 2
OPTN	optineurin
PA	phosphatic acid
PAG	peroxisome degradation via autophagy
PARP1	poly(ADP-ribose)-polymerase 1
PAZ	pexophagy zeocin-resistant
PB	PHOX and BEM1P
PDD	peroxisome degradation-deficient
PE	phosphatidylethanolamine
PERK	protein kinase RNA-like ER kinase
PI	phosphoinositide
PI(3,4,5)P3	phosphatidylinositol 3,4,5-trisphosphate
PI3P	phosphatidylinositol 3-phosphate
PI4P	phosphatidylinositol 4-phosphate
PIAS	protein inhibitor of activated STAT
PKA	protein kinase A
PKB	protein kinase B
PKC	protein kinase C
PP2A	serine/threonine protein phosphatase 2 A
PRAS40	40 kDa proline-rich AKT substrate
PS	proline/serine-rich
PYK2	proline-rich tyrosine kinase 2
RAB	RAS-related in brain
RALB	RAS like proto-oncogene B

---

RAPTOR	regulatory-associated protein of mTOR
RB1CC1	retinoblastoma 1-inducible coiled-coil 1
REDD1	regulation of DNA damage response 1
RHEB	RAS homologue enriched in brain
RUBICON	RUN domain BECN1-interacting and cysteine-rich containing protein
SCF	SKP1–CUL1–F-box-protein
SKP2	S-phase kinase-associated protein 2
SLR	sequestosome-1-like receptor
SNAP29	synaptosome associated protein 29
SNARE	soluble N-ethylmaleimide sensitive factor attachment receptor
SQSTM1	sequestosome 1
STBD1	starch-binding domain-containing protein 1
STING	stimulator of interferon genes
STK36	serine/threonine kinase 36
STX17	syntaxin17
SUMO	small ubiquitin-related modifier
TAX1BP1	TAX1 binding protein 1
TBC1D7	TBC1 domain family member 7
TBK1	TANK-binding kinase 1
TFEB	transcription factor EB
TIP60	HIV-1 Tat interacting protein, 60kDa
TNF $\alpha$	tumour necrosis factor alpha
TOR	target of rapamycin
TRAF	TNF receptor-associated factor
TSC	tuberous sclerosis complex
UBD	ubiquitin-binding domain
ULK	UNC-51-like kinase
UNC-51	uncoordinated movement-51
UPR	unfolded protein response
UVRAG	UV radiation resistance associated protein

VAMP8	vesicle associated membrane protein 8
v-ATPase	vacuolar H <sup>+</sup> -ATPase
VPS	vacuolar protein sorting
WIPI	WD-repeat protein interacting with phosphoinositides

**Amino acids**

<b>Amino acid</b>	<b>Single letter code</b>
Alanine	A
Cysteine	C
Aspartic acid	D
Glutamic acid	E
Phenylalanine	F
Glycine	G
Histidine	H
Isoleucine	I
Lysine	K
Leucine	L
Methionine	M
Asparagine	N
Proline	P
Glutamine	Q
Arginine	R
Serine	S
Threonine	T
Valine	V
Tryptophan	W
Tyrosine	Y
any amino acid	x
aromatic amino acid	Ω
hydrophobic amino acid	Ψ

## 1. Summary

Macroautophagy is a cellular degradation process targeting long-lived and/or toxic proteins and protein aggregates as well as superfluous and damaged organelles. Through its course, autophagy maintains cell homeostasis and integrity. In addition to its function on basal levels, autophagic activity can be increased when cells are exposed to stressors like nutrient deprivation, hypoxia or pathogen invasion. In accordance with its essential role in cellular health, autophagy is implicated in the development and progression of various diseases, among them several types of cancer. Additionally, anticancer drugs used in chemotherapy induce cytoprotective autophagy in cancer cells, leading to impaired efficiency of these compounds. Consequently, autophagy modulation accompanying cancer therapy might enhance successful treatment. Based on the fact that the ULK1 complex is a key signalling node in the autophagy network, the overall aim of this study was the evaluation of the ULK1 kinase activity and the protein interactions within the ULK1 complex in regard to their functions for the regulation of autophagy.

Previous studies proposed increased ULK1 stability and activity through ubiquitination, however deubiquitination events and the mediating deubiquitinases (DUBs) have not been characterized in the context of ULK1 activity regulation. Using the partially selective deubiquitinase inhibitor WP1130, we confirmed posttranslational modification of ULK1 by ubiquitination, which resulted in ULK1 aggregation and transfer to the aggresome. This was accompanied by a loss of kinase activity and reduced autophagy induction.

The scaffolding protein ATG13 recruits the catalytically active kinase ULK1 and the regulatory proteins ATG101 and RB1CC1 to stably form the ULK1 complex. Additionally, the GABARAP protein subfamily as well as phospholipids have been determined as interaction partners of ATG13.

Using mutational analysis, we identified the amino acids in ATG13 mediating the binding to RB1CC1, ULK1 and ATG101. Through generating ATG13 mutants, the ULK1 complex formation, starvation-induced recruitment to the autophagosome initiation site and autophagy inducing capacities of the particular protein-protein and protein-phospholipid interactions were examined. The study revealed that the ATG13-ATG101 interaction is of essential relevance for autophagy induction. Furthermore, targeting the binding of ULK1 to ATG13 revealed only a mild phenotype of autophagy inhibition.

In summary, these results indicate that the ATG101-ATG13 interaction is the most promising target to control the ULK1 complex activity. Additionally, modulating the ULK1 kinase activity might be an effective approach to regulate the autophagic response.

## 2. Zusammenfassung

Makroautophagie ist ein zellulärer Prozess zum Abbau von langlebigen und/oder schädlichen Proteinen, Proteinaggregaten und beschädigten Zellorganellen. Neben der essentiellen Funktion zum Erhalt der zellulären Homöostase, fungiert Autophagie auch als Adaptionsmechanismus während akuter Stressbedingungen wie Unterversorgung mit Nährstoffen und Sauerstoff oder Infektionen. Dementsprechend ist die Deregulation des Autophagieprozesses mit malignen Erkrankungen wie Krebs und neurodegenerativen Krankheiten assoziiert. Weiterhin kann eine radio- oder chemotherapeutische Behandlung von Tumoren zu einer Induktion der zytoprotektiven Autophagie führen und das Überleben von Krebszellen positiv beeinflussen. Deshalb ist eine Kombination aus konventioneller Krebstherapie und gezielter Autophagieregulation eine erfolgsversprechende Möglichkeit zur Behandlung von Tumoren.

Im Zentrum des Autophagienetzwerks steht die Proteinkinase ULK1, weshalb die Modulation von Autophagie über die Regulation der Kinaseaktivität von ULK1 naheliegend ist. In vorangegangenen Studien wurde eine positive Regulierung der ULK1-Stabilität und -Aktivität durch Ubiquitylierung gezeigt. Allerdings wurde dabei der Einfluss von Deubiquitinasen (DUB) zur Regulierung der ULK1-Ubiquitylierung nicht untersucht. Mithilfe des semi-selektiven DUB Inhibitors WP1130 konnte die posttranslationale Modifikation von ULK1 durch Ubiquitylierung bestätigt werden. Die Verwendung von WP1130 führte zu einer ULK1-Aggregation und anschließendem Transfer zu den Aggresomen. Damit einhergehend wurde ein Verlust der ULK1-Kinaseaktivität und Induzierbarkeit von Autophagie detektiert.

Zusammen mit ULK1 bilden die regulatorischen Proteinen ATG13, ATG101 und RB1CC1 den ULK1-Komplex. ATG13 funktioniert dabei als Plattform zur Rekrutierung der ULK1-Komplex-bildenden Proteine. Darüber hinaus ist bekannt, dass ATG13 mit Phospholipiden und Mitgliedern der GABARAP Proteinfamilie interagiert. Mithilfe von Mutationsanalysen konnten die Aminosäurereste in ATG13 identifiziert werden, welche die Bindung mit den Interaktionspartnern ULK1, ATG101 und RB1CC1 vermitteln. Durch die Etablierung von ATG13-Mutanten wurde der Einfluss der jeweiligen Protein-Protein- und Protein-Phospholipid-Interaktionen auf die ULK1-Komplexassemblierung, die Rekrutierung zum Autophagosomenursprung und die Induktion von Autophagie untersucht. Es zeigte sich, dass die Interaktion von ATG13 mit ATG101 essentiell für die ULK1-Komplex-abhängige Induktion der Autophagie ist. Zusätzlich erzielte die Blockade der ULK1-ATG13 Assoziation nur eine milde Inhibition der Autophagieinduktion.

Zusammenfassend konnte gezeigt werden, dass die Modulation der ATG13-ATG101 Interaktion sowie der ULK1-Kinaseaktivität ein vielversprechender Ansatz zur Regulation von autophagischen Prozessen darstellt.

### 3. Introduction

#### 3.1 Autophagy – recycle for a better life!

The term autophagy is derived from the Greek words “autos” meaning “self” and “phagein” translating to “to eat”. Consistent with its literal meaning this cellular process indeed resembles the self-digestion of cellular material within a cell. This autophagic cargo comprises damaged, aberrant, and toxic proteins, protein aggregates and organelles, which become degraded by hydrolytic proteases in the lysosome. The remaining disintegrated building blocks like amino acids and lipids are then reused for *de novo* protein synthesis and maintenance of energy metabolism. Depending on the route on which the cargo is transported to the lysosome, autophagy is subdivided into three distinct forms (Figure 1). During microautophagy, cellular contents are directly ingested by invagination of the lysosomal membrane (Li et al., 2012a). Chaperone-mediated autophagy (CMA) is of relevance for substrate proteins with a pentapeptide motif recognized by the constitutive chaperone heat shock-cognate protein of 70 kDa (hsc70), which translocates the cargo into the lysosomal lumen by interacting with the lysosome-associated protein 2A (LAMP2A) (Cuervo and Wong, 2014). A third and up to date best characterized form of autophagy is macroautophagy that is commonly referred to as simply autophagy. This multi-step process utilizes a membrane compartment originating from the mitochondria, Golgi network, endoplasmic reticulum (ER), recycling endosomes and/or the plasma membrane called phagophore to trap the cytoplasmic entities destined for disposal and upon closure gives rise to a double-membraned vesicle. The so called autophagosome finally fuses with the lysosome into an autolysosome for successful cargo degradation (Yin et al., 2016).

These autophagy pathways are universally conserved from yeast to higher eukaryotes and next to the ubiquitin proteasome system are essential for functional metabolism and cell integrity. While the ubiquitin proteasome system is mainly responsible for degradation of short-lived regulatory proteins, autophagy degrades long-lived proteins and organelles (Mizushima et al., 2008; Schreiber and Peter, 2014). Another major difference between these two degradation systems is that the proteasome hydrolyses unfolded proteins one by one, whereas autophagy disposes its cargo in a single step by delivering it into the lysosomal lumen (Levine and Klionsky, 2004; Reggiori and Klionsky, 2006).

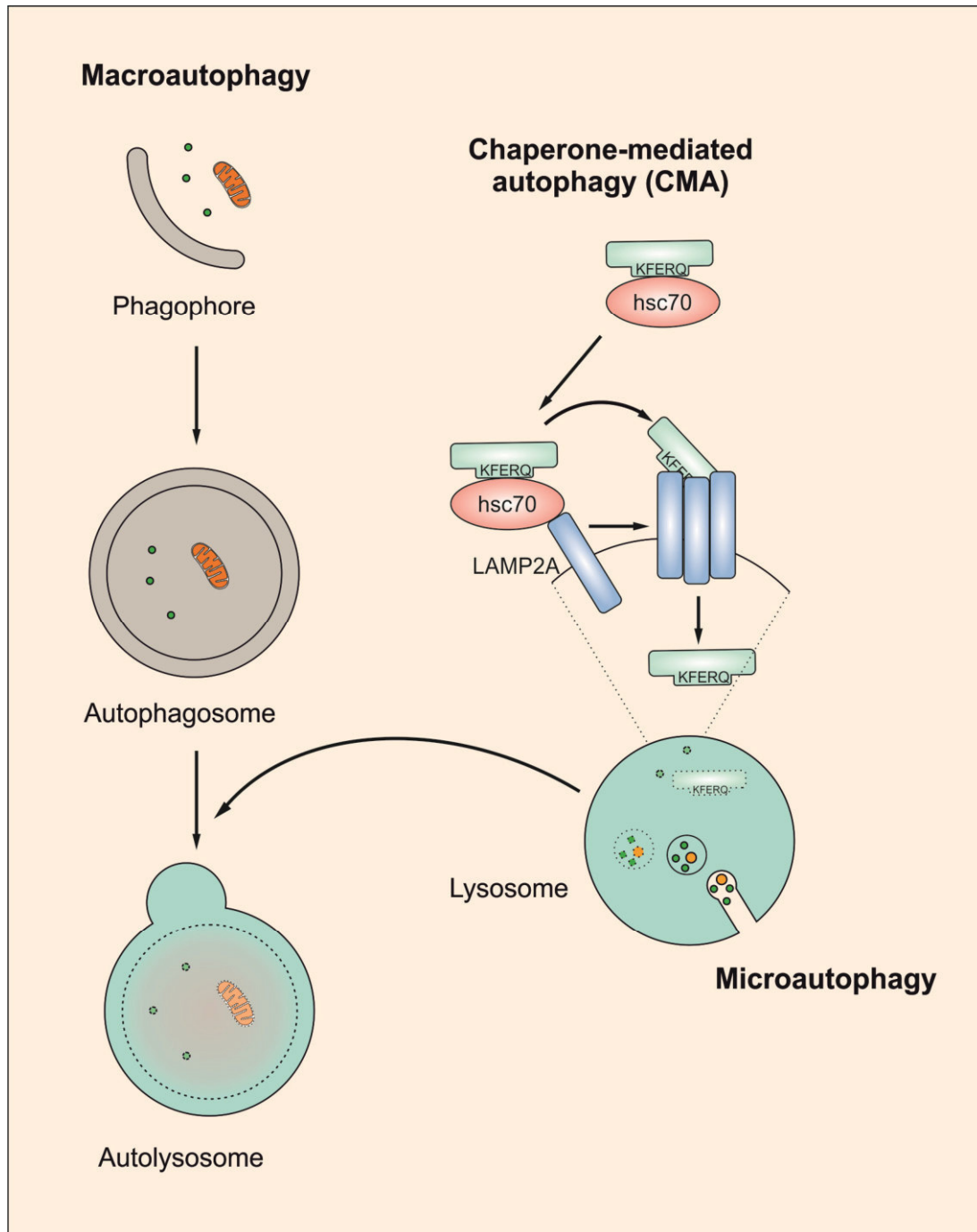


**Figure 1: Three major types of autophagy:** During macroautophagy, a unique membrane compartment called the phagophore is formed, which recruits the autophagic cargo to its proximity and encircles the cytoplasmic material upon closure of the phagophore into an autophagosome. The autophagosome subsequently fuses with a lysosome giving rise to the autolysosome and subjects the autophagic cargo to hydrolytic degradation by lysosomal hydrolases. The chaperone-mediated autophagy (CMA) exerts the chaperone protein hsc70 to recognize a pentapeptide motif present in the amino acid sequence of all CMA substrates. Motifs can become accessible for chaperone recognition after protein unfolding, protein disassembly from multiprotein complexes, or release of membrane-bound proteins. Hsc70 targets the CMA substrate to the lysosomal surface and activates the single-span membrane protein LAMP2A to oligomerize into a pore complex which then translocates the substrate proteins across the lysosomal membrane. During microautophagy invagination of the lysosomal membrane randomly occurs by lateral segregation of lipids and local exclusion of large transmembrane proteins. In an active and ATP-dependent process this bulge extends and specializes into an autophagic tube which forms an autophagic body at its tip that expands into a vesicle. After vesicle scission hydrolyses in the lysosomal lumen break down the vesicle and its content and permeases recycle nutrients to the cytoplasm.

Macroautophagy, or hereafter referred to as autophagy, can be rather unselective or exceptionally specific. On demand for essential metabolic building blocks and energy, unselective autophagy becomes activated and degrades various, nonessential cytoplasmic constituents. Oppositely, cargo-specific degradation serves as a quality control system removing superfluous or damaged organelles and protein aggregates that otherwise can be toxic to the cell (Youle and Narendra, 2011). Consequently, cargo-depending subgroups for the selective degradation process have been named: mitophagy for mitochondrial degradation (Lemasters, 2005), aggrephagy for degradation of aggregated proteins (Overbye et al., 2007), pexophagy for peroxisome degradation (Klionsky, 1997), ribophagy for degradation of mature ribosomes (Kraft et al., 2008), ER-phagy for endoplasmic reticulum degradation (Bernales et al., 2006), lipophagy for lipid droplet degradation (Singh et al., 2009), nucleophagy for nuclear envelope degradation (Park et al., 2009), and ferritinophagy for ferritin degradation (Asano et al., 2011).

In addition to its housekeeping role to maintain cellular homeostasis, autophagy can be upregulated during metabolic, genotoxic or hypoxic stress conditions and acts as an adaptive mechanism essential for cell survival. This is especially the case during the neonatal period bridging transplacental supply *in utero* and nutrient supply by maternal milk suckling (Medina et al., 1996). During this time the newborn is exposed to starvation by nutrient shortage which can be survived only by autophagy upregulation (Kuma et al., 2004).

Moreover, next to cytoplasmic entities autophagy can also degrade invading pathogens like bacteria and viruses which is referred to as xenophagy and is an essential process during immune responses (Jordan and Randall, 2012; Knodler and Celli, 2011; Levine, 2005; Vergne et al., 2006).

Inferring from its role in cellular health, dysregulation of autophagy is implicated in development and progression of various diseases like cancer, neurodegenerative diseases such as Alzheimer's and Parkinson's, myopathies, and heart and liver diseases (Dikic et al., 2010; Levine and Kroemer, 2008; Mizushima et al., 2008; Mowers et al., 2016).

The person inventing the term autophagy is Christian de Duve, a scientist and Nobel laureate especially known for his discovery of lysosomes. Following the development and technical improvement of electron microscopy in the 1950s, he was able to detect double membraned vesicles containing cytoplasmic material that were later identified as autophagosomes (Deter et al., 1967). Moving on to the early 1990s, Professor Ohsumi and colleagues reported the first autophagy defective mutants in yeast followed by identification of about 30 genes essential in autophagy induction and progression (Harding et al., 1995; Kamada et al., 2000; Mizushima et al., 1999; Shintani et al., 1999; Tanida et al., 1999; Thumm et al., 1994; Tsukada and Ohsumi, 1993). With the introduction of comprehensive genome sequencing, identification of genes coding for autophagy-

involved proteins in yeast, mammals, and plants revealed the high conservation of the autophagy process among eukaryotes (Reggiori and Klionsky, 2002).

Back then, several laboratories investigating autophagy and autophagy-related pathways in yeast originally used their own nomenclature e.g. APG (Tsukada and Ohsumi, 1993), and AUT for autophagy (Thumm et al., 1994), CVT for cytoplasm-to-vacuole targeting (Harding et al., 1996; Harding et al., 1995), GSA for glucose-induced selective autophagy (Yuan et al., 1997), PAG for peroxisome degradation via autophagy (Sakai et al., 1998), PAZ for pexophagy zeocin-resistant (Mukaiyama et al., 2002), and PDD for peroxisome degradation-deficient (Titorenko et al., 1995). As this caused great confusion among researchers, the abbreviation ATG for autophagy-related was officially selected after discussions at the first Gordon Research Conference on “Autophagy in Stress, Development, and Disease” in 2003 (Klionsky et al., 2003).

### 3.1.1 Autophagy regulation – pulling the trigger

Autophagy is a tightly regulated process being of essential importance for cellular health and homeostasis. Concomitantly, many factors of intrinsically and extrinsically origin contribute to autophagy regulation. The supply of amino acids, oxygen and growth factors is as important as the energy status of the cell to control autophagy induction. Also, stressors like ER and DNA damage or cellular  $Ca^{2+}$  levels have regulatory effects on autophagy signalling. Apparently, most signalling pathways inducing autophagy accumulate in the mechanistic target of rapamycin complex 1 (mTORC1). This complex was first found to be implicated in autophagy regulation in the yeast *Saccharomyces cerevisiae* where inhibition of the Tor kinase activity by rapamycin resulted in autophagy induction even under growing conditions (Noda and Ohsumi, 1998).

The mammalian mTORC1 contains seven core subunits: the catalytic TOR kinase, mammalian lethal with SEC13 protein (MLST8, also known as GβL ) (Kim et al., 2003), DEP domain containing MTOR-interacting protein (DEPTOR) (Peterson et al., 2009), 40 kDa proline-rich AKT substrate (PRAS40) (Sancak et al., 2007; Thedieck et al., 2007; Wang et al., 2007), regulatory-associated protein of mTOR (RAPTOR) (Hara et al., 2002; Kim et al., 2002) and the TTI1/TEL2 complex (Kaizuka et al., 2010). The PRAS40 subunit has regulatory functions within the complex by inhibiting TOR kinase activity under conditions that induce autophagy, such as nutrient or serum deprivation (Sancak et al., 2007; Thedieck et al., 2007; Vander Haar et al., 2007; Wang et al., 2007), indicating that mTORC1 acts as a gatekeeper for autophagy induction which has to be inactivated prior to autophagy-inducing signal transmission.

In the case of autophagy regulation by intracellular amino acid levels, a so-called “inside-out” signalling model has been established (Zoncu et al., 2011) (Figure 2). Here, amino acids accumulate in the lysosomal lumen, where their levels are recognized by a vacuolar H<sup>+</sup>-ATPase (v-ATPase) (Zoncu et al., 2011). This v-ATPase further interacts with the guanine nucleotide exchange factor (GEF) protein lysosomal adapter of mTOR (LAMTOR, previously called Ragulator, consisting of the subunits MAPKSP1, ROBLD3 and c11orf59) (Bar-Peled et al., 2012; Sancak et al., 2010), that tethers the RAG GTPase protein complex comprising heterodimers of RAGA or B and RAGC or D to the lysosomal surface (Kim et al., 2008; Sancak et al., 2008). While amino acid levels are high, the GEF activity of LAMTOR is enhanced, activating the RAG heterodimer (GTP-loaded RAGA/B and GDP-loaded RAGC/D), which subsequently recruits mTORC1 to the lysosomal surface (Zoncu et al., 2011). Through this intracellular relocation, mTORC1 retrieves proximity to its activator RAS homologue enriched in brain (RHEB) (Sancak et al., 2008). Like RAG, RHEB is a small GTPase, which in GTP-bound state enhances mTOR activity (Dibble et al., 2012). In response to depleted amino acid levels the GEF activity of LAMTOR is decreased, which results in the release of mTORC1 from the lysosome and its inactivation (Zoncu et al., 2011) (Figure 2).

Additionally a negative regulator for the RAG GTPases called the GTPase activating proteins toward Rags 1 (GATOR1) complex is activated in response to amino acid deprivation (Bar-Peled et al., 2013). GATOR1 has GTPase-activating protein (GAP) activity for RAGA and B, thereby favouring GDP-loaded RAGA/B and GTP-loaded RAGC/D and inactivating mTORC1. Consequently, inhibition of the GATOR1 subunits (DEPDC5, Nprl2, and Nprl3) makes mTORC1 signalling resistant to amino acid deprivation (Bar-Peled et al., 2013).

Also, RHEB activity can be inhibited by the tuberous sclerosis complex (TSC) which includes TSC1, TSC2 and RAS-related in brain (RAB) GTPase-activating protein TBC1 domain family member 7 (TBC1D7) (Dibble et al., 2012; Inoki et al., 2003a).

Another signalling pathway regulating mTORC1 activity is executed by the AMP-activated protein kinase (AMPK), which is regulated by cellular energy status measured by the AMP to ATP ratio. AMPK is a heterotrimeric complex consisting of a catalytic kinase domain-containing  $\alpha$ 1/2-subunit and the regulatory subunits  $\beta$ 1/2 and  $\gamma$ 1/2/3 (Davies et al., 1994).

When AMP levels are high and energy status of the cell is low, AMPK becomes activated and phosphorylates TSC2. This event in turn results in increased GAP activity of TSC2 towards RHEB, resulting in the inactivation of mTORC1 and initiation of autophagy (Inoki et al., 2003b). As a second level of regulation, AMPK can directly regulate mTORC1 function by phosphorylating RAPTOR, leading to 14-3-3 binding and allosteric inhibition of mTORC1 (Gwinn et al., 2008; Lee et al., 2010).

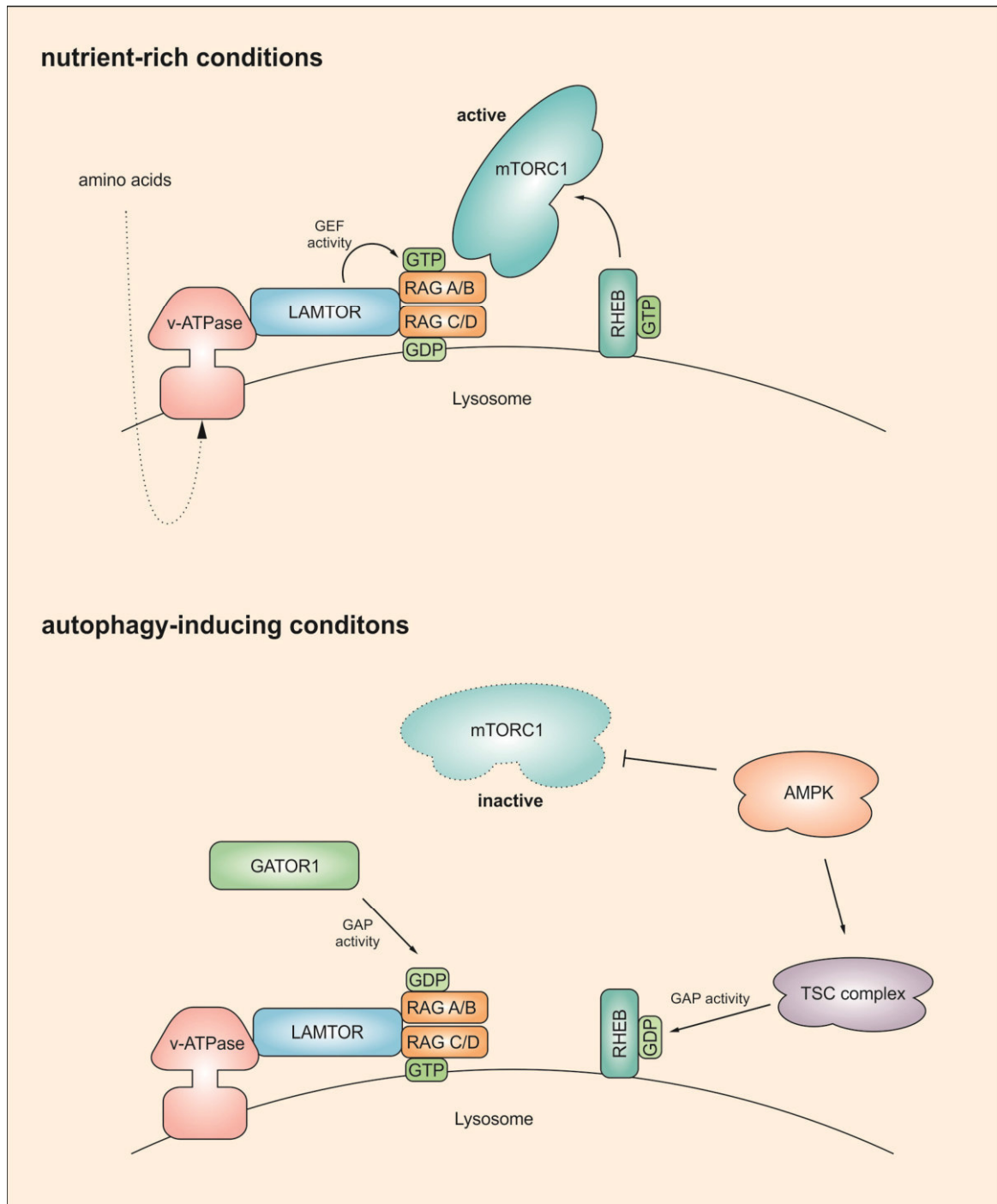


**Figure 2 Amino acid-dependent regulation of mTORC1:** Amino acids accumulate in the lysosomal lumen, where they stimulate signals to a vacuolar  $H^+$ -ATPase (v-ATPase) through an inside-out mechanism. The v-ATPase tethers LAMTOR to the lysosome, controls the LAMTOR-RAG GTPase complex interaction and induces the guanine exchange factor (GEF) activity of LAMTOR to promote loading of RAGA/B with GTP. Subsequently, the active RAG complex (RAGA/B-GTP-RAGC/D-GDP) binds to mTORC1 and recruits it to the lysosome, proximally located to the mTORC1 activator RHEB. Active, GTP-bound RHEB potently activates mTORC1 which then executes its inhibitory activity on the autophagy machinery. During autophagy-inducing conditions the RAG complex is inactivated by GATOR1 resulting in dissociation of mTORC1 from the lysosome and its diffuse localisation throughout the cytoplasm. Additionally, the TSC complex inhibits the mTORC1 activator RHEB. The ATP levels-sensing kinase complex AMPK exerts its autophagy-inducing activity via direct mTORC1 inactivation by phosphorylation events or activation of the GAP activity of the TSC complex to inhibit RHEB.

Noteworthy, AMPK is not just activated by the cellular energy level, but is also affected during the DNA damage response resulting in autophagy induction, where activation of TSC2 protein expression causes downregulation of the entire mTORC1 axis (Feng et al., 2005; Stambolic et al., 2001) and activation of AMPK (Budanov and Karin, 2008).

Besides autophagy regulation through signalling cascades, AMPK executes epigenetic control on autophagy-related gene expression. During persistent glucose starvation, the AMPK subunit  $\alpha 2$  accumulates in the nucleus where it downregulates S-phase kinase-associated protein 2 (SKP2), a cofactor of the E3 ubiquitin ligase SKP1–CUL1–F-box-protein (SCF) (Shin et al., 2016). This abrogates the permanent SCF-SKP2-mediated ubiquitination and degradation of the coactivator-associated arginine methyltransferase 1 (CARM1), which then exerts its transcriptional co-activator function on autophagy-related and lysosomal genes through the transcription factor EB (TFEB) (Shin et al., 2016). Another major physiologic circumstance regulating autophagy is the sufficient supply of oxygen to the cell. Chronic and moderate hypoxia induce autophagy via the hypoxia-inducible factor-1 (HIF-1) and the protein kinase C (PKC $\delta$ ) and c-Jun-N terminal kinase 1 (JNK1) pathway (Mazure and Pouyssegur, 2010). HIF-1 is a transcriptional regulator of hypoxia-associated genes and it also upregulates the expression of two BH3 domain-containing pro-autophagic proteins: B-cell lymphoma 2 (BCL-2)-interacting protein 3 (BNIP3) and BNIP3-like (BNIP3L, also known as NIX) (Bellot et al., 2009; Guo et al., 2001). These in turn replace another pro-autophagic protein BECN1 from the BCL-2 family proteins, freeing it to participate in autophagosome formation (Bellot et al., 2009). Adding to this, JNK1, activated by PKC $\delta$ , phosphorylates BCL-2, which additionally promotes dissociation of BECN1 from BCL-2 (Chen et al., 2008). Another HIF-1 target gene is regulation of DNA damage response 1 (REDD1), which promotes association of 14-3-3 to mTORC1 and inhibition of mTOR kinase activity (Ben Sahra et al., 2011; Brugarolas et al., 2004; DeYoung et al., 2008).

During rapid and severe oxygen fluctuation conditions, as it occurs for example under ischemia injury, autophagy is induced by HIF-1 independent pathways. Sensing of hypoxia by AMPK and resulting mTORC1 inhibition have been reported (Cam et al., 2010; Papandreou et al., 2008) as well as autophagy induction by the unfolded protein response (UPR) (Rouschop et al., 2010). The UPR is sensitive to unfolded proteins in the ER (Buchberger et al., 2010) which is mediated by three ER stressors: activation of transcription factor 6 (ATF6), ER to nucleus signalling 1 (ERN1, also known as IRE1 (inositol-requiring enzyme 1)) and eukaryotic translation initiation factor 2- $\alpha$  kinase 3 (EIF2AK3, also known as PERK (protein kinase RNA-like ER kinase)) (Appenzeller-Herzog and Hall, 2012; Ron and Walter, 2007). In an inactivated state, the latter are bound to the ER chaperone heat shock 70 kDa protein 5 (HSPA5), while in response to UPR, autophagy becomes activated by both the EIF2AK3 and

ATF6 pathways, but is negatively affected by ERN1 (Appenzeller-Herzog and Hall, 2012; Ogata et al., 2006; Yamazaki et al., 2009).

For completeness, it should be mentioned that amongst others growth factors, pro-inflammatory cytokines, and the Wnt pathway circumvent autophagy induction. Growth factors, such as insulin and insulin-like growth factor 1, and pro-inflammatory cytokines such as tumour necrosis factor  $\alpha$  (TNF $\alpha$ ) act via conceptually similar mechanisms by inhibiting the TSC complex and thus activating mTORC1 (Inoki et al., 2002; Lee et al., 2007; Ma et al., 2005; Manning et al., 2002; Potter et al., 2002; Roux et al., 2004). The canonical Wnt signalling pathway, a major regulator of cell growth, proliferation, polarity, differentiation, and development, inhibits glycogen synthase kinase 3 beta (GSK3- $\beta$ ), which normally phosphorylates and promotes TSC2 activity and thereby activates mTORC1 (Inoki et al., 2006).

### **3.2 The who is who in autophagy signalling**

Autophagy progression is tightly regulated by the core ATG proteins at every step, from sensing the environment, via autophagy initiation, phagophore development and elongation, maturation of the autophagosome, until fusion with lysosomes (Lamb et al., 2013) (Figure 3). The ULK1 complex is the central regulation node of autophagy initiation, mediating the transmission of the signal to the membrane source at which the nucleation of the isolation membrane occurs. This is followed by the recruitment of the VPS34 complex and activation of its lipid kinase activity by ULK1-mediated phosphorylation leading to abundant phosphatidylinositol 3-phosphate (PI3P) levels (Russell et al., 2013). This remodelling of the membrane composition distinguishes the isolation membrane from its membrane source and secondly recruits PI3P effector proteins like WIPs and DFCP1. During the elongation stage, expansion of the isolation membrane occurs and the cargo destined for degradation is located to the isolation membrane by autophagy receptor proteins and the ATG8 protein family members. Before closure of the isolation membrane the ATG proteins dissociate, and only the ATG8 family members remain attached (Karanasios et al., 2013; Polson et al., 2010). The final fusion step with the lysosome is then mediated by soluble N-ethylmaleimide sensitive factor attachment receptor (SNARE) proteins (Itakura et al., 2012).

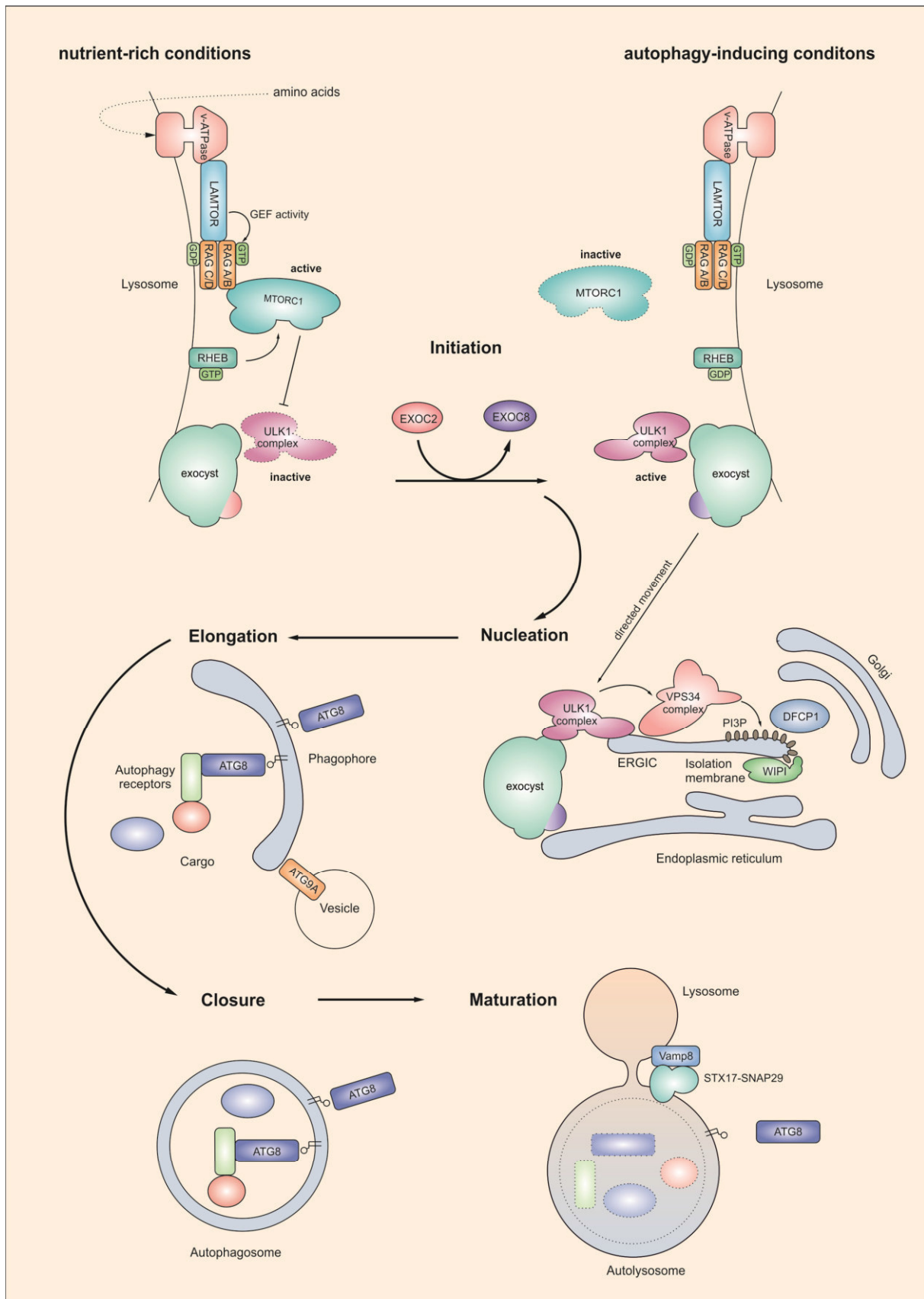


**Figure 3: The autophagy process:** Under nutrient-rich conditions, the mTORC1 complex is tethered and activated on the lysosomal surface where it executes its inhibitory function on the ULK1 complex. By autophagy induction through amino acid starvation conditions, mTORC1 dissociates and the ULK1 complex is released from mTORC1 repression. The active ULK1 complex is then shuttled to the autophagosome formation site possibly by the exocyst, which substitutes its subunit EXOC2

to EXOC8 under starvation conditions. The origin of the autophagosome formation site possibly exists at the ERGIC (ER-Golgi intermediate compartment), where localisation of the ULK1 triggers nucleation of the isolation membrane by recruitment and activation of the autophagic machinery. The VPS34 lipid kinase complex generates PI3P, thereby distinguishing the isolation membrane from the ERGIC by its unique lipid and protein composition. Secondly, PI3P recruits PI3P binding factors, such as DFCP1 and WIPI proteins. Growing of the isolation membrane is possibly driven by ER standing lipid synthesizing enzymes. After budding from the ER association, elongation of the isolation membrane to form the phagophore is driven by the membrane transfer protein ATG9A. The phagophore becomes sequestered with lipidated ATG8 proteins that recruit the autophagic cargo via autophagy receptors to the phagophore. Prior to the closure of the phagophore into the autophagosome, the autophagic core complexes with the exception of the ATG8 proteins, dissociate from the phagophore. Lastly, the autophagosome fuses with a lysosome with the help of the SNARE complex VAMP8 and STX17-SNAP29. The ATG8 proteins present on the outer autophagosomal membrane become recycled by dissociation from PE, while the inner membrane and the components in the autolysosomal lumen become degraded by hydrolases. Permeases allow the release of building blocks like amino acids and lipids into the cytoplasm where they are available for cellular processes.

### 3.2.1 The ULK1 protein complex - a star is born

In 1993 Tsukada and Ohsumi initiated a global screen for autophagy loss-of function yeast strains, resulting in the *apg1* gene being the first found to mediate autophagy-defects by gene knockout in *Saccharomyces cerevisiae* (Tsukada and Ohsumi, 1993). Following studies revealed a serine/threonine protein kinase as the gene product which was subsequently termed Atg1 (originally *apg1*) (Matsuura et al., 1997). Interestingly, this protein displayed 39.8 % sequence identity and 52.7 % similarity in its N-terminal kinase domain to the previously identified *Caenorhabditis elegans* kinase uncoordinated movement-51 (UNC-51) (Matsuura et al., 1997), which was reported to be essential for axonal elongation (Ogura et al., 1994). Though many species like *Caenorhabditis elegans* (Ogura et al., 1994) and *Drosophila melanogaster* (Scott et al., 2004) possess only one gene coding for Atg1 and its orthologues, vertebrates in contrast have at least five serine/threonine protein kinases in their genome displaying considerable homology to yeast Atg1 in their kinase domain (Chan and Tooze, 2009). The first identified mammalian homologues were the two most closely related UNC-51-like kinases 1 and 2 (ULK1/2) possessing 78 % amino acid identity in their catalytic domains and an overall homology of 52 % (Kuroyanagi et al., 1998; Tomoda et al., 1999; Yan et al., 1998; Yan et al., 1999). Next to the catalytically active kinase domain in their N terminus, ULK1/2 harbour a proline/serine-rich (PS) domain and a C-terminal domain which both mediate binding to interaction partners (Chan and Tooze, 2009).

The other UNC-51-related kinases ULK3, ULK4 and serine/threonine kinase 36 (STK36, also known as fused) display homology in their kinase domain only, but lack the unique C-terminal domain of ULK1 and ULK2 (Maloverjan et al., 2010a; Maloverjan et al., 2010b; Maloverjan et al., 2007).

The essential role of Atg1 orthologues for autophagy induction has been confirmed in several organisms such as *Caenorhabditis elegans* (Ogura et al., 1994) and *Drosophila melanogaster* (Scott et

al., 2004). In contrast, the role of the ULKs in higher eukaryotes is controversially discussed. First knockdown experiments using siRNA demonstrated abolished autophagy induction only after targeting both ULK1 and 2, but not for the single knockdowns, indicating redundant functions for these kinases (Chan et al., 2007). Similar observations were made in mice models: *Ulk1*<sup>-/-</sup> as well as *Ulk2*<sup>-/-</sup> knockout mice are born viable and survive the short starvation period after birth (Cheong et al., 2011; Kundu et al., 2008; Lee and Tournier, 2011). In contrast, *Ulk1/2*<sup>-/-</sup> mice are born alive but display early neonatal lethality, again emphasizing redundant functions of the two kinase homologues in autophagy (Cheong et al., 2011; McAlpine et al., 2013). In accordance with these observations, McAlpine et al. reported a complete block of autophagy induction by amino acid or glucose deprivation in murine embryonic fibroblasts (MEFs) isolated from their *Ulk1/2*<sup>-/-</sup> mice (McAlpine et al., 2013). Controversially, Cheong et al. observed inhibited autophagy induction only by amino acid withdrawal, while increasing ammonia concentrations occurring during glucose deprivation still resulted in an autophagy induction response in MEF cells isolated from their mouse model, which suggests the existence of ULK1/2-independent autophagy pathways (Cheong et al., 2011). This was supported by a third knockout model, where *Ulk1/2*<sup>-/-</sup> DT40 cells also displayed ULK1/2-independent autophagy (Alers et al., 2011). An interesting observation was made by Chan et al., who found that autophagy is blocked by overexpression of ULK1 (Chan et al., 2007). Furthermore, this effect was independent from the ULK1 kinase activity but mediated by the N-terminal region of residues 1-351 indicating a unique set of functions (Chan et al., 2007).

It is also noteworthy, that despite their redundant activity in overall autophagy, ULK1 and ULK2 seem to act independently in specialized cellular processes. First of all, only *Ulk1*<sup>-/-</sup> mice display compromised clearance of mitochondria during erythropoiesis (Kundu et al., 2008), which might be explained by the fact that only ULK1 is reported to be involved in mitophagy (Joo et al., 2011). Secondly, localization of ULK1 and ULK2 differs severely. While ULK1 is primarily located in the cytosol, ULK2 preferentially localizes to the nucleus, where it displays ULK1- and maybe even autophagy-independent functions e.g. regulation of poly(ADP-ribose)-polymerase 1 (PARP1) activity (Joshi et al., 2016; Shin et al., 2015). Autophagy-independent roles for ULK1/2 have been established also in lipid metabolism and glucose uptake. Here, ULK1 and ULK2 display opposite functions. While ULK1 knockdown enhances fatty acid uptake but reduces oxidation, ULK2 knockdown has converse effects (Ro et al., 2013).

To execute its function in the autophagy signalling pathway, ULK1 is incorporated into a 3 MDa complex by the scaffolding protein ATG13 together with ATG101 and Retinoblastoma 1-inducible coiled-coil 1 (RB1CC1, also called focal adhesion kinase-interacting protein of 200 kDa (FIP200)) (Chan et al., 2009; Ganley et al., 2009; Hieke et al., 2015; Hosokawa et al., 2009a; Jung et al., 2009; Suzuki

et al., 2015a). Because ULK1 is the only protein with catalytic activity, the complex was consequently named ULK1 complex, which features a permanent complex formation in mammals unaffected by the cellular nutrient status (Chang and Neufeld, 2009; Ganley et al., 2009; Hara et al., 2008; Hosokawa et al., 2009a; Hosokawa et al., 2009b; Jung et al., 2009).

Similar to ULK1, the orthologue of ATG13 was among the proteins primarily identified as autophagy-essential during the global yeast screening (Funakoshi et al., 1997). By performing an *in silico* analysis of the non-redundant NCBI protein database, the human protein with the accession number AAH02378 (a putative product of the KIAA0652 gene) was identified as the potential mammalian ATG13 homolog (Meijer et al., 2007). This is supported by the fact that cells carrying an ATG13 knockout are defective in ULK1 complex assembly and autophagy induction (Kaizuka and Mizushima, 2015). Moreover, *Atg13*<sup>-/-</sup> mice die *in utero* and embryos show growth retardation and myocardial growth defects (Kaizuka and Mizushima, 2015).

The ATG13 protein can roughly be divided into a strictly structured N-terminal part and an intrinsically disordered region mapped to the C terminus (Fujioka et al., 2014; Mei et al., 2014). The N terminus of ATG13 comprises a HORMA domain, a structured region first identified and named after the *Saccharomyces cerevisiae* proteins Hop1, Rev7, and Mad2, which display sequence similarities but no functional overlaps (Aravind and Koonin, 1998). In all of these proteins, the HORMA domain is highly conserved, mediating protein-protein interactions through a structurally unique mechanism. Usually two functionally distinct regions organise the HORMA domain: the N-terminal core region and a C-terminal safety belt (Rosenberg and Corbett, 2015). In the case of Mad2, the HORMA domain can adapt an open or closed state and this conformational conversion is essential for protein binding. The ATG13 HORMA domain corresponds to the closed C-Mad2 structure, which raised speculations of a possible conformational change mediated by phosphorylation of a phosphor sensor motif within the HORMA domain (Jao et al., 2013). Only after crystallisation of the ATG13-ATG101 protein interaction it became clear that ATG101 as well harbours a HORMA domain in an open O-Mad2 conformation, complementing the ATG13 C-Mad2-like HORMA structure (Michel et al., 2015; Qi et al., 2015; Suzuki et al., 2015a).

ATG101, the product of the mammalian C12orf44 gene, is the most recently identified ULK1 complex component and direct binding partner of ATG13 (Hosokawa et al., 2009b; Mercer et al., 2009). Though it shows a weak sequence similarity to yeast *Atg17*, there exists no obvious homologue in the yeast *Saccharomyces cerevisiae*, hence the nomenclature ATG101 was chosen (Mercer et al., 2009). Interestingly, ATG101 is conserved in higher eukaryotes like flies and worms and even in the fission yeast *Schizosaccharomyces pombe* (Steffan, 2010).

Importantly, when mutating ATG13 or ATG101 to inhibit protein interaction, ATG101 cannot incorporate into the ULK1 complex leading to impaired autophagy induction (Suzuki et al., 2015a) (chapter 4.3). Though the ATG101 function within the ULK1 complex is not entirely clarified, it might work as a regulatory subunit that recruits downstream targets through a unique WF finger in its HORMA domain (Qi et al., 2015; Suzuki et al., 2015a).

The interaction sites for ULK1 and RB1CC1 were previously roughly mapped to the human ATG13 C terminus (Jung et al., 2009). In depth studies revealed the extreme C terminus comprising the ULK1 binding platform with deletion of the last three amino acids in ATG13 being sufficient to abolish ULK1 complex formation (Hieke et al., 2015) (chapter 4.1). The RB1CC1 interaction hub was distinguishably mapped from the ULK1 interaction site as a 26 amino acid stretch in the C terminus of ATG13 (Alers et al., 2011). Surprisingly, though formation of the ULK1 complex was abolished and recruitment of the ULK1 complex members to the autophagosome formation site under starvation conditions was absent, inhibition of the ATG13-ULK1 interaction had only minor effects on autophagy induction and blocking of the ATG13-RB1CC1 complex formation did not have an impact at all (Hieke et al., 2015) (chapter 4.3).

This is particularly surprising, since knockout of RB1CC1 just like ATG13 results in impaired autophagy (Hara et al., 2008). Systemic *Rb1cc1* knockout in mice is lethal with embryonic death at mid/late gestation stage, which is associated with heart failure and liver degeneration (Gan et al., 2006). Several pieces of information hint that this might not only be due to its function in autophagy but its collaboration in several other signalling pathways. Known interaction partners and functions of RB1CC1 are binding to stathmin (Maucuer et al., 1995) and listeria monocytogenes surface protein ActA (Pfeuffer et al., 2000), the direct inhibition of the focal adhesion kinase (FAK) and proline-rich tyrosine kinase 2 (PYK2) activities (Abbi et al., 2002; Ueda et al., 2000), disruption of the TSC complex formation (Gan et al., 2005), regulation of p53 and TSC1 protein stability (Chano et al., 2006; Melkounian et al., 2005), scaffolding of TNF receptor-associated factor 2 (TRAF2) and apoptosis signal-regulating kinase 1 (ASK1) to facilitate signalling for JNK1 activation (Gan et al., 2006), regulation of p21 expression via protein inhibitor of activated STAT  $\gamma$  (PIAS $\gamma$ ) interaction (Martin et al., 2008), and regulation of Retinoblastoma 1 transcription (Chano et al., 2002a; Kontani et al., 2003).

Mammalian RB1CC1 is majorly unstructured but depicts a large coiled-coil region containing a leucine zipper motif and a putative nuclear localization signal (Chano et al., 2002a). This is highly conserved as human and mouse RB1CC1 share around 90 % sequence identity and a similar domain structure (Chano et al., 2002b). Interestingly, no yeast homolog has been identified so far, though yeast Atg17 has been proposed as a functional counterpart due to functional overlap in the autophagy signalling

pathway (Hara and Mizushima, 2009). Since known interaction partners mediate diverse, largely non-overlapping functions, including regulation of microtubule dynamics, cell adhesion and migration signalling, stress response, cell proliferation and cell growth, and associate with various regions in RB1CC1, it is possible that RB1CC1 can exert multiple biochemical functions through different domains simultaneously. This is also illustrated by its diverse cellular localization to the cytoplasm (Gan et al., 2005; Gan et al., 2006; Maucuer et al., 1995; Pfeuffer et al., 2000; Ueda et al., 2000), focal adhesions (Abbi et al., 2002), and the nucleus (Chano et al., 2002b; Melkounian et al., 2005).

A (microtubule-associated protein 1) light chain 3 ((MAP1)LC3)-interacting region (LIR) is situated upstream of the RB1CC1 interaction site in ATG13 (Alemu et al., 2012; Birgisdottir et al., 2013). This motif mediates interaction with the ATG8 protein family members (chapter 1.2.6). Though the interaction was experimentally verified, no functional relevance has been reported so far (Suzuki et al., 2014) (chapter 4.3).

Additionally to protein interaction partners, ATG13 contains a highly conserved phospholipid binding motif at its extreme N terminus, that facilitates interaction with phosphatic acid (PA), phosphatidylinositol 3-phosphate (PI3P), phosphatidylinositol 4-phosphate (PI4P) and to a lesser extent with phosphatidylinositol 3,4,5-trisphosphate (PI(3,4,5)P3) (Karanasios et al., 2013). Necessity of this site is questionable though, since opposite observations have been reported. Karanasios et al. found inhibited ATG13 translocation and autophagosome formation (Karanasios et al., 2013) while our research group detected no autophagy-inhibitory effects upon mutation of this motif (chapter 4.3).

### **3.2.2 Upstream regulation of the ULK1 complex or: Why is life always that complicated?**

MTORC1 and AMPK, two protein kinases with opposite regulatory functions in the upstream autophagy induction pathway, both mediate their signalling via the ULK1 complex (Hosokawa et al., 2009a; Mack et al., 2012). Accordingly, the phosphorylation status within the ULK1 complex dramatically changes in response to the nutrient status. Under growing conditions, mTORC1 associates with the ULK1 complex, either by interaction of RAPTOR with the PS domain of ULK1 (Hosokawa et al., 2009a) or direct mTOR binding to the kinase domain of ULK1 (Lee et al., 2010). Subsequently, active mTOR phosphorylates ULK1 thereby negatively regulating its kinase activity (Ganley et al., 2009; Hosokawa et al., 2009a; Jung et al., 2009).

Phosphorylation sites in ULK1 are plenty, but of these especially the phosphorylation status of S<sup>638</sup> and S<sup>758</sup> (in human ULK1, corresponding to S<sup>637</sup> and S<sup>757</sup> in murine ULK1) severely changes during starvation (Dorsey et al., 2009; Kim et al., 2011; Shang et al., 2011). It is generally accepted that S<sup>758</sup> is phosphorylated by mTOR, though its effect on ULK1 function is controversially discussed. Kim et al. reported inhibitory effects of phosphorylated S<sup>758</sup> on the association of ULK1 and AMPK, and accordingly blockade of autophagy (Kim et al., 2011). Shang et al. on the other hand postulated that phosphorylation of S<sup>758</sup> promotes the ULK1-AMPK interaction. They further speculated that this interaction actually retains ULK1 from its function in autophagy and thereby blocks autophagic flux under nutrient-rich conditions (Shang and Wang, 2011). Adding to this complex model is the second phosphorylation site S<sup>638</sup> in ULK1, which can be phosphorylated both by mTOR and AMPK according to Shang et al., while others identified S<sup>638</sup> solely as an AMPK target (Egan et al., 2011a; Mack et al., 2012; Shang et al., 2011). Surprisingly, similar to S<sup>758</sup>, phosphorylation of S<sup>638</sup> decreases during starvation despite enhanced AMPK activity (Shang et al., 2011).

Other AMPK-mediated phosphorylation events target S<sup>317</sup> and S<sup>556</sup> in ULK1 (in murine ULK1 additionally S<sup>777</sup>) (Bach et al., 2011; Kim et al., 2011; Lee et al., 2010; Mack et al., 2012). Contrary to S<sup>638</sup>, phosphorylation of these sites increases upon glucose or amino acid deprivation and is required for ULK1 kinase activity and function in autophagy (Egan et al., 2011a; Egan et al., 2011b; Kim et al., 2011). These data indicate a very complex regulation of ULK1 activity, where AMPK alone can induce or inhibit ULK1 function solely by phosphorylating distinct serine residues.

The inscrutable role of AMPK in ULK1 regulation and autophagy induction extends to the ULK1 complex subunit ATG13, which is phosphorylated by AMPK at S<sup>224</sup> and additionally by mTOR at S<sup>258</sup>. Importantly, the phosphorylation is strong under nutrient rich conditions and decreases upon starvation, accompanied by increased ULK1 kinase activity (Puente et al., 2016). These data further emphasize the dual role of AMPK and possibly its fine-tuning function in autophagy.

The complexity of this phosphorylation-mediated regulatory network is increased by the existence of feedback loops that positively or negatively regulate the autophagy process. Active ULK1 is able to phosphorylate RAPTOR at numerous sites (S<sup>855</sup>, S<sup>859</sup>, S<sup>792</sup>) which leads to hindered substrate docking of e.g. the eukaryotic translation initiation factor 4E-binding protein 1 (4E-BP1) and negatively regulates mTORC1 activity, which consequently increases autophagic activity (Dunlop et al., 2011). For contrary effects, ULK1 can directly phosphorylate AMPK and inhibit its kinase activity and autophagy-inducing functions (Löffler et al., 2011).

Moreover, it is important to mention that most research groups investigating ULK1 phosphorylation did not account dephosphorylating events as a major tool for catalytic activity control. The

serine/threonine protein phosphatase 2 A (PP2A) was identified to dephosphorylate S<sup>757</sup> and S<sup>637</sup> upon autophagy induction, thereby operating against mTOR and AMPK (Wong et al., 2015).

Additionally, other kinases have been reported to phosphorylate ULK1 e.g. protein kinase B (PKB, also known as AKT) at S<sup>774</sup> upon insulin treatment (Bach et al., 2011) and S<sup>1042</sup> by protein kinase A (PKA) (Dorsey et al., 2009), both leading to rather inactivated ULK1.

As a last remark it should be mentioned that posttranslational modifications other than protein phosphorylation are just as important in the regulatory machinery. Exemplarily the acetylation of ULK1 at K<sup>162</sup> and K<sup>606</sup> by the acetyltransferase HIV-1 Tat interacting protein, 60kDa (TIP60) should be stated, which is required for autophagy induction by growth factor deprivation (Lin et al., 2012). Additionally, ubiquitination of ULK1 by the E3-ligase TNF receptor-associated factor 6 (TRAF6) with K<sup>63</sup>-linked chains enhances its protein stability and function (Nazio et al., 2013).

### 3.2.3 Downstream signalling of the ULK1 complex: phosphorylation<sup>2</sup>

Subsequent to the successful activation of ULK1 by autophagy inducing signalling pathways, the ULK1 complex translocates to the autophagosome formation site to mediate signalling to the downstream autophagy machinery (Chan et al., 2007; Ganley et al., 2009; Hara et al., 2008; Hosokawa et al., 2009a; Itakura and Mizushima, 2010; Jung et al., 2009). This directed movement of the ULK1 complex might be facilitated by the exocyst, a large hetero-octameric complex, which is commonly known as a dynamic scaffold platform for protein complexes (Bodemann et al., 2011). In this model, the ULK1 complex is associated with an inactive exocyst complex component 2 (EXOC2)-containing exocyst complex in the perinuclear region under nutrient rich conditions. In response to starvation, the GTPase RAS like proto-oncogene B (RALB) becomes activated and promotes replacement of EXOC2 by EXOC8. The EXOC8-containing exocyst complex then translocates to vesicular structures, possibly the autophagosome initiation sites and additionally recruits other autophagy protein complexes thereby bringing the autophagy machinery into close proximity (Bodemann et al., 2011).

In addition to the subcellular complex localisation, the kinase activity of ULK1 is of central relevance for autophagy signalling. A protein interaction database (Chatr-Aryamontri et al., 2017) (and <https://thebiogrid.org/113996/summary/homo-sapiens/ulk1.html>) collecting low- and high-throughput data currently lists 50 unique interactors for ULK1 which overlaps with a large number of substrates already reported for ULK1. The optimal ULK1 substrate motif features preferences for hydrophobic residues M or L at the -3 position and aromatic residues like Y at the +2 position (Egan et al., 2015).

Within the ULK1 complex, ULK1 autophosphorylates and transphosphorylates its interaction partners ATG13, RB1CC1 and ATG101 (Chan et al., 2007; Egan et al., 2015; Ganley et al., 2009; Hara et al., 2008; Hosokawa et al., 2009a; Jung et al., 2009). It has been argued that the ULK1 autophosphorylation mainly regulates its conformation, the exposure of the CTD and by this means its interaction with putative interaction partners (Chan et al., 2007; Chan et al., 2009; Chan and Tooze, 2009). For ATG13 several ULK1-dependent phosphorylation sites have been identified (Egan et al., 2015). Among these, phosphorylation at S<sup>318</sup> in ATG13 has an essential function in mitophagy, where it translocates to depolarized mitochondria following ULK1-mediated phosphorylation and promotes mitochondrial degradation (Joo et al., 2011). Notably, in this context ATG13 displays a ULK1-independent function, as the phosphorylation leads to dissociation from the ULK1 complex.

Alers et al. identified five more ULK1-dependent phosphorylation sites in a kinase assay, though mutation of these sites in ATG13 did not have an effect on ATG13 function and autophagy initiation (Alers et al., 2011).

Additionally, ULK1 target sites were reported for RB1CC1, though their functional meaning was not examined (Egan et al., 2015). The same accounts for ATG101. Here, phosphorylation by ULK1 at S<sup>11</sup> and S<sup>203</sup> was identified, however the relevance for autophagy signalling was not further investigated (Egan et al., 2015).

Other ULK1 substrates are in part members of the autophagy core protein complexes like activating molecule in beclin1-regulated autophagy (AMBRA1), beclin1 (BECN1), and ATG14L (Nazio et al., 2013; Park et al., 2016; Russell et al., 2013) which will be discussed in the following sections (chapter 1.2.4). Additionally identified target proteins are FUN14 domain containing 1 (FUNDC1), a mitochondrial resident protein that is phosphorylated at S<sup>17</sup> leading to increased mitophagy (Wu et al., 2014), and stimulator of interferon genes (STING) (Konno et al., 2013).

### 3.2.4 VPS34 lipid kinase complex: running down the Pipeline

The downstream signalling of the ULK1 complex takes a very interesting turn, as the downstream target is the VPS34 lipid kinase complex, which catalyses the generation of phosphatidylinositol 3-phosphate (PI3P) (Itakura and Mizushima, 2010; Matsunaga et al., 2010).

The VPS34 complex comprises the catalytic lipid kinase subunit VPS34, and the accessory proteins VPS15, BECN1, ATG14L (also known as beclin-1 associated autophagy-related key regulator (Barkor)), and UV radiation resistance associated protein (UVRAG) (Itakura et al., 2008; Kihara et al., 2001a; Liang et al., 1999; Matsunaga et al., 2009; Sun et al., 2008; Zhong et al., 2009). As ATG14L and UVRAG

are mutually exclusive subunits, the ATG14L-containing complex is referred to as complex I, while UVRAG is present in complex II. Both have distinct functions, with complex I facilitating autophagy initiation (Matsunaga et al., 2010; Zhong et al., 2009), whereas complex II is integrated into autophagosome maturation (Liang et al., 2006; Liang et al., 2008). The high conservation of the VPS34 complexes from yeast to higher eukaryotes emphasizes its essential role in the autophagy machinery (Kihara et al., 2001b; Obara et al., 2006).

The lipid kinase VPS34 produces PI3P by phosphorylating phosphoinositide (PI) at the 3' position of the inositol ring. Generation of PI3P originates a membrane compartment with unique lipid composition that is distinguishable from the regular ER, where no PI3P is present in the membrane (Gillooly et al., 2000).

The function of VPS15 in this complex is not quite clear, though its essential importance for VPS34 complex activity was demonstrated (Yan et al., 2009). VPS15 might be a pseudo kinase, as it harbours a protein kinase domain whose function and possible substrates are uncertain. Moreover, for the yeast homolog Vps15 a membrane anchor function by a myristoylation tag is published, which might mirror its function in higher eukaryotes (Herman et al., 1991).

The BECN1 subunit acts as a scaffold protein for the recruitment of further regulatory subunits to the complex. The interaction with the VPS34-VPS15 core complex is not constitutive, but is induced upon autophagy induction. Under growing conditions, BECN1 rather interacts with GAPR1, a myristoylated protein that is present in lipid-enriched microdomains of the Golgi network and thereby keeping it from the VPS34 complex (Shoji-Kawata et al., 2013). Additionally, BECN1 associates with the anti-autophagic protein BCL-2 via its BH3 domain, and thereby becomes sequestered to mitochondria (Pattingre et al., 2005). During autophagy induction BCL-2 is phosphorylated by JNK1, thus freeing BECN1 from BCL-2 and inducing proper VPS34 complex formation and autophagy progression (Wei et al., 2008). Moreover, BECN1 becomes phosphorylated at S<sup>91</sup> by AMPK and S<sup>14</sup> by ULK1 which enhances activity of the VPS34 complex and positively regulates autophagy (Kim et al., 2013b; Russell et al., 2013).

One BECN1-interacting protein is ATG14L (Matsunaga et al., 2010), and levels of ATG14L severely influence the stability of both BECN1 and VPS34, indicating the essential role of ATG14L for the VPS34 complex functionality (Itakura et al., 2008). ATG14L localizes to the ER, a putative site for autophagosome formation, even under growing conditions (Matsunaga et al., 2010). This observation suggests that ATG14L is the driving force in recruiting the subcomponents of the VPS34 complex to the ER (Matsunaga et al., 2010). Moreover, ATG14L might link the VPS34 complex to the ULK1 complex, since ATG14L directly interacts with the HORMA domain in ATG13 (Jao et al., 2013).

Additionally, ATG14L becomes phosphorylated by ULK1, which stimulates the kinase activity of the VPS34 complex facilitating phagophore and autophagosome formation (Park et al., 2016).

Recently, the nuclear receptor binding factor 2 (NRBF2) was identified as a new interaction partner of the VPS34 complex I. The association was reported to be mediated either by binding to VPS15 (Cao et al., 2014) or ATG14L (Zhong et al., 2014). NRBF2 promotes the dimerization of the ATG14L-containing VPS34 complex to increase the lipid kinase activity of VPS34 (Young et al., 2016). Despite the activation of VPS34, the function of NRBF2 in the autophagy signalling network is not answered conclusively. Experimental approaches using NRBF2 knockdown detected an increased autophagic flux, assigning a rather autophagy-inhibiting function to NRBF2 (Zhong et al., 2014). Contrary, other studies observed defective autophagy upon NRBF2 knockdown and knockout indicating autophagy-promoting effects (Cao et al., 2014; Lu et al., 2014). Very recently, mTORC1-mediated NRBF2 regulation by phosphorylation has been described (Ma et al., 2017). The mTOR-dependent phosphorylation sites become dephosphorylated under starvation conditions, which increase the binding preference of NRBF2 to the VPS34 complex. This facilitates VPS34 complex assembly, association with the ULK1 complex and progression of autophagic signalling.

Another regulatory subunit of the VPS34 complex is AMBRA1 (Fimia et al., 2007). Similar to BECN1, AMBRA1 interacts with BCL-2 under growing conditions, thereby sequestering it to mitochondria. By nutrient deprivation, AMBRA1 is released from this interaction and incorporated into the VPS34 complex, which is essential for its lipid kinase activity (Strappazzon et al., 2011). Another report suggests that AMBRA1 specifically binds to the dynein motor complex under growing conditions through direct interaction with dynein light chain 1 (DLC1) (Di Bartolomeo et al., 2010; Fimia et al., 2011). Upon starvation, AMBRA1 is released from this interaction by ULK1-mediated phosphorylation, which facilitates VPS34 complex translocation to the ER, where it initiates autophagosome formation (Di Bartolomeo et al., 2010; Fimia et al., 2011). In a positive feedback loop, AMBRA1 supports ULK1 ubiquitination by TRAF6, which enhances ULK1 stabilization and function (Nazio et al., 2013). AMBRA1 therefore adapts an interesting role in the autophagy signalling network, as it is not just a cofactor of BECN1 but also a crucial upstream regulator of the autophagy-inducing ULK1 complex (Fimia et al., 2011).

UVRAG, the VPS34 complex II subunit, binds to BECN1 by competing with ATG14L for the same binding site and thereby integrates the complex in the course of the autophagosome maturation (Li et al., 2012b; Sun et al., 2008). Its mode of action is not clear, but implementation in membrane curving is one possibility. It has been reported that UVRAG interacts with bax-interacting factor 1 (BIF1) (Takahashi et al., 2007), which harbours an N-BAR domain, known to bind membranes and cause them to undergo curvature (Itoh and De Camilli, 2006). This suggests that UVRAG recruits BIF1

to deform membranes. A putative negative regulator of UVRAG is RUN domain BECN1-interacting and cysteine-rich containing protein (RUBICON), which is integrated into the VPS34 complex II via UVRAG, where it inhibits VPS34 lipid kinase activity (Matsunaga et al., 2009; Sun et al., 2010; Zhong et al., 2009). Moreover, mTOR phosphorylates UVRAG, thereby enhancing UVRAG-RUBICON interaction and suppression of autophagosome maturation (Kim et al., 2015).

### 3.2.5 The PI3P effector proteins: PlmPing it up

The generated PI3P functions as a new platform to recruit downstream effectors for autophagy signalling. One of these effector proteins is double FYVE domain-containing protein 1 (DFCP1) (Cheung et al., 2001; Derubeis et al., 2000; Ridley et al., 2001), which binds PI3P via its two FYVE domains. Among the FYVE-domain-containing proteins, DFCP1 displays a unique localization to the ER and Golgi network (Cheung et al., 2001) instead of endosomal membranes (Ridley et al., 2001). This might be due to an ER-targeting domain that is dominant over the two FYVE domains (Axe et al., 2008).

In contrast, the WD-repeat protein interacting with phosphoinositides (WIPI) protein family binds PI3P via a seven-bladed  $\beta$ -propeller. In mammals four isoforms exist (WIPI1-4), though only WIPI1 and WIPI 2 are recruited to the autophagosomal membrane (Polson et al., 2010; Proikas-Cezanne et al., 2004). The WD-40 motif-containing proteins belong to the PROPPIN family, which is conserved from yeast to humans (Baskaran et al., 2012). Members of this family harbour two PI3P binding sites functioning in concert with a hydrophobic loop, which mediates membrane binding, explaining the specificity of the PROPPINS for membrane-bound PI3P (Baskaran et al., 2012; Watanabe et al., 2012). Interestingly, though WIPIs and DFCP1 both target PI3P, their cellular localization slightly differs. WIPI2 colocalizes with ATG14L, a marker for the isolation membrane, while DFCP1 is in close proximity (Itakura and Mizushima, 2010). Therefore, it has been suggested that DFCP1 localizes to the omegasome, a ring-like structure emanating from the isolation membrane, rather than to the isolation membrane itself.

### 3.2.6 Two ubiquitin-like protein complexes: tag me whole again

Ubiquitination is a posttranslational modification by covalent conjugation of the protein ubiquitin to a target protein, and this mechanism is essential to numerous processes such as cell cycle

progression, apoptosis, cell proliferation and differentiation (Weissman, 2001). The multistep mechanism involves at least three types of enzymes: (I) The ubiquitin-activating enzyme E1, forming a thiol-ester bond with the C-terminal glycine of ubiquitin in an ATP-consuming reaction; (II) the ubiquitin-carrier enzyme E2, which ubiquitin is transferred to, and (III) the ubiquitin protein ligase E3, which catalyses the transfer of ubiquitin to the amino group of a lysine in the substrate protein (Figure 4). Several ubiquitin homologs have been found e.g. neural precursor cell expressed, developmentally down-regulated gene 8 (NEDD8) and small ubiquitin-related modifier (SUMO) resembling amino acid sequence homology with ubiquitin, whereas others show only functional resemblance.

One of these is the autophagic protein ATG12, which becomes activated by the E1 enzyme ATG7, is then transferred to the E2 enzyme ATG10, and eventually attaches to ATG5 via an isopeptide bond (Kaiser et al., 2012; Mizushima et al., 1998a; Mizushima et al., 1998b; Otomo et al., 2013).

The second ubiquitin-like mechanism implicated in autophagy involves the ATG8 protein family members. After translation, these proteins are immediately processed by the protease ATG4 to expose a C-terminal glycine residue (Kirisako et al., 2000). The conjugation reaction for ATG8 proteins also involves ATG7 as the E1 enzyme (Taherbhoy et al., 2011), whereas ATG3 functions as the carrier enzyme E2 (Ichimura et al., 2000; Noda et al., 2011). Interestingly, the target of the ATG8 family members is not a protein, but the membrane-anchored lipid phosphatidylethanolamine (PE) (Geng and Klionsky, 2008; Ichimura et al., 2000).

Remarkable about these two processes is the absence of an E3 enzyme. Instead, the E2 enzymes directly recognize the substrates. In the case of the ATG8-PE conjugation, the ATG5-ATG12 conjugate has E3-like functions, since it associates with ATG3 and enhances its E2 activity (Metlagel et al., 2013). ATG12 binds tightly to ATG3 (Metlagel et al., 2013) and ATG5 recognizes negatively charged membranes (Romanov et al., 2012), thereby bringing the ATG8-ATG3 complex into proximity with PE. Hence, mice lacking ATG5 or ATG12 have no lipidated ATG8 proteins, are defective in autophagy and not viable (Kuma et al., 2004; Malhotra et al., 2015). The same is true for ATG7 knockdown and knockout (Komatsu et al., 2005).

The ATG5-ATG12 conjugate complexes with ATG16L1, and by dimerization of ATG16L1 eventually forms a supracomplex of about 800 kDa (Fujioka et al., 2010; Mizushima et al., 2003). ATG16L1 is dispensable for E3-like function of ATG12-ATG5, but is essential for the localization of the complex to autophagy-related membranes (Fujita et al., 2008b; Romanov et al., 2012). How ATG16L1 accomplishes this function is curious, since it has no membrane-recognizing motif. One possibility is its interaction with the Golgi resident small GTPase RAB33B (Itoh et al., 2008) or the ULK1 complex subunit RB1CC1 (Gammoh et al., 2013; Nishimura et al., 2013). Both proteins do not recognize PI3P

though, which is essential for the ATG5-ATG12-ATG16L1 complex formation (Itakura and Mizushima, 2010). The solution might be WIPI2, which was recently found to interact with ATG16L1 as well, and an ATG16L1 mutant able to bind RB1CC1 but not WIPI2 was not able to rescue starvation-induced autophagy in ATG16L knockout cells (Dooley et al., 2014).

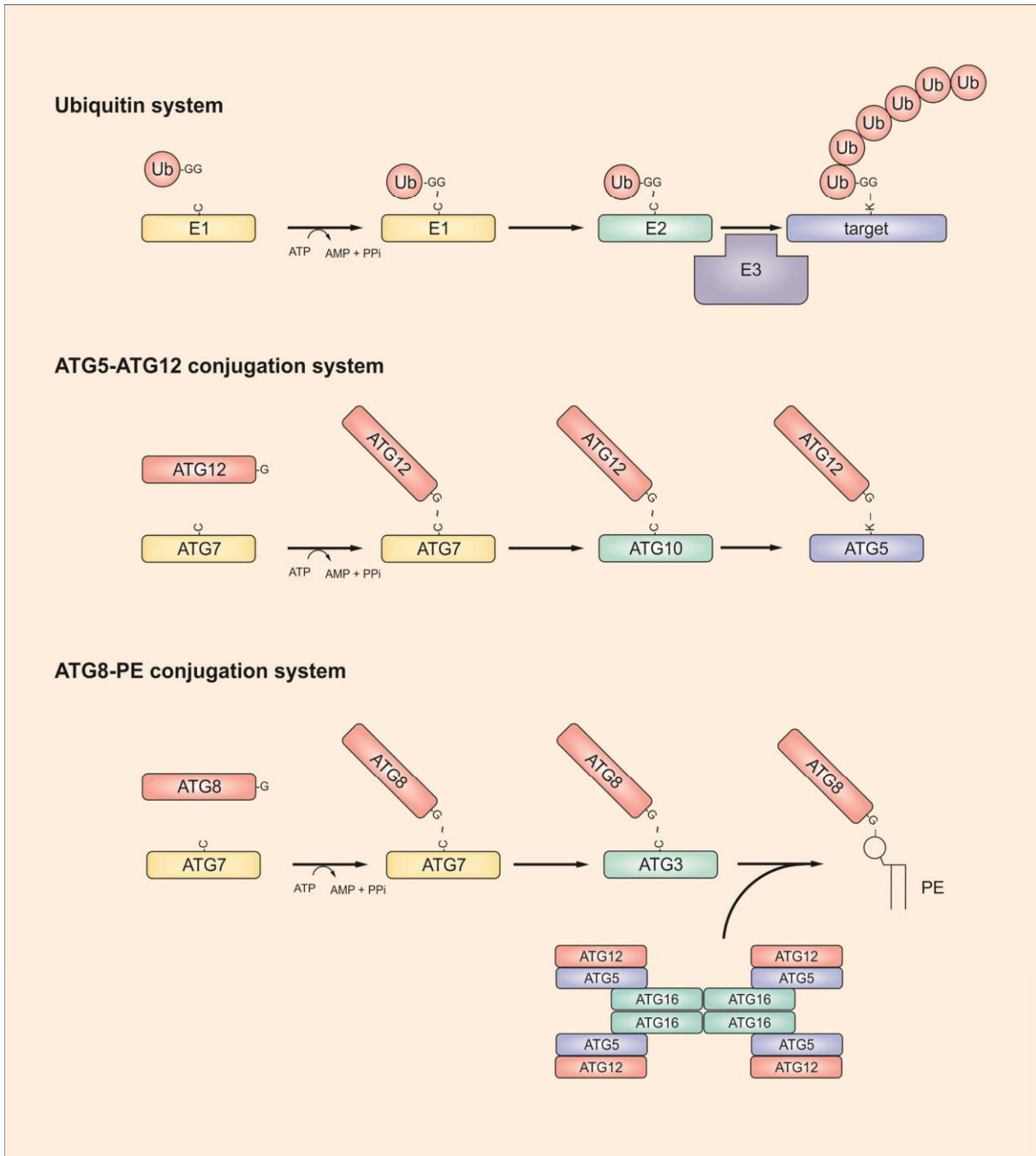


**Figure 4: The ubiquitin-like conjugation systems in autophagy:** The ubiquitin conjugation system comprises three main enzymes essential for ubiquitination. The ubiquitin-activating enzyme E1 forms a thiol-ester bond with the C-terminal glycine of ubiquitin in an ATP-consuming process. Subsequently, the ubiquitin is transferred to the ubiquitin-conjugating enzyme or ubiquitin-carrier enzyme E2 by a transthioleation reaction, again involving the C terminus of ubiquitin. Finally, the ubiquitin protein ligase E3 catalyses the loading of ubiquitin from the E2 enzyme to the  $\epsilon$ -amino group of a lysine residue on the substrate. ATG12 becomes activated by the E1-like enzyme ATG7, is transferred to the E2-like conjugation enzyme ATG10 and eventually covalently associates with ATG5 via an isopeptide bond. The ATG5-ATG12 conjugate forms a large complex together with ATG16L. The ATG8 proteins are synthesized as precursors which are immediately processed by the

protease ATG4 to reveal the C-terminal glycine. The E1-like ATG7 activates ATG8, which is then transferred to the E2-like enzyme ATG3. The conjugation of ATG8 to the lipid phosphatidylethanolamine (PE) is catalysed by ATG3 and the E3-like ATG5-ATG12-ATG16L complex. Modified from (Ohsumi, 2001).

For the ATG8 protein family eight members have been identified so far, which, based on amino acid similarities, can be divided into two subgroups (Shpilka et al., 2011): the (MAP1)LC3 subfamily comprises LC3A (with two variants originating from alternative splicing), LC3B, LC3B2 and LC3C, whereas the Gamma-aminobutyric acid A receptor-associated protein (GABARAP) subfamily contains GABARAP, GABARAPL1, GABARAPL2 (also known as GATE-16) and GABARAPL3. It is noteworthy that the expression of GABARAPL3 has been demonstrated on the transcriptional level only (Xin et al., 2001), the corresponding open reading frame might therefore represent a pseudogene.

The ATG8 proteins function during expansion and closure of autophagosomal membranes (Fujita et al., 2008a; Nakatogawa et al., 2007; Stolz et al., 2014; Weidberg et al., 2011; Weidberg et al., 2010). Though both subfamilies are essential for autophagy induction (Tanida et al., 2004), their functions are non-redundant during autophagosome biogenesis. LC3 subfamily members were shown to promote elongation of phagophore membranes before GABARAP-mediated maturation and possible sealing of the autophagosome (Weidberg et al., 2010). In contrast, a subsequent study in *Caenorhabditis elegans* reported that LC3 functions downstream of GABARAP during developmental autophagy (Manil-Segalen et al., 2014).

Notably, a recent report employing murine hexaknockout cells for the LC3 and GABARAP subfamilies described that ATG8 proteins are dispensable for autophagosome formation and only the GABARAPs were found to be essential for autophagosome-lysosome fusion (Nguyen et al., 2016).

### 3.2.7 Autophagy receptors: trash is my major

Another important function of ATG8 proteins is the linkage of the autophagosome with the cargo via so-called autophagy receptors, thereby fostering selective engulfment by the autophagosome. To achieve this, most autophagy receptors harbour a LIR motif for ATG8 protein binding and an ubiquitin-binding domain (UBD) for cargo recognition (Kirkin et al., 2009b; Slobodkin and Elazar, 2013; Wild et al., 2014; Xu et al., 2015). Hence, mutation of the LIR motif in autophagy receptors ablates ATG8 protein recruitment and blocks autophagy (Kirkin et al., 2009a; Novak et al., 2010; Pankiv et al., 2007; von Muhlinen et al., 2012).

The core consensus sequence of the LIR motif is  $\Omega xx\Psi$ , where  $\Omega$  and  $\Psi$  are aromatic (W/F/Y) and hydrophobic (L/I/V) residues, respectively, and the two residues in between can be any other amino acids (Ichimura et al., 2008a; Noda et al., 2008; Pankiv et al., 2007). Structural studies reveal three

key features of the LIR motif: the aromatic amino acid side chain ( $\Omega$ ) and the downstream conserved hydrophobic amino acid residue ( $\Psi$ ) each plug into a hydrophobic pocket of the ATG8 protein, and preferentially one or more acidic residues are needed upstream of the LIR sequence (Noda et al., 2010), which bind to the basic side chains of the ATG8 proteins (Ichimura et al., 2008b; Pankiv et al., 2007).

The autophagy receptors are divided into three subgroups: (1) the sequestosome-1-like receptor (SLR) group consists of sequestosome 1 (SQSTM1, also known as p62), neighbour of BRCA1 gene 1 (NBR1), nuclear domain 10 protein 52 (NDP52), Tax1-binding protein 1 (TAX1BP1), and optineurin (OPTN) (Birgisdottir et al., 2013); (2) the mitophagy receptor group with FUN14 domain-containing 1 (FUNDC1), BNIP3, and BNIP3L (Birgisdottir et al., 2013); and (3) the specialized receptors starch-binding domain-containing protein 1 (STBD1) and the E3 ubiquitin ligase CBL1.

The first identified and yet best studied autophagy receptor is SQSTM1, comprising the LIR sequence WTHL, an UBD domain preferentially binding  $K^{48}$ - and  $K^{63}$ -linked di-ubiquitin rather than mono-ubiquitin (Long et al., 2008) and a PB1 domain, which facilitates oligomerization as a homodimer or with NBR1 in order to act independently or cooperatively during cargo recognition (Lamark et al., 2009). Interestingly, though NBR1 is closely related with SQSTM1 through structural similarities of the UBD and PB1 domain (Walinda et al., 2014), the Y-type LIR motif (YIII) of NBR1 is interacting preferentially with GABARAPL1 (Rozenknop et al., 2011).

The autophagy receptors NDP52 and OPTN are both involved in xenophagy for clearing pathogens such as Salmonella, Listeria, Shigella, and Mycobacteria (Mostowy et al., 2011; Thurston et al., 2009; Watson et al., 2012). Both receptors are remarkably, as they contain unique and non-canonical LIR motifs. NDP52 interacts preferentially with LC3C via its LIR sequence ILVV, which lacks the aromatic residue at position 1. Hence the mode of interaction is different, as NDP52 does not reach the hydrophobic pocket that normally binds the aromatic residue ( $\Omega$ ) in a canonical LIR (von Muhlinen et al., 2012). Of note, NDP52 comprises a galectin-8-binding region (Galbi), which targets NDP52 to galectin-8-decorated bacteria-containing vesicles, thereby promoting an ubiquitin-independent mode of action for NDP52 in xenophagy (Kim et al., 2013a; Thurston et al., 2012; Xie et al., 2015).

OPTN is the most recently identified autophagy receptor, with the canonical LIR motif FVEI, but unique features as it comprises a serine residue upstream of its LIR sequence, that is modified to phosphoserine by TANK-binding kinase 1 (TBK1) (Wild et al., 2011). This phosphorylation works as an activating event through which the binding affinity to LC3B is severely increased (Rogov et al., 2013; Wild et al., 2011). Like NDP52, OPTN can recognize autophagic cargo independent of ubiquitination with its coiled-coil domain that directly binds to protein aggregates (Korac et al., 2013).

TAX1BP1 shows homology with NDP52 since it contains the same non-canonical LIR motif. Though it is recruited to autophagosomes and subjected to autophagy turnover, its role in xenophagy is unknown (Newman et al., 2012; Thurston et al., 2009).

In contrast to the SLRs, the mitophagy receptors do not harbour an UBD, but are integral proteins of the outer mitochondrial membrane. Though BNIP3 and BNIP3L have the identical core LIR motif, BNIP3 interacts with LC3B, while BNIP3L prefers GABARAPL1 (Novak et al., 2010). Probably, residues flanking the LIR motif are crucial for this selectivity. The third mitophagy receptor is FUNDC1, which has an interesting mode of action involving dephosphorylation of its LIR motif for enhanced binding affinity to LC3B (Liu et al., 2012).

In this context, it is important to note, that LIR motifs have been mapped to proteins which do not function as classical autophagy receptors. For example most members of the core autophagy machinery contain a LIR motif. In ATG13 and ULK1 LIR motifs have been found to preferentially bind GABARAPs (Alemu et al., 2012; Behrends et al., 2010; Okazaki et al., 2000). In the case of ULK1 it was suggested that the interaction with GABARAPs effects spatial regulation of the ULK1 complex and promotes ULK1 activation (Alemu et al., 2012; Joachim and Tooze, 2016; Kraft et al., 2012). Interestingly, this is independent of GABARAP lipidation and membrane localisation, suggesting a yet unknown function for the ATG8 proteins (Joachim and Tooze, 2016).

### **3.2.8 The autolysosome: it all goes down in a bubble**

In the last step of the autophagy process, the autophagosome fuses with the lysosome for effective cargo degradation. For classical fusion of vesicles with their target membrane bound compartments, SNARE complexes are essential. The autolysosome formation is no exception. Implicated SNARE complexes are the binary target-SNARE (t-SNARE) complex Syntaxin17–synaptosome associated protein 29 (STX17-SNAP29) present on the autophagosome, and the vesicle-SNARE (v-SNARE) vesicle associated membrane protein 8 (VAMP8) localised to the lysosome (Diao et al., 2015). In a preliminary model, ATG14L, a member of the VSP34 complex, binds the SNARE core domain of STX17 through its coiled coil domain, thereby stabilizing the STX17-SNAP29 binary t-SNARE complex and promoting STX17-SNAP29-VAMP8-mediated autophagosome fusion with the lysosome (Diao et al., 2015; Liu et al., 2015). Notably, this model is not supported by other studies. Itakura et al. found no colocalization of ATG14L with STX17 (Itakura et al., 2012) and others identified STX17 even as an upstream effector of ATG14L, promoting recruitment of ATG14L to the autophagosome formation site (Hamasaki et al., 2013).

### 3.2.9 The Autophagosomal membrane source – the essential question of life:

#### Where am I coming from?

The debate on the origin of the autophagosomal membrane continues to this date and ER, mitochondria, Golgi network, recycling endosomes, and even the plasma membrane have been proposed as membrane sources (Lamb et al., 2013).

With the discovery of DFCP1 as a PI3P-binding protein, investigation of the autophagosomal origin made progress by monitoring PI3P generation during autophagy. PI3P enriched compartments were found to dynamically connect to the ER (Axe et al., 2008; Hayashi-Nishino et al., 2009; Walker et al., 2008; Yla-Anttila et al., 2009), and in depth electron tomography studies identified a subdomain of the ER that encircles the isolation membrane both from the inside and outside (Hayashi-Nishino et al., 2009). Since the isolation membrane is continuous with the ER network, it was suggested that autophagosomes originate from a specific portion of the ER (Hayashi-Nishino et al., 2009). The cradle surrounding the isolation membrane was suggested to be the omegasome (Hamasaki et al., 2013), which had been described before as an  $\Omega$ -shaped structure (Walker et al., 2008).

However, it has been reported that the emerging autophagic puncta appear always distinct from the ER strands, though they remain constantly proximal during autophagosome biogenesis (Karanasios et al., 2013). This observation and a study detecting transfer of an artificial mitochondrial marker from the mitochondrial outer membrane to the autophagosomal membrane (Hailey et al., 2010) lead to the conclusion that mitochondria associated ER membranes (MAMs) might be the origin of the isolation membrane (Hamasaki et al., 2013; Karanasios et al., 2013).

Additionally, Golgi-localized RABs were found to regulate autophagosome formation and expansion. E.g. RAB1 is essential for the formation of DFCP1-positive omegasomes (Huang et al., 2011; Mochizuki et al., 2013; Winslow et al., 2010; Zoppino et al., 2010), and RAB33B is found on Golgi vesicles and autophagosomes, where it interacts with ATG16L1 and promotes autophagy (Itoh et al., 2008).

Subsequent studies proposed two ER-associated membrane compartments as the origin of the isolation membrane: the ER-Golgi intermediate compartment (ERGIC) (Ge et al., 2013; Ge et al., 2014; Karanasios et al., 2016) and the ER exit sites (ERES) (Graef et al., 2013). Through super-resolution microscopy it was clarified that the ULK1 complex is associated with ERGIC markers, which is possibly the earliest autophagy-specific structure, from which the isolation membrane and omegasome originate (Karanasios et al., 2016).

Once the isolation membrane has been initiated, it expands at a rapid rate (Karanasios et al., 2013). As the ER is the main site of lipid synthesizing enzymes in the cell (van Meer et al., 2008), it is likely

that a subset of these is involved in isolation membrane formation and expansion (Karanasios et al., 2013). However, when the autophagosome detaches from the omegasome, these ER-resident enzymes are probably retained in the ER and the membrane expansion is driven rather by vesicular fusion. A candidate protein for this is ATG9A, which may act as a lipid transfer protein, delivering membrane pieces from one compartment to another (Lamb et al., 2013). ATG9A is the only polytopic integral membrane protein in the ATG family. Both the N and C termini of ATG9A are cytosolic, with six transmembrane domains in between (Young et al., 2006). Under nutrient rich conditions, ATG9A resides on the trans-Golgi network and on recycling and late endosomes (Longatti et al., 2012; Orsi et al., 2012; Webber and Tooze, 2010; Young et al., 2006), while it partially colocalizes with LC3 positive compartments during starvation (Webber and Tooze, 2010; Weerasekara et al., 2014; Yamada et al., 2005; Young et al., 2006). Notably, although knockdown experiments revealed the ATG9A necessity in autophagosome formation (Orsi et al., 2012; Yamada et al., 2005; Young et al., 2006), the association of ATG9A positive structures with phagophores and autophagosomes is very dynamic and without incorporation of the ATG9A vesicles into the autophagosome (Orsi et al., 2012).

Primarily the ATG9A function was observed as ULK1-dependent by regulating the starvation-induced redistribution of ATG9A from the trans-Golgi network to endosomes (Young et al., 2006), probably by phosphorylation events mediated by ULK1 and AMPK (Weerasekara et al., 2014). In contrast, a recent study proposed a parallel action of ULK1 and ATG9A, as the nucleation of autophagosomes is initiated by the ULK1 complex on ER tubulovesicular regions marked by ATG9A vesicles (Karanasios et al., 2016).

## 4. Summary of papers

### 4.1 Paper 1

#### **Expression of a ULK1/2 binding-deficient ATG13 variant can partially restore autophagic activity in ATG13-deficient cells**

Nora Hieke, Antje S Löffler, Takeshi Kaizuka, Niklas Berleth, Philip Böhler, Stefan Drießen, Fabian Stuhldreier, Olena Friesen, Kaivon Assani, Katharina Schmitz, Christoph Peter, Britta Diedrich, Jörn Dengjel, Petter Holland, Anne Simonsen, Sebastian Wesselborg, Noboru Mizushima & Björn Stork

*Autophagy*, 11:9, 1471-1483, September 2015

Autophagy is a cellular process for the degradation of proteins, aggregates and organelles in order to balance cell homeostasis. Additionally to its basal activity, autophagy can be induced by stressors like amino acid or glucose deprivation or hypoxia. A key regulatory node in the autophagy network is the ULK1 complex, which comprises the serine/threonine kinase ULK1/2 and the accessory proteins ATG13, RB1CC1 and ATG101. We identified the minimal region in ATG13 that is required for ULK1/2 interaction. Deletion of the last three amino acids in the C terminus of ATG13 ablates interaction with ULK1/2 and inhibits recruitment of ULK1 to the autophagy initiating core complex. Moreover, ULK1 mediated phosphorylation of ATG13 is blocked, and localization of ULK1 and ATG13 to the autophagosome formation sites upon autophagy induction is also suppressed. Surprisingly, in cells expressing an ATG13 mutant lacking ULK1 interaction, autophagy induction by starvation is only partially blocked. These findings lead us to speculate that autophagy induction might be triggered by several pathways dependent and independent of the interaction between ATG13 and ULK1.

#### **Author contribution:**

NH, ASL and TK designed the experiments, generated cell lines and performed immunoblot analyses. NH and ASL performed cloning of cDNA constructs and immuno- and affinity purifications. NH performed flow cytometry analyses and confocal imaging of GFP-ULK1 and HA-ATG13, of endogenous LC3 and SQSTM1/p62, and of mRFP-EGFP-rLC3. TK performed gel filtration analysis and the GFP-ULK1 and HA-ATG13 puncta analysis. NB, PB, SD, FS, KS and CP gave technical support. KA

performed quantification of fluorescent micrographs. BD and JD performed mass spectrometric analyses. PH and AS designed and performed the long-lived protein degradation assay. NH and BS wrote the manuscript. NH, ASL, TK, SW, NM and BS analyzed and interpreted the data. SW, NM and BS supervised the project. All authors discussed the results and commented on the manuscript.

## 4.2 Paper 2

### **Deubiquitinase inhibition by WP1130 leads to ULK1 aggregation and blockade of autophagy**

Stefan Drießen, Niklas Berleth, Olena Friesen, Antje S Löffler, Philip Böhrer, Nora Hieke, Fabian Stuhldreier, Christoph Peter, Kay O Schink, Sebastian W Schultz, Harald Stenmark, Petter Holland, Anne Simonsen, Sebastian Wesselborg & Björn Stork

*Autophagy*, 11:9, 1458-1470, September 2015

The ULK1 complex is a central regulator of autophagy, a degradative pathway responsible for the clearance of toxic cellular entities as well as for cell survival. ULK1 is a protein kinase transmitting signals sensing autophagy-inducing conditions to the autophagosome formation site to induce autophagy progression. It is tightly regulated by upstream kinases e.g. mTORC1 and AMPK. Other posttranslational modifications are reported for ULK1 and of these, ubiquitination is thought to positively effect ULK1 activity. We applied the compound WP1130, a deubiquitinase inhibitor and indeed, ubiquitination of ULK1 was subsequently increased. Strikingly, increased ubiquitination lead to decreased ULK1 levels in the soluble fraction but promoted ULK1-positive aggresome formation, accompanied by the loss of ULK1 kinase activity towards its phosphorylation target AMPK. In accordance with this, WP1130 further blocked autophagic flux, which emphasized the importance of ULK1 and its kinase activity for autophagy induction. We therefore propose the modulation of the ULK1 ubiquitination status as a promising approach to regulate ULK1 kinase activity.

#### **Author contribution:**

SD designed the experiments, generated cDNA constructs, transfected cell lines and performed immunopurification experiments. OF performed flow cytometry experiments. SD and ASL performed in vitro kinase assay. SD and NH performed immunoblot analysis. SD, KOS and SWS performed confocal laser scanning microscopy and live cell imaging. PH and AS designed and performed the long-lived protein degradation assay. BS wrote the manuscript. SD, OF, ASL, NH, HS, AS, SW and BS analyzed and interpreted the data. SW, HS, AS and BS supervised the project. All authors discussed the results and commented on the manuscript.

### 4.3 Paper 3

#### **Systematic analysis of ATG13 domain requirements for autophagy induction**

Nora Wallot-Hieke, Neha Verma, David Schlütermann, Niklas Berleth, Jana Deitersen, Philip Böhrer, Fabian Stuhldreier, Wenxian Wu, Christoph Peter, Sabine Seggewiss, Holger Gohlke, Noboru Mizushima, Björn Stork

*Accepted in Autophagy*

ATG13 is a subunit of the ULK1 complex, a core autophagy-regulating complex important for autophagy induction. Here, ATG13 functions as a scaffolding protein recruiting ULK1/2, RB1CC1 and ATG101 to the ULK1 complex. Additionally, ATG13 harbours a phospholipid binding site and a LIR motif, facilitating its interaction with phospholipids and proteins of the ATG8 family, respectively. By mutational analysis, we mapped the interaction sites of RB1CC1 and ATG101 in ATG13. In a next step, we applied various ATG13 mutants lacking interaction sites for its binding partners and analysed ULK1 complex formation, recruitment of the complex to the autophagosome formation site upon autophagy induction, and their capacity to regulate autophagy. While the inhibition of the interaction of ATG13 with RB1CC1 or ATG101 had severe effects on complex formation, only inhibited binding to ATG101 blocked autophagic flux. Moreover, the inhibition of ATG8 protein and phospholipid binding did not effect the complex formation and had only minor effects on autophagy induction. In summary, these data support an essential role of the ATG13-ATG101 interaction for autophagy.

#### **Author contribution:**

NWH designed the experiments, generated cDNA constructs and cell lines, and performed immuno- and affinity purifications and immunoblot analyses. NWH performed flow cytometry analyses, confocal imaging, and size exclusion chromatography. DS, NB, JD, PB, FS, WW, SS and CP gave technical support. NV and HG performed computational alanine scanning and MM-GB/SA calculations. NWH and BS wrote the manuscript. NWH, NV, HG, NM and BS analyzed and interpreted the data. HG, NM and BS supervised the project. All authors discussed the results and commented on the manuscript.

## 5. Discussion

The ULK1 protein kinase complex is an essential signalling node for the induction of autophagy. The core ULK1 complex consists of the serine/threonine protein kinase ULK1 and the accessory proteins ATG13, RB1CC1 and ATG101. As the first factor in the autophagy initiation network, modulation of the complex's activity is a promising tool for autophagy regulation. The complex assembly is driven by the scaffolding protein ATG13, whereas the catalytic subunit ULK1 is required for signal transmission to the downstream autophagy machinery. To elucidate the importance of these processes in the course of autophagy, we performed systemic analysis of the ATG13 domains. It has been published, that the amino acids R<sup>10</sup>, K<sup>11</sup>, K<sup>15</sup> and K<sup>18</sup> in ATG13 mediate the binding to phospholipids (Karanasios et al., 2013) and F<sup>407</sup> and I<sup>410</sup> (ATG13 isoform 2, Uniprot identifier: O75143-2) comprise the LIR motif (Alemu et al., 2012) (Figure 5). The interaction sites of ATG101, ULK1 and RB1CC1 in ATG13 were mapped in our studies. We found the amino acids I<sup>131</sup>, R<sup>133</sup>, V<sup>134</sup> and Y<sup>138</sup> of ATG13 being mandatory for the interaction with ATG101 (Figure 5). The amino acid sequence V<sup>348</sup>-M<sup>373</sup> of ATG13 comprises the RB1CC1 interaction site, and the last three amino acids TLQ<sup>480</sup> in ATG13 are crucial for ULK1/2 binding. Secondly, we designed ATG13 mutants targeting the specific protein interactions, expressed them in ATG13 knockout cells and analysed the autophagic flux during starvation.

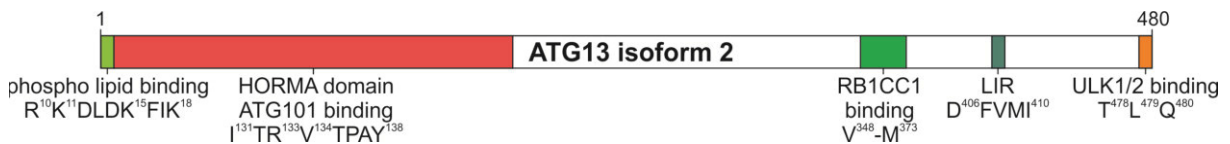


**Figure 5: ATG13 domain structure:** The ULK1 complex subunit ATG13 comprises a phospholipid binding motif at its extreme N terminus followed by a HORMA domain mediating ATG101 interaction. The C terminus contains the RB1CC1 binding site, a LIR motif mediating interaction with the ATG8 subfamily of the GABARAPs, and a binding site for the kinases ULK1 and ULK2. Amino acids carrying a sequence position were mutated in this study to abrogate corresponding protein or phospholipid interactions. The depicted ATG13 corresponds to the isoform 2 of human ATG13 as has been used in this study.

Our analyses revealed the strongest effect on autophagy regulation by targeting the ATG101-ATG13 protein interaction. This was accompanied by a dissociated ULK1 complex and ATG101 present as a monomer only, which is similar to the situation in ATG13 knockout cells (Kaizuka and Mizushima, 2015).

The severe defect of autophagy provoked by blocking the ATG13-ATG101 interaction has two possible reasons: Firstly, we and others observed a strong reduction in ATG13 and ATG101 protein levels when the respective binding partner was missing (Kaizuka and Mizushima, 2015; Suzuki et al., 2015b). This suggests a protein stabilizing function for the ATG13-ATG101 interaction, which - if

missing - results in altered protein functionality in the autophagic process. In this context it is noteworthy, that crystallisation studies revealed two hydrophobic pockets formed at the ATG13-ATG101 interface, which are composed of residues from both proteins. The amino acids Y<sup>138</sup>, R<sup>139</sup>, R<sup>142</sup> and K<sup>143</sup> in ATG13 form one of these sites, which is proximal to the amino acids I<sup>131</sup>, R<sup>133</sup>, V<sup>134</sup> and Y<sup>138</sup> identified by us to mediate ATG101 interaction (Qi et al., 2015). Next to the direct protein-protein interaction mediated by these amino acids, another possibility is the disruption of the hydrophobic pocket through mutation of the amino acids and thereby weakening the ATG13-ATG101 association.

Secondly, ATG101 harbours a unique WF finger in its HORMA domain, which might recruit regulatory proteins to the ULK1 complex essential for autophagy (Qi et al., 2015; Suzuki et al., 2015a). Qi et al. found the WF finger being partially sequestered in a hydrophobic pocket, and the conformational flexibility seems to be altered by the ATG13-ATG101 interaction, suggesting that the exposure of this motif is regulated (Qi et al., 2015).

Notably, these alternatives are not mutually exclusive but are rather both of importance for autophagy signalling. Mutations of the ATG13 interaction site as well as in the WF finger in ATG101 blocked autophagy induction by starvation (Suzuki et al., 2015b).

These data in combination with our findings still do not clarify if the ATG13-ATG101 interaction itself is mandatory for the autophagy process, or if rather the binding induces a conformational change of the WF finger, making it available for the association with possible interaction partners. Future studies have to reveal if ATG101 recruits accessory proteins to the ULK1 complex, whether this is regulated (e.g. by plugging the WF finger from the hydrophobic pocket), and if this contributes to the ULK1 activity and/or autophagy signalling.

A phospholipid binding motif exists proximal to the HORMA domain in ATG13 (Karanasios et al., 2013). Mutation of the domain did not have an effect on autophagy induction during nutrient withdrawal and only mild effects on mTOR-inhibited autophagy. This is in clear contrast to the report that established this site. Karanasios et al. detected inhibited ATG13 recruitment to phagophores and autophagy deficiency when this motif was mutated (Karanasios et al., 2013).

Similar results were obtained for the LIR domain in ATG13. Mutation of this motif did not have an inhibitory effect on autophagy, but on the contrary depicted increased autophagic flux when measured by accumulation of lipidated LC3 during nutrient withdrawal. In our opinion, two explanations might exist for this data. Firstly, autophagic flux might be enhanced, which is not supported by our other data. Recruitment of the ULK1 complex as well as WIPI2 and ATG16L to the phagophore was unaltered upon ATG13 LIR motif mutation. Secondly, increased overall lipidation of LC3 might occur in the cells expressing the ATG13 mutant, which could be facilitated by enhanced

LC3 expression, ATG4 protease activity, activity of the lipidation machinery or LC3 protein stability. Either way, our findings show that the LIR motif in ATG13 is not in any way as essential for autophagy as it is for ULK1. Here, the LIR motif mediates localisation of the ULK1 complex to the phagophore by GABARAPs and promotes autophagy induction (Joachim and Tooze, 2016).

Another surprising observation was that the blockade of the ATG13-RB1CC1 interaction is of marginal importance for autophagy signalling. This was unexpected, firstly because the ULK1 complex was disrupted by inhibited interaction and recruitment of ATG13 and RB1CC1 to the autophagosome initiation site was ablated. Secondly, the proteins ATG13 and RB1CC1 themselves are essential in autophagy (Gan et al., 2006; Hara et al., 2008). This lead us to the conclusion that the interaction of ATG13 and RB1CC1 is not mandatory, but their function in autophagy is. In this context it has to be noted that Chen et al. mapped the ATG13 interaction site in RB1CC1, identifying the amino acid sequence LQFL<sup>585</sup> as the ATG13-binding platform. Mutation of these residues abrogated the ATG13 interaction and remarkably blocked autophagy, which is in considerable contrast to our observations (Chen et al., 2016). We can only speculate why these results are so contradictory. It is possible that our ATG13 mutant does not completely lack RB1CC1 interaction, though we confirmed disrupted binding to RB1CC1 when employing assays to detect single protein-protein interactions. Additionally, we found destabilized RB1CC1 levels in the cells expressing the ATG13 mutant similar to ATG13 knockout cells, which further suggests inhibited interaction with ATG13.

Many interaction partners of RB1CC1 are known, among them TSC1 (Gan et al., 2005). TSC1 is a subunit of the TSC complex, which initiates autophagy by direct mTOR inactivation (Inoki et al., 2003b). When RB1CC1 binds TSC1, the TSC complex is disrupted, and mTOR is released from its inactivation, thereby blocking autophagy initiation (Gan et al., 2005). In the report of Chen et al. the interaction of RB1CC1 with TSC1 was increased upon RB1CC1 mutation, which might result in inhibited TSC complex formation and autophagic block, though this was not investigated further in this study (Chen et al., 2016).

Finally, we analysed the role of the ULK1-ATG13 interaction in autophagy regulation. We were surprised to find that only three amino acids in ATG13 comprise the minimal ULK1/2 interaction site. It remains a speculation if the TLQ motif presents the direct binding site for ULK1/2 or is of structural relevance for the ULK1/2 interaction. Short peptide motifs at the C terminus of proteins like the TLQ motif in ATG13 are bound by PDZ domains of the interacting partners (Harris and Lim, 2001; Lee and Zheng, 2010), and indeed, the TLQ motif resembles a PDZ domain ligand class I (Harris and Lim, 2001). Moreover, the threonine in the ATG13 TLQ motif was phosphorylated in a ULK1 kinase assay, suggesting a regulatory role for PDZ binding (Alers et al., 2011). Though exchange of this residue to

alanine did not have an effect on ULK1-binding and autophagy induction, it might affect interactions with other binding partners.

Another possibility is that the TLQ motif is important for structural conformation of the ULK1-binding site. In yeast Atg13, a MIT-interacting motif (MIM) was reported, that binds the microtubule interacting and transport (MIT) domain in Atg1 (Fujioka et al., 2014). Though there hardly exists any sequence similarities between yeast and human ATG13, a structural homology might be conserved, which might be destroyed by TLQ deletion. Since the C-terminal domain of ATG13 is mostly intrinsically disordered, crystallisation approaches failed to investigate structured regions within the C terminus (Michel et al., 2015). Still, Fujioka et al. suggested a conservation of the MIM domain and identified two phenylalanine residues as the key amino acids for ULK1 interaction. However, mutation of these phenylalanines to alanines in human ATG13 did not have an effect on ATG13-ULK1 interaction or binding to any other known interaction partner. We concluded that the suggested MIM domain might not be present in mammalian ATG13, but we cannot exclude a structural relevance of the TLQ motif rather than being the direct interaction platform for ULK1/s.

The finding, that autophagy is only slightly blocked when interaction with ULK1 is inhibited was unexpected. One explanation could be that ULK1 can execute its function in autophagy independent of the ULK1 complex. Other binding partners might exist, that recruit ULK1 to the autophagosome formation site. ULK1 comprises a LIR motif, which facilitates interaction with GABARAP and which reportedly sequesters ULK1 to the isolation membrane (Joachim and Tooze, 2016). However, in our experiments, we did not observe detectable ULK1 accumulation during starvation when interaction with ATG13 was abolished. This might be due to very dynamic association of ULK1 with the isolation membrane in the absence of ATG13 or only a minor portion of ULK1 becomes recruited, which is not detectable by confocal microscopy. Live cell imaging combined with super-resolution microscopy might be a helpful tool to clarify this question.

Another possibility is the existence of ULK1/2-independent autophagy pathways, which probably become activated when the ULK1 axis is blocked (Alers et al., 2011; Cheong et al., 2011; Choi et al., 2016; Gao et al., 2016; Manzoni et al., 2016).

Importantly, though the ATG13-ULK1 interaction is not essential for autophagy induction, the ULK1 kinase activity indeed is. First of all, a kinase dead mutant of ULK1 had a dominant negative effect on autophagosome formation (Hara et al., 2008). Secondly, in our experiments with WP1130, ubiquitylated ULK1 was incorporated into aggresomes and lost its kinase activity, associated with a blockage in autophagy. Since the list of ULK1 interaction partners and phosphorylation targets is long, it is conceivable that its kinase activity is dominant over its interaction with ATG13.

Nazio et al. reported increased ULK1 kinase activity by ubiquitination through TRAF6 (Nazio et al., 2013). We tried to elucidate the enzymes responsible for deubiquitination and hence inactivation of ULK1. To identify the deubiquitinases (DUB) acting on ULK1, we applied the partially specific DUB inhibitor WP1130. Indeed, we found increased ubiquitination of ULK1, but in contrast to our expectation, this led to transfer of ubiquitylated ULK1 to aggresomes. We speculated that this is either because of an overload of the proteasome by abundant levels of ubiquitylated proteins, or because WP1130 disrupts a ULK1 specific ubiquitin conjugation-deconjugation cycle. Subsequently we screened the DUBs that are reportedly regulated by WP1130, but none of these effected the WP1130-induced ULK1 aggregation. It is feasible that another yet unreported DUB might act in this scenario. Since there are 79 active DUBs encoded in the human genome, identifying a specific DUB might be difficult (Komander et al., 2009). We therefore performed a DUB profiling assay with WP1130 using a library of 35 recombinant DUBs including those known to be inhibited by WP1130. Surprisingly, none of the screened DUBs showed inhibited activity upon WP1130 treatment.

We cannot exclude that WP1130 has other functions in addition to DUB inhibition, which effect either ULK1 or proteins regulating ULK1.

Summarizing our results we concluded that the ATG13-ATG101 interaction is the most promising target to regulate autophagy. The crystal structure of the interacting HORMA domains was elucidated, showing that the protein interaction is constitutive and independent on other proteins (Michel et al., 2015; Qi et al., 2015; Suzuki et al., 2015b). Additionally, the amino acids in ATG101 and ATG13 mediating protein association were identified, which is advantageous when designing or searching for a peptide or compound interfering with the ATG13-ATG101 interaction. Finally, we see considerable potential in ULK1 kinase activity modulation for autophagy regulation. Here, several more or less specific inhibitors have been published, that have already been shown to effect autophagy *in vitro* and *in vivo* (Egan et al., 2015; Lazarus et al., 2015; Lazarus and Shokat, 2015; Petherick et al., 2015).

## 6. References

- Abbi, S., Ueda, H., Zheng, C., Cooper, L.A., Zhao, J., Christopher, R., and Guan, J.L.** (2002). Regulation of focal adhesion kinase by a novel protein inhibitor FIP200. *Mol Biol Cell* *13*, 3178-3191.
- Alemu, E.A., Lamark, T., Torgersen, K.M., Birgisdottir, A.B., Larsen, K.B., Jain, A., Olsvik, H., Overvatn, A., Kirkin, V., and Johansen, T.** (2012). ATG8 family proteins act as scaffolds for assembly of the ULK complex: sequence requirements for LC3-interacting region (LIR) motifs. *J Biol Chem* *287*, 39275-39290.
- Alers, S., Löffler, A.S., Paasch, F., Dieterle, A.M., Keppeler, H., Lauber, K., Campbell, D.G., Fehrenbacher, B., Schaller, M., Wesselborg, S., and Stork, B.** (2011). Atg13 and FIP200 act independently of Ulk1 and Ulk2 in autophagy induction. *Autophagy* *7*, 1423-1433.
- Appenzeller-Herzog, C., and Hall, M.N.** (2012). Bidirectional crosstalk between endoplasmic reticulum stress and mTOR signaling. *Trends Cell Biol* *22*, 274-282.
- Aravind, L., and Koonin, E.V.** (1998). The HORMA domain: a common structural denominator in mitotic checkpoints, chromosome synapsis and DNA repair. *Trends Biochem Sci* *23*, 284-286.
- Asano, T., Komatsu, M., Yamaguchi-Iwai, Y., Ishikawa, F., Mizushima, N., and Iwai, K.** (2011). Distinct mechanisms of ferritin delivery to lysosomes in iron-depleted and iron-replete cells. *Mol Cell Biol* *31*, 2040-2052.
- Axe, E.L., Walker, S.A., Manifava, M., Chandra, P., Roderick, H.L., Habermann, A., Griffiths, G., and Ktistakis, N.T.** (2008). Autophagosome formation from membrane compartments enriched in phosphatidylinositol 3-phosphate and dynamically connected to the endoplasmic reticulum. *J Cell Biol* *182*, 685-701.
- Bach, M., Larance, M., James, D.E., and Ramm, G.** (2011). The serine/threonine kinase ULK1 is a target of multiple phosphorylation events. *Biochem J* *440*, 283-291.
- Bar-Peled, L., Chantranupong, L., Cherniack, A.D., Chen, W.W., Ottina, K.A., Grabiner, B.C., Spear, E.D., Carter, S.L., Meyerson, M., and Sabatini, D.M.** (2013). A Tumor suppressor complex with GAP activity for the Rag GTPases that signal amino acid sufficiency to mTORC1. *Science* *340*, 1100-1106.
- Bar-Peled, L., Schweitzer, L.D., Zoncu, R., and Sabatini, D.M.** (2012). Ragulator is a GEF for the rag GTPases that signal amino acid levels to mTORC1. *Cell* *150*, 1196-1208.
- Baskaran, S., Ragusa, M.J., Boura, E., and Hurley, J.H.** (2012). Two-site recognition of phosphatidylinositol 3-phosphate by PROPPINs in autophagy. *Mol Cell* *47*, 339-348.
- Behrends, C., Sowa, M.E., Gygi, S.P., and Harper, J.W.** (2010). Network organization of the human autophagy system. *Nature* *466*, 68-76.
- Bellot, G., Garcia-Medina, R., Gounon, P., Chiche, J., Roux, D., Pouyssegur, J., and Mazure, N.M.** (2009). Hypoxia-induced autophagy is mediated through hypoxia-inducible factor induction of BNIP3 and BNIP3L via their BH3 domains. *Mol Cell Biol* *29*, 2570-2581.
- Ben Sahra, I., Regazzetti, C., Robert, G., Laurent, K., Le Marchand-Brustel, Y., Auburger, P., Tanti, J.F., Giorgetti-Peraldi, S., and Bost, F.** (2011). Metformin, independent of AMPK, induces mTOR inhibition and cell-cycle arrest through REDD1. *Cancer Res* *71*, 4366-4372.
- Bernales, S., McDonald, K.L., and Walter, P.** (2006). Autophagy counterbalances endoplasmic reticulum expansion during the unfolded protein response. *PLoS Biol* *4*, e423.
- Birgisdottir, A.B., Lamark, T., and Johansen, T.** (2013). The LIR motif - crucial for selective autophagy. *J Cell Sci* *126*, 3237-3247.
- Bodemann, B.O., Orvedahl, A., Cheng, T., Ram, R.R., Ou, Y.H., Formstecher, E., Maiti, M., Hazelett, C.C., Wauson, E.M., Balakireva, M., Camonis, J.H., Yeaman, C., Levine, B., and White, M.A.** (2011). RalB and the exocyst mediate the cellular starvation response by direct activation of autophagosome assembly. *Cell* *144*, 253-267.
- Brugarolas, J., Lei, K., Hurley, R.L., Manning, B.D., Reiling, J.H., Hafen, E., Witters, L.A., Ellisen, L.W., and Kaelin, W.G., Jr.** (2004). Regulation of mTOR function in response to hypoxia by REDD1 and the TSC1/TSC2 tumor suppressor complex. *Genes Dev* *18*, 2893-2904.
- Buchberger, A., Bukau, B., and Sommer, T.** (2010). Protein quality control in the cytosol and the endoplasmic reticulum: brothers in arms. *Mol Cell* *40*, 238-252.
- Budanov, A.V., and Karin, M.** (2008). p53 target genes sestrin1 and sestrin2 connect genotoxic stress and mTOR signaling. *Cell* *134*, 451-460.
- Cam, H., Easton, J.B., High, A., and Houghton, P.J.** (2010). mTORC1 signaling under hypoxic conditions is controlled by ATM-dependent phosphorylation of HIF-1alpha. *Mol Cell* *40*, 509-520.
- Cao, Y., Wang, Y., Abi Saab, W.F., Yang, F., Pessin, J.E., and Backer, J.M.** (2014). NRBF2 regulates macroautophagy as a component of Vps34 Complex I. *Biochem J* *461*, 315-322.
- Chan, E.Y., Kir, S., and Tooze, S.A.** (2007). siRNA screening of the kinome identifies ULK1 as a multidomain modulator of autophagy. *J Biol Chem* *282*, 25464-25474.
- Chan, E.Y., Longatti, A., McKnight, N.C., and Tooze, S.A.** (2009). Kinase-inactivated ULK proteins inhibit autophagy via their conserved C-terminal domains using an Atg13-independent mechanism. *Mol Cell Biol* *29*, 157-171.
- Chan, E.Y., and Tooze, S.A.** (2009). Evolution of Atg1 function and regulation. *Autophagy* *5*, 758-765.
- Chang, Y.Y., and Neufeld, T.P.** (2009). An Atg1/Atg13 complex with multiple roles in TOR-mediated autophagy regulation. *Mol Biol Cell* *20*, 2004-2014.

- Chano, T., Ikegawa, S., Kontani, K., Okabe, H., Baldini, N., and Saeki, Y. (2002a). Identification of RB1CC1, a novel human gene that can induce RB1 in various human cells. *Oncogene* 21, 1295-1298.
- Chano, T., Ikegawa, S., Saito-Ohara, F., Inazawa, J., Mabuchi, A., Saeki, Y., and Okabe, H. (2002b). Isolation, characterization and mapping of the mouse and human RB1CC1 genes. *Gene* 291, 29-34.
- Chano, T., Saji, M., Inoue, H., Minami, K., Kobayashi, T., Hino, O., and Okabe, H. (2006). Neuromuscular abundance of RB1CC1 contributes to the non-proliferating enlarged cell phenotype through both RB1 maintenance and TSC1 degradation. *Int J Mol Med* 18, 425-432.
- Chatr-Aryamontri, A., Oughtred, R., Boucher, L., Rust, J., Chang, C., Kolas, N.K., O'Donnell, L., Oster, S., Theesfeld, C., Sellam, A., Stark, C., Breitkreutz, B.J., Dolinski, K., and Tyers, M. (2017). The BioGRID interaction database: 2017 update. *Nucleic Acids Res* 45, D369-D379.
- Chen, J.L., Lin, H.H., Kim, K.J., Lin, A., Forman, H.J., and Ann, D.K. (2008). Novel roles for protein kinase Cdelta-dependent signaling pathways in acute hypoxic stress-induced autophagy. *J Biol Chem* 283, 34432-34444.
- Chen, S., Wang, C., Yeo, S., Liang, C.C., Okamoto, T., Sun, S., Wen, J., and Guan, J.L. (2016). Distinct roles of autophagy-dependent and -independent functions of FIP200 revealed by generation and analysis of a mutant knock-in mouse model. *Genes Dev* 30, 856-869.
- Cheong, H., Lindsten, T., Wu, J., Lu, C., and Thompson, C.B. (2011). Ammonia-induced autophagy is independent of ULK1/ULK2 kinases. *Proc Natl Acad Sci U S A* 108, 11121-11126.
- Cheung, P.C., Trinkle-Mulcahy, L., Cohen, P., and Lucocq, J.M. (2001). Characterization of a novel phosphatidylinositol 3-phosphate-binding protein containing two FYVE fingers in tandem that is targeted to the Golgi. *Biochem J* 355, 113-121.
- Choi, H., Merceron, C., Mangiavini, L., Seifert, E.L., Schipani, E., Shapiro, I.M., and Risbud, M.V. (2016). Hypoxia promotes noncanonical autophagy in nucleus pulposus cells independent of MTOR and HIF1A signaling. *Autophagy* 12, 1631-1646.
- Cuervo, A.M., and Wong, E. (2014). Chaperone-mediated autophagy: roles in disease and aging. *Cell Res* 24, 92-104.
- Davies, S.P., Hawley, S.A., Woods, A., Carling, D., Haystead, T.A., and Hardie, D.G. (1994). Purification of the AMP-activated protein kinase on ATP-gamma-sepharose and analysis of its subunit structure. *Eur J Biochem* 223, 351-357.
- Derubeis, A.R., Young, M.F., Jia, L., Robey, P.G., and Fisher, L.W. (2000). Double FYVE-containing protein 1 (DFCP1): isolation, cloning and characterization of a novel FYVE finger protein from a human bone marrow cDNA library. *Gene* 255, 195-203.
- Deter, R.L., Baudhuin, P., and De Duve, C. (1967). Participation of lysosomes in cellular autophagy induced in rat liver by glucagon. *J Cell Biol* 35, C11-16.
- DeYoung, M.P., Horak, P., Sofer, A., Sgroi, D., and Ellisen, L.W. (2008). Hypoxia regulates TSC1/2-mTOR signaling and tumor suppression through REDD1-mediated 14-3-3 shuttling. *Genes Dev* 22, 239-251.
- Di Bartolomeo, S., Corazzari, M., Nazio, F., Oliverio, S., Lisi, G., Antonioli, M., Pagliarini, V., Matteoni, S., Fuoco, C., Giunta, L., D'Amelio, M., Nardacci, R., Romagnoli, A., Piacentini, M., Cecconi, F., and Fimia, G.M. (2010). The dynamic interaction of AMBRA1 with the dynein motor complex regulates mammalian autophagy. *J Cell Biol* 191, 155-168.
- Diao, J., Liu, R., Rong, Y., Zhao, M., Zhang, J., Lai, Y., Zhou, Q., Wilz, L.M., Li, J., Vivona, S., Pfuetzner, R.A., Brunger, A.T., and Zhong, Q. (2015). ATG14 promotes membrane tethering and fusion of autophagosomes to endolysosomes. *Nature* 520, 563-566.
- Dibble, C.C., Elis, W., Menon, S., Qin, W., Klekota, J., Asara, J.M., Finan, P.M., Kwiatkowski, D.J., Murphy, L.O., and Manning, B.D. (2012). TBC1D7 is a third subunit of the TSC1-TSC2 complex upstream of mTORC1. *Mol Cell* 47, 535-546.
- Dikic, I., Johansen, T., and Kirkin, V. (2010). Selective autophagy in cancer development and therapy. *Cancer Res* 70, 3431-3434.
- Dooley, H.C., Razi, M., Polson, H.E., Girardin, S.E., Wilson, M.I., and Tooze, S.A. (2014). WIPI2 links LC3 conjugation with PI3P, autophagosome formation, and pathogen clearance by recruiting Atg12-5-16L1. *Mol Cell* 55, 238-252.
- Dorsey, F.C., Rose, K.L., Coenen, S., Prater, S.M., Cavett, V., Cleveland, J.L., and Caldwell-Busby, J. (2009). Mapping the phosphorylation sites of Ulk1. *J Proteome Res* 8, 5253-5263.
- Dunlop, E.A., Hunt, D.K., Acosta-Jaquez, H.A., Fingar, D.C., and Tee, A.R. (2011). ULK1 inhibits mTORC1 signaling, promotes multisite Raptor phosphorylation and hinders substrate binding. *Autophagy* 7, 737-747.
- Egan, D., Kim, J., Shaw, R.J., and Guan, K.L. (2011a). The autophagy initiating kinase ULK1 is regulated via opposing phosphorylation by AMPK and mTOR. *Autophagy* 7, 643-644.
- Egan, D.F., Chun, M.G., Vamos, M., Zou, H., Rong, J., Miller, C.J., Lou, H.J., Raveendra-Panickar, D., Yang, C.C., Sheffler, D.J., Teriete, P., Asara, J.M., Turk, B.E., Cosford, N.D., and Shaw, R.J. (2015). Small Molecule Inhibition of the Autophagy Kinase ULK1 and Identification of ULK1 Substrates. *Mol Cell* 59, 285-297.
- Egan, D.F., Shackelford, D.B., Mihaylova, M.M., Gelino, S., Kohnz, R.A., Mair, W., Vasquez, D.S., Joshi, A., Gwinn, D.M., Taylor, R., Asara, J.M., Fitzpatrick, J., Dillin, A., Viollet, B., Kundu, M., Hansen, M., and Shaw, R.J. (2011b). Phosphorylation of ULK1 (hATG1) by AMP-activated protein kinase connects energy sensing to mitophagy. *Science* 331, 456-461.
- Feng, Z., Zhang, H., Levine, A.J., and Jin, S. (2005). The coordinate regulation of the p53 and mTOR pathways in cells. *Proc Natl Acad Sci U S A* 102, 8204-8209.
- Fimia, G.M., Di Bartolomeo, S., Piacentini, M., and Cecconi, F. (2011). Unleashing the Ambra1-Beclin 1 complex from dynein chains: Ulk1 sets Ambra1 free to induce autophagy. *Autophagy* 7, 115-117.
- Fimia, G.M., Stoykova, A., Romagnoli, A., Giunta, L., Di Bartolomeo, S., Nardacci, R., Corazzari, M., Fuoco, C., Ucar, A., Schwartz, P., Gruss, P., Piacentini, M., Chowdhury, K., and Cecconi, F. (2007). Ambra1 regulates autophagy and development of the nervous system. *Nature* 447, 1121-1125.

- Fujioka, Y., Noda, N.N., Nakatogawa, H., Ohsumi, Y., and Inagaki, F. (2010). Dimeric coiled-coil structure of *Saccharomyces cerevisiae* Atg16 and its functional significance in autophagy. *J Biol Chem* 285, 1508-1515.
- Fujioka, Y., Suzuki, S.W., Yamamoto, H., Kondo-Kakuta, C., Kimura, Y., Hirano, H., Akada, R., Inagaki, F., Ohsumi, Y., and Noda, N.N. (2014). Structural basis of starvation-induced assembly of the autophagy initiation complex. *Nat Struct Mol Biol* 21, 513-521.
- Fujita, N., Hayashi-Nishino, M., Fukumoto, H., Omori, H., Yamamoto, A., Noda, T., and Yoshimori, T. (2008a). An Atg4B mutant hampers the lipidation of LC3 paralogues and causes defects in autophagosome closure. *Mol Biol Cell* 19, 4651-4659.
- Fujita, N., Itoh, T., Omori, H., Fukuda, M., Noda, T., and Yoshimori, T. (2008b). The Atg16L complex specifies the site of LC3 lipidation for membrane biogenesis in autophagy. *Mol Biol Cell* 19, 2092-2100.
- Funakoshi, T., Matsuura, A., Noda, T., and Ohsumi, Y. (1997). Analyses of APG13 gene involved in autophagy in yeast, *Saccharomyces cerevisiae*. *Gene* 192, 207-213.
- Gammoh, N., Florey, O., Overholtzer, M., and Jiang, X. (2013). Interaction between FIP200 and ATG16L1 distinguishes ULK1 complex-dependent and -independent autophagy. *Nat Struct Mol Biol* 20, 144-149.
- Gan, B., Melkounian, Z.K., Wu, X., Guan, K.L., and Guan, J.L. (2005). Identification of FIP200 interaction with the TSC1-TSC2 complex and its role in regulation of cell size control. *J Cell Biol* 170, 379-389.
- Gan, B., Peng, X., Nagy, T., Alcaraz, A., Gu, H., and Guan, J.L. (2006). Role of FIP200 in cardiac and liver development and its regulation of TNF $\alpha$  and TSC-mTOR signaling pathways. *J Cell Biol* 175, 121-133.
- Ganley, I.G., Lam du, H., Wang, J., Ding, X., Chen, S., and Jiang, X. (2009). ULK1.ATG13.FIP200 complex mediates mTOR signaling and is essential for autophagy. *J Biol Chem* 284, 12297-12305.
- Gao, Y., Liu, Y., Hong, L., Yang, Z., Cai, X., Chen, X., Fu, Y., Lin, Y., Wen, W., Li, S., Liu, X., Huang, H., Vogt, A., Liu, P., Yin, X.M., and Li, M. (2016). Golgi-associated LC3 lipidation requires V-ATPase in noncanonical autophagy. *Cell Death Dis* 7, e2330.
- Ge, L., Melville, D., Zhang, M., and Schekman, R. (2013). The ER-Golgi intermediate compartment is a key membrane source for the LC3 lipidation step of autophagosome biogenesis. *Elife* 2, e00947.
- Ge, L., Zhang, M., and Schekman, R. (2014). Phosphatidylinositol 3-kinase and COPII generate LC3 lipidation vesicles from the ER-Golgi intermediate compartment. *Elife* 3, e04135.
- Geng, J., and Klionsky, D.J. (2008). The Atg8 and Atg12 ubiquitin-like conjugation systems in macroautophagy. 'Protein modifications: beyond the usual suspects' review series. *EMBO Rep* 9, 859-864.
- Gillooly, D.J., Morrow, I.C., Lindsay, M., Gould, R., Bryant, N.J., Gaullier, J.M., Parton, R.G., and Stenmark, H. (2000). Localization of phosphatidylinositol 3-phosphate in yeast and mammalian cells. *Embo J* 19, 4577-4588.
- Graef, M., Friedman, J.R., Graham, C., Babu, M., and Nunnari, J. (2013). ER exit sites are physical and functional core autophagosome biogenesis components. *Mol Biol Cell* 24, 2918-2931.
- Guo, K., Searfoss, G., Krolkowski, D., Pagnoni, M., Franks, C., Clark, K., Yu, K.T., Jaye, M., and Ivashchenko, Y. (2001). Hypoxia induces the expression of the pro-apoptotic gene BNIP3. *Cell Death Differ* 8, 367-376.
- Gwinn, D.M., Shackelford, D.B., Egan, D.F., Mihaylova, M.M., Mery, A., Vasquez, D.S., Turk, B.E., and Shaw, R.J. (2008). AMPK phosphorylation of raptor mediates a metabolic checkpoint. *Mol Cell* 30, 214-226.
- Hailey, D.W., Rambold, A.S., Satpute-Krishnan, P., Mitra, K., Sougrat, R., Kim, P.K., and Lippincott-Schwartz, J. (2010). Mitochondria supply membranes for autophagosome biogenesis during starvation. *Cell* 141, 656-667.
- Hamasaki, M., Furuta, N., Matsuda, A., Nezu, A., Yamamoto, A., Fujita, N., Oomori, H., Noda, T., Haraguchi, T., Hiraoka, Y., Amano, A., and Yoshimori, T. (2013). Autophagosomes form at ER-mitochondria contact sites. *Nature* 495, 389-393.
- Hara, K., Maruki, Y., Long, X., Yoshino, K., Oshiro, N., Hidayat, S., Tokunaga, C., Avruch, J., and Yonezawa, K. (2002). Raptor, a binding partner of target of rapamycin (TOR), mediates TOR action. *Cell* 110, 177-189.
- Hara, T., and Mizushima, N. (2009). Role of ULK-FIP200 complex in mammalian autophagy: FIP200, a counterpart of yeast Atg17? *Autophagy* 5, 85-87.
- Hara, T., Takamura, A., Kishi, C., Iemura, S., Natsume, T., Guan, J.L., and Mizushima, N. (2008). FIP200, a ULK-interacting protein, is required for autophagosome formation in mammalian cells. *J Cell Biol* 181, 497-510.
- Harding, T.M., Hefner-Gravink, A., Thumm, M., and Klionsky, D.J. (1996). Genetic and phenotypic overlap between autophagy and the cytoplasm to vacuole protein targeting pathway. *J Biol Chem* 271, 17621-17624.
- Harding, T.M., Morano, K.A., Scott, S.V., and Klionsky, D.J. (1995). Isolation and characterization of yeast mutants in the cytoplasm to vacuole protein targeting pathway. *J Cell Biol* 131, 591-602.
- Harris, B.Z., and Lim, W.A. (2001). Mechanism and role of PDZ domains in signaling complex assembly. *J Cell Sci* 114, 3219-3231.
- Hayashi-Nishino, M., Fujita, N., Noda, T., Yamaguchi, A., Yoshimori, T., and Yamamoto, A. (2009). A subdomain of the endoplasmic reticulum forms a cradle for autophagosome formation. *Nat Cell Biol* 11, 1433-1437.
- Herman, P.K., Stack, J.H., DeModena, J.A., and Emr, S.D. (1991). A novel protein kinase homolog essential for protein sorting to the yeast lysosome-like vacuole. *Cell* 64, 425-437.
- Hieke, N., Löffler, A.S., Kaizuka, T., Berleth, N., Böhrer, P., Drießen, S., Stuhldreier, F., Friesen, O., Assani, K., Schmitz, K., Peter, C., Diedrich, B., Dengjel, J., Holland, P., Simonsen, A., Wesselborg, S., Mizushima, N., and Stork, B. (2015). Expression of a ULK1/2 binding-deficient ATG13 variant can partially restore autophagic activity in ATG13-deficient cells. *Autophagy* 11, 1471-1483.

- Hosokawa, N., Hara, T., Kaizuka, T., Kishi, C., Takamura, A., Miura, Y., Iemura, S., Natsume, T., Takehana, K., Yamada, N., Guan, J.L., Oshiro, N., and Mizushima, N. (2009a). Nutrient-dependent mTORC1 association with the ULK1-Atg13-FIP200 complex required for autophagy. *Mol Biol Cell* 20, 1981-1991.
- Hosokawa, N., Sasaki, T., Iemura, S., Natsume, T., Hara, T., and Mizushima, N. (2009b). Atg101, a novel mammalian autophagy protein interacting with Atg13. *Autophagy* 5, 973-979.
- Huang, J., Birmingham, C.L., Shahnazari, S., Shiu, J., Zheng, Y.T., Smith, A.C., Campellone, K.G., Heo, W.D., Gruenheid, S., Meyer, T., Welch, M.D., Ktistakis, N.T., Kim, P.K., Klionsky, D.J., and Brumell, J.H. (2011). Antibacterial autophagy occurs at PI(3)P-enriched domains of the endoplasmic reticulum and requires Rab1 GTPase. *Autophagy* 7, 17-26.
- Ichimura, Y., Kirisako, T., Takao, T., Satomi, Y., Shimonishi, Y., Ishihara, N., Mizushima, N., Tanida, I., Kominami, E., Ohsumi, M., Noda, T., and Ohsumi, Y. (2000). A ubiquitin-like system mediates protein lipidation. *Nature* 408, 488-492.
- Ichimura, Y., Kominami, E., Tanaka, K., and Komatsu, M. (2008a). Selective turnover of p62/A170/SQSTM1 by autophagy. *Autophagy* 4, 1063-1066.
- Ichimura, Y., Kumanomidou, T., Sou, Y.S., Mizushima, T., Ezaki, J., Ueno, T., Kominami, E., Yamane, T., Tanaka, K., and Komatsu, M. (2008b). Structural basis for sorting mechanism of p62 in selective autophagy. *J Biol Chem* 283, 22847-22857.
- Inoki, K., Li, Y., Xu, T., and Guan, K.L. (2003a). Rheb GTPase is a direct target of TSC2 GAP activity and regulates mTOR signaling. *Genes Dev* 17, 1829-1834.
- Inoki, K., Li, Y., Zhu, T., Wu, J., and Guan, K.L. (2002). TSC2 is phosphorylated and inhibited by Akt and suppresses mTOR signalling. *Nat Cell Biol* 4, 648-657.
- Inoki, K., Ouyang, H., Zhu, T., Lindvall, C., Wang, Y., Zhang, X., Yang, Q., Bennett, C., Harada, Y., Stankunas, K., Wang, C.Y., He, X., MacDougald, O.A., You, M., Williams, B.O., and Guan, K.L. (2006). TSC2 integrates Wnt and energy signals via a coordinated phosphorylation by AMPK and GSK3 to regulate cell growth. *Cell* 126, 955-968.
- Inoki, K., Zhu, T., and Guan, K.L. (2003b). TSC2 mediates cellular energy response to control cell growth and survival. *Cell* 115, 577-590.
- Itakura, E., Kishi-Itakura, C., and Mizushima, N. (2012). The hairpin-type tail-anchored SNARE syntaxin 17 targets to autophagosomes for fusion with endosomes/lysosomes. *Cell* 151, 1256-1269.
- Itakura, E., Kishi, C., Inoue, K., and Mizushima, N. (2008). Beclin 1 forms two distinct phosphatidylinositol 3-kinase complexes with mammalian Atg14 and UVRAG. *Mol Biol Cell* 19, 5360-5372.
- Itakura, E., and Mizushima, N. (2010). Characterization of autophagosome formation site by a hierarchical analysis of mammalian Atg proteins. *Autophagy* 6, 764-776.
- Itoh, T., and De Camilli, P. (2006). BAR, F-BAR (EFC) and ENTH/ANTH domains in the regulation of membrane-cytosol interfaces and membrane curvature. *Biochim Biophys Acta* 1761, 897-912.
- Itoh, T., Fujita, N., Kanno, E., Yamamoto, A., Yoshimori, T., and Fukuda, M. (2008). Golgi-resident small GTPase Rab33B interacts with Atg16L and modulates autophagosome formation. *Mol Biol Cell* 19, 2916-2925.
- Jao, C.C., Ragusa, M.J., Stanley, R.E., and Hurley, J.H. (2013). A HORMA domain in Atg13 mediates PI 3-kinase recruitment in autophagy. *Proc Natl Acad Sci U S A* 110, 5486-5491.
- Joachim, J., and Tooze, S.A. (2016). GABARAP activates ULK1 and traffics from the centrosome dependent on Golgi partners WAC and GOLGA2/GM130. *Autophagy* 12, 892-893.
- Joo, J.H., Dorsey, F.C., Joshi, A., Hennessy-Walters, K.M., Rose, K.L., McCastlain, K., Zhang, J., Iyengar, R., Jung, C.H., Suen, D.F., Steeves, M.A., Yang, C.Y., Prater, S.M., Kim, D.H., Thompson, C.B., Youle, R.J., Ney, P.A., Cleveland, J.L., and Kundu, M. (2011). Hsp90-Cdc37 chaperone complex regulates Ulk1- and Atg13-mediated mitophagy. *Mol Cell* 43, 572-585.
- Jordan, T.X., and Randall, G. (2012). Manipulation or capitulation: virus interactions with autophagy. *Microbes Infect* 14, 126-139.
- Joshi, A., Iyengar, R., Joo, J.H., Li-Harms, X.J., Wright, C., Marino, R., Winborn, B.J., Phillips, A., Temirov, J., Sciarretta, S., Kriwacki, R., Peng, J., Shelat, A., and Kundu, M. (2016). Nuclear ULK1 promotes cell death in response to oxidative stress through PARP1. *Cell Death Differ* 23, 216-230.
- Jung, C.H., Jun, C.B., Ro, S.H., Kim, Y.M., Otto, N.M., Cao, J., Kundu, M., and Kim, D.H. (2009). ULK-Atg13-FIP200 complexes mediate mTOR signaling to the autophagy machinery. *Mol Biol Cell* 20, 1992-2003.
- Kaiser, S.E., Mao, K., Taherbhoy, A.M., Yu, S., Olszewski, J.L., Duda, D.M., Kurinov, I., Deng, A., Fenn, T.D., Klionsky, D.J., and Schulman, B.A. (2012). Noncanonical E2 recruitment by the autophagy E1 revealed by Atg7-Atg3 and Atg7-Atg10 structures. *Nat Struct Mol Biol* 19, 1242-1249.
- Kaizuka, T., Hara, T., Oshiro, N., Kikkawa, U., Yonezawa, K., Takehana, K., Iemura, S., Natsume, T., and Mizushima, N. (2010). Tti1 and Tel2 are critical factors in mammalian target of rapamycin complex assembly. *J Biol Chem* 285, 20109-20116.
- Kaizuka, T., and Mizushima, N. (2015). Atg13 Is Essential for Autophagy and Cardiac Development in Mice. *Mol Cell Biol* 36, 585-595.
- Kamada, Y., Funakoshi, T., Shintani, T., Nagano, K., Ohsumi, M., and Ohsumi, Y. (2000). Tor-mediated induction of autophagy via an Apg1 protein kinase complex. *J Cell Biol* 150, 1507-1513.
- Karanasios, E., Stapleton, E., Manifava, M., Kaizuka, T., Mizushima, N., Walker, S.A., and Ktistakis, N.T. (2013). Dynamic association of the ULK1 complex with omegasomes during autophagy induction. *J Cell Sci* 126, 5224-5238.
- Karanasios, E., Walker, S.A., Okkenhaug, H., Manifava, M., Hummel, E., Zimmermann, H., Ahmed, Q., Domart, M.C., Collinson, L., and Ktistakis, N.T. (2016). Autophagy initiation by ULK complex assembly on ER tubulovesicular regions marked by ATG9 vesicles. *Nat Commun* 7, 12420.

- Kihara, A., Kabeya, Y., Ohsumi, Y., and Yoshimori, T.** (2001a). Beclin-phosphatidylinositol 3-kinase complex functions at the trans-Golgi network. *EMBO Rep* 2, 330-335.
- Kihara, A., Noda, T., Ishihara, N., and Ohsumi, Y.** (2001b). Two distinct Vps34 phosphatidylinositol 3-kinase complexes function in autophagy and carboxypeptidase Y sorting in *Saccharomyces cerevisiae*. *J Cell Biol* 152, 519-530.
- Kim, B.W., Hong, S.B., Kim, J.H., Kwon, D.H., and Song, H.K.** (2013a). Structural basis for recognition of autophagic receptor NDP52 by the sugar receptor galectin-8. *Nat Commun* 4, 1613.
- Kim, D.H., Sarbassov, D.D., Ali, S.M., King, J.E., Latek, R.R., Erdjument-Bromage, H., Tempst, P., and Sabatini, D.M.** (2002). mTOR interacts with raptor to form a nutrient-sensitive complex that signals to the cell growth machinery. *Cell* 110, 163-175.
- Kim, D.H., Sarbassov, D.D., Ali, S.M., Latek, R.R., Guntur, K.V., Erdjument-Bromage, H., Tempst, P., and Sabatini, D.M.** (2003). GbetaL, a positive regulator of the rapamycin-sensitive pathway required for the nutrient-sensitive interaction between raptor and mTOR. *Mol Cell* 11, 895-904.
- Kim, E., Goraksha-Hicks, P., Li, L., Neufeld, T.P., and Guan, K.L.** (2008). Regulation of TORC1 by Rag GTPases in nutrient response. *Nat Cell Biol* 10, 935-945.
- Kim, J., Kim, Y.C., Fang, C., Russell, R.C., Kim, J.H., Fan, W., Liu, R., Zhong, Q., and Guan, K.L.** (2013b). Differential regulation of distinct Vps34 complexes by AMPK in nutrient stress and autophagy. *Cell* 152, 290-303.
- Kim, J., Kundu, M., Viollet, B., and Guan, K.L.** (2011). AMPK and mTOR regulate autophagy through direct phosphorylation of Ulk1. *Nat Cell Biol* 13, 132-141.
- Kim, Y.M., Jung, C.H., Seo, M., Kim, E.K., Park, J.M., Bae, S.S., and Kim, D.H.** (2015). mTORC1 phosphorylates UVRAG to negatively regulate autophagosome and endosome maturation. *Mol Cell* 57, 207-218.
- Kirisako, T., Ichimura, Y., Okada, H., Kabeya, Y., Mizushima, N., Yoshimori, T., Ohsumi, M., Takao, T., Noda, T., and Ohsumi, Y.** (2000). The reversible modification regulates the membrane-binding state of Apg8/Aut7 essential for autophagy and the cytoplasm to vacuole targeting pathway. *J Cell Biol* 151, 263-276.
- Kirkin, V., Lamark, T., Sou, Y.S., Bjorkoy, G., Nunn, J.L., Bruun, J.A., Shvets, E., McEwan, D.G., Clausen, T.H., Wild, P., Bilusic, I., Theurillat, J.P., Overvatn, A., Ishii, T., Elazar, Z., Komatsu, M., Dikic, I., and Johansen, T.** (2009a). A role for NBR1 in autophagosomal degradation of ubiquitinated substrates. *Mol Cell* 33, 505-516.
- Kirkin, V., McEwan, D.G., Novak, I., and Dikic, I.** (2009b). A role for ubiquitin in selective autophagy. *Mol Cell* 34, 259-269.
- Klionsky, D.J.** (1997). Protein transport from the cytoplasm into the vacuole. *J Membr Biol* 157, 105-115.
- Klionsky, D.J., Cregg, J.M., Dunn, W.A., Jr., Emr, S.D., Sakai, Y., Sandoval, I.V., Sibirny, A., Subramani, S., Thumm, M., Veenhuis, M., and Ohsumi, Y.** (2003). A unified nomenclature for yeast autophagy-related genes. *Dev Cell* 5, 539-545.
- Knodler, L.A., and Celli, J.** (2011). Eating the strangers within: host control of intracellular bacteria via xenophagy. *Cell Microbiol* 13, 1319-1327.
- Komander, D., Clague, M.J., and Urbe, S.** (2009). Breaking the chains: structure and function of the deubiquitinases. *Nat Rev Mol Cell Biol* 10, 550-563.
- Komatsu, M., Waguri, S., Ueno, T., Iwata, J., Murata, S., Tanida, I., Ezaki, J., Mizushima, N., Ohsumi, Y., Uchiyama, Y., Kominami, E., Tanaka, K., and Chiba, T.** (2005). Impairment of starvation-induced and constitutive autophagy in Atg7-deficient mice. *J Cell Biol* 169, 425-434.
- Konno, H., Konno, K., and Barber, G.N.** (2013). Cyclic dinucleotides trigger ULK1 (ATG1) phosphorylation of STING to prevent sustained innate immune signaling. *Cell* 155, 688-698.
- Kontani, K., Chano, T., Ozaki, Y., Tezuka, N., Sawai, S., Fujino, S., Saeki, Y., and Okabe, H.** (2003). RB1CC1 suppresses cell cycle progression through RB1 expression in human neoplastic cells. *Int J Mol Med* 12, 767-769.
- Korac, J., Schaeffer, V., Kovacevic, I., Clement, A.M., Jungblut, B., Behl, C., Terzic, J., and Dikic, I.** (2013). Ubiquitin-independent function of optineurin in autophagic clearance of protein aggregates. *J Cell Sci* 126, 580-592.
- Kraft, C., Deplazes, A., Sohrmann, M., and Peter, M.** (2008). Mature ribosomes are selectively degraded upon starvation by an autophagy pathway requiring the Ubp3p/Bre5p ubiquitin protease. *Nat Cell Biol* 10, 602-610.
- Kraft, C., Kijanska, M., Kalie, E., Siergiejuk, E., Lee, S.S., Semplicio, G., Stoffel, I., Brezovich, A., Verma, M., Hansmann, I., Ammerer, G., Hofmann, K., Tooze, S., and Peter, M.** (2012). Binding of the Atg1/ULK1 kinase to the ubiquitin-like protein Atg8 regulates autophagy. *Embo J* 31, 3691-3703.
- Kuma, A., Hatano, M., Matsui, M., Yamamoto, A., Nakaya, H., Yoshimori, T., Ohsumi, Y., Tokuhiya, T., and Mizushima, N.** (2004). The role of autophagy during the early neonatal starvation period. *Nature* 432, 1032-1036.
- Kundu, M., Lindsten, T., Yang, C.Y., Wu, J., Zhao, F., Zhang, J., Selak, M.A., Ney, P.A., and Thompson, C.B.** (2008). Ulk1 plays a critical role in the autophagic clearance of mitochondria and ribosomes during reticulocyte maturation. *Blood* 112, 1493-1502.
- Kuroyanagi, H., Yan, J., Seki, N., Yamanouchi, Y., Suzuki, Y., Takano, T., Muramatsu, M., and Shirasawa, T.** (1998). Human ULK1, a novel serine/threonine kinase related to UNC-51 kinase of *Caenorhabditis elegans*: cDNA cloning, expression, and chromosomal assignment. *Genomics* 51, 76-85.
- Lamark, T., Kirkin, V., Dikic, I., and Johansen, T.** (2009). NBR1 and p62 as cargo receptors for selective autophagy of ubiquitinated targets. *Cell Cycle* 8, 1986-1990.
- Lamb, C.A., Yoshimori, T., and Tooze, S.A.** (2013). The autophagosome: origins unknown, biogenesis complex. *Nat Rev Mol Cell Biol* 14, 759-774.
- Lazarus, M.B., Novotny, C.J., and Shokat, K.M.** (2015). Structure of the human autophagy initiating kinase ULK1 in complex with potent inhibitors. *ACS Chem Biol* 10, 257-261.

- Lazarus, M.B., and Shokat, K.M.** (2015). Discovery and structure of a new inhibitor scaffold of the autophagy initiating kinase ULK1. *Bioorg Med Chem* 23, 5483-5488.
- Lee, D.F., Kuo, H.P., Chen, C.T., Hsu, J.M., Chou, C.K., Wei, Y., Sun, H.L., Li, L.Y., Ping, B., Huang, W.C., He, X., Hung, J.Y., Lai, C.C., Ding, Q., Su, J.L., Yang, J.Y., Sahin, A.A., Hortobagyi, G.N., Tsai, F.J., Tsai, C.H., and Hung, M.C.** (2007). IKK beta suppression of TSC1 links inflammation and tumor angiogenesis via the mTOR pathway. *Cell* 130, 440-455.
- Lee, E.J., and Tournier, C.** (2011). The requirement of uncoordinated 51-like kinase 1 (ULK1) and ULK2 in the regulation of autophagy. *Autophagy* 7, 689-695.
- Lee, H.J., and Zheng, J.J.** (2010). PDZ domains and their binding partners: structure, specificity, and modification. *Cell Commun Signal* 8, 8.
- Lee, J.W., Park, S., Takahashi, Y., and Wang, H.G.** (2010). The association of AMPK with ULK1 regulates autophagy. *PLoS One* 5, e15394.
- Lemasters, J.J.** (2005). Selective mitochondrial autophagy, or mitophagy, as a targeted defense against oxidative stress, mitochondrial dysfunction, and aging. *Rejuvenation Res* 8, 3-5.
- Levine, B.** (2005). Eating oneself and uninvited guests: autophagy-related pathways in cellular defense. *Cell* 120, 159-162.
- Levine, B., and Klionsky, D.J.** (2004). Development by self-digestion: molecular mechanisms and biological functions of autophagy. *Dev Cell* 6, 463-477.
- Levine, B., and Kroemer, G.** (2008). Autophagy in the pathogenesis of disease. *Cell* 132, 27-42.
- Li, W.W., Li, J., and Bao, J.K.** (2012a). Microautophagy: lesser-known self-eating. *Cell Mol Life Sci* 69, 1125-1136.
- Li, X., He, L., Che, K.H., Funderburk, S.F., Pan, L., Pan, N., Zhang, M., Yue, Z., and Zhao, Y.** (2012b). Imperfect interface of Beclin1 coiled-coil domain regulates homodimer and heterodimer formation with Atg14L and UVRAG. *Nat Commun* 3, 662.
- Liang, C., Feng, P., Ku, B., Dotan, I., Canaani, D., Oh, B.H., and Jung, J.U.** (2006). Autophagic and tumour suppressor activity of a novel Beclin1-binding protein UVRAG. *Nat Cell Biol* 8, 688-699.
- Liang, C., Lee, J.S., Inn, K.S., Gack, M.U., Li, Q., Roberts, E.A., Vergne, I., Deretic, V., Feng, P., Akazawa, C., and Jung, J.U.** (2008). Beclin1-binding UVRAG targets the class C Vps complex to coordinate autophagosome maturation and endocytic trafficking. *Nat Cell Biol* 10, 776-787.
- Liang, X.H., Jackson, S., Seaman, M., Brown, K., Kempkes, B., Hibshoosh, H., and Levine, B.** (1999). Induction of autophagy and inhibition of tumorigenesis by beclin 1. *Nature* 402, 672-676.
- Lin, S.Y., Li, T.Y., Liu, Q., Zhang, C., Li, X., Chen, Y., Zhang, S.M., Lian, G., Ruan, K., Wang, Z., Zhang, C.S., Chien, K.Y., Wu, J., Li, Q., Han, J., and Lin, S.C.** (2012). GSK3-TIP60-ULK1 signaling pathway links growth factor deprivation to autophagy. *Science* 336, 477-481.
- Liu, L., Feng, D., Chen, G., Chen, M., Zheng, Q., Song, P., Ma, Q., Zhu, C., Wang, R., Qi, W., Huang, L., Xue, P., Li, B., Wang, X., Jin, H., Wang, J., Yang, F., Liu, P., Zhu, Y., Sui, S., and Chen, Q.** (2012). Mitochondrial outer-membrane protein FUNDC1 mediates hypoxia-induced mitophagy in mammalian cells. *Nat Cell Biol* 14, 177-185.
- Liu, R., Zhi, X., and Zhong, Q.** (2015). ATG14 controls SNARE-mediated autophagosome fusion with a lysosome. *Autophagy* 11, 847-849.
- Löffler, A.S., Alers, S., Dieterle, A.M., Keppeler, H., Franz-Wachtel, M., Kundu, M., Campbell, D.G., Wesselborg, S., Alessi, D.R., and Stork, B.** (2011). Ulk1-mediated phosphorylation of AMPK constitutes a negative regulatory feedback loop. *Autophagy* 7, 696-706.
- Long, J., Gallagher, T.R., Cavey, J.R., Sheppard, P.W., Ralston, S.H., Layfield, R., and Searle, M.S.** (2008). Ubiquitin recognition by the ubiquitin-associated domain of p62 involves a novel conformational switch. *J Biol Chem* 283, 5427-5440.
- Longatti, A., Lamb, C.A., Razi, M., Yoshimura, S., Barr, F.A., and Tooze, S.A.** (2012). TBC1D14 regulates autophagosome formation via Rab11- and ULK1-positive recycling endosomes. *J Cell Biol* 197, 659-675.
- Lu, J., He, L., Behrends, C., Araki, M., Araki, K., Jun Wang, Q., Catanzaro, J.M., Friedman, S.L., Zong, W.X., Fiel, M.I., Li, M., and Yue, Z.** (2014). NRBF2 regulates autophagy and prevents liver injury by modulating Atg14L-linked phosphatidylinositol-3 kinase III activity. *Nat Commun* 5, 3920.
- Ma, L., Chen, Z., Erdjument-Bromage, H., Tempst, P., and Pandolfi, P.P.** (2005). Phosphorylation and functional inactivation of TSC2 by Erk implications for tuberous sclerosis and cancer pathogenesis. *Cell* 121, 179-193.
- Ma, X., Zhang, S., He, L., Rong, Y., Brier, L.W., Sun, Q., Liu, R., Fan, W., Chen, S., Yue, Z., Kim, J., Guan, K.L., Li, D., and Zhong, Q.** (2017). MTORC1-mediated NRBF2 phosphorylation functions as a switch for the class III PtdIns3K and autophagy. *Autophagy* 13, 592-607.
- Mack, H.I., Zheng, B., Asara, J.M., and Thomas, S.M.** (2012). AMPK-dependent phosphorylation of ULK1 regulates ATG9 localization. *Autophagy* 8, 1197-1214.
- Malhotra, R., Warne, J.P., Salas, E., Xu, A.W., and Debnath, J.** (2015). Loss of Atg12, but not Atg5, in pro-opiomelanocortin neurons exacerbates diet-induced obesity. *Autophagy* 11, 145-154.
- Maloverjan, A., Piirsoo, M., Kasak, L., Peil, L., Osterlund, T., and Kogerman, P.** (2010a). Dual function of UNC-51-like kinase 3 (Ulk3) in the Sonic hedgehog signaling pathway. *J Biol Chem* 285, 30079-30090.
- Maloverjan, A., Piirsoo, M., Michelson, P., Kogerman, P., and Osterlund, T.** (2010b). Identification of a novel serine/threonine kinase ULK3 as a positive regulator of Hedgehog pathway. *Exp Cell Res* 316, 627-637.
- Maloveryan, A., Finta, C., Osterlund, T., and Kogerman, P.** (2007). A possible role of mouse Fused (STK36) in Hedgehog signaling and Gli transcription factor regulation. *J Cell Commun Signal* 1, 165-173.
- Manil-Segalen, M., Lefebvre, C., Jenzer, C., Trichet, M., Boulogne, C., Satiat-Jeunemaitre, B., and Legouis, R.** (2014). The *C. elegans* LC3 acts downstream of GABARAP to degrade autophagosomes by interacting with the HOPS subunit VPS39. *Dev Cell* 28, 43-55.

- Manning, B.D., Tee, A.R., Logsdon, M.N., Blenis, J., and Cantley, L.C.** (2002). Identification of the tuberous sclerosis complex-2 tumor suppressor gene product tuberin as a target of the phosphoinositide 3-kinase/akt pathway. *Mol Cell* *10*, 151-162.
- Manzoni, C., Mamais, A., Roosen, D.A., Dihanich, S., Soutar, M.P., Plun-Favreau, H., Bandopadhyay, R., Hardy, J., Tooze, S.A., Cookson, M.R., and Lewis, P.A.** (2016). mTOR independent regulation of macroautophagy by Leucine Rich Repeat Kinase 2 via Beclin-1. *Sci Rep* *6*, 35106.
- Martin, N., Schwamborn, K., Urlaub, H., Gan, B., Guan, J.L., and Dejean, A.** (2008). Spatial interplay between PIASy and FIP200 in the regulation of signal transduction and transcriptional activity. *Mol Cell Biol* *28*, 2771-2781.
- Matsunaga, K., Morita, E., Saitoh, T., Akira, S., Ktistakis, N.T., Izumi, T., Noda, T., and Yoshimori, T.** (2010). Autophagy requires endoplasmic reticulum targeting of the PI3-kinase complex via Atg14L. *J Cell Biol* *190*, 511-521.
- Matsunaga, K., Saitoh, T., Tabata, K., Omori, H., Satoh, T., Kurotori, N., Maejima, I., Shirahama-Noda, K., Ichimura, T., Isoe, T., Akira, S., Noda, T., and Yoshimori, T.** (2009). Two Beclin 1-binding proteins, Atg14L and Rubicon, reciprocally regulate autophagy at different stages. *Nat Cell Biol* *11*, 385-396.
- Matsuura, A., Tsukada, M., Wada, Y., and Ohsumi, Y.** (1997). Apg1p, a novel protein kinase required for the autophagic process in *Saccharomyces cerevisiae*. *Gene* *192*, 245-250.
- Maucuer, A., Camonis, J.H., and Sobel, A.** (1995). Stathmin interaction with a putative kinase and coiled-coil-forming protein domains. *Proc Natl Acad Sci U S A* *92*, 3100-3104.
- Mazure, N.M., and Pouyssegur, J.** (2010). Hypoxia-induced autophagy: cell death or cell survival? *Curr Opin Cell Biol* *22*, 177-180.
- McAlpine, F., Williamson, L.E., Tooze, S.A., and Chan, E.Y.** (2013). Regulation of nutrient-sensitive autophagy by uncoordinated 51-like kinases 1 and 2. *Autophagy* *9*, 361-373.
- Medina, J.M., Tabernero, A., Tovar, J.A., and Martin-Barrientos, J.** (1996). Metabolic fuel utilization and pyruvate oxidation during the postnatal period. *J Inher Metab Dis* *19*, 432-442.
- Mei, Y., Su, M., Soni, G., Salem, S., Colbert, C.L., and Sinha, S.C.** (2014). Intrinsically disordered regions in autophagy proteins. *Proteins* *82*, 565-578.
- Meijer, W.H., van der Klei, I.J., Veenhuis, M., and Kiel, J.A.** (2007). ATG genes involved in non-selective autophagy are conserved from yeast to man, but the selective Cvt and pexophagy pathways also require organism-specific genes. *Autophagy* *3*, 106-116.
- Melkounian, Z.K., Peng, X., Gan, B., Wu, X., and Guan, J.L.** (2005). Mechanism of cell cycle regulation by FIP200 in human breast cancer cells. *Cancer Res* *65*, 6676-6684.
- Mercer, C.A., Kaliappan, A., and Dennis, P.B.** (2009). A novel, human Atg13 binding protein, Atg101, interacts with ULK1 and is essential for macroautophagy. *Autophagy* *5*, 649-662.
- Metlagel, Z., Otomo, C., Takaesu, G., and Otomo, T.** (2013). Structural basis of ATG3 recognition by the autophagic ubiquitin-like protein ATG12. *Proc Natl Acad Sci U S A* *110*, 18844-18849.
- Michel, M., Schwarten, M., Decker, C., Nagel-Steger, L., Willbold, D., and Weiergraber, O.H.** (2015). The mammalian autophagy initiator complex contains 2 HORMA domain proteins. *Autophagy* *11*, 2300-2308.
- Mizushima, N., Kuma, A., Kobayashi, Y., Yamamoto, A., Matsubae, M., Takao, T., Natsume, T., Ohsumi, Y., and Yoshimori, T.** (2003). Mouse Apg16L, a novel WD-repeat protein, targets to the autophagic isolation membrane with the Apg12-Apg5 conjugate. *J Cell Sci* *116*, 1679-1688.
- Mizushima, N., Levine, B., Cuervo, A.M., and Klionsky, D.J.** (2008). Autophagy fights disease through cellular self-digestion. *Nature* *451*, 1069-1075.
- Mizushima, N., Noda, T., and Ohsumi, Y.** (1999). Apg16p is required for the function of the Apg12p-Apg5p conjugate in the yeast autophagy pathway. *Embo J* *18*, 3888-3896.
- Mizushima, N., Noda, T., Yoshimori, T., Tanaka, Y., Ishii, T., George, M.D., Klionsky, D.J., Ohsumi, M., and Ohsumi, Y.** (1998a). A protein conjugation system essential for autophagy. *Nature* *395*, 395-398.
- Mizushima, N., Sugita, H., Yoshimori, T., and Ohsumi, Y.** (1998b). A new protein conjugation system in human. The counterpart of the yeast Apg12p conjugation system essential for autophagy. *J Biol Chem* *273*, 33889-33892.
- Mochizuki, Y., Ohashi, R., Kawamura, T., Iwanari, H., Kodama, T., Naito, M., and Hamakubo, T.** (2013). Phosphatidylinositol 3-phosphatase myotubularin-related protein 6 (MTMR6) is regulated by small GTPase Rab1B in the early secretory and autophagic pathways. *J Biol Chem* *288*, 1009-1021.
- Mostowy, S., Sancho-Shimizu, V., Hamon, M.A., Simeone, R., Brosch, R., Johansen, T., and Cossart, P.** (2011). p62 and NDP52 proteins target intracytosolic *Shigella* and *Listeria* to different autophagy pathways. *J Biol Chem* *286*, 26987-26995.
- Mowers, E.E., Sharifi, M.N., and Macleod, K.F.** (2016). Autophagy in cancer metastasis. *Oncogene*.
- Mukaiyama, H., Oku, M., Baba, M., Samizo, T., Hammond, A.T., Glick, B.S., Kato, N., and Sakai, Y.** (2002). Paz2 and 13 other PAZ gene products regulate vacuolar engulfment of peroxisomes during micropexophagy. *Genes Cells* *7*, 75-90.
- Nakatogawa, H., Ichimura, Y., and Ohsumi, Y.** (2007). Atg8, a ubiquitin-like protein required for autophagosome formation, mediates membrane tethering and hemifusion. *Cell* *130*, 165-178.
- Nazio, F., Strappazzon, F., Antonioli, M., Bielli, P., Cianfanelli, V., Bordin, M., Gretzmeier, C., Dengjel, J., Piacentini, M., Fimia, G.M., and Cecconi, F.** (2013). mTOR inhibits autophagy by controlling ULK1 ubiquitylation, self-association and function through AMBRA1 and TRAF6. *Nat Cell Biol* *15*, 406-416.
- Newman, A.C., Scholefield, C.L., Kemp, A.J., Newman, M., Mclver, E.G., Kamal, A., and Wilkinson, S.** (2012). TBK1 kinase addiction in lung cancer cells is mediated via autophagy of Tax1bp1/Ndp52 and non-canonical NF-kappaB signalling. *PLoS One* *7*, e50672.

- Nguyen, T.N., Padman, B.S., Usher, J., Oorschot, V., Ramm, G., and Lazarou, M.** (2016). Atg8 family LC3/GABARAP proteins are crucial for autophagosome-lysosome fusion but not autophagosome formation during PINK1/Parkin mitophagy and starvation. *J Cell Biol* 215, 857-874.
- Nishimura, T., Kaizuka, T., Cadwell, K., Sahani, M.H., Saitoh, T., Akira, S., Virgin, H.W., and Mizushima, N.** (2013). FIP200 regulates targeting of Atg16L1 to the isolation membrane. *EMBO Rep* 14, 284-291.
- Noda, N.N., Kumeta, H., Nakatogawa, H., Satoo, K., Adachi, W., Ishii, J., Fujioka, Y., Ohsumi, Y., and Inagaki, F.** (2008). Structural basis of target recognition by Atg8/LC3 during selective autophagy. *Genes Cells* 13, 1211-1218.
- Noda, N.N., Ohsumi, Y., and Inagaki, F.** (2010). Atg8-family interacting motif crucial for selective autophagy. *FEBS Lett* 584, 1379-1385.
- Noda, N.N., Satoo, K., Fujioka, Y., Kumeta, H., Ogura, K., Nakatogawa, H., Ohsumi, Y., and Inagaki, F.** (2011). Structural basis of Atg8 activation by a homodimeric E1, Atg7. *Mol Cell* 44, 462-475.
- Noda, T., and Ohsumi, Y.** (1998). Tor, a phosphatidylinositol kinase homologue, controls autophagy in yeast. *J Biol Chem* 273, 3963-3966.
- Novak, I., Kirkin, V., McEwan, D.G., Zhang, J., Wild, P., Rozenknop, A., Rogov, V., Lohr, F., Popovic, D., Occhipinti, A., Reichert, A.S., Terzic, J., Dotsch, V., Ney, P.A., and Dikic, I.** (2010). Nix is a selective autophagy receptor for mitochondrial clearance. *EMBO Rep* 11, 45-51.
- Obara, K., Sekito, T., and Ohsumi, Y.** (2006). Assortment of phosphatidylinositol 3-kinase complexes--Atg14p directs association of complex I to the pre-autophagosomal structure in *Saccharomyces cerevisiae*. *Mol Biol Cell* 17, 1527-1539.
- Ogata, M., Hino, S., Saito, A., Morikawa, K., Kondo, S., Kanemoto, S., Murakami, T., Taniguchi, M., Tanii, I., Yoshinaga, K., Shiosaka, S., Hammarback, J.A., Urano, F., and Imaizumi, K.** (2006). Autophagy is activated for cell survival after endoplasmic reticulum stress. *Mol Cell Biol* 26, 9220-9231.
- Ogura, K., Wicky, C., Magnenat, L., Tobler, H., Mori, I., Muller, F., and Ohshima, Y.** (1994). *Caenorhabditis elegans* unc-51 gene required for axonal elongation encodes a novel serine/threonine kinase. *Genes Dev* 8, 2389-2400.
- Ohsumi, Y.** (2001). Molecular dissection of autophagy: two ubiquitin-like systems. *Nat Rev Mol Cell Biol* 2, 211-216.
- Okazaki, N., Yan, J., Yuasa, S., Ueno, T., Kominami, E., Masuho, Y., Koga, H., and Muramatsu, M.** (2000). Interaction of the Unc-51-like kinase and microtubule-associated protein light chain 3 related proteins in the brain: possible role of vesicular transport in axonal elongation. *Brain Res Mol Brain Res* 85, 1-12.
- Orsi, A., Razi, M., Dooley, H.C., Robinson, D., Weston, A.E., Collinson, L.M., and Tooze, S.A.** (2012). Dynamic and transient interactions of Atg9 with autophagosomes, but not membrane integration, are required for autophagy. *Mol Biol Cell* 23, 1860-1873.
- Otomo, C., Metlagel, Z., Takaesu, G., and Otomo, T.** (2013). Structure of the human ATG12~ATG5 conjugate required for LC3 lipidation in autophagy. *Nat Struct Mol Biol* 20, 59-66.
- Overbye, A., Fengsrud, M., and Seglen, P.O.** (2007). Proteomic analysis of membrane-associated proteins from rat liver autophagosomes. *Autophagy* 3, 300-322.
- Pankiv, S., Clausen, T.H., Lamark, T., Brech, A., Bruun, J.A., Outzen, H., Overvatn, A., Bjorkoy, G., and Johansen, T.** (2007). p62/SQSTM1 binds directly to Atg8/LC3 to facilitate degradation of ubiquitinated protein aggregates by autophagy. *J Biol Chem* 282, 24131-24145.
- Papandreou, I., Lim, A.L., Laderoute, K., and Denko, N.C.** (2008). Hypoxia signals autophagy in tumor cells via AMPK activity, independent of HIF-1, BNIP3, and BNIP3L. *Cell Death Differ* 15, 1572-1581.
- Park, J.M., Jung, C.H., Seo, M., Otto, N.M., Grunwald, D., Kim, K.H., Moriarity, B., Kim, Y.M., Starker, C., Nho, R.S., Voytas, D., and Kim, D.H.** (2016). The ULK1 complex mediates MTORC1 signaling to the autophagy initiation machinery via binding and phosphorylating ATG14. *Autophagy* 12, 547-564.
- Park, Y.E., Hayashi, Y.K., Bonne, G., Arimura, T., Noguchi, S., Nonaka, I., and Nishino, I.** (2009). Autophagic degradation of nuclear components in mammalian cells. *Autophagy* 5, 795-804.
- Pattingre, S., Tassa, A., Qu, X., Garuti, R., Liang, X.H., Mizushima, N., Packer, M., Schneider, M.D., and Levine, B.** (2005). Bcl-2 antiapoptotic proteins inhibit Beclin 1-dependent autophagy. *Cell* 122, 927-939.
- Peterson, T.R., Laplante, M., Thoreen, C.C., Sancak, Y., Kang, S.A., Kuehl, W.M., Gray, N.S., and Sabatini, D.M.** (2009). DEPTOR is an mTOR inhibitor frequently overexpressed in multiple myeloma cells and required for their survival. *Cell* 137, 873-886.
- Petherick, K.J., Conway, O.J., Mpamhanga, C., Osborne, S.A., Kamal, A., Saxty, B., and Ganley, I.G.** (2015). Pharmacological inhibition of ULK1 kinase blocks mammalian target of rapamycin (mTOR)-dependent autophagy. *J Biol Chem* 290, 28726.
- Pfeuffer, T., Goebel, W., Laubinger, J., Bachmann, M., and Kuhn, M.** (2000). LaXp180, a mammalian ActA-binding protein, identified with the yeast two-hybrid system, co-localizes with intracellular *Listeria monocytogenes*. *Cell Microbiol* 2, 101-114.
- Polson, H.E., de Lartigue, J., Rigden, D.J., Reedijk, M., Urbe, S., Clague, M.J., and Tooze, S.A.** (2010). Mammalian Atg18 (WIPI2) localizes to omegasome-anchored phagophores and positively regulates LC3 lipidation. *Autophagy* 6, 506-522.
- Potter, C.J., Pedraza, L.G., and Xu, T.** (2002). Akt regulates growth by directly phosphorylating Tsc2. *Nat Cell Biol* 4, 658-665.
- Proikas-Cezanne, T., Waddell, S., Gaugel, A., Frickey, T., Lupas, A., and Nordheim, A.** (2004). WIPI-1alpha (WIPI49), a member of the novel 7-bladed WIPI protein family, is aberrantly expressed in human cancer and is linked to starvation-induced autophagy. *Oncogene* 23, 9314-9325.
- Puente, C., Hendrickson, R.C., and Jiang, X.** (2016). Nutrient-regulated Phosphorylation of ATG13 Inhibits Starvation-induced Autophagy. *J Biol Chem* 291, 6026-6035.

- Qi, S., Kim, D.J., Stjepanovic, G., and Hurley, J.H.** (2015). Structure of the Human Atg13-Atg101 HORMA Heterodimer: an Interaction Hub within the ULK1 Complex. *Structure* 23, 1848-1857.
- Reggiori, F., and Klionsky, D.J.** (2002). Autophagy in the eukaryotic cell. *Eukaryot Cell* 1, 11-21.
- Reggiori, F., and Klionsky, D.J.** (2006). Atg9 sorting from mitochondria is impaired in early secretion and VFT-complex mutants in *Saccharomyces cerevisiae*. *J Cell Sci* 119, 2903-2911.
- Ridley, S.H., Ktistakis, N., Davidson, K., Anderson, K.E., Manifava, M., Ellson, C.D., Lipp, P., Bootman, M., Coadwell, J., Nazarian, A., Erdjument-Bromage, H., Tempst, P., Cooper, M.A., Thuring, J.W., Lim, Z.Y., Holmes, A.B., Stephens, L.R., and Hawkins, P.T.** (2001). FENS-1 and DFCP1 are FYVE domain-containing proteins with distinct functions in the endosomal and Golgi compartments. *J Cell Sci* 114, 3991-4000.
- Ro, S.H., Jung, C.H., Hahn, W.S., Xu, X., Kim, Y.M., Yun, Y.S., Park, J.M., Kim, K.H., Seo, M., Ha, T.Y., Arriaga, E.A., Bernlohr, D.A., and Kim, D.H.** (2013). Distinct functions of Ulk1 and Ulk2 in the regulation of lipid metabolism in adipocytes. *Autophagy* 9, 2103-2114.
- Rogov, V.V., Suzuki, H., Fiskin, E., Wild, P., Kniss, A., Rozenknop, A., Kato, R., Kawasaki, M., McEwan, D.G., Lohr, F., Guntert, P., Dikic, I., Wakatsuki, S., and Dotsch, V.** (2013). Structural basis for phosphorylation-triggered autophagic clearance of *Salmonella*. *Biochem J* 454, 459-466.
- Romanov, J., Walczak, M., Ibricic, I., Schuchner, S., Ogris, E., Kraft, C., and Martens, S.** (2012). Mechanism and functions of membrane binding by the Atg5-Atg12/Atg16 complex during autophagosome formation. *Embo J* 31, 4304-4317.
- Ron, D., and Walter, P.** (2007). Signal integration in the endoplasmic reticulum unfolded protein response. *Nat Rev Mol Cell Biol* 8, 519-529.
- Rosenberg, S.C., and Corbett, K.D.** (2015). The multifaceted roles of the HORMA domain in cellular signaling. *J Cell Biol* 211, 745-755.
- Rouschop, K.M., van den Beucken, T., Dubois, L., Niessen, H., Bussink, J., Savelkoul, K., Keulers, T., Mujcic, H., Landuyt, W., Voncken, J.W., Lambin, P., van der Kogel, A.J., Koritzinsky, M., and Wouters, B.G.** (2010). The unfolded protein response protects human tumor cells during hypoxia through regulation of the autophagy genes MAP1LC3B and ATG5. *J Clin Invest* 120, 127-141.
- Roux, P.P., Ballif, B.A., Anjum, R., Gygi, S.P., and Blenis, J.** (2004). Tumor-promoting phorbol esters and activated Ras inactivate the tuberous sclerosis tumor suppressor complex via p90 ribosomal S6 kinase. *Proc Natl Acad Sci U S A* 101, 13489-13494.
- Rozenknop, A., Rogov, V.V., Rogova, N.Y., Lohr, F., Guntert, P., Dikic, I., and Dotsch, V.** (2011). Characterization of the interaction of GABARAPL-1 with the LIR motif of NBR1. *J Mol Biol* 410, 477-487.
- Russell, R.C., Tian, Y., Yuan, H., Park, H.W., Chang, Y.Y., Kim, J., Kim, H., Neufeld, T.P., Dillin, A., and Guan, K.L.** (2013). ULK1 induces autophagy by phosphorylating Beclin-1 and activating VPS34 lipid kinase. *Nat Cell Biol* 15, 741-750.
- Sakai, Y., Koller, A., Rangell, L.K., Keller, G.A., and Subramani, S.** (1998). Peroxisome degradation by microautophagy in *Pichia pastoris*: identification of specific steps and morphological intermediates. *J Cell Biol* 141, 625-636.
- Sancak, Y., Bar-Peled, L., Zoncu, R., Markhard, A.L., Nada, S., and Sabatini, D.M.** (2010). Ragulator-Rag complex targets mTORC1 to the lysosomal surface and is necessary for its activation by amino acids. *Cell* 141, 290-303.
- Sancak, Y., Peterson, T.R., Shaul, Y.D., Lindquist, R.A., Thoreen, C.C., Bar-Peled, L., and Sabatini, D.M.** (2008). The Rag GTPases bind raptor and mediate amino acid signaling to mTORC1. *Science* 320, 1496-1501.
- Sancak, Y., Thoreen, C.C., Peterson, T.R., Lindquist, R.A., Kang, S.A., Spooner, E., Carr, S.A., and Sabatini, D.M.** (2007). PRAS40 is an insulin-regulated inhibitor of the mTORC1 protein kinase. *Mol Cell* 25, 903-915.
- Schreiber, A., and Peter, M.** (2014). Substrate recognition in selective autophagy and the ubiquitin-proteasome system. *Biochim Biophys Acta* 1843, 163-181.
- Scott, R.C., Schuldiner, O., and Neufeld, T.P.** (2004). Role and regulation of starvation-induced autophagy in the *Drosophila* fat body. *Dev Cell* 7, 167-178.
- Shang, L., Chen, S., Du, F., Li, S., Zhao, L., and Wang, X.** (2011). Nutrient starvation elicits an acute autophagic response mediated by Ulk1 dephosphorylation and its subsequent dissociation from AMPK. *Proc Natl Acad Sci U S A* 108, 4788-4793.
- Shang, L., and Wang, X.** (2011). AMPK and mTOR coordinate the regulation of Ulk1 and mammalian autophagy initiation. *Autophagy* 7, 924-926.
- Shin, H.J., Kim, H., Oh, S., Lee, J.G., Kee, M., Ko, H.J., Kweon, M.N., Won, K.J., and Baek, S.H.** (2016). AMPK-SKP2-CARM1 signalling cascade in transcriptional regulation of autophagy. *Nature* 534, 553-557.
- Shin, S.H., Lee, E.J., Chun, J., Hyun, S., and Kang, S.S.** (2015). ULK2 Ser 1027 Phosphorylation by PKA Regulates Its Nuclear Localization Occurring through Karyopherin Beta 2 Recognition of a PY-NLS Motif. *PLoS One* 10, e0127784.
- Shintani, T., Mizushima, N., Ogawa, Y., Matsuura, A., Noda, T., and Ohsumi, Y.** (1999). Apg10p, a novel protein-conjugating enzyme essential for autophagy in yeast. *Embo J* 18, 5234-5241.
- Shoji-Kawata, S., Sumpter, R., Leveno, M., Campbell, G.R., Zou, Z., Kinch, L., Wilkins, A.D., Sun, Q., Pallauf, K., MacDuff, D., Huerta, C., Virgin, H.W., Helms, J.B., Eerland, R., Tooze, S.A., Xavier, R., Lenschow, D.J., Yamamoto, A., King, D., Lichtarge, O., Grishin, N.V., Spector, S.A., Kaloyanova, D.V., and Levine, B.** (2013). Identification of a candidate therapeutic autophagy-inducing peptide. *Nature* 494, 201-206.
- Shpilka, T., Weidberg, H., Pietrovski, S., and Elazar, Z.** (2011). Atg8: an autophagy-related ubiquitin-like protein family. *Genome Biol* 12, 226.
- Singh, R., Kaushik, S., Wang, Y., Xiang, Y., Novak, I., Komatsu, M., Tanaka, K., Cuervo, A.M., and Czaja, M.J.** (2009). Autophagy regulates lipid metabolism. *Nature* 458, 1131-1135.

- Slobodkin, M.R., and Elazar, Z.** (2013). The Atg8 family: multifunctional ubiquitin-like key regulators of autophagy. *Essays Biochem* 55, 51-64.
- Stambolic, V., MacPherson, D., Sas, D., Lin, Y., Snow, B., Jang, Y., Benchimol, S., and Mak, T.W.** (2001). Regulation of PTEN transcription by p53. *Mol Cell* 8, 317-325.
- Steffan, J.S.** (2010). Does Huntingtin play a role in selective macroautophagy? *Cell Cycle* 9, 3401-3413.
- Stolz, A., Ernst, A., and Dikic, I.** (2014). Cargo recognition and trafficking in selective autophagy. *Nat Cell Biol* 16, 495-501.
- Strappazzon, F., Vietri-Rudan, M., Campello, S., Nazio, F., Florenzano, F., Fimia, G.M., Piacentini, M., Levine, B., and Cecconi, F.** (2011). Mitochondrial BCL-2 inhibits AMBRA1-induced autophagy. *Embo J* 30, 1195-1208.
- Sun, Q., Fan, W., Chen, K., Ding, X., Chen, S., and Zhong, Q.** (2008). Identification of Barkor as a mammalian autophagy-specific factor for Beclin 1 and class III phosphatidylinositol 3-kinase. *Proc Natl Acad Sci U S A* 105, 19211-19216.
- Sun, Q., Westphal, W., Wong, K.N., Tan, I., and Zhong, Q.** (2010). Rubicon controls endosome maturation as a Rab7 effector. *Proc Natl Acad Sci U S A* 107, 19338-19343.
- Suzuki, H., Kaizuka, T., Mizushima, N., and Noda, N.N.** (2015a). Structure of the Atg101-Atg13 complex reveals essential roles of Atg101 in autophagy initiation. *Nat Struct Mol Biol* 22, 572-580.
- Suzuki, H., Tabata, K., Morita, E., Kawasaki, M., Kato, R., Dobson, R.C., Yoshimori, T., and Wakatsuki, S.** (2014). Structural basis of the autophagy-related LC3/Atg13 LIR complex: recognition and interaction mechanism. *Structure* 22, 47-58.
- Suzuki, S.W., Yamamoto, H., Oikawa, Y., Kondo-Kakuta, C., Kimura, Y., Hirano, H., and Ohsumi, Y.** (2015b). Atg13 HORMA domain recruits Atg9 vesicles during autophagosome formation. *Proc Natl Acad Sci U S A* 112, 3350-3355.
- Taherbhoy, A.M., Tait, S.W., Kaiser, S.E., Williams, A.H., Deng, A., Nourse, A., Hammel, M., Kurinov, I., Rock, C.O., Green, D.R., and Schulman, B.A.** (2011). Atg8 transfer from Atg7 to Atg3: a distinctive E1-E2 architecture and mechanism in the autophagy pathway. *Mol Cell* 44, 451-461.
- Takahashi, Y., Coppola, D., Matsushita, N., Cualing, H.D., Sun, M., Sato, Y., Liang, C., Jung, J.U., Cheng, J.Q., Mule, J.J., Pledger, W.J., and Wang, H.G.** (2007). Bif-1 interacts with Beclin 1 through UVRAG and regulates autophagy and tumorigenesis. *Nat Cell Biol* 9, 1142-1151.
- Tanida, I., Mizushima, N., Kiyooka, M., Ohsumi, M., Ueno, T., Ohsumi, Y., and Kominami, E.** (1999). Apg7p/Cvt2p: A novel protein-activating enzyme essential for autophagy. *Mol Biol Cell* 10, 1367-1379.
- Tanida, I., Ueno, T., and Kominami, E.** (2004). LC3 conjugation system in mammalian autophagy. *Int J Biochem Cell Biol* 36, 2503-2518.
- Thedieck, K., Polak, P., Kim, M.L., Molle, K.D., Cohen, A., Jeno, P., Arriemerlou, C., and Hall, M.N.** (2007). PRAS40 and PRR5-like protein are new mTOR interactors that regulate apoptosis. *PLoS One* 2, e1217.
- Thumm, M., Egner, R., Koch, B., Schlumpberger, M., Straub, M., Veenhuis, M., and Wolf, D.H.** (1994). Isolation of autophagocytosis mutants of *Saccharomyces cerevisiae*. *FEBS Lett* 349, 275-280.
- Thurston, T.L., Ryzhakov, G., Bloor, S., von Muhlinen, N., and Randow, F.** (2009). The TBK1 adaptor and autophagy receptor NDP52 restricts the proliferation of ubiquitin-coated bacteria. *Nat Immunol* 10, 1215-1221.
- Thurston, T.L., Wandel, M.P., von Muhlinen, N., Foeglein, A., and Randow, F.** (2012). Galectin 8 targets damaged vesicles for autophagy to defend cells against bacterial invasion. *Nature* 482, 414-418.
- Titorenko, V.I., Keizer, I., Harder, W., and Veenhuis, M.** (1995). Isolation and characterization of mutants impaired in the selective degradation of peroxisomes in the yeast *Hansenula polymorpha*. *J Bacteriol* 177, 357-363.
- Tomoda, T., Bhatt, R.S., Kuroyanagi, H., Shirasawa, T., and Hatten, M.E.** (1999). A mouse serine/threonine kinase homologous to *C. elegans* UNC51 functions in parallel fiber formation of cerebellar granule neurons. *Neuron* 24, 833-846.
- Tsukada, M., and Ohsumi, Y.** (1993). Isolation and characterization of autophagy-defective mutants of *Saccharomyces cerevisiae*. *FEBS Lett* 333, 169-174.
- Ueda, H., Abbi, S., Zheng, C., and Guan, J.L.** (2000). Suppression of Pyk2 kinase and cellular activities by FIP200. *J Cell Biol* 149, 423-430.
- van Meer, G., Voelker, D.R., and Feigenson, G.W.** (2008). Membrane lipids: where they are and how they behave. *Nat Rev Mol Cell Biol* 9, 112-124.
- Vander Haar, E., Lee, S.I., Bandhakavi, S., Griffin, T.J., and Kim, D.H.** (2007). Insulin signalling to mTOR mediated by the Akt/PKB substrate PRAS40. *Nat Cell Biol* 9, 316-323.
- Vergne, I., Singh, S., Roberts, E., Kyei, G., Master, S., Harris, J., de Haro, S., Naylor, J., Davis, A., Delgado, M., and Deretic, V.** (2006). Autophagy in immune defense against *Mycobacterium tuberculosis*. *Autophagy* 2, 175-178.
- von Muhlinen, N., Akutsu, M., Ravenhill, B.J., Foeglein, A., Bloor, S., Rutherford, T.J., Freund, S.M., Komander, D., and Randow, F.** (2012). LC3C, bound selectively by a noncanonical LIR motif in NDP52, is required for antibacterial autophagy. *Mol Cell* 48, 329-342.
- Walinda, E., Morimoto, D., Sugase, K., Konuma, T., Tochio, H., and Shirakawa, M.** (2014). Solution structure of the ubiquitin-associated (UBA) domain of human autophagy receptor NBR1 and its interaction with ubiquitin and polyubiquitin. *J Biol Chem* 289, 13890-13902.
- Walker, S., Chandra, P., Manifava, M., Axe, E., and Ktistakis, N.T.** (2008). Making autophagosomes: localized synthesis of phosphatidylinositol 3-phosphate holds the clue. *Autophagy* 4, 1093-1096.
- Wang, L., Harris, T.E., Roth, R.A., and Lawrence, J.C., Jr.** (2007). PRAS40 regulates mTORC1 kinase activity by functioning as a direct inhibitor of substrate binding. *J Biol Chem* 282, 20036-20044.
- Watanabe, Y., Kobayashi, T., Yamamoto, H., Hoshida, H., Akada, R., Inagaki, F., Ohsumi, Y., and Noda, N.N.** (2012). Structure-based analyses reveal distinct binding sites for Atg2 and phosphoinositides in Atg18. *J Biol Chem* 287, 31681-31690.

- Watson, R.O., Manzanillo, P.S., and Cox, J.S.** (2012). Extracellular *M. tuberculosis* DNA targets bacteria for autophagy by activating the host DNA-sensing pathway. *Cell* *150*, 803-815.
- Webber, J.L., and Tooze, S.A.** (2010). Coordinated regulation of autophagy by p38alpha MAPK through mAtg9 and p38IP. *Embo J* *29*, 27-40.
- Weerasekara, V.K., Panek, D.J., Broadbent, D.G., Mortenson, J.B., Mathis, A.D., Logan, G.N., Prince, J.T., Thomson, D.M., Thompson, J.W., and Andersen, J.L.** (2014). Metabolic-stress-induced rearrangement of the 14-3-3zeta interactome promotes autophagy via a ULK1- and AMPK-regulated 14-3-3zeta interaction with phosphorylated Atg9. *Mol Cell Biol* *34*, 4379-4388.
- Wei, Y., Pattingre, S., Sinha, S., Bassik, M., and Levine, B.** (2008). JNK1-mediated phosphorylation of Bcl-2 regulates starvation-induced autophagy. *Mol Cell* *30*, 678-688.
- Weidberg, H., Shpilka, T., Shvets, E., Abada, A., Shimron, F., and Elazar, Z.** (2011). LC3 and GATE-16 N termini mediate membrane fusion processes required for autophagosome biogenesis. *Dev Cell* *20*, 444-454.
- Weidberg, H., Shvets, E., Shpilka, T., Shimron, F., Shinder, V., and Elazar, Z.** (2010). LC3 and GATE-16/GABARAP subfamilies are both essential yet act differently in autophagosome biogenesis. *Embo J* *29*, 1792-1802.
- Weissman, A.M.** (2001). Themes and variations on ubiquitylation. *Nat Rev Mol Cell Biol* *2*, 169-178.
- Wild, P., Farhan, H., McEwan, D.G., Wagner, S., Rogov, V.V., Brady, N.R., Richter, B., Korac, J., Waidmann, O., Choudhary, C., Dotsch, V., Bumann, D., and Dikic, I.** (2011). Phosphorylation of the autophagy receptor optineurin restricts *Salmonella* growth. *Science* *333*, 228-233.
- Wild, P., McEwan, D.G., and Dikic, I.** (2014). The LC3 interactome at a glance. *J Cell Sci* *127*, 3-9.
- Winslow, A.R., Chen, C.W., Corrochano, S., Acevedo-Arozena, A., Gordon, D.E., Peden, A.A., Lichtenberg, M., Menzies, F.M., Ravikumar, B., Imarisio, S., Brown, S., O'Kane, C.J., and Rubinsztein, D.C.** (2010). alpha-Synuclein impairs macroautophagy: implications for Parkinson's disease. *J Cell Biol* *190*, 1023-1037.
- Wong, P.M., Feng, Y., Wang, J., Shi, R., and Jiang, X.** (2015). Regulation of autophagy by coordinated action of mTORC1 and protein phosphatase 2A. *Nat Commun* *6*, 8048.
- Wu, W., Tian, W., Hu, Z., Chen, G., Huang, L., Li, W., Zhang, X., Xue, P., Zhou, C., Liu, L., Zhu, Y., Li, L., Zhang, L., Sui, S., Zhao, B., and Feng, D.** (2014). ULK1 translocates to mitochondria and phosphorylates FUNDC1 to regulate mitophagy. *EMBO Rep* *15*, 566-575.
- Xie, X., Li, F., Wang, Y., Lin, Z., Cheng, X., Liu, J., Chen, C., and Pan, L.** (2015). Molecular basis of ubiquitin recognition by the autophagy receptor CALCOCO2. *Autophagy* *11*, 1775-1789.
- Xin, Y., Yu, L., Chen, Z., Zheng, L., Fu, Q., Jiang, J., Zhang, P., Gong, R., and Zhao, S.** (2001). Cloning, expression patterns, and chromosome localization of three human and two mouse homologues of GABA(A) receptor-associated protein. *Genomics* *74*, 408-413.
- Xu, Z., Yang, L., Xu, S., Zhang, Z., and Cao, Y.** (2015). The receptor proteins: pivotal roles in selective autophagy. *Acta Biochim Biophys Sin (Shanghai)* *47*, 571-580.
- Yamada, T., Carson, A.R., Caniggia, I., Umebayashi, K., Yoshimori, T., Nakabayashi, K., and Scherer, S.W.** (2005). Endothelial nitric-oxide synthase antisense (NOS3AS) gene encodes an autophagy-related protein (APG9-like2) highly expressed in trophoblast. *J Biol Chem* *280*, 18283-18290.
- Yamazaki, H., Hiramatsu, N., Hayakawa, K., Tagawa, Y., Okamura, M., Ogata, R., Huang, T., Nakajima, S., Yao, J., Paton, A.W., Paton, J.C., and Kitamura, M.** (2009). Activation of the Akt-NF-kappaB pathway by subtilase cytotoxin through the ATF6 branch of the unfolded protein response. *J Immunol* *183*, 1480-1487.
- Yan, J., Kuroyanagi, H., Kuroiwa, A., Matsuda, Y., Tokumitsu, H., Tomoda, T., Shirasawa, T., and Muramatsu, M.** (1998). Identification of mouse ULK1, a novel protein kinase structurally related to *C. elegans* UNC-51. *Biochem Biophys Res Commun* *246*, 222-227.
- Yan, J., Kuroyanagi, H., Tomemori, T., Okazaki, N., Asato, K., Matsuda, Y., Suzuki, Y., Ohshima, Y., Mitani, S., Masuho, Y., Shirasawa, T., and Muramatsu, M.** (1999). Mouse ULK2, a novel member of the UNC-51-like protein kinases: unique features of functional domains. *Oncogene* *18*, 5850-5859.
- Yan, Y., Flinn, R.J., Wu, H., Schnur, R.S., and Backer, J.M.** (2009). hVps15, but not Ca<sup>2+</sup>/CaM, is required for the activity and regulation of hVps34 in mammalian cells. *Biochem J* *417*, 747-755.
- Yin, Z., Pascual, C., and Klionsky, D.J.** (2016). Autophagy: machinery and regulation. *Microb Cell* *3*, 588-596.
- Yla-Anttila, P., Vihinen, H., Jokitalo, E., and Eskelinen, E.L.** (2009). 3D tomography reveals connections between the phagophore and endoplasmic reticulum. *Autophagy* *5*, 1180-1185.
- Youle, R.J., and Narendra, D.P.** (2011). Mechanisms of mitophagy. *Nat Rev Mol Cell Biol* *12*, 9-14.
- Young, A.R., Chan, E.Y., Hu, X.W., Kochl, R., Crawshaw, S.G., High, S., Hailey, D.W., Lippincott-Schwartz, J., and Tooze, S.A.** (2006). Starvation and ULK1-dependent cycling of mammalian Atg9 between the TGN and endosomes. *J Cell Sci* *119*, 3888-3900.
- Young, L.N., Cho, K., Lawrence, R., Zoncu, R., and Hurley, J.H.** (2016). Dynamics and architecture of the NRB2-containing phosphatidylinositol 3-kinase complex I of autophagy. *Proc Natl Acad Sci U S A* *113*, 8224-8229.
- Yuan, W., Tuttle, D.L., Shi, Y.J., Ralph, G.S., and Dunn, W.A., Jr.** (1997). Glucose-induced microautophagy in *Pichia pastoris* requires the alpha-subunit of phosphofruktokinase. *J Cell Sci* *110 ( Pt 16)*, 1935-1945.
- Zhong, Y., Morris, D.H., Jin, L., Patel, M.S., Karunakaran, S.K., Fu, Y.J., Matuszak, E.A., Weiss, H.L., Chait, B.T., and Wang, Q.J.** (2014). Nrbf2 protein suppresses autophagy by modulating Atg14L protein-containing Beclin 1-Vps34 complex architecture and reducing intracellular phosphatidylinositol-3 phosphate levels. *J Biol Chem* *289*, 26021-26037.

- Zhong, Y., Wang, Q.J., Li, X., Yan, Y., Backer, J.M., Chait, B.T., Heintz, N., and Yue, Z.** (2009). Distinct regulation of autophagic activity by Atg14L and Rubicon associated with Beclin 1-phosphatidylinositol-3-kinase complex. *Nat Cell Biol* *11*, 468-476.
- Zoncu, R., Bar-Peled, L., Efeyan, A., Wang, S., Sancak, Y., and Sabatini, D.M.** (2011). mTORC1 senses lysosomal amino acids through an inside-out mechanism that requires the vacuolar H(+)-ATPase. *Science* *334*, 678-683.
- Zoppino, F.C., Militello, R.D., Slavin, I., Alvarez, C., and Colombo, M.I.** (2010). Autophagosome formation depends on the small GTPase Rab1 and functional ER exit sites. *Traffic* *11*, 1246-1261.

## 7. Curriculum Vitae

### PERSONAL DATA

<b>Name</b>	Nora Wallot-Hieke
<b>Date of Birth</b>	February 26th, 1986
<b>Address</b>	Erftrasse 18, 40219 Düsseldorf, Germany
<b>Phone</b>	+49 (0)17625485965
<b>Mail</b>	<a href="mailto:nora.hieke@uni-duesseldorf.de">nora.hieke@uni-duesseldorf.de</a>

### DOCTORATE

09/2012 to 09/2017	<b>Heinrich-Heine University Düsseldorf</b> Doctorate at the Institute of Molecular Medicine (Prof. Dr. rer. nat. Björn Stork)
01 to 04/2015	<b>University of Tokyo, Japan</b> Visiting researcher at the Graduate School of Medicine and Faculty of Medicine (Prof. PD Noboru Mizushima)
12/2011 to 05/2012	<b>Friedrich-Alexander University Erlangen-Nürnberg</b> Research assistant at the Department of Internal Medicine III (Prof. Dr. med. Jörg Distler)

### ACADEMIA

09/2008 to 11/2011	<b>RWTH Aachen University</b> Master's degree course "Biotechnology/Molecular Biotechnology" Certificate: Master of Science (Grade 1.6)
09/2008 to 03/2009	<b>Osaka University, Japan</b> Internship at the Division of Chemical Engineering, Taya Lab (Bioreaction Engineering)
10/2005 to 09/2008	<b>RWTH Aachen University</b> Bachelor's degree course "Biotechnology/Molecular Biotechnology" Certificate: Bachelor of Science (Grade 2.0)

### PROFESSIONAL ACTIVITY

02/2011 to 11/2011	<b>Institute of Immunology, RWTH Aachen University</b> Student assistant
03/2009 to 07/2010	<b>Life Sciences, Fraunhofer Institute of Production Technologies (IPT)</b> Student assistant
10/2007 to 03/2008	<b>Institute of Biotechnology, RWTH Aachen University</b> Student assistant

## COLLEGE

- 1996 to 2005      **Grammar school**, Georg-Cantor Gymnasium Halle an der Saale  
Certificate: Allgemeine Hochschulreife (Grade 1.4)
- 09/2002 to 07/2003      **Kanagawa-Sogo School Yokohama, Japan**  
Exchange year

## 8. Publications and conference contributions

**Wallot-Hieke, N., Verma, N., Schlütermann, D., Berleth, N., Deitersen, J., Böhler, P., Stuhldreier, F., Wu, W., Peter, C., Gohlke, H., Mizushima, N., Stork, B.** Systematic analysis of ATG13 domain requirements for autophagy induction. Accepted in *Autophagy* 2017

**Hieke, N., Löffler, A.S., Kaizuka, T., Berleth, N., Böhler, P., Drießen, S., Stuhldreier, F., Friesen, O., Assani, K., Schmitz, K., Peter, C., Diedrich, B., Dengjel, J., Holland, P., Simonsen, A., Wesselborg, S., Mizushima, N., and Stork, B.** (2015). Expression of a ULK1/2 binding-deficient ATG13 variant can partially restore autophagic activity in ATG13-deficient cells. *Autophagy* 11, 1471-1483

**Drießen, S., Berleth, N., Friesen, O., Löffler, A.S., Böhler, P., Hieke, N., Stuhldreier, F., Peter, C., Schink, K.O., Schultz, S.W., Stenmark, H., Holland, P., Simonsen, A., Wesselborg, S., Stork, B.** (2015) Deubiquitinase inhibition by WP1130 leads to ULK1 aggregation and blockade of autophagy. *Autophagy* 11, 1458-1470

**Dieterle, A.M., Böhler, P., Keppeler, H., Alers, S., Berleth, N., Drießen, S., Hieke, N., Pietkiewicz, S., Löffler, A.S., Peter, C., Gray, A., Leslie, N.R., Shinohara, H., Kurosaki, T., Engelke, M., Wienands, J., Bonin, M., Wesselborg, S., Stork, B.** (2014). PDK1 controls upstream PI3K expression and PIP3 generation. *Oncogene*. 33, 3043-3053

**FRIAS Black forest winter conference – Autophagy Membrane Trafficking & Dynamics in Ageing and Disease**, Germany, Lenzkirch, 2016

Poster: Direct interaction of ATG13 with RB1CC1 is dispensable for autophagy induction

**Keystone symposia- Autophagy: Fundamentals to Disease**, USA, Austin, 2014

Poster: Direct interaction of ULK1 with the ATG13-RB1CC1-ATG101 core complex is dispensable for autophagy induction



# Paper 1



# Expression of a ULK1/2 binding-deficient ATG13 variant can partially restore autophagic activity in ATG13-deficient cells

Nora Hieke,<sup>1,†</sup> Antje S Löffler,<sup>1,†</sup> Takeshi Kaizuka,<sup>2,3,†</sup> Niklas Berleth,<sup>1</sup> Philip Böhler,<sup>1</sup> Stefan Drießen,<sup>1</sup> Fabian Stuhldreier,<sup>1</sup> Olena Friesen,<sup>1</sup> Kaivon Assani,<sup>4</sup> Katharina Schmitz,<sup>1</sup> Christoph Peter,<sup>1</sup> Britta Diedrich,<sup>5</sup> Jörn Dengjel,<sup>5</sup> Petter Holland,<sup>6</sup> Anne Simonsen,<sup>6</sup> Sebastian Wesselborg,<sup>1</sup> Noboru Mizushima,<sup>2,3</sup> and Björn Stork<sup>1,\*</sup>

<sup>1</sup>Institute of Molecular Medicine I; Heinrich-Heine-University; Düsseldorf, Germany; <sup>2</sup>Department of Biochemistry and Molecular Biology; Graduate School and Faculty of Medicine; University of Tokyo; Tokyo, Japan; <sup>3</sup>Department of Physiology and Cell Biology; Tokyo Medical and Dental University; Tokyo, Japan; <sup>4</sup>Center for Microbial Pathogenesis; The Research Institute at Nationwide Children's Hospital; Columbus, OH USA; <sup>5</sup>Department of Dermatology; Medical Center; ZBSA Center for Biological Systems Analysis; BIOS Centre for Biological Signaling Studies; Freiburg Institute for Advanced Studies; University of Freiburg; Freiburg, Germany; <sup>6</sup>Institute of Basic Medical Sciences; Faculty of Medicine; University of Oslo; Oslo, Norway

<sup>†</sup>These authors contributed equally to this work.

**Keywords:** ATG13, ATG101, autophagy, RB1CC1, ULK1

**Abbreviations:** ACTB/ $\beta$ -actin, actin,  $\beta$ ; AMPK, AMP-activated protein kinase; ATG, autophagy-related; Baf A1, bafilomycin A<sub>1</sub>; BECN1, Beclin 1, autophagy-related; EBSS, Earle's balanced salt solution; GFP, green fluorescent protein; GST, glutathione S-transferase; KO, knockout; LIR, LC3-interacting region; MAP1LC3/LC3, microtubule-associated protein 1 light chain 3; MEF, mouse embryonic fibroblast; MIM, MIT-interacting motif; MIT, microtubule interacting and transport; (M)TOR, (mechanistic) target of rapamycin (serine/threonine kinase); PAS, phagophore assembly site; PtdIns3K, phosphatidylinositol 3-kinase; RB1CC1/FIP200, RB1-inducible coiled-coil 1; SQSTM1/p62, sequestosome 1; ULK1/2, unc-51 like autophagy activating kinase 1/2.

Autophagy describes an intracellular process responsible for the lysosome-dependent degradation of cytosolic components. The ULK1/2 complex comprising the kinase ULK1/2 and the accessory proteins ATG13, RB1CC1, and ATG101 has been identified as a central player in the autophagy network, and it represents the main entry point for autophagy-regulating kinases such as MTOR and AMPK. It is generally accepted that the ULK1 complex is constitutively assembled independent of nutrient supply. Here we report the characterization of the ATG13 region required for the binding of ULK1/2. This binding site is established by an extremely short peptide motif at the C terminus of ATG13. This motif is mandatory for the recruitment of ULK1 into the autophagy-initiating high-molecular mass complex. Expression of a ULK1/2 binding-deficient ATG13 variant in ATG13-deficient cells resulted in diminished but not completely abolished autophagic activity. Collectively, we propose that autophagy can be executed by mechanisms that are dependent or independent of the ULK1/2-ATG13 interaction.

## Introduction

Macroautophagy (hereafter referred to as autophagy) describes a process for the degradation of cytoplasmic contents including long-lived, misfolded or aggregated proteins, or entire organelles. In yeast and higher eukaryotic cells this mechanism is evolutionarily conserved and represents a major player in the degradation network next to the ubiquitin-proteasome-system. Under regular physiologic conditions, basal autophagy executes a critical role in cell homeostasis through protein and organelle quality control. However, autophagy can be upregulated under stress conditions like ATP or amino acid deprivation, hypoxia, growth factor withdrawal, DNA damage, or intracellular pathogens. During

autophagy, phagophores form at phosphatidylinositol-3-phosphate (PtdIns3P)-enriched microdomains in the endoplasmic reticulum (ER) termed omegasomes, and the expanding phagophores engulf portions of cytoplasmic material. Closure of this membrane compartment gives rise to autophagosomes. Autophagosomes are double-membraned vesicles which then fuse with endosomes and lysosomes resulting in the formation of autolysosomes.<sup>1</sup> Lysosomal hydrolases subsequently degrade the cargo as well as the inner vesicular membrane, and the resulting building blocks such as amino or fatty acids are made available for *de novo* protein synthesis, ATP generation, and so forth.

On the molecular level, autophagy-related (ATG) gene products as well as several non-ATG proteins regulate all steps

\*Correspondence to: Björn Stork; Email: bjoern.stork@uni-duesseldorf.de  
Submitted: 09/02/2014; Revised: 06/22/2015; Accepted: 06/27/2015  
<http://dx.doi.org/10.1080/15548627.2015.1068488>

of the autophagic flux, including vesicle nucleation, elongation, closure, and fusion with endosomes and lysosomes.<sup>2</sup> With regard to autophagy initiation, the ULK1/2 kinase complex has been characterized as central gatekeeper. In 2009, several groups clarified the composition of this complex and its molecular regulation by the upstream nutrient-sensing MTORC1.<sup>3-8</sup> The macromolecular ULK1/2 (unc51-like autophagy activating kinase 1/2) complex with a molecular mass of approximately 3 MDa is comprised of the Ser/Thr protein kinase ULK1/2 and the accessory proteins ATG13, RB1CC1/FIP200 (RB1-inducible coiled-coil 1), and ATG101.<sup>3-5</sup> In the currently accepted model, the components of the ULK1/2 complex are constitutively associated irrespectively of nutrient supply. Under nutrient-rich conditions, MTORC1 interacts with the ULK1/2 complex, resulting in the inactivation of the complex by MTOR-dependent phosphorylation of ULK1/2 and ATG13 and thus in the inhibition of autophagy. During nutrient deprivation, MTORC1 dissociates from the complex, leading to the activation of the complex by ULK1/2-dependent autophosphorylation and transphosphorylation of ATG13 and RB1CC1 and thus to autophagy induction. However, it appears that the above-described model represents a rather simplistic view. For example, the MTOR-dependent phospho-sites of ATG13 or the ULK1/2-dependent phospho-sites of RB1CC1 have not been reported so far, and the importance of ULK1/2-dependent phosphorylation of ATG13 has been questioned.<sup>9</sup> Furthermore, it has been recently shown that ULK1 is directly controlled by other kinases, e.g. the energy-sensing AMP-activated protein kinase (AMPK) or AKT,<sup>10-14</sup> and by alternative post-translational modifications, e.g. acetylation or ubiquitination.<sup>15,16</sup> With regard to ULK1 ubiquitination, it appears that this is another mode of action for how MTOR influences ULK1 activity. It has been reported that MTORC1 phosphorylates AMBRA1 and thus inhibits TRAF6-mediated ubiquitination of ULK1, which is required for stabilization and activation.<sup>16</sup> Downstream of ULK1, several substrates have been identified to mediate the proautophagic function of this kinase, including AMBRA1, BECN1, or DAPK3/ZIPK (death-associated protein kinase 3).<sup>17-19</sup> Of note, ULK1-independent mechanisms of autophagy induction have been proposed as well.<sup>9,20</sup> In contrast, both ATG13 and RB1CC1 appear to be unequivocally required for starvation-induced autophagy.<sup>3,4,6-9,21,22</sup>

In this study, we further elucidated the molecular details of how the ULK1/2 kinase complex regulates autophagy. We observed that the interaction of ATG13 and ULK1/2 requires the last 2 amino acids LQ of ATG13. Deletion of this short peptide motif constitutes an ULK1/2 binding-deficient ATG13 variant, which retains regular binding to RB1CC1 and ATG101. Accordingly, the disruption of the ULK1/2-ATG13 interaction excludes ULK1 but not ATG13 from the autophagy-initiating high-molecular mass complex and abolishes recruitment of ULK1 to the phagophore assembly site (PAS). Interestingly, we observed that autophagy is not completely inhibited in cells expressing the ULK1/2 binding-deficient

variant of ATG13. We hypothesize that the interaction of ATG13 and ULK1/2 is not necessarily required for autophagy induction by amino acid deprivation and that ULK1/2-ATG13 interaction-dependent and -independent mechanisms contribute to autophagy.

## Results

### The interaction between ULK1/2 and ATG13 is controlled by the extreme C terminus of ATG13

The binding site of ULK1 within ATG13 has been roughly mapped to the last 57 amino acids of the C terminus of ATG13.<sup>7</sup> In order to characterize the binding motif essential for the interaction with ULK1/2, we made use of different truncated ATG13 variants, lacking the last amino acid Gln 480/Q480 (1AAAΔ), the last 2 amino acids Leu,Gln480/LQ480 (2AAAΔ), or the last 3 amino acids Thr,Leu,Gln480/TLQ480 (3AAAΔ, amino acid numbering of human isoform 2, Uniprot identifier O75143-2). The latter sequence has previously gained our interest since it contains a putative ULK1 phosphorylation site (Thr478).<sup>9</sup> We also included the 57AAAΔ variant as positive control and an F429A and F433A (F429A,F433A) double mutant of ATG13, since it has been previously suggested that these 2 phenylalanine residues might be orthologous to hydrophobic residues of the MIT-interacting motif (MIM) domain in yeast Atg13 mediating the interaction with yeast Atg1.<sup>23</sup> We transiently coexpressed GST fusion proteins of full-length ATG13 or the different ATG13 variants in Flp-In<sup>TM</sup> T-REx<sup>TM</sup> 293 cells expressing GFP-tagged full-length ULK1 (GFP-ULK1) or full-length ULK2 (GFP-ULK2), and performed affinity purifications using glutathione-sepharose 4B beads. Only GST-ATG13, GST-ATG13<sup>1AAAΔ</sup> and GST-ATG13<sup>F429A,F433A</sup> purified GFP-ULK1 and GFP-ULK2 from Flp-In<sup>TM</sup> T-REx<sup>TM</sup> 293 cells in considerable amounts, whereas GST-ATG13<sup>2AAAΔ</sup> and GST-ATG13<sup>3AAAΔ</sup> only purified minute amounts of GFP-ULK1 or GFP-ULK2, similar to the 57AAAΔ variant (Fig. 1A, middle panels). All GST-ATG13 variants purified similar amounts of RB1CC1, except for the 57AAAΔ variant which revealed slightly reduced binding to RB1CC1 (Fig. 1A, middle panels). In a vice versa approach, the GFP-tagged ULK proteins were immunopurified using GFP-Trap<sup>®</sup> beads. Again, only GST-ATG13 and GST-ATG13<sup>1AAAΔ</sup> revealed strong interaction with GFP-ULK1 and GFP-ULK2, whereas only low amounts of GST-ATG13<sup>2AAAΔ</sup>, GST-ATG13<sup>3AAAΔ</sup>, and GST-ATG13<sup>57AAAΔ</sup> were purified with these 2 proteins (Fig. 1A, right panels). GST-ATG13<sup>F429A,F433A</sup> was clearly purified with GFP-ULK1 but to a lesser extent with GFP-ULK2. In the next step, we investigated whether starvation has an effect on the binding of GFP-ULK1 to the different ATG13 variants. For that, we repeated affinity and immunopurification experiments described above with GST fusion proteins of wild-type ATG13 and ATG13<sup>3AAAΔ</sup>. As a control, we included a C-terminally truncated version of ULK1 which does not interact with ATG13. Again the ATG13<sup>3AAAΔ</sup> variant did not purify GFP-ULK1 and was itself only slightly purified by GFP-ULK1, independent of nutrient supply

(Fig. 1B, middle and right panels). The weak purification of GFP-ULK proteins with 2AAAΔ, 3AAAΔ and 57AAAΔ mutant proteins, and the weak association of these ATG13 variants with GFP-ULKs are probably caused by the heterodimerization of overexpressed GST-ATG13 variants with endogenous ATG13 since ATG13 has been suggested to form dimers.<sup>3</sup> Indeed, endogenous ATG13 can be detected in GFP-ULK1 immunopurifications (Fig. 1B, right panels). Similarly, RB1CC1 was purified with GFP-ULK1/2 (Fig. 1A and B, right panels), further supporting the presence of endogenous ATG13 (although we could not exclude a direct interaction between ULK1/2 and RB1CC1 at this stage, see below). In order to avoid potential heterodimerization of endogenous ATG13 with overexpressed GST-ATG13 variants, we employed GFP-ULK1-expressing *atg13*<sup>-/-</sup> (*Atg13* knockout [KO]) murine embryonic fibroblasts (MEFs),<sup>14</sup> that were reconstituted with either HA-tagged full-length ATG13 or the corresponding 3AAAΔ deletion mutant. In accordance with our observations previously described, GFP-ULK1 associated with full-length ATG13, but not with ATG13<sup>3AAAΔ</sup> (Fig. 1C). Finally, we reconstituted the *Atg13* KO MEFs with different ATG13 variants and analyzed their interaction with endogenous ULK1. Again only wild-type ATG13, ATG13<sup>1AAAΔ</sup> and ATG13<sup>F429A,F433A</sup> associated with endogenous ULK1, and again this interaction was not affected by nutrient supply. In contrast, ATG13<sup>2AAAΔ</sup>, ATG13<sup>3AAAΔ</sup>, and ATG13<sup>57AAAΔ</sup> did not interact with ULK1. The abolished interaction between ULK1 and ATG13<sup>3AAAΔ</sup> was also confirmed by a mass spectrometry-based SILAC approach (Fig. S1). Since the ATG13<sup>2AAAΔ</sup> and the ATG13<sup>3AAAΔ</sup> variants retained normal RB1CC1 binding but no ULK1 binding, it is unlikely that the direct association of ULK1 with RB1CC1 plays a prominent role during the assembly of the heterotetrameric complex. This was also confirmed by the observation that ULK1 was not coimmunopurified with RB1CC1 from

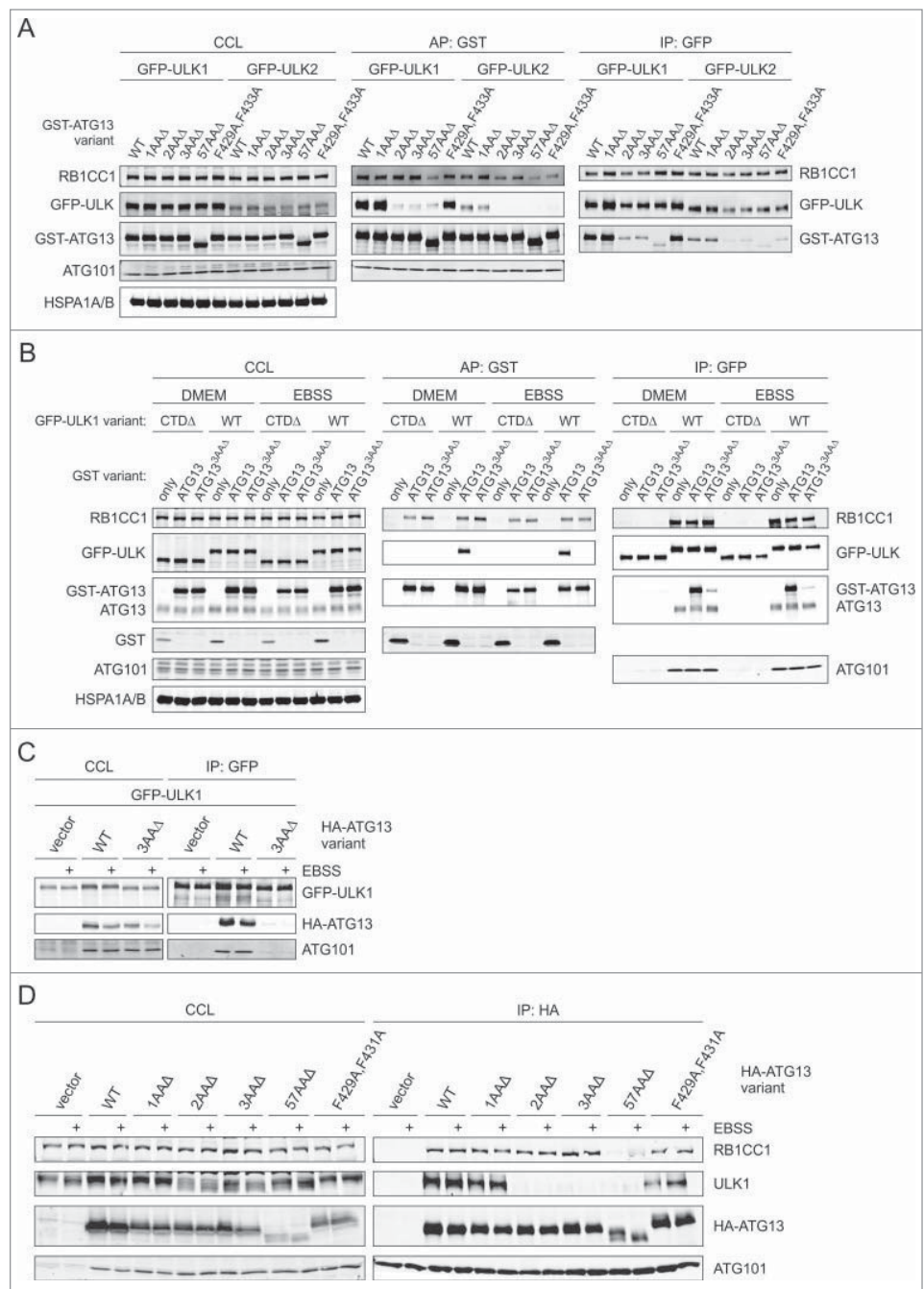


**Figure 1.** For figure legend, see page 1474.

lysates derived from *Atg13* KO MEFs (Fig. S2A). Similarly, a direct interaction between ATG101 and ULK1 was not detectable in *Atg13* KO MEFs (Fig. S2B). Collectively, these data indicate that the interaction between ULK1/2 and ATG13 is mainly controlled by the last 2 amino acids LQ480 of ATG13. Although the ATG13 amino acid sequence shows only weak conservation among species (Fig. S3A), the C-terminal TLQ motif is extremely conserved in vertebrates (Fig. S3B).

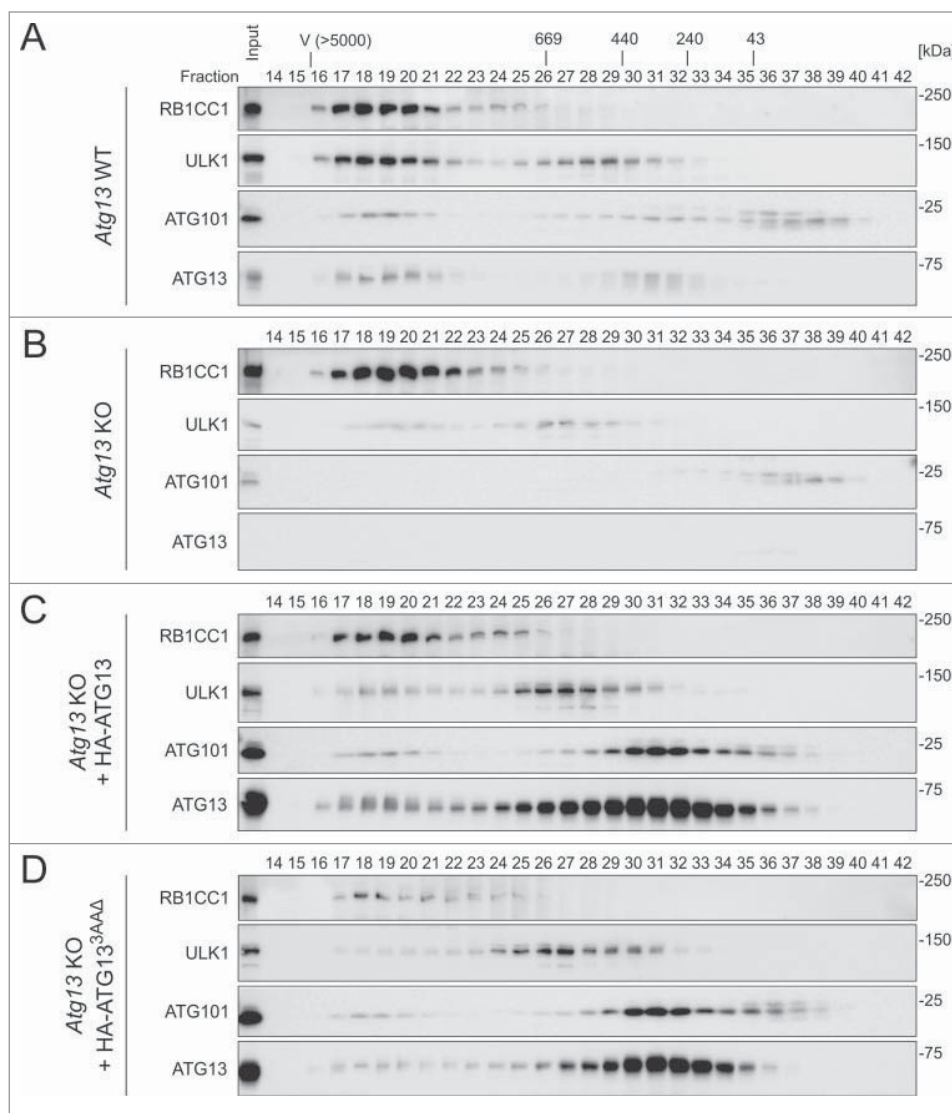


**Figure 2.** The TLQ480 motif of ATG13 is required for recruitment of ULK1 to the autophagy-regulating complex and the phagophore assembly site. (A to D) S100 fractions of wild-type, *Atg13* KO or *Atg13* KO MEFs reconstituted with either HA-ATG13 or HA-ATG13<sup>3AAAΔ</sup> were separated by size exclusion chromatography on a Superose 6 column. Each fraction was analyzed by immunoblotting with anti-RB1CC1, anti-ULK1, anti-ATG101 and anti-ATG13 antibodies. Positions of the molecular mass standards (in kDa) are shown at the top. V, void fraction.

complex in cells expressing the ULK1/2 binding-deficient ATG13<sup>3AAAΔ</sup> variant. We deliberately chose the 3AAAΔ variant for this and the following experiments, since it apparently cannot bind ULK proteins similar to the 2AAAΔ variant, but additionally lacks the putative phospho-acceptor Thr478. To analyze ULK1 recruitment, S100 fractions of wild-type, *Atg13* KO, and *Atg13* KO MEFs reconstituted with either full-length HA-ATG13 or HA-ATG13<sup>3AAAΔ</sup> were subjected to size exclusion chromatography. For wild-type MEFs, RB1CC1, ULK1, ATG13, and ATG101 were mainly detected in fractions corresponding to a molecular mass of ~3 MDa (Fig. 2A) as previously reported.<sup>3-5</sup> ULK1, ATG13

### The incorporation of ULK1 into the autophagy-initiating complex is mediated by a short peptide motif of ATG13

Next, we were interested whether ULK1 is still recruited to the previously described macromolecular autophagy-initiating

and ATG101 were also eluted in fractions according to lower molecular mass complexes of ~300 to 600 kDa (ULK1), 200 to 400 kDa (ATG13 and ATG101), and <40 kDa (ATG101), confirming previous observations.<sup>4,5</sup> In the absence of ATG13,

**Figure 1 (See previous page).** The last 2 amino acids (LQ480) of ATG13 mediate interaction with ULK1/2. (A) Flp-In<sup>TM</sup> T-REx<sup>TM</sup> 293 cells inducibly expressing GFP-tagged full-length ULK1 (GFP-ULK1) or full-length ULK2 (GFP-ULK2) were transiently transfected with vectors encoding GST-ATG13 (WT), GST-ATG13<sup>1AAAΔ</sup> (1AAAΔ), GST-ATG13<sup>2AAAΔ</sup> (2AAAΔ), GST-ATG13<sup>3AAAΔ</sup> (3AAAΔ), GST-ATG13<sup>57AAAΔ</sup> (57AAAΔ) or GST-ATG13<sup>F429A,F433A</sup> 12 h before expression of GFP-ULK variants was induced by doxycycline. After 6 h of GFP-ULK induction, cells were lysed and GST affinity purifications (middle panels) or GFP immunoprecipitations (right panels) were performed. Cleared cellular lysates (CCL) and purified proteins were subjected to SDS-PAGE and analyzed by immunoblotting for RB1CC1, GFP, GST, ATG101, or HSPA1A/B. (B) Flp-In<sup>TM</sup> T-REx<sup>TM</sup> 293 cells inducibly expressing GFP-tagged ULK1 lacking the C-terminal domain (CTDΔ) or full-length ULK1 (WT) were transiently transfected with vectors encoding GST (only), GST-ATG13 (ATG13) or GST-ATG13<sup>3AAAΔ</sup> (ATG13<sup>3AAAΔ</sup>) 12 h before expression of GFP-ULK variants was induced by doxycycline. After 4 h of GFP-ULK induction, cells were cultured in regular medium or starvation medium (EBSS) for 2 h. Cells were lysed and GST affinity purifications (middle panels) or GFP immunoprecipitations (right panels) were performed. Cleared cellular lysates (CCL) and purified proteins were subjected to SDS-PAGE and analyzed by immunoblotting for RB1CC1, GFP, ATG13, GST, ATG101, or HSPA1A/B. (C) GFP-ULK1-expressing *Atg13* KO MEFs retrovirally transfected with empty vector or cDNA encoding HA-ATG13 (WT) or HA-ATG13<sup>3AAAΔ</sup> (3AAAΔ) were cultured in regular medium or starvation medium (EBSS) for 2 h. Cells were lysed and GFP-immunoprecipitations were performed. CCLs and purified proteins were subjected to SDS-PAGE and analyzed by immunoblotting for ULK1, ATG13, or ATG101. (D) *Atg13* KO MEFs retrovirally transfected with empty vector or cDNA encoding HA-ATG13 (WT), HA-ATG13<sup>1AAAΔ</sup> (1AAAΔ), HA-ATG13<sup>2AAAΔ</sup> (2AAAΔ), HA-ATG13<sup>3AAAΔ</sup> (3AAAΔ), HA-ATG13<sup>57AAAΔ</sup> (57AAAΔ) or HA-ATG13<sup>F429A,F433A</sup> were cultured in regular medium or starvation medium (EBSS) for 2 h. Cells were lysed and HA-immunoprecipitations were performed. CCLs and purified proteins were subjected to SDS-PAGE and analyzed by immunoblotting for RB1CC1, ULK1, ATG13, or ATG101.

ULK1 and ATG101 overall levels are decreased and predominantly present in low molecular fractions, i.e. ~300 to 600 kDa for ULK1 and <40 kDa for ATG101 (Fig. 2B). This indicates that ATG13 is essential for the recruitment of ULK1 and ATG101 to the high molecular mass complex established by RB1CC1. Again confirming previous results, the distribution of RB1CC1 is not affected by the absence of ATG13.<sup>4,5</sup> The size exclusion chromatography pattern of *Atg13* KO MEFs reconstituted with HA-tagged full-length ATG13 generally resembles the one observed for wild-type MEFs (Fig. 2C). Furthermore, the overall protein levels of ULK1 and ATG101 are normalized or even increased compared to the levels in wild-type or *Atg13* KO MEFs, which is probably caused by the stabilizing effects of ATG13.<sup>3-5,7</sup> Since ATG13 protein levels are higher in this reconstituted cell line than in wild-type MEFs, the main portion of ATG13—and thus the main portions of ULK1 and ATG101—are present in fractions corresponding to 200 to 500 kDa, and only small amounts are incorporated in the high molecular mass complex. Nevertheless, all 3 proteins and RB1CC1 are present in fractions corresponding to the ~3 MDa complex. For the *Atg13* KO MEFs reconstituted with HA-ATG13<sup>3AAA</sup>, only ATG101 was shifted to fractions corresponding to the ~3 MDa complex, while ULK1 largely remained in fractions comprising lower molecular mass complexes of ~300 to 600 kDa (Fig. 2D). To confirm the importance of the TLQ-motif for ULK1 recruitment by an independent approach, we transfected the cells described above with cDNA encoding GFP-ULK1 and analyzed starvation-induced formation of GFP-ULK1 puncta. The number of GFP-ULK1 puncta per cell was significantly reduced in cells either lacking ATG13 or expressing the ULK1 binding-deficient variants 3AAAΔ or 57AAAΔ (Fig. 3). Furthermore, colocalization of GFP-ULK1 and HA-ATG13 was only observed for wild-type ATG13 and almost completely absent in the 3AAAΔ or 57AAAΔ versions. Collectively, these results indicate that the interaction of ATG13 with ULK1 and the recruitment of ULK1 to the autophagy-initiating complex are dependent on the last 3 amino acids of ATG13. Deletion of this TLQ480 motif is sufficient to exclude ULK1 from the complex and to impair recruitment of ULK1 to the phagophore assembly site (PAS).

**The direct interaction of ATG13 and ULK1 and the recruitment of ULK1 to the autophagy-initiating complex are not necessarily required for autophagy**

Next we addressed the question of whether the presence of ULK1 within the ~3 MDa complex is essential for autophagy induction upon starvation. For this purpose, we stably transfected differently reconstituted *Atg13* KO MEFs with cDNA encoding mCitrine-MAP1LC3/LC3 and analyzed lysosomal degradation of mCitrine-LC3 upon starvation by flow cytometry. In wild-type MEFs and *Atg13* KO MEFs reconstituted with wild-type HA-ATG13, HA-ATG13<sup>1AAA</sup>, or HA-ATG13<sup>F429A,F433A</sup> incubation in EBSS resulted in strong lysosome-dependent degradation of mCitrine-LC3, which in turn was blocked by addition of bafilomycin A<sub>1</sub> (Fig. 4A). In contrast, EBSS-induced degradation of mCitrine-LC3 did not occur in *Atg13* KO MEFs. Of note, in MEFs expressing HA-ATG13<sup>2AAA</sup>, HA-

ATG13<sup>3AAA</sup>, or HA-ATG13<sup>57AAA</sup> the autophagic degradation of mCitrine-LC3 was clearly reduced, but not completely absent (Fig. 4A). Generally, these observations confirmed previous results establishing the importance of the ULK1/2-ATG13 interaction for autophagy induction<sup>3,4,6,7</sup> but apparently some autophagic activity remains even in the absence of this interaction. We also investigated LC3B turnover in *Atg13* KO MEFs transfected with empty vector or cDNA encoding either full-length HA-ATG13 or HA-ATG13<sup>3AAA</sup> by immunoblotting. LC3B-I and -II levels remained unaltered in control-transfected *Atg13* KO MEFs upon EBSS treatment (Fig. 4B). Interestingly, autophagy was induced in both HA-ATG13- and HA-ATG13<sup>3AAA</sup>-expressing cells as detected by increased LC3B-II levels in EBSS/bafilomycin A<sub>1</sub>-treated cells compared to DMEM-bafilomycin A<sub>1</sub>-treated cells (Fig. 4B). Similar observations were made for SQSTM1/p62, which bridges LC3 and ubiquitinated substrates and thus serves as readout for autophagic degradation.<sup>24</sup> SQSTM1 accumulation observed in *Atg13* KO MEFs was absent in both HA-ATG13- and HA-ATG13<sup>3AAA</sup>-expressing MEFs (Fig. 4B). Furthermore, ULK1 stabilization was evident only in HA-ATG13-expressing cells, whereas *Atg13* KO and HA-ATG13<sup>3AAA</sup>-expressing MEFs depicted clearly reduced ULK1 levels (Fig. 4B). In turn, ATG101 was stabilized by both ATG13 variants (Fig. 4B). These ATG13-dependent effects on ULK1 and ATG101 expression levels were already apparent in the size exclusion analyses described above (Fig. 2). We also analyzed phosphorylation of ATG13 Ser318, which has been previously identified as ULK1-dependent phospho-acceptor site during mitophagy.<sup>25</sup> While we observed a clear increase in Ser318 phosphorylation in HA-ATG13-expressing cells upon EBSS treatment, this was not the case in cells expressing the ULK1 binding-deficient HA-ATG13<sup>3AAA</sup> variant (Fig. 4B). This data suggest that 1) a direct interaction between ULK1 and ATG13 is necessary for Ser318 phosphorylation and 2) phosphorylation of this site is not absolutely required for starvation-induced autophagy. The latter was confirmed by expression of a Ser318-to-Ala (S318A) ATG13 mutant in *Atg13* KO MEFs, which mounts a normal autophagic response (data not shown). In summary, the mCitrine-LC3 degradation assay clearly supported the importance of the ULK1-ATG13 interaction for starvation-induced autophagy. However, both the mCitrine-LC3 degradation assay and the LC3 turnover assay suggest that the ULK1 binding-deficient ATG13 variants can at least partially restore autophagic activity. To further elucidate this latter aspect, we performed immunofluorescence of endogenous LC3B and SQSTM1 (Fig. 5). *Atg13* KO MEFs showed almost no increased LC3B puncta formation upon starvation and bafilomycin A<sub>1</sub> treatment (Fig. 5A, upper panels). MEFs reconstituted with full-length HA-ATG13 showed formation of LC3B-positive structures upon starvation, which could be further increased by addition of bafilomycin A<sub>1</sub> (Fig. 5A, middle panels). HA-ATG13<sup>3AAA</sup>-expressing MEFs revealed a similar tendency, although overall LC3 puncta numbers were reduced in cells incubated in DMEM or EBSS compared to full-length ATG13-expressing MEFs (Fig. 5A, lower panels). Again, analogous observations were made for SQSTM1. *Atg13* KO MEFs did not show a prominent

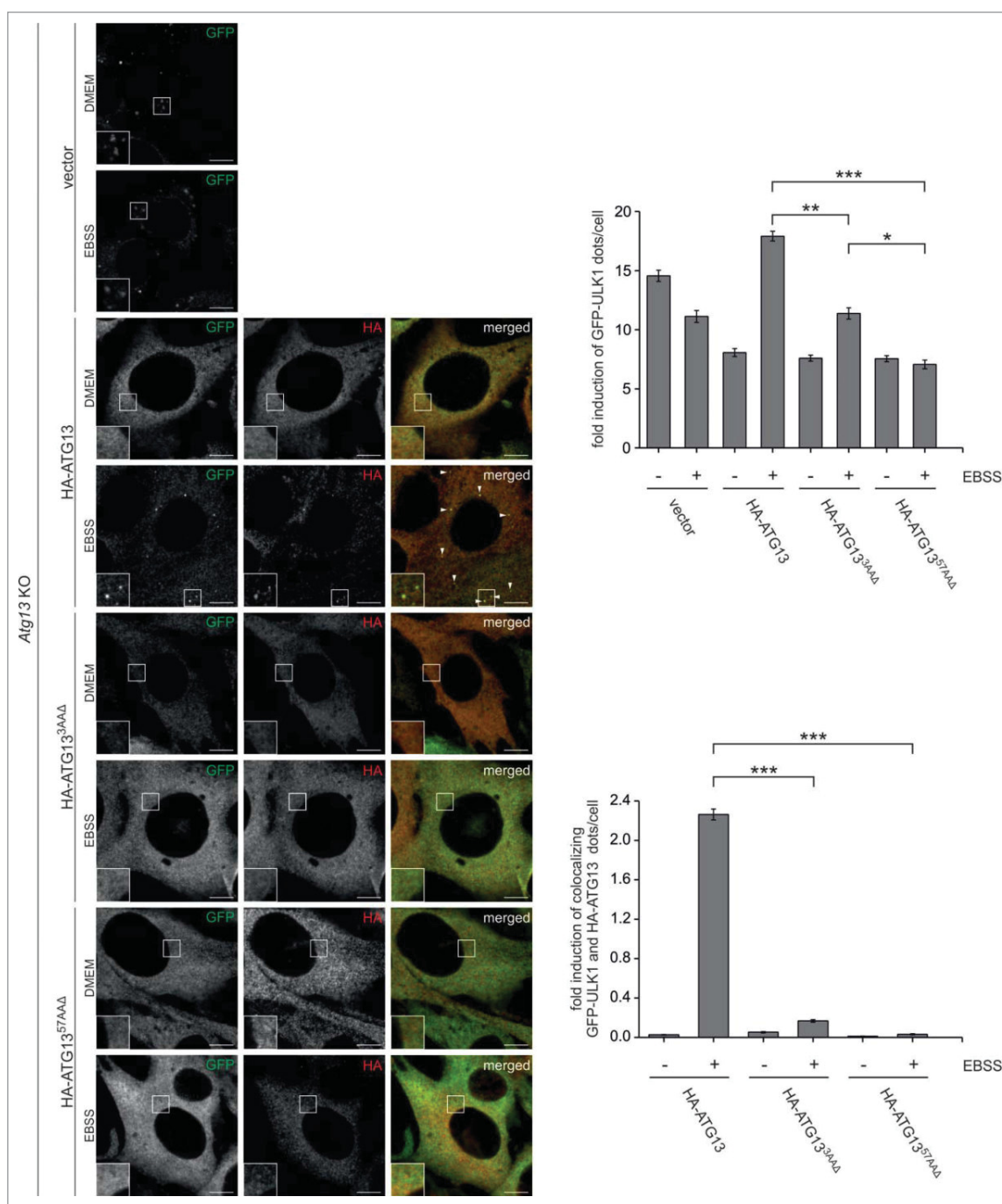


**Figure 3.** ULK1 does not localize with ULK1 binding-deficient variants of ATG13. GFP-ULK1-expressing *Atg13* KO MEFs retrovirally transfected with empty vector or cDNA encoding HA-ATG13, HA-ATG13<sup>3AAA</sup> or HA-ATG13<sup>57AAA</sup> were cultured in regular medium or starvation medium (EBSS) for 2 h. Cells were fixed and analyzed by immunofluorescence microscopy using anti-GFP and anti-HA antibodies. Scale bar: 10  $\mu$ m. The number of GFP-ULK1 dots and colocalization of GFP-ULK1 and HA-ATG13 dots were quantified from at least 220 cells using Fiji software and data represent mean  $\pm$  SEM. \* $P$  < 0.05, \*\* $P$  < 0.01, \*\*\* $P$  < 0.001 (Student *t* test, 2-sample assuming unequal variances).

increase in SQSTM1-positive structures upon EBSS treatment in the presence of bafilomycin A<sub>1</sub>, whereas this was clearly the case for both cell lines expressing the 2 different ATG13 variants (Fig. 5B). In order to more robustly analyze the autophagic flux, we generated cell lines stably expressing the tandem fluorescent

mRFP-EGFP-LC3B chimeric protein for the detection of early and late autophagic activity.<sup>26</sup> In *Atg13* KO MEFs, only mRFP-EGFP-double-positive structures, which may represent protein aggregates generated under autophagy-deficient conditions, were detectable upon starvation for 2 h, whereas both reconstituted

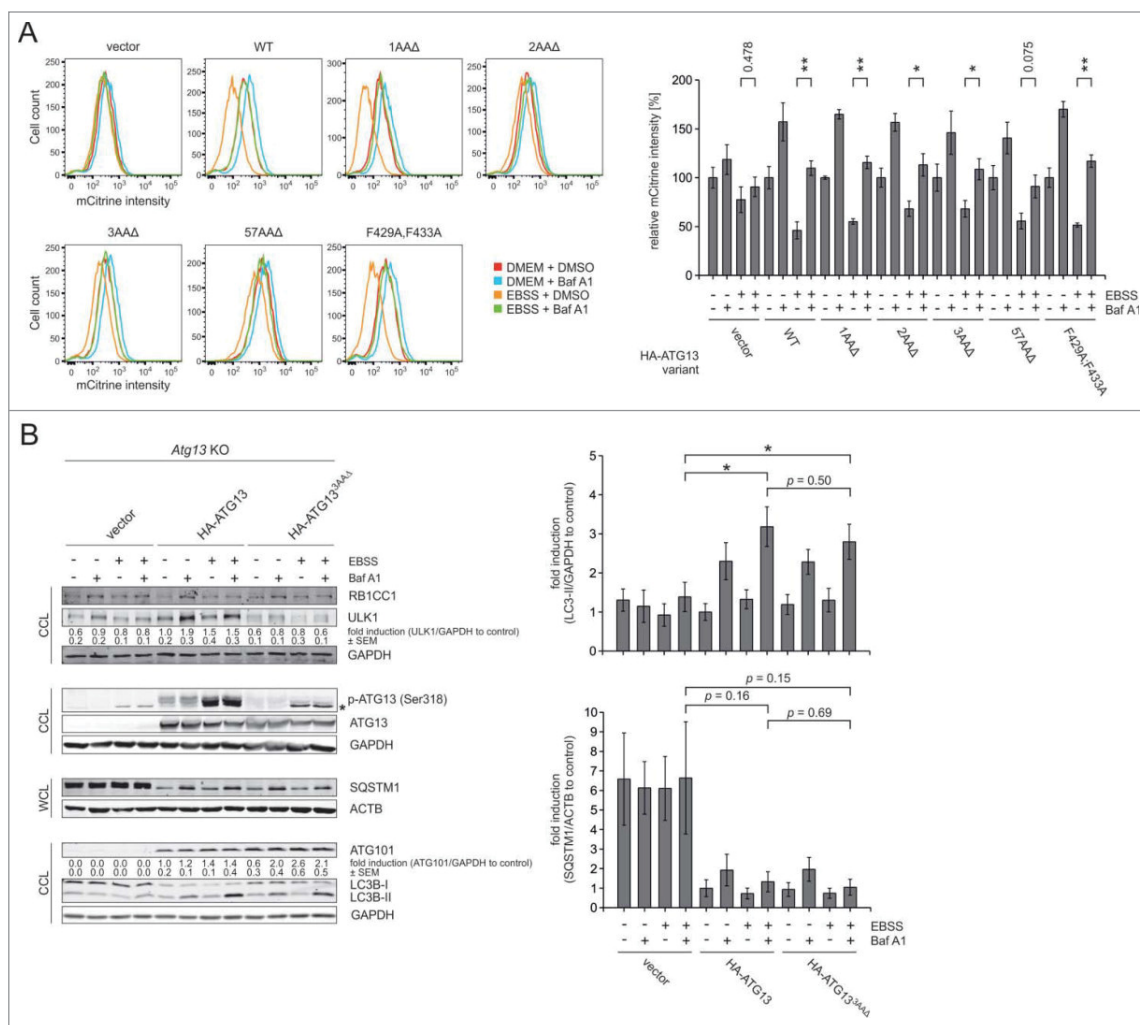


**Figure 4.** ATG13<sup>3AAΔ</sup> supports mCitrine-LC3 degradation in *Atg13* KO MEFs but does not support ULK1 stabilization. **(A)** MEFs stably expressing mCitrine-LC3 and the indicated ATG13 variants were cultured in regular medium or starvation medium (EBSS) with or without 40 nM baflomycin A<sub>1</sub> (Baf A1) for 10 h. Total cellular mCitrine-LC3 signals were analyzed by flow cytometry. Cell debris was eliminated by gating. Representative FACS data from 3 independent experiments is shown in the panels. The median of fluorescence intensity was plotted in a bar diagram. Values are expressed as a percentage of the mean of cells cultured in regular medium. Data represent mean ± SEM. \**P* < 0.05, \*\**P* < 0.01 (Student *t* test, 2-sample assuming unequal variances). **(B)** *Atg13* KO MEFs retrovirally transfected with empty vector or cDNA encoding HA-ATG13 or HA-ATG13<sup>3AAΔ</sup> were incubated in culture medium (DMEM) or starvation medium (EBSS) in the presence or absence of 40 nM baflomycin A<sub>1</sub> for 2 h. Cells were lysed and lysates (either cleared cellular lysates, CCL, or whole cellular lysates, WCL) were subjected to immunoblotting for RB1CC1, ULK1, phospho-ATG13 (Ser318), ATG13, SQSTM1/p62, ATG101, LC3B, ACTB, and GAPDH. Asterisk indicates a nonspecific background band. Data shown are representative of at least 3 independent experiments. Fold changes were calculated by dividing each normalized ratio (protein to loading control) by the average of the ratios of the control lane (HA-ATG13 + DMEM, *n* ≥ 3). Results are mean ± SEM and are given below the corresponding blots (ULK1 and ATG101) or are plotted as bar diagram (LC3-II and SQSTM1/p62). \**P* < 0.05, \*\**P* < 0.01 (Student *t* test, 2-sample assuming unequal variances).

MEF cell lines revealed mRFP-single-positive structures presumably representing autolysosomes (Fig. 6A). Finally, we performed a long-lived protein degradation assay. Although statistically not significant, it again appeared that the ATG13<sup>3AAΔ</sup> variant can partially compensate the autophagy-defective phenotype of *Atg13* KO MEFs (Fig. 6B).

In the past, several noncanonical autophagy signaling pathways have been proposed, including ULK1/2-, BECN1/VPS30-PIK3C3/VPS34- and ATG5-ATG7-independent processes.<sup>20,27,28</sup> Since the majority of our autophagy readouts were based on LC3

lipidation, we can exclude ATG5-ATG7-independent effects. However, we investigated whether the partial restoration of autophagy observed for ATG13<sup>3AAΔ</sup>-expressing MEFs depends on ULK1/2 or the PtdIns3K class III complex. The observation that autophagic flux can partially be restored independent of the ULK1-ATG13 interaction does not necessarily imply that the process is ULK1/2-independent. We performed *Ulk1/2* RNAi experiments in *Atg13* KO MEFs transfected with empty vector or cDNA encoding either full-length HA-ATG13 or HA-ATG13<sup>3AAΔ</sup> and analyzed LC3 turnover by immunoblotting (Fig. S4A). However,

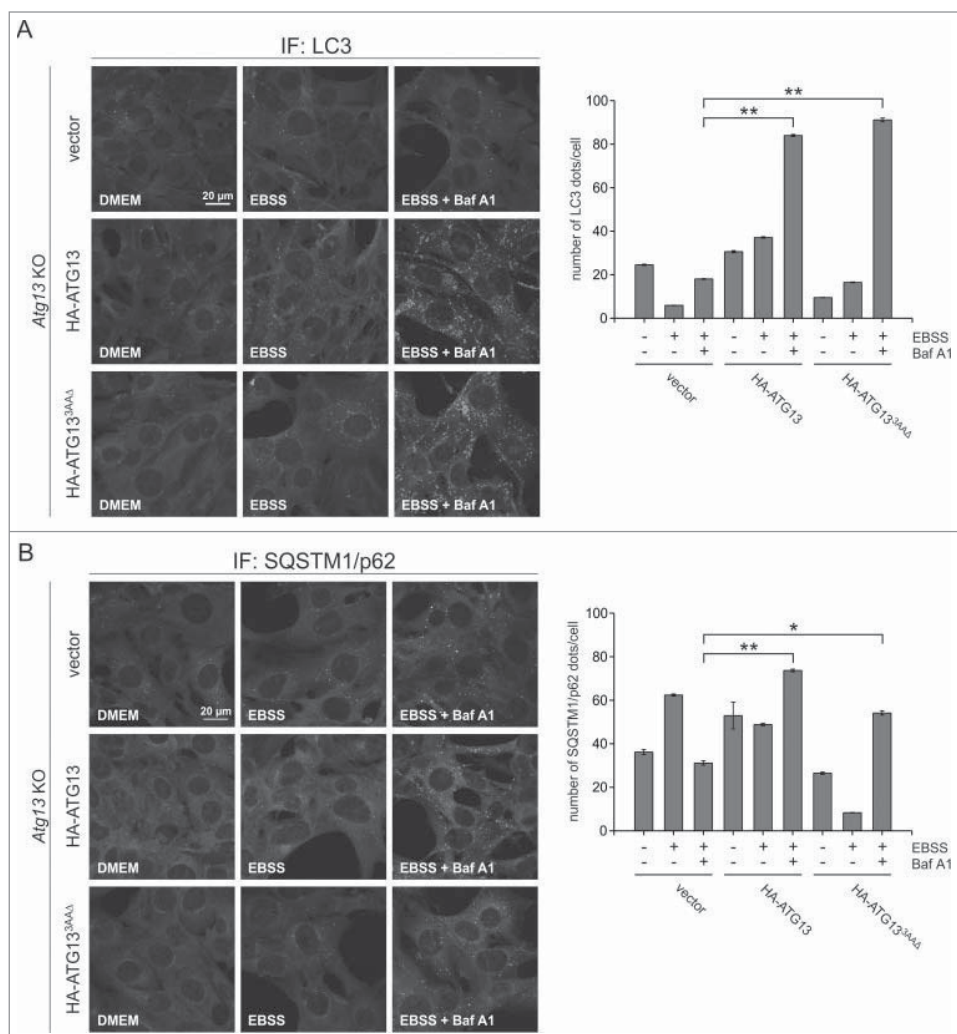


**Figure 5.** ATG13<sup>3AAΔ</sup> supports starvation-induced accumulation of LC3 and SQSTM1/p62 puncta in the presence of bafilomycin A<sub>1</sub> in *Atg13* KO MEFs. **(A and B)** *Atg13* KO MEFs retrovirally transfected with empty vector or cDNA encoding full-length HA-ATG13 or HA-ATG13<sup>3AAΔ</sup> were grown on glass coverslips for 24 h and then incubated in culture medium (DMEM) or starvation medium (EBSS) in the presence or absence of 40 nM bafilomycin A<sub>1</sub> for 2 h. Cells were fixed and LC3B **(A)** or SQSTM1/p62 **(B)** were detected by confocal laser-scanning microscopy. Fiji software was used to process and count the puncta. At least 505 cells were scored for each condition. Data represent mean ± SEM. \**P* < 0.05, \*\**P* < 0.01 (Student *t* test, 2-sample assuming unequal variances).

from these results, it is difficult to interpret the relevance of ULK1. This is in line with observations made in *Ulk1/2* DKO MEFs, in which LC3-II levels clearly increase upon starvation (ref.<sup>29</sup> and own observation). With regard to the PtdIns3K class III complex, we pursued 2 approaches. First we used *Becn1* siRNA similar to the experiments described above (Fig. S4B). Since BECN1 knock-down efficiency appeared to be insufficient, we employed the PtdIns3K class III inhibitor 3-methyladenine (3-MA). 3-MA blocked autophagy in both HA-ATG13- or HA-ATG13<sup>3AAΔ</sup>-expressing MEFs (Fig. S4C), indicating that PtdIns3K class III activity is important for the observed phenomenon.

Taken together, our results suggest that autophagy induction depends on the interaction between ULK1/2 and ATG13—

which is mediated by a short C-terminal motif of ATG13—but that autophagic capacity can be partially restored by the ULK1/2 binding-deficient variant of ATG13. Apparently, this remaining autophagic competence depends on the core autophagy signaling machinery, i.e. the PtdIns3K class III complex and the LC3-conjugation system.

## Discussion

The mammalian ULK1/2-ATG13-RB1CC1-ATG101 complex is essential for the initiating steps of autophagy. In recent years, the molecular details of how this complex regulates autophagy have been deciphered. It is generally accepted that the complex is constitutively assembled, independently of nutrient supply. It has been proposed that the proautophagic activity of the ULK1/2 complex is mainly controlled by the upstream kinases MTOR, PRKA/AMPK, or AKT. Here, we identified a short ULK1/2 binding motif at the C terminus of ATG13, which is composed of the last 3 amino acids TLQ480. Furthermore, we demonstrated that this motif is essential for the recruitment of ULK1 into the autophagy-regulating complex and to the PAS. Although lysosomal degradation of mCitricine-LC3 was slightly compromised in cells expressing the C-terminal truncated version of ATG13, we

surprisingly observed that the direct association of ULK1/2 with ATG13 is not absolutely required to support the induction of autophagy.

Our data reveal that the last 3 amino acids of ATG13 represent or at least contribute to the core interaction site for ULK1/2. Thus, we clearly fine-mapped the ULK1-interaction site, which has been previously mapped to amino acids 384 to 517 (amino acid numbering of human isoform 1; corresponds to amino acids 347 to 480 of human isoform 2).<sup>7</sup> In our view, there exist 2 possibilities how the last 3 amino acids of ATG13 might mediate ULK1/2 binding: 1) these amino acids represent the direct binding site for ULK1/2, or 2) these amino acids are structurally relevant for the ULK1/2 binding site. With regard to the first

possibility, short peptide motifs at the C terminus of proteins are bound by PDZ (postsynaptic density 95, PSD-95; discs large, Dlg; zonula occludens-1, ZO-1) domains.<sup>30-32</sup> Of note, it has been proposed that ULK1 itself harbors a PDZ binding motif at its C terminus.<sup>6,33,34</sup> However, the C terminus of ULK1 is not very conserved across species, and the reported YVA motif in murine ULK1 cannot be found in human ULK1. In contrast, the TLQ480 motif of ATG13 is highly conserved across vertebrate species (including *H. sapiens*, *M. musculus*, *G. gallus*, *F. catus*, *C. familiaris*, *B. taurus*, *D. rerio*), resembles a class I PDZ domain ligand,<sup>30,32,35</sup> and binding specificity might be regulated by phosphorylation of Thr478. Indeed, we have previously proposed that Thr478 might be a ULK1-dependent phospho-acceptor site.<sup>9</sup> However, mutation of Thr478 to either phospho-deficient alanine or phospho-mimicking glutamic acid did not modulate ULK1 binding (data not shown). Furthermore, ULK1/2 has not been characterized as PDZ-domain-containing protein so far. Nevertheless, it is tempting to speculate that the C-terminal peptide motif of ATG13 represents a PDZ-domain binding ligand. Alternatively, the last 3 amino acids are structurally important for the ULK1/2 binding site. Fujioka et al. have reported the X-ray crystallographic analysis of the interaction of yeast Atg13 with Atg1 and Atg17.<sup>23</sup> Atg13 binds tandem microtubule interacting and transport (tMIT) domains in Atg1 via a 2-part MIT-interacting motif. These Atg1 binding regions in Atg13 have been recently confirmed by hydrogen-deuterium exchange coupled to mass spectrometry.<sup>36</sup> Fujioka et al. suggest that the MIT-MIM interaction is conserved in mammals, and ULK1 was purified by a GST fusion protein comprising the last 60 amino acids of ATG13. According to the authors, the C-terminal half of the MIM domain is established by the amino acids of the

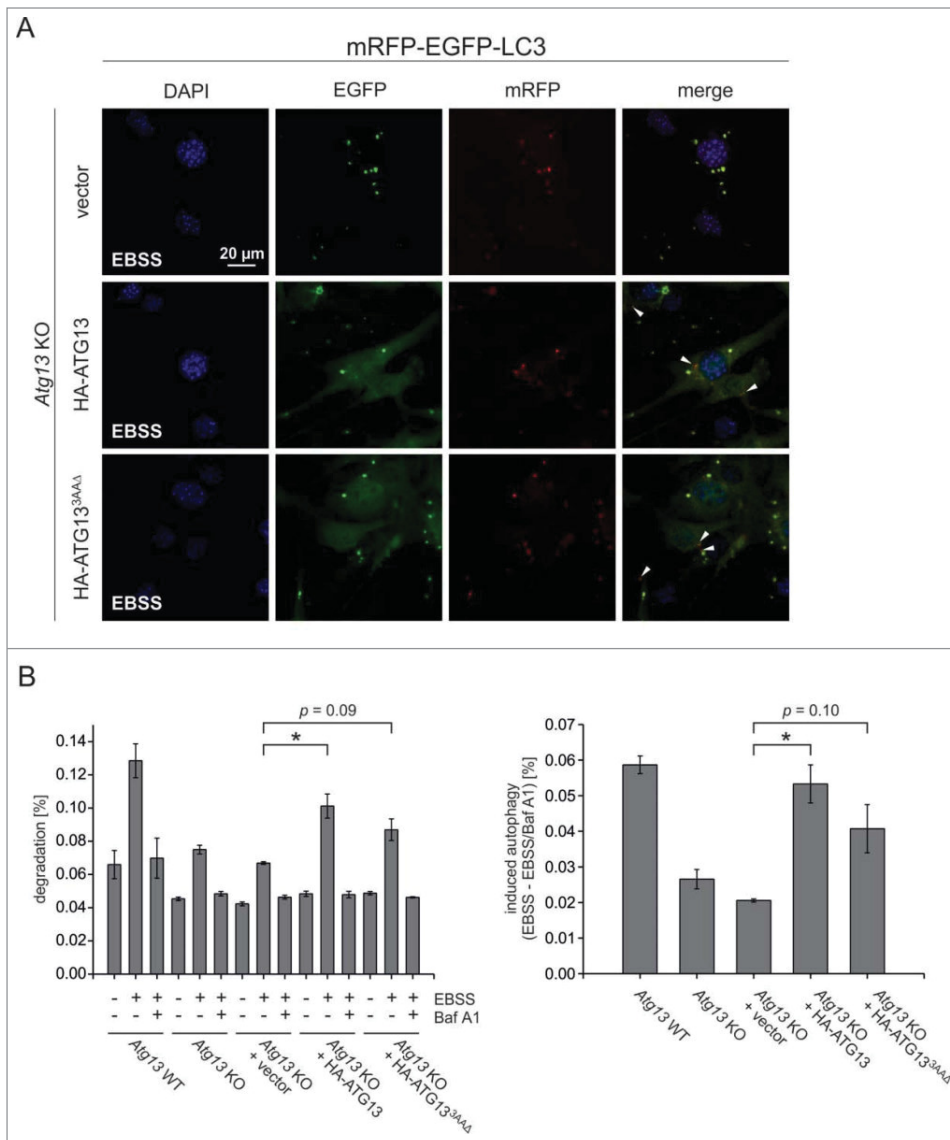


**Figure 6.** ATG13<sup>3AAΔ</sup> can partially restore autophagic flux in *Atg13* KO MEFs and supports long-lived protein degradation. (A) *Atg13* KO MEFs retrovirally transfected with empty vector or cDNA encoding full-length HA-ATG13 or HA-ATG13<sup>3AAΔ</sup> were additionally retrovirally transfected with pMSCVblast/mRFP-EGFP-rLC3. Cells were incubated in starvation medium (EBSS) for 2 h, fixed, and analyzed by confocal laser scanning microscopy. Autolysosomes are indicated by white arrow heads. (B) Cellular proteins of the indicated MEF cells were labeled with L-[<sup>14</sup>C]valine as described in the Materials and Methods section. Cells were washed and treated with the indicated medium (control or EBSS ± Baf A1) for 4 h. For each sample, the radioactivity of the acid-soluble fraction of the medium and the radioactivity in the cells remaining in the well were measured. Percent degradation was assessed as the acid-soluble radioactivity of the medium divided by the total radioactivity (left diagram). Additionally, induction of autophagy was assessed by subtracting percent degradation of EBSS/Baf A1-treated cells from percent degradation of EBSS-treated cells (right diagram). Data shown are mean of triplicates of averaged duplicates ± SEM; \**P* < 0.05 (Student *t* test, 2-sample assuming unequal variances).

ATG13 C terminus.<sup>23</sup> Thus, it is also feasible that the deletion of the TLQ480 motif disrupts the structure of the MIM domain, ultimately abolishing the interaction with ULK1. Fujioka et al. suggest that Phe429 and Phe433 are part of the N-terminal half of the MIM domain of the mammalian ATG13. However,

mutation of these 2 phenylalanine residues to alanine did not impair ATG13 function in our analyses. Collectively, future experiments and structural analyses will have to reveal the existence of a MIM domain in mammalian ATG13 and the exact function of the TLQ480 motif.

In the recent past, several ULK1-interacting partners have been identified which might contribute to the recruitment of ULK1 to the PAS. For example, it has been suggested that ULK1 might interact directly with RB1CC1.<sup>3</sup> The authors used recombinant proteins in an in vitro binding assay. In contrast, Jung et al. and Hosokawa et al. see a prominent dependency on ATG13 for the ULK1-RB1CC1 interaction,<sup>4,7</sup> which corresponds to our observations. The ATG13<sup>3AAA</sup> protein retains normal RB1CC1 binding, but ULK1 cannot be purified by affinity purification or immunopurification with this truncated protein. Furthermore, ULK1 and RB1CC1 cannot be coimmunopurified from lysates of *Atg13* KO MEFs. The same holds true for a potential interaction between ULK1 and ATG101, which has been suggested for the *C. elegans* orthologs UNC-51/ATG-1 and EPG-9/ATG-101.<sup>37</sup> Whereas these results might be explained by our cell lysis conditions (0.3% CHAPS), we additionally showed 1) by size exclusion chromatography that ULK1 is not part of the high molecular mass complex in HA-ATG13<sup>3AAA</sup>-expressing MEFs and 2) by confocal microscopy that GFP-ULK1 is not efficiently recruited to the PAS in these MEFs. Collectively, our data do not support the hypothesis that ULK1 is recruited to the PAS in general and to the high molecular mass complex in particular via direct interaction with RB1CC1 or ATG101, respectively. Similarly, we assume that previously reported alternative “PAS recruitment options”—i.e. via protein binding to ATG8 proteins or via direct lipid binding—play only a minor role compared to the direct ULK1-ATG13 interaction. Admittedly, we cannot entirely exclude that a transient or low-affinity interaction between ULK1 and ATG13<sup>3AAA</sup> might support autophagy induction. Our affinity/immunopurification experiments and the size exclusion experiments are in vitro approaches and depend on the overexpression of at least one of the 2 components. However, some of our observations clearly show that the association between ULK1 and the ATG13 mutants is severely compromised, e.g. the missing stabilization of ULK1 by ATG13<sup>3AAA</sup> or the absent colocalization of these 2 proteins as detected by immunofluorescence.

We employed different readout methods to analyze autophagy in cells expressing the TLQ-deleted variant of ATG13. Although these assays confirm the importance of the ULK1-ATG13 interaction for autophagy induction, it appears that autophagic activity is at least partially restored in ATG13<sup>3AAA</sup>-expressing cells. Our results likely reflect that starvation-induced autophagy cannot entirely be blocked by the disruption of the ULK1/2-ATG13 interaction. In general, 2 mechanisms might explain the observed restoration of autophagic activity by ATG13<sup>3AAA</sup>: 1) ULK1/2-independent autophagy pathways or 2) ULK1/2-dependent but ULK1/2-ATG13 interaction-independent autophagy pathways. So far, we cannot easily distinguish between these 2 possibilities. It has been previously shown that amino acid starvation-induced autophagy is largely blocked in ULK1/2 double-deficient MEFs,

indicating that this autophagic pathway requires ULK1/2 activity.<sup>20,29</sup> However, McAlpine et al. state that detectable levels of amino acid starvation-induced autophagy in form of LC3 lipidation are still observable following double knockout of ULK1/2.<sup>29</sup> This is in accordance with our own observations (data not shown). Additionally, ULK1/2-independent autophagy has been proposed for other stimuli (i.e. glucose starvation) or other cellular systems (i.e. chicken DT40 B lymphocytes).<sup>9,20</sup> We performed *Ulk1/2* siRNA experiments in ATG13<sup>3AAA</sup>-expressing cells and analyzed LC3 turnover. However, so far we cannot convincingly determine the functional role of ULK1 for the partial autophagic flux. In order to clarify this issue, one approach would be the reconstitution of *Ulk1*, *Ulk2*, and *Atg13* triple-knockout cells with single components. What we can say so far is that the partial autophagic flux in ATG13<sup>3AAA</sup>-expressing cells depends on other conventional autophagy signaling modules, i.e. the BECN1-PIK3C3 complex and the LC3 conjugation system.

Collectively, our data challenge the current view of a constitutively assembled ULK1/2 complex as unequivocal requirement for autophagy induction. Future experiments will have to reveal the relative contribution of pathways dependent or independent of the ULK1/2-ATG13 interaction to autophagy. Furthermore, one might speculate that different (selective) autophagic processes might vary in their dependency on this interaction. Interestingly, Joo et al. reported that mitochondrial damage triggers ULK1 activation and ULK1-dependent phosphorylation of ATG13, which then leads to the release of ATG13 and its translocation to the damaged mitochondria.<sup>25</sup> These data suggest a phosphorylation-dependent regulation of the ULK1-ATG13 interaction during selective autophagy processes. Finally, Kraft et al. report for the yeast orthologs that the autophagy defects of an *Atg1* binding-deficient *Atg13* mutant are less pronounced than the defects of a complete *Atg13* knockout,<sup>38</sup> similarly indicating a differential requirement for this interaction. Although the majority of the relevant components of this autophagy-initiating complex are identified, apparently the molecular dynamics of their interplay are far from being completely understood.

## Materials and Methods

### Antibodies and reagents

Antibodies against ACTB/ $\beta$ -actin (clone AC-74, Sigma-Aldrich, A5316), ATG101 (Sigma-Aldrich, SAB4200175), ATG13 (Sigma-Aldrich, SAB4200100), ATG13 pSer318 (Rockland Immunochemicals, 600-401-C49), GAPDH (clone 6C5, Abcam, ab8245), GFP (Roche, 11814460001, ChromoTek, 3h9, and Nacalai Tesque, 04404-84), GST (GE Healthcare, 27-4577-01), HA (Covance, MMS-101R), HSPA1A/B (BD Transduction Laboratories, 610607), LC3B (Cell Signaling Technology, 2775, and MBL International, PM036), RB1CC1 (Bethyl Laboratories, A301-536A), SQSTM1/p62 (MBL, PM045, and PROGEN Biotechnik, GP62-C), and ULK1 (clone D8H5, Cell Signaling Technology, 8054, or Sigma-Aldrich, A7481) were used. Alternatively, antibodies for ATG101 and RB1CC1 have been previously described.<sup>5,22</sup> IRDye 800- or IRDye 680-

conjugated secondary antibodies were purchased from LI-COR Biosciences (926-32210/11, 926-68070/71, 926-68024 and 926-32214), Alexa Fluor® 488-conjugated goat anti-rat IgG (H<sup>+</sup>L) antibodies and Alexa Fluor® 568-conjugated goat anti-mouse IgG (H<sup>+</sup>L) antibodies from Life Technologies (A-11006 and A-11031), and Alexa Fluor® 647-conjugated goat anti-rabbit IgG (H<sup>+</sup>L) antibodies from Jackson ImmunoResearch Laboratories (111-605-003). Bafilomycin A<sub>1</sub> was obtained from Sigma-Aldrich (B1793). [<sup>14</sup>C]Valine (NEC291EU050UC) was purchased from PerkinElmer.

### Cell lines and cell culture

Wild-type and *Atg13* KO MEFs were kindly provided by Xiaodong Wang.<sup>14</sup> Generation of Flp-In<sup>TM</sup> T-REx<sup>TM</sup> 293 cells inducibly expressing GFP-ULK1 or GFP-ULK1<sup>CTDA</sup> was previously described.<sup>39</sup> The vector pcDNA5/FRT/TO-GFP containing human *ULK2* cDNA was kindly provided by Dario Alessi. This vector was cotransfected with pOG44 (Life Technologies, V6005-20) into Flp-In<sup>TM</sup> T-REx<sup>TM</sup> 293 cells (Life Technologies, R780-07). Stable transfectants were selected with 200 µg/ml hygromycin B (Life Technologies, 10687-010) and 5 µg/ml blasticidin (Life Technologies, A11139-02). MEFs and Flp-In<sup>TM</sup> T-REx<sup>TM</sup> 293 cell lines were cultured in DMEM (4.5 g/l D-glucose) supplemented with 10% FCS, 100 U/ml penicillin and 100 µg/ml streptomycin (PAA Laboratories GmbH, E15-810) in a 5% CO<sub>2</sub> humidified atmosphere at 37°C. For induction of GFP-ULK1/2 expression, Flp-In<sup>TM</sup> T-REx<sup>TM</sup> 293 GFP-ULK1/2 cells were stimulated with 0.1 µg/ml doxycycline (Clontech, 631311) for 4 to 6 h. For starvation treatment, cells were washed with Earle's Balanced Salt Solution (EBSS, Gibco, 24010-043) and incubated in EBSS for the indicated time periods.

### Expression constructs and transfections

pEGB-6P/ATG13 (human isoform 2) and pEGB-6P/3AAA were kindly provided by Dario Alessi (MRC Protein Phosphorylation Unit, College of Life Sciences, University of Dundee, UK). All other pEGB-6P/ATG13 variants were generated by site-directed mutagenesis. Transient transfection of Flp-In<sup>TM</sup> T-REx<sup>TM</sup> 293 cells with pEGB-6P vectors was performed using Lipofectamine<sup>TM</sup> 2000 or Lipofectamine<sup>TM</sup> 3000 (Life Technologies, 11668019 and L3000015). Human cDNAs encoding either HA-tagged full-length ATG13 (isoform 2) or ATG13 mutants were cloned into pMSCVpuro (Clontech Laboratories, Takara Bio, 631461) for retroviral infection of MEFs. pMSCVblast/GFP-ULK1 was generated by cloning *GFP-ULK1* cDNA from pcDNA5/FRT/TO-GFP-ULK1 (previously described in ref. 39) into pMSCVblast, which was generated by replacing the puromycin resistance cassette of pMSCVpuro by a blasticidin resistance cassette amplified from pcDNA<sup>TM</sup>6/TR (Life Technologies, V1025-20). To generate pMSCVblast/mCitrine-LC3 plasmid, the cDNA encoding human LC3 was subcloned into pMSCVblast together with mCitrine. pMSCVblast/mRFP-EGFP-rLC3 expression vector was generated by cloning of *mRFP-EGFP-rLC3* cDNA from pmRFP-EGFP-rLC3 (kindly provided by Tamotsu Yoshimori, Department of Genetics,

Osaka University Graduate School of Medicine, Japan) into pMSCVblast. For the production of recombinant retroviruses, Plat-E cells (kindly provided by Toshio Kitamura, Institute of Medical Science, University of Tokyo, Japan) were transfected with pMSCVpuro- or pMSCVblast-based retroviral vectors using FuGENE® 6 or FuGENE® HD transfection reagent (Roche, 11988387001 and 04709713001). *Atg13* KO MEF cells were incubated with retroviral supernatant fractions containing 3 to 8 µg/ml Polybrene (Sigma-Aldrich, H9268-106) and selected in medium containing 2.5 µg/ml puromycin (InvivoGen, ant-pr-1) or 35 µg/ml blasticidin (InvivoGen, ant-bl-1).

### Affinity and immunopurification and immunoblotting

Cells were lysed in lysis buffer (50 mM Tris-HCl, pH 7.5, 150 mM NaCl, 0.3% [v/v] CHAPS [Carl Roth GmbH + Co. KG, 1479.3] or 1% Triton X-100 [Carl Roth GmbH + Co. KG, 3051.2], 1 mM EDTA, 1 mM EGTA, 1 mM Na<sub>3</sub>VO<sub>4</sub>, 50 mM NaF, 5 mM Na<sub>4</sub>P<sub>2</sub>O<sub>7</sub>, 0.27 M sucrose [Carl Roth GmbH + Co. KG, 4621.1], protease inhibitor cocktail [Sigma-Aldrich, P2714]) for 30 min on ice. Lysates were flash frozen and/or directly clarified by centrifugation at 17,000 *g* for 15 min at 4°C. Equal protein amounts were determined by Bradford method. Alternatively, whole cell lysates were prepared by direct addition of sample buffer (125 mM Tris-HCl, pH 6.8, 17.2% [v/v] glycerol, 4.1% [w/v] SDS [AppliChem GmbH, A7249], 200 µg/ml bromophenol blue, 2% [v/v] β-mercaptoethanol) to the cells and subsequent sonification. Lysates were subjected to 6–15% SDS-PAGE. Proteins were transferred to PVDF membranes (Merck, Millipore, IPFL00010) and immunoblot analysis was performed using the indicated primary antibodies and appropriate IRDye® 800- or IRDye® 680-conjugated secondary antibodies (LI-COR Biosciences). Signals were detected with an Odyssey® Infrared Imaging system (LI-COR Biosciences). For affinity or immunopurification of GST-, GFP- or HA-tagged proteins, clarified lysates were incubated with either glutathione sepharose 4B beads (GE Healthcare, 17-0756-01), GFP-trap® beads (ChromoTek, gta-200) or monoclonal anti-HA agarose beads (clone HA-7, Sigma-Aldrich, A2095) at 4°C for 1.5 to 3 h or overnight with rotation. For immunopurification of untagged proteins, clarified lysates were incubated with corresponding antibodies and protein A and G sepharose (GE Healthcare, 17-5280-01 and 17-0618-01) mixed in equal parts at 4°C overnight. Purified proteins were washed at least 3 times with lysis buffer and analyzed by immunoblotting.

### Size-exclusion chromatography

MEFs were lysed in a hypotonic buffer (40 mM Tris HCl, pH 7.5, and Complete EDTA-free protease inhibitor cocktail [Roche, 0505648900]) by repeated passages (15 times) through a 1-ml syringe with a 27-gauge needle and incubation on ice for 20 min following addition of NaCl to a final concentration of 150 mM. The homogenates were centrifuged at 13,000 × *g* for 15 min, and the supernatant fractions were further centrifuged at 100,000 × *g* for 60 min. The supernatant fractions (S100 fractions) were then filtered with Ultrafree-MC 0.45-µm filter unit (Millipore, UFC30HV00) and applied to a Superose 6 column

(GE Healthcare, 17-5172-01). Subsequently, 0.5-ml fractions were collected at a flow rate of 0.5 ml/min with elution buffer (40 mM Tris-HCl, pH 7.5, 150 mM NaCl). The fractions were then analyzed by immunoblotting. The column was calibrated with thyroglobulin (669 kDa), ferritin (440 kDa), catalase (240 kDa), and ovalbumin (43 kDa).

### Confocal laser scanning microscopy

For immunofluorescent staining of LC3B and SQSTM1/p62, cells were grown on glass coverslips overnight, stimulated as indicated and fixed in 4% formaldehyde solution, following incubation with primary antibodies overnight and secondary antibodies for 1 h in 0.05% saponin (Sigma-Aldrich, 47036) in phosphate-buffered saline (Gibco, 14190-094). Subsequently, cells were stained with 1  $\mu$ g/ml DAPI (Carl Roth GmbH + Co. KG, 6335.1) and embedded in Mowiol 4-88 (Carl Roth GmbH + Co. KG, 0713.1). MEF cells stably expressing mRFP-EGFP-rLC3B were stained with DAPI only. Samples were analyzed on a Leica TCS SP2 confocal laser-scanning microscope (Wetzlar, Germany). For immunofluorescent staining of GFP-ULK1 and HA-ATG13, cells were grown on glass coverslips, stimulated as indicated and fixed in 4% formaldehyde solution, permeabilized with 50  $\mu$ g/ml digitonin (Wako, 043-21376) in phosphate-buffered saline (Gibco, 14200-075), and stained with anti-GFP rat monoclonal antibodies and anti-HA mouse monoclonal antibodies. As secondary antibodies Alexa Fluor<sup>®</sup> 488-conjugated anti-rat IgG and Alexa Fluor<sup>®</sup> 568-conjugated anti-mouse IgG antibodies were used. Samples were analyzed with a confocal laser microscope (FV1000D; Olympus, Tokyo, Japan) using a 60x PlanApoN oil immersion lens (1.42 NA; Olympus). DAPI was excited at 405 nm, EGFP or Alexa Fluor<sup>®</sup> 488 at 488 nm, Alexa Fluor<sup>®</sup> 568 at 559 nm, mRFP at 594 nm and Alexa Fluor<sup>®</sup> 647 at 633 nm wavelengths.

### Flow cytometry

Cells stably expressing mCitrine-LC3 were cultured in the indicated medium for 10 h, harvested with 0.05% trypsin-EDTA, and washed once with phosphate-buffered saline. The samples were analyzed using an LSRFortessa flow cytometer (Becton Dickinson, Heidelberg, Germany).

### Long-lived protein degradation assay

Cells were incubated for 72 h with 0.125  $\mu$ Ci/ml L-[<sup>14</sup>C] valine-supplemented medium, followed by 2 washes and a 16 h chase in fresh medium containing 10 mM nonradioactive L-valine to allow degradation of short-lived proteins. Next, the cells were washed and treated with the indicated medium for 4 h. For each sample, the radioactivity of the acid-soluble fraction of the medium and the radioactivity in the cells remaining in the well were measured.

### Statistical analysis

For western blotting, fold changes were calculated by dividing each normalized density ratio (protein of interest to loading control) by the average of the density ratios of the control lane (control

lane: fold change = 1.00,  $n \geq 3$ ). Results are mean  $\pm$  SEM and are given below the corresponding blots or are depicted in a bar diagram. For GFP-ULK1, HA-ATG13, LC3B and SQSTM1/p62 immunofluorescence, the number of GFP-ULK1 dots, LC3B dots, SQSTM1 dots and colocalizing GFP-ULK1 and HA-ATG13 dots were quantified from at least 220 cells using Fiji software and data represent mean  $\pm$  SEM. For mCitrine-LC3B degradation, data represent the mean of the median fluorescence intensity (5,000 cells/experiment; 3 independent experiments)  $\pm$  SEM. Values are expressed as a percentage of the mean of cells cultured in regular medium (DMEM without bafilomycin A<sub>1</sub>). For the long-lived protein degradation assay, the radioactivity of the acid-soluble fraction of the medium and the radioactivity in the cells remaining in the well were measured for each sample. Percent degradation was assessed as the acid-soluble radioactivity of the medium divided by the total radioactivity. Additionally, induction of autophagy was assessed by subtracting percent degradation of EBSS/Baf A1-treated cells from percent degradation of EBSS-treated cells. Data shown are mean of triplicates of averaged duplicates  $\pm$  SEM and are depicted in bar diagrams. For all analyses, *P* values were determined by the Student *t* test (2-samples, unequal variances) and the significance levels were set as follows: \* indicates *P* < 0.05, \*\* indicates *P* < 0.01, \*\*\* indicates *P* < 0.001.

### Disclosure of Potential Conflicts of Interest

No potential conflicts of interest were disclosed.

### Acknowledgments

We thank Toshio Kitamura for providing Plat-E cells, Dario Alessi for providing pEGB-6P/ATG13, pEGB-6P/ATG13<sup>3AAA</sup> and pcDNA5/FRT/TO-GFP-ULK2, Tamotsu Yoshimori for providing pmRFP-EGFP-rLC3, and Xiaodong Wang for providing wild-type and *Atg13* KO MEFs.

### Funding

This work was supported by the Deutsche Forschungsgemeinschaft STO 864/3-1 and STO 864/4-1 (to B.S.), the Research Committee of the Medical Faculty of the Heinrich-Heine-University Düsseldorf 58/2013 (to B.S.), the Düsseldorf School of Oncology (to S.W. and B.S.; funded by the Comprehensive Cancer Center Düsseldorf/Deutsche Krebshilfe and the Medical Faculty of the Heinrich-Heine-University Düsseldorf), the Japan Society for the Promotion of Science (JSPS) KAKENHI Grants-in-Aid for Scientific Research on Innovative Areas (Grant Number 25111005) (to N.M.), and the JSPS Postdoctoral Fellowship (short-term) for North American and European Researchers (Grant Number PE 14784) (to N.H.).

### Supplemental Material

Supplemental data for this article can be accessed on the publisher's website.

## References

- Klionsky DJ, Eskelinen EL, Deretic V. Autophagosomes, phagosomes, autolysosomes, phagolysosomes, autophagolysosomes. . . Wait, I'm confused. *Autophagy* 2014; 10:549-51; PMID:2465794; <http://dx.doi.org/10.4161/autophagy.28448>
- Mizushima N, Yoshimori T, Ohsumi Y. The role of Atg proteins in autophagosome formation. *Annu Rev Cell Dev Biol* 2011; 27:107-32; PMID:21801009; <http://dx.doi.org/10.1146/annurev-cellbio-092910-154005>
- Ganley IG, Lam du H, Wang J, Ding X, Chen S, Jiang X. ULK1-ATG13-FIP200 complex mediates mTOR signaling and is essential for autophagy. *J Biol Chem* 2009; 284:12297-305; PMID:19258318
- Hosokawa N, Hara T, Kaizuka T, Kishi C, Takamura A, Miura Y, Iemura S, Natsume T, Takehana K, Yamada N, et al. Nutrient-dependent mTORC1 association with the ULK1-Atg13-FIP200 complex required for autophagy. *Mol Biol Cell* 2009; 20:1981-91; PMID:19211835; <http://dx.doi.org/10.1091/mbc.E08-12-1248>
- Hosokawa N, Sasaki T, Iemura S, Natsume T, Hara T, Mizushima N. Atg101, a novel mammalian autophagy protein interacting with Atg13. *Autophagy* 2009; 5:973-9; PMID:19597335; <http://dx.doi.org/10.4161/autophagy.5.7.9296>
- Chan EY, Longatti A, McKnight NC, Tooze SA. Kinase-inactivated ULK proteins inhibit autophagy via their conserved C-terminal domains using an Atg13-independent mechanism. *Mol Cell Biol* 2009; 29:157-71; PMID:18936157; <http://dx.doi.org/10.1128/MCB.01082-08>
- Jung CH, Jun CB, Ro SH, Kim YM, Otto NM, Cao J, Kundu M, Kim DH. ULK-Atg13-FIP200 complexes mediate mTOR signaling to the autophagy machinery. *Mol Biol Cell* 2009; 20:1992-2003; PMID:19225151 <http://dx.doi.org/10.1091/mbc.E08-12-1249>
- Mercer CA, Kaliappan A, Dennis PB. A novel, human Atg13 binding protein, Atg101, interacts with ULK1 and is essential for macroautophagy. *Autophagy* 2009; 5:649-62; PMID:19287211; <http://dx.doi.org/10.4161/autophagy.5.5.8249>
- Alers S, Löffler AS, Paasch F, Dieterle AM, Keppeler H, Lauber K, Campbell DG, Fehrenbacher B, Schaller M, Wesselborg S, et al. Atg13 and FIP200 act independently of Ulk1 and Ulk2 in autophagy induction. *Autophagy* 2011; 7:1423-33; PMID:22024743; <http://dx.doi.org/10.4161/autophagy.7.12.18027>
- Bach M, Larance M, James DE, Ramm G. The serine/threonine kinase ULK1 is a target of multiple phosphorylation events. *Biochem J* 2011; 440:283-91; PMID:21819378; <http://dx.doi.org/10.1042/BJ20101894>
- Egan DF, Shackelford DB, Mihaylova MM, Gelino S, Kohnz RA, Mair W, Vasquez DS, Joshi A, Gwinn DM, Taylor R, et al. Phosphorylation of ULK1 (hATG1) by AMP-activated protein kinase connects energy sensing to mitophagy. *Science* 2011; 331:456-61; PMID:21205641; <http://dx.doi.org/10.1126/science.1196371>
- Kim J, Kundu M, Viollet B, Guan KL. AMPK and mTOR regulate autophagy through direct phosphorylation of Ulk1. *Nat Cell Biol* 2011; 13:132-41; PMID:21258367; <http://dx.doi.org/10.1038/ncb2152>
- Mack HI, Zheng B, Asara JM, Thomas SM. AMPK-dependent phosphorylation of ULK1 regulates ATG9 localization. *Autophagy* 2012; 8:1197-214; PMID:22932492; <http://dx.doi.org/10.4161/autophagy.20586>
- Shang L, Chen S, Du F, Li S, Zhao L, Wang X. Nutrient starvation elicits an acute autophagic response mediated by Ulk1 dephosphorylation and its subsequent dissociation from AMPK. *Proc Natl Acad Sci USA* 2011; 108:4788-93; PMID:21383122; <http://dx.doi.org/10.1073/pnas.1100844108>
- Lin SY, Li TY, Liu Q, Zhang C, Li X, Chen Y, Zhang SM, Lian G, Ruan K, Wang Z, et al. GSK3-TIP60-ULK1 signaling pathway links growth factor deprivation to autophagy. *Science* 2012; 336:477-81; PMID:22539723; <http://dx.doi.org/10.1126/science.1217032>
- Nazio F, Strappazzon F, Antonioni M, Bielli P, Cianfanelli V, Bordin M, Gretzmeier C, Dengej J, Piacentini M, Fimia GM, et al. mTOR inhibits autophagy by controlling ULK1 ubiquitylation, self-association and function through AMBRA1 and TRAF6. *Nat Cell Biol* 2013; 15:406-16; PMID:23524951; <http://dx.doi.org/10.1038/ncb2708>
- Di Bartolomeo S, Corazzari M, Nazio F, Oliverio S, Lisi G, Antonioni M, Pagliarini V, Matteoni S, Fuoco C, Giunta L, et al. The dynamic interaction of AMBRA1 with the dynein motor complex regulates mammalian autophagy. *J Cell Biol* 2010; 191:155-68; PMID:20921139; <http://dx.doi.org/10.1083/jcb.201002100>
- Russell RC, Tian Y, Yuan H, Park HW, Chang YY, Kim J, Kim H, Neufeld TP, Dillin A, Guan KL. ULK1 induces autophagy by phosphorylating Beclin-1 and activating VPS34 lipid kinase. *Nat Cell Biol* 2013; 15:741-50; PMID:23685627; <http://dx.doi.org/10.1038/ncb2757>
- Tang HW, Wang YB, Wang SL, Wu MH, Lin SY, Chen GC. Atg1-mediated myosin II activation regulates autophagosome formation during starvation-induced autophagy. *EMBO J* 2011; 30:636-51; PMID:21169900; <http://dx.doi.org/10.1038/emboj.2010.338>
- Cheong H, Lindsten T, Wu J, Lu C, Thompson CB. Ammonia-induced autophagy is independent of ULK1/ULK2 kinases. *Proc Natl Acad Sci USA* 2011; 108:11121-6; PMID:21690395; <http://dx.doi.org/10.1073/pnas.1107969108>
- Chang YY, Neufeld TP. An Atg1/Atg13 complex with multiple roles in TOR-mediated autophagy regulation. *Mol Biol Cell* 2009; 20:2004-14; PMID:19225150; <http://dx.doi.org/10.1091/mbc.E08-12-1250>
- Hara T, Takamura A, Kishi C, Iemura S, Natsume T, Guan JL, Mizushima N. FIP200, a ULK-interacting protein, is required for autophagosome formation in mammalian cells. *J Cell Biol* 2008; 181:497-510; PMID:18443221; <http://dx.doi.org/10.1083/jcb.200712064>
- Fujioka Y, Suzuki SW, Yamamoto H, Kondo-Kakuta C, Kimura Y, Hirano H, Akada R, Inagaki F, Ohsumi Y, Noda NN. Structural basis of starvation-induced assembly of the autophagy initiation complex. *Nat Struct Mol Biol* 2014 21(6):513-21; PMID:24793651
- Klionsky DJ, Abdalla FC, Abeliovich H, Abraham RT, Acevedo-Arozena A, Adeli K, Agholme L, Agnello M, Agostinis P, Aguirre-Ghisso JA, et al. Guidelines for the use and interpretation of assays for monitoring autophagy. *Autophagy* 2012; 8:445-544; PMID:22966490; <http://dx.doi.org/10.4161/autophagy.19496>
- Joo JH, Dorsey FC, Joshi A, Hennessy-Walters KM, Rose KL, McCastlain K, Zhang J, Iyengar R, Jung CH, Suen DF, et al. Hsp90-Cdc37 chaperone complex regulates Ulk1- and Atg13-mediated mitophagy. *Mol Cell* 2011; 43:572-85; PMID:21855797; <http://dx.doi.org/10.1016/j.molcel.2011.06.018>
- Kimura S, Noda T, Yoshimori T. Dissection of the autophagosome maturation process by a novel reporter protein, tandem fluorescent-tagged LC3. *Autophagy* 2007; 3:452-60; PMID:17534139; <http://dx.doi.org/10.4161/autophagy.4451>
- Nishida Y, Arakawa S, Fujitani K, Yamaguchi H, Mizuta T, Kanaseki T, Komatsu M, Otsu K, Tsujimoto Y, Shimizu S. Discovery of Atg5/Atg7-independent alternative macroautophagy. *Nature* 2009; 461:654-8; PMID:19794493; <http://dx.doi.org/10.1038/nature08455>
- Scarlatti F, Maffei R, Beau I, Codogno P, Ghidoni R. Role of non-canonical Beclin 1-independent autophagy in cell death induced by resveratrol in human breast cancer cells. *Cell Death Differ* 2008; 15:1318-29; PMID:18421301; <http://dx.doi.org/10.1038/cdd.2008.51>
- McAlpine F, Williamson LE, Tooze SA, Chan EY. Regulation of nutrient-sensitive autophagy by uncoordinated 51-like kinases 1 and 2. *Autophagy* 2013; 9:361-73; PMID:23291478; <http://dx.doi.org/10.4161/autophagy.23066>
- Harris BZ, Lim WA. Mechanism and role of PDZ domains in signaling complex assembly. *J Cell Sci* 2001; 114:3219-31; PMID:11591811
- Lee HJ, Zheng JJ. PDZ domains and their binding partners: structure, specificity, and modification. *Cell Commun Signal* 2010; 8:8; PMID:20509869; <http://dx.doi.org/10.1186/1478-811X-8-8>
- Nourry C, Grant SG, Borg JP. PDZ domain proteins: plug and play!. *Sci STKE* 2003; 2003:RE7; PMID:12709532
- Chan EY, Kir S, Tooze SA. siRNA screening of the kinome identifies ULK1 as a multidomain modulator of autophagy. *J Biol Chem* 2007; 282:25464-74; PMID:17595159; <http://dx.doi.org/10.1074/jbc.M703663200>
- Tomoda T, Kim JH, Zhan C, Hatten ME. Role of Unc51.1 and its binding partners in CNS axon outgrowth. *Genes Dev* 2004; 18:541-58; PMID:15014045; <http://dx.doi.org/10.1101/gad.1151204>
- Songyang Z, Fanning AS, Fu C, Xu J, Marfatia SM, Chishti AH, Crompton A, Chan AC, Anderson JM, Cantley LC. Recognition of unique carboxyl-terminal motifs by distinct PDZ domains. *Science* 1997; 275:73-7; PMID:8974395; <http://dx.doi.org/10.1126/science.275.5296.73>
- Stjepanovic G, Davies CW, Stanley RE, Ragusa MJ, Kim DJ, Hurley JH. Assembly and dynamics of the autophagy-initiating Atg1 complex. *Proc Natl Acad Sci USA* 2014 111(35):12793-8; PMID:25139988
- Liang Q, Yang P, Tian E, Han J, Zhang H. The C. elegans ATG101 homolog EPG-9 directly interacts with EPG-1/Atg13 and is essential for autophagy. *Autophagy* 2012; 8:1426-33; PMID:22885670; <http://dx.doi.org/10.4161/autophagy.21163>
- Kraft C, Kijanska M, Kalie E, Siergiejuk E, Lee SS, Semplicio G, Stoffel I, Brezovich A, Verma M, Hansmann I, et al. Binding of the Atg1/ULK1 kinase to the ubiquitin-like protein Atg8 regulates autophagy. *EMBO J* 2012; 31:3691-703; PMID:22885598; <http://dx.doi.org/10.1038/emboj.2012.225>
- Löffler AS, Alers S, Dieterle AM, Keppeler H, Franz-Wachtel M, Kundu M, Campbell DG, Wesselborg S, Alessi DR, Stork B. Ulk1-mediated phosphorylation of AMPK constitutes a negative regulatory feedback loop. *Autophagy* 2011; 7:696-706; PMID:21460634; <http://dx.doi.org/10.4161/autophagy.7.7.15451>

## Supplementary Figures

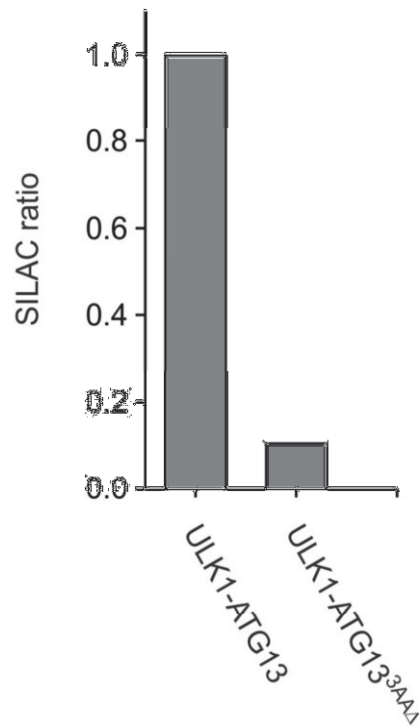


**Figure S1.** The interaction between ULK1 and ATG13 is severely compromised by deletion of the TLQ480 motif. *Atg13* KO MEFs retrovirally transfected with empty vector or cDNA encoding HA-ATG13 or HA-ATG13<sup>3AAΔ</sup> were labeled with light (R0K0), medium (R6K4) or heavy (R10K8) arginine/lysine. Cells were lysed and HA immunopurifications were performed. Purified proteins were analyzed by mass spectrometry as described in the supplementary Material and Methods section. Unnormalized SILAC ratios for ULK1 obtained from MaxQuant were normalized to the ratio of ATG13.

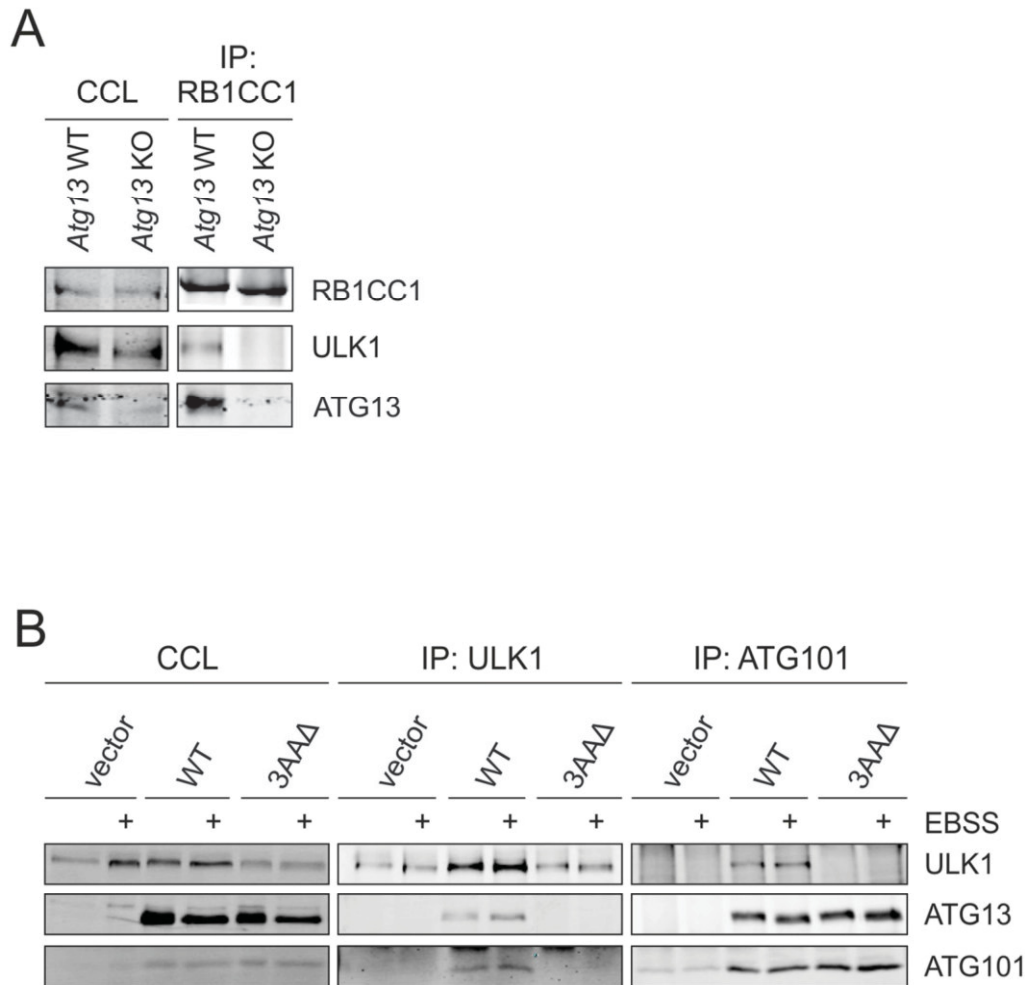
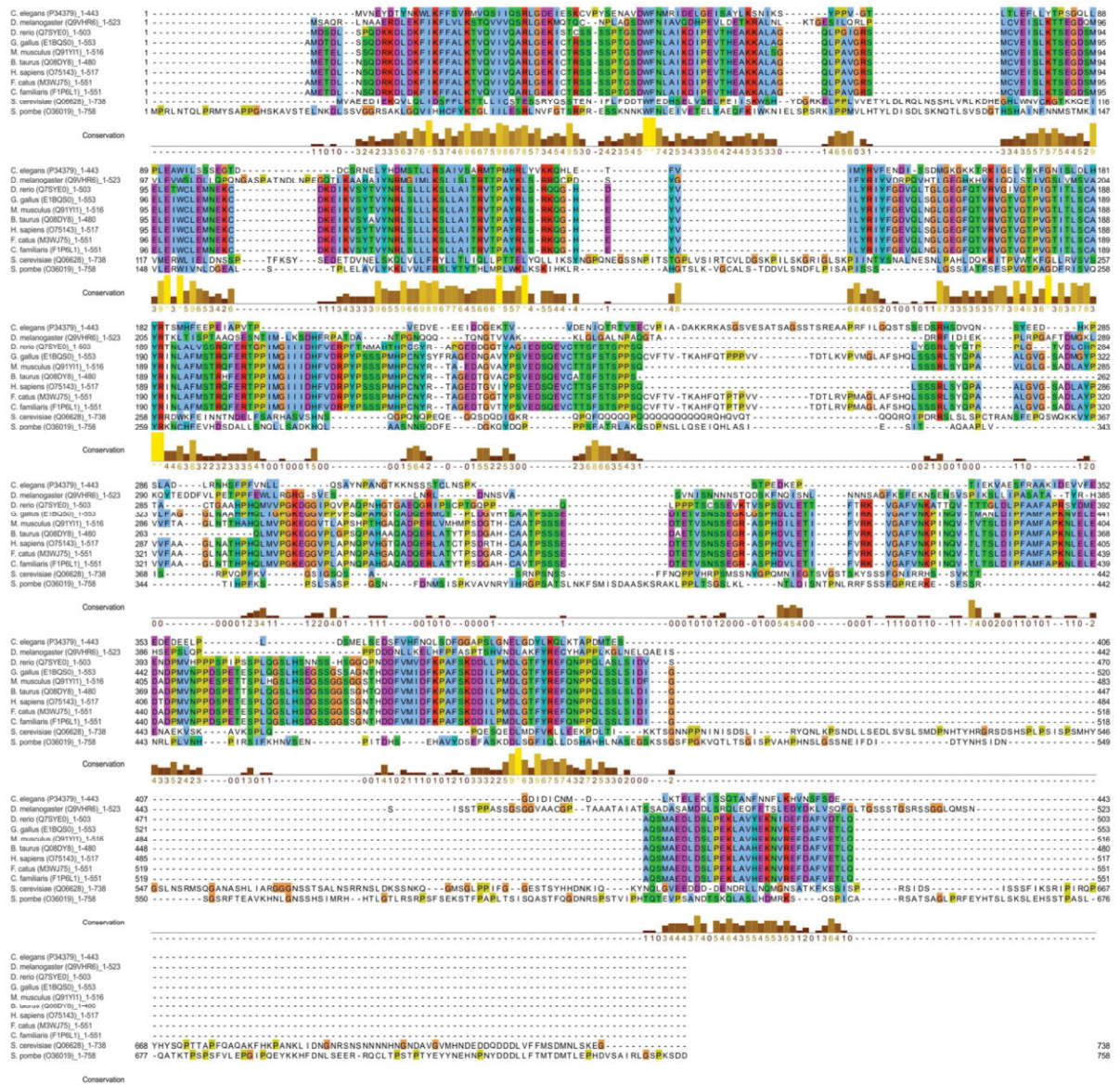


**Figure S2.** ULK1 cannot be copurified with RB1CC1 or ATG101 in the absence of full-length ATG13. **(A)** Wild-type or *Atg13* KO MEFs were lysed and anti-RB1CC1 immunopurifications were performed. Cleared cellular lysates (CCL) and purified proteins were subjected to SDS-PAGE and analyzed by immunoblotting for RB1CC1, ULK1, or ATG13. **(B)** *Atg13* KO MEFs retrovirally transfected with empty vector or cDNA encoding HA-ATG13 (WT) or HA-ATG13<sup>3AAAΔ</sup> (3AAAΔ) were incubated in full medium or starvation medium (EBSS). Cells were lysed and anti-ULK1 (middle panels) or anti-ATG101 (right panels) immunopurifications were performed. CCLs and purified proteins were subjected to SDS-PAGE and analyzed by immunoblotting for ULK1, ATG13, or ATG101.

A



B

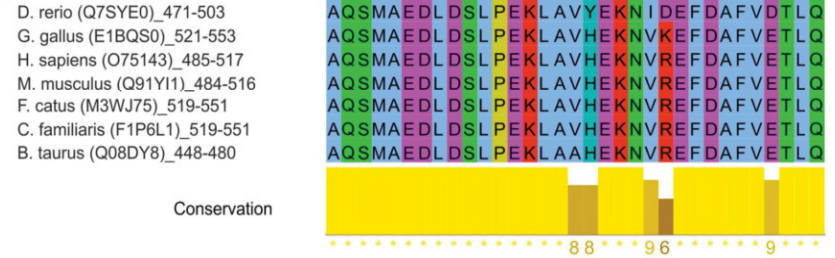


**Figure S3.** Amino acid alignment of ATG13/Atg13 proteins. (A) Full length ATG13/Atg13 proteins were aligned using Clustal Omega (<http://www.ebi.ac.uk/Tools/msa/clustalo/>). Alignments were coloured using Jalview software. Amino acid sequences derive from the

following species: *Caenorhabditis elegans* (UniProt ID P34379), *Drosophila melanogaster* (Q9VHR6), *Danio rerio* (Q7SYE0), *Gallus gallus* (E1BQS0), *Mus musculus* (Q91YI1), *Bos taurus* (Q08DY8), *Homo sapiens* (O75143), *Felis catus* (M3WJ75), *Canis familiaris* (F1P6L1), *Saccharomyces cerevisiae* (Q06628), and *Schizosaccharomyces pombe* (O36019). **(B)** C-terminal parts of the indicated ATG13 proteins were aligned as in (A).

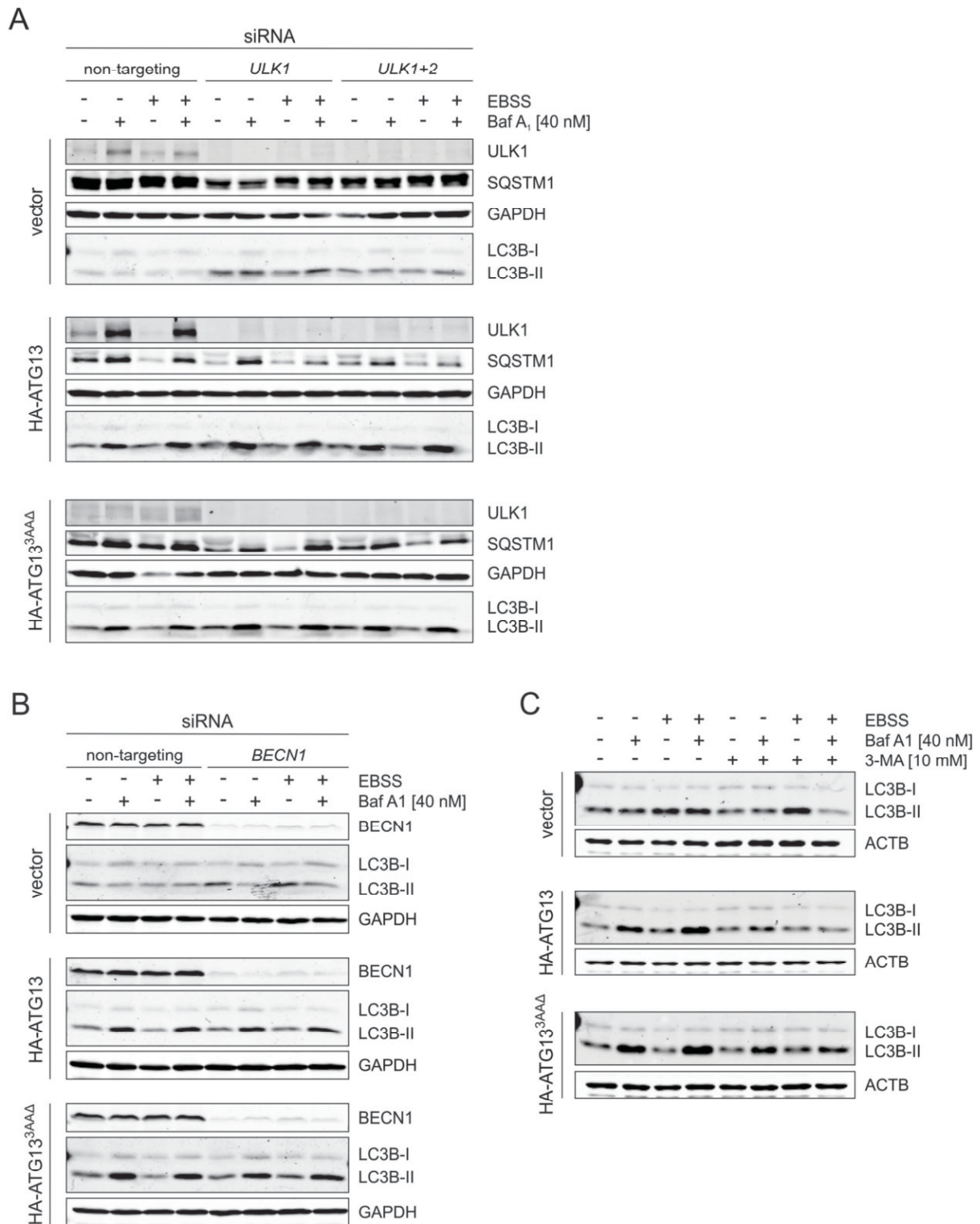


**Figure S4.** Partial restoration of autophagic flux by ATG13<sup>3AAΔ</sup> depends on the BECN1-PIK3C3/VPS34 complex. **(A and B)** *Atg13* KO MEFs retrovirally transfected with empty vector or cDNA encoding HA-ATG13 or HA-ATG13<sup>3AAΔ</sup> were transiently transfected with the indicated siRNAs. Cells were incubated in full medium or starvation medium (EBSS) for 2 h in

the absence or presence of 40 nM bafilomycin A<sub>1</sub> (Baf A1). Cells were lysed and whole cellular lysates were subjected to SDS-PAGE and analyzed by immunoblotting for ULK1, SQSTM1, GAPDH, BECN1 or LC3. (C) MEFs described in (A and B) were incubated in full medium or starvation medium (EBSS) for 2 h in the absence or presence of 40 nM bafilomycin A<sub>1</sub> (Baf A1) and/or 10 mM 3-MA. Cells were lysed and whole cellular lysates were subjected to SDS-PAGE and analyzed by immunoblotting for LC3 or ACTB.

## Supplementary Materials and Methods

siRNA-mediated knockdown of *Ulk1*, *Ulk2* and *Becn1*

MEFs were seeded on a 24-well plate overnight. Cells were transfected using Lipofectamine<sup>®</sup> RNAiMAX (Life Technologies, 13778-150) according to the manufacturer's instructions with 20 nM ON-TARGETplus SMARTpool<sup>®</sup> siRNA (Dharmacon, Thermo Scientific) targeting *Ulk1* (L-040155-00-0005), *Ulk2* (L-040619-00-0005) or *Becn1* (L-055895-00-0005), or a non-targeting control pool (D-001810-10-05). Knockdown efficiency was analyzed by immunoblotting.

### *Mass Spectrometry*

#### Sample preparation

Protein mixtures were reduced with Dithiothreitol (Sigma Aldrich, 43815) and alkylated with Iodacetamide (Sigma Aldrich, I11A49) and subsequently separated by SDS-PAGE using 4-12% Bis-Tris mini gradient gels (NuPAGE, Life Technologies, NP0335BOX). The gel lanes were cut into 10 equal slices, proteins were in-gel digested with trypsin (Promega, V5113),<sup>1</sup> and the resulting peptide mixtures were processed on StageTips using C18 material (3M Empore C18, IVA Analysetechnik, 2215) as described previously.<sup>2</sup>

#### MS analysis

Mass spectrometric measurements were performed essentially as described<sup>3</sup> on an LTQ Orbitrap XL mass spectrometer (Serial #: 01599B, Thermo Fisher Scientific, Langensfeld, Germany) coupled to an Agilent 1200 nanoflow-HPLC (Agilent Technologies, Waldbronn, Germany) or a NanoLC Ultra (Serial #: 11-01-15-215, Eksigent, Darmstadt, Germany). HPLC-column tips (fused silica) with 75 µm inner diameter (New Objective, FS360-75-10-N-5-C25)

were self-packed with Reprosil-Pur 120 ODS-3 (Dr. Maisch, r13.aq) to a length of 20 cm. Samples were applied directly onto the column without pre-column. A gradient of A (0.5% acetic acid [high purity, LGC Promochem, 33209-1L-GL] in water) and B (0.5% acetic acid in 80% acetonitrile [LC-MS grade, Promochem, SO-9340-B025] in water) with increasing organic proportion was used for peptide separation (loading of sample with 2% B; separation ramp: from 10-30% B within 80 min). The flow rate was 250 nl/min and for sample application 500 nl/min. The mass spectrometer was operated in the data-dependent mode and switched automatically between MS (max. of  $1 \times 10^6$  ions) and MS/MS. Each MS scan was followed by a maximum of 5 MS/MS scans in the linear ion trap using normalized collision energy of 35% and a target value of 5000. Parent ions with a charge state from  $z=1$  and unassigned charge states were excluded for fragmentation. The mass range for MS was  $m/z = 370$  to 2000. The resolution was set to 60,000. Mass-spectrometric parameters were as follows: spray voltage 2.3 kV; no sheath and auxiliary gas flow; ion-transfer tube temperature 125°C.

#### Identification of proteins and protein ratio assignment using MaxQuant

The MS raw data files were uploaded into the MaxQuant software<sup>4</sup> version 1.3.0.5., which performs peak detection and generates peak lists of mass error-corrected peptides using the following parameters: carbamidomethylcysteine was set as fixed modification, methionine oxidation and protein amino-terminal acetylation were set as variable modifications. Three miss-cleavages were allowed, enzyme specificity was trypsin/P + DP, and the MS/MS tolerance was set to 0.5 Da. Peak lists were searched by Andromeda for peptide identification using a Uniprot mouse database from September 2012 containing common contaminants such as keratins and enzymes used for in-gel digestion (55299 entries). The

database was complemented by the sequence of human ATG13 (O75143). Peptide lists were further used by MaxQuant to identify and relatively quantify proteins using the following parameters: peptide, and protein false discovery rates were set to 0.01, maximum peptide posterior error probability (PEP) was set to 1, minimum peptide length was set to 7, the PEP was based on Andromeda score, minimum number of peptides for protein identification was set to one, which must be unique, and for protein quantitation a ratio count of 2 was required. Identified proteins were requantified.

#### Data analysis

Unnormalized SILAC ratios for ULK1 obtained from MaxQuant were normalized to the ratio of ATG13.

### Supplementary References

1. Shevchenko A, Tomas H, Havlis J, Olsen JV, Mann M. In-gel digestion for mass spectrometric characterization of proteins and proteomes. *Nat Protoc* 2006; 1:2856-60.
2. Rappsilber J, Mann M, Ishihama Y. Protocol for micro-purification, enrichment, pre-fractionation and storage of peptides for proteomics using StageTips. *Nat Protoc* 2007; 2:1896-906.
3. Sprenger A, Weber S, Zarai M, Engelke R, Nascimento JM, Gretzmeier C, Hilpert M, Boerries M, Has C, Busch H, et al. Consistency of the proteome in primary human keratinocytes with respect to gender, age, and skin localization. *Mol Cell Proteomics* 2013; 12:2509-21.
4. Cox J, Mann M. MaxQuant enables high peptide identification rates, individualized p.p.b.-range mass accuracies and proteome-wide protein quantification. *Nat Biotechnol* 2008; 26:1367-72.

# Paper 2



# Deubiquitinase inhibition by WP1130 leads to ULK1 aggregation and blockade of autophagy

Stefan Drießen,<sup>1</sup> Niklas Berleth,<sup>1</sup> Olena Friesen,<sup>1</sup> Antje S Löffler,<sup>1</sup> Philip Böhler,<sup>1</sup> Nora Hieke,<sup>1</sup> Fabian Stuhldreier,<sup>1</sup> Christoph Peter,<sup>1</sup> Kay O Schink,<sup>2</sup> Sebastian W Schultz,<sup>2</sup> Harald Stenmark,<sup>2</sup> Petter Holland,<sup>3</sup> Anne Simonsen,<sup>3</sup> Sebastian Wesselborg,<sup>1</sup> and Björn Stork<sup>1,\*</sup>

<sup>1</sup>Institute of Molecular Medicine; Heinrich-Heine-University; Düsseldorf, Germany; <sup>2</sup>Department of Biochemistry; Institute for Cancer Research; The Norwegian Radium Hospital; Oslo, Norway; <sup>3</sup>Institute of Basic Medical Sciences; Faculty of Medicine; University of Oslo; Oslo, Norway

**Keywords:** autophagy, deubiquitinases, ubiquitination, ULK1, WP1130

**Abbreviations:** ACTB/ $\beta$ -actin, actin,  $\beta$ ; AMBRA1, autophagy/Beclin 1 regulator 1; AMPK, AMP-activated protein kinase; ATG, autophagy related; Baf A1, bafilomycin A<sub>1</sub>; BECN1, Beclin 1, autophagy related; Dox, doxycycline; DUB, deubiquitinases; EBSS, Earle's balanced salt solution; GFP, green fluorescent protein; MAP1LC3/LC3, microtubule-associated protein 1 light chain 3; MBP, myelin basic protein; MTOR, mechanistic target of rapamycin (serine/threonine kinase); MTORC1, MTOR complex 1; PtdIns3K, phosphatidylinositol 3-kinase; PRKA, protein kinase, AMP-activated; SQSTM1/p62, sequestosome 1; TRAF6, TNF receptor-associated factor 6, E3 ubiquitin protein ligase; TUBE, tandem ubiquitin binding entity; UCH, ubiquitin carboxyl-terminal hydrolase; ULK1, unc-51 like autophagy activating kinase 1; USP, ubiquitin-specific peptidase; WT, wild type.

Autophagy represents an intracellular degradation process which is involved in both regular cell homeostasis and disease settings. In recent years, the molecular machinery governing this process has been elucidated. The ULK1 kinase complex consisting of the serine/threonine protein kinase ULK1 and the adapter proteins ATG13, RB1CC1, and ATG101, is centrally involved in the regulation of autophagy initiation. This complex is in turn regulated by the activity of different nutrient- or energy-sensing kinases, including MTOR, AMPK, and AKT. However, next to phosphorylation processes it has been suggested that ubiquitination of ULK1 positively influences ULK1 function. Here we report that the inhibition of deubiquitinases by the compound WP1130 leads to increased ULK1 ubiquitination, the transfer of ULK1 to aggresomes, and the inhibition of ULK1 activity. Additionally, WP1130 can block the autophagic flux. Thus, treatment with WP1130 might represent an efficient tool to inhibit the autophagy-initiating ULK1 complex and autophagy.

## Introduction

Macroautophagy (hereafter referred to as autophagy) is an intracellular degradation process contributing to the recycling of long-lived, aggregated or misfolded proteins, or even entire organelles. During this process, the cargo to be degraded becomes enveloped within a double-membrane vesicle (referred to as an autophagosome), which is then transported to and fuses with lysosomes. Autophagy occurs at basal levels in most cell lines in order to sustain cellular homeostasis. However, autophagy can also be actively induced upon stress conditions such as nutrient- or energy-depletion, intracellular pathogens, oxidative or ER stress. In the past 2 decades, the molecular understanding of the machinery governing autophagy has substantially increased. Autophagy-related (ATG) gene products mediate all steps of the autophagic flux, including vesicle nucleation, elongation, closure, and fusion with lysosomes.<sup>1</sup> Next to ATG proteins, several non-ATG proteins are centrally involved in the regulation of autophagy, including the nutrient- and energy-sensing kinases MTOR

(mechanistic target of rapamycin [serine/threonine kinase]) or AMP-activated protein kinase (AMPK).<sup>1,2</sup> The ATGs can be grouped into several functional units.<sup>1</sup> Two macromolecular protein complexes regulate the initiation of the autophagic process, i.e. the ULK1 protein kinase complex and the class III phosphatidylinositol 3-kinase (PtdIns3K) lipid kinase complex.<sup>1</sup> The ULK1 core complex consists of the serine/threonine protein kinase ULK1 (unc-51 like autophagy activating kinase 1) and the adapter proteins ATG13, RB1CC1/FIP200 (RB1-inducible coiled-coil 1), and ATG101. ULK1 is one of the 5 mammalian orthologs of yeast Atg1. In 2009, several groups reported the mechanistic details for how this complex is assembled and receives input from the upstream MTOR complex 1 (MTORC1).<sup>3–6</sup> In the current model, MTORC1 associates with the ULK1 complex under nutrient-rich conditions and keeps the complex in an inactive state by phosphorylating ULK1 and ATG13. Upon nutrient depletion, MTORC1 dissociates from this complex and the MTOR-dependent inhibitory ULK1-sites become dephosphorylated. This in turn leads to the activation of

\*Corresponding author: Björn Stork; Email: bjoern.stork@uni-duesseldorf.de  
Submitted: 03/25/2014; Revised: 06/16/2015; Accepted: 06/24/2015  
<http://dx.doi.org/10.1080/15548627.2015.1067359>

ULK1, ULK1 autophosphorylation and ULK1-dependent ATG13-RB1CC1 transphosphorylation.<sup>7-11</sup> However, central aspects of this model remain unresolved, including the identification of the MTOR-dependent phospho-sites of ATG13 or the ULK1-dependent phospho-sites of RB1CC1. Additionally, the importance of the ULK1-dependent ATG13 phospho-sites has been challenged by our group.<sup>12</sup> Another level of complexity is added to the above described model by the fact that other kinases have been reported to regulate the ULK1 complex, including AMPK and AKT/PKB,<sup>13-17</sup> and that alternative post-translational modifications of ULK1 have been described, including acetylation and ubiquitination.<sup>18,19</sup> Recently Nazio et al. have shown that AMBRA1, which is a component of the class III PtdIns3K complex, not only becomes phosphorylated by ULK1, but in turn recruits the E3-ligase TRAF6 (TNF receptor-associated factor 6).<sup>19</sup> TRAF6 apparently supports Lys63/K63-linked ULK1 ubiquitination, leading to the stabilization and activation of ULK1.<sup>19</sup> To date, several ULK1 substrates presumably mediating its proautophagic function have been identified, such as AMBRA1, BECN1, or DAPK3/ZIPK (death-associated protein kinase 3).<sup>20-22</sup> Recently, it has been reported that yeast Atg1 phosphorylates Atg9.<sup>23</sup> Furthermore, we were able to demonstrate that ULK1 phosphorylates all 3 subunits of AMPK, ultimately leading to the inhibition of AMPK activity.<sup>24</sup>

Although there are the above-described hints that the ULK1 complex is regulated by ubiquitination, the overall picture as to how this posttranslational modification regulates the ULK1 complex is incomplete. Furthermore, the role of deubiquitinases (DUBs) for the regulation of autophagy is completely uncharacterized. In the present work, we made use of the partially selective DUB inhibitor WP1130 (also known as degrasyn), which has originally been identified during a library screen for small compounds that inhibit IL6-induced phosphorylation of STAT3.<sup>25,26</sup> We demonstrate that treatment of cells with this compound leads to the recruitment of ULK1 to aggresomes. This relocalization is most likely caused by an increased ubiquitination status of ULK1. We further observed that ULK1 activity is severely compromised upon ULK1 recruitment to aggresomes. Additionally, treatment with WP1130 leads to the blockade of the autophagic flux. Taken together, we propose that WP1130 represents an efficient tool to inhibit autophagy in general and to modulate ULK1 activity in particular. Next to the direct inhibition of ULK1 kinase activity, the regulation of ULK1 ubiquitination might be an effective approach to modulate the autophagic response.

## Results

### WP1130 treatment induces the transfer of ULK1 to aggresomes

It has previously been reported that ULK1 function is controlled by ubiquitination.<sup>19</sup> Additionally, it has been speculated that the deubiquitinase (DUB) inhibitor WP1130 might increase autophagy.<sup>27</sup> Accordingly, we aimed at the in-depth characterization of this compound with regard to autophagy signaling. We

made use of the previously described Flp-In<sup>TM</sup> T-REx<sup>TM</sup> 293 cells inducibly expressing GFP-ULK1 upon doxycycline treatment.<sup>24</sup> Interestingly, incubation with 5  $\mu$ M WP1130 resulted in decreased levels of GFP-ULK1. (Fig. 1A) A similar observation was made for GFP-ULK2 (Fig. S1A). Next we investigated whether the reduced GFP-ULK1 protein levels were caused by proteasomal degradation. However, treatment with the proteasome inhibitors MG132 or bortezomib did not abolish the WP1130-induced reduction of GFP-ULK1, indicating that the deubiquitinase inhibitor WP1130 reduces GFP-ULK1 levels without the involvement of the proteasome (Fig. 1B)

It has been previously reported that WP1130 induces the formation of juxtannuclear aggresomes.<sup>27</sup> Additionally, it has been shown that the tyrosine kinases BCR-ABL and JAK2 are recruited to these aggresomes upon WP1130 treatment, which then results in inhibition of their kinase activity.<sup>26,28</sup> Accordingly, we speculated that GFP-ULK1 might not be degraded by proteolysis but might be instead transferred to aggresome-like structures upon WP1130 treatment. To test this, we analyzed the effect of WP1130 treatment on the localization of GFP-ULK1 by confocal microscopy. Indeed, incubation with WP1130 resulted in the recruitment of GFP-ULK1 to juxtannuclear punctate structures (Fig. 1C and Fig. S1B). Similarly, GFP-ULK2 was also recruited to these aggresomes upon WP1130 treatment (Fig. S1C). Furthermore, recruitment to aggresomes did not require ULK1 activity since a kinase-dead version of GFP-ULK1 was also translocated to these juxtannuclear punctate structures (Fig. S1C). The WP1130-induced recruitment of GFP-ULK1 to aggresomes was also monitored by live-cell imaging (Movies S1-S3). We observed that small GFP-ULK1 aggregates are already formed upon induction of GFP-ULK1 expression (Movie S1). However, formation of these small peripheral aggregates was clearly enhanced by WP1130 treatment (Movie S2). Furthermore, WP1130 treatment induced the translocation of these aggregates to the perinuclear aggresome (Movie S2). It has been previously reported that microtubule disruption with nocodazole inhibits aggresome formation.<sup>29</sup> Indeed, parallel incubation of cells with WP1130 and nocodazole abolished aggresome formation and led to the generation of smaller GFP-ULK1 aggregates in the periphery (Movie S3). Further analysis of the aggresomes revealed that these structures comprised ubiquitin—including K63-linked ubiquitin—and MAP1LC3/LC3 (microtubule-associated protein 1 light chain 3), and to a minor extent contained SQSTM1/p62. (Fig. S2) To confirm these microscopy observations by an independent biochemical assay, we analyzed the WP1130-dependent distribution of GFP-ULK1 in Triton X-100-soluble and -insoluble fractions. Notably, WP1130 treatment led to the redistribution of GFP-ULK1 from the soluble to the insoluble fraction (Fig. 1D) Taken together, WP1130 treatment does not result in the proteolytic degradation of GFP-ULK1 but induces its transfer to aggresomes.

It has been previously observed that overexpression of GFP-ULK1 leads to the formation of cytosolic GFP-positive puncta.<sup>30</sup> In order to exclude that the observed effect is just an overexpression artifact, we analyzed the protein levels and distribution of endogenous ULK1 upon WP1130 treatment in 3 different cell

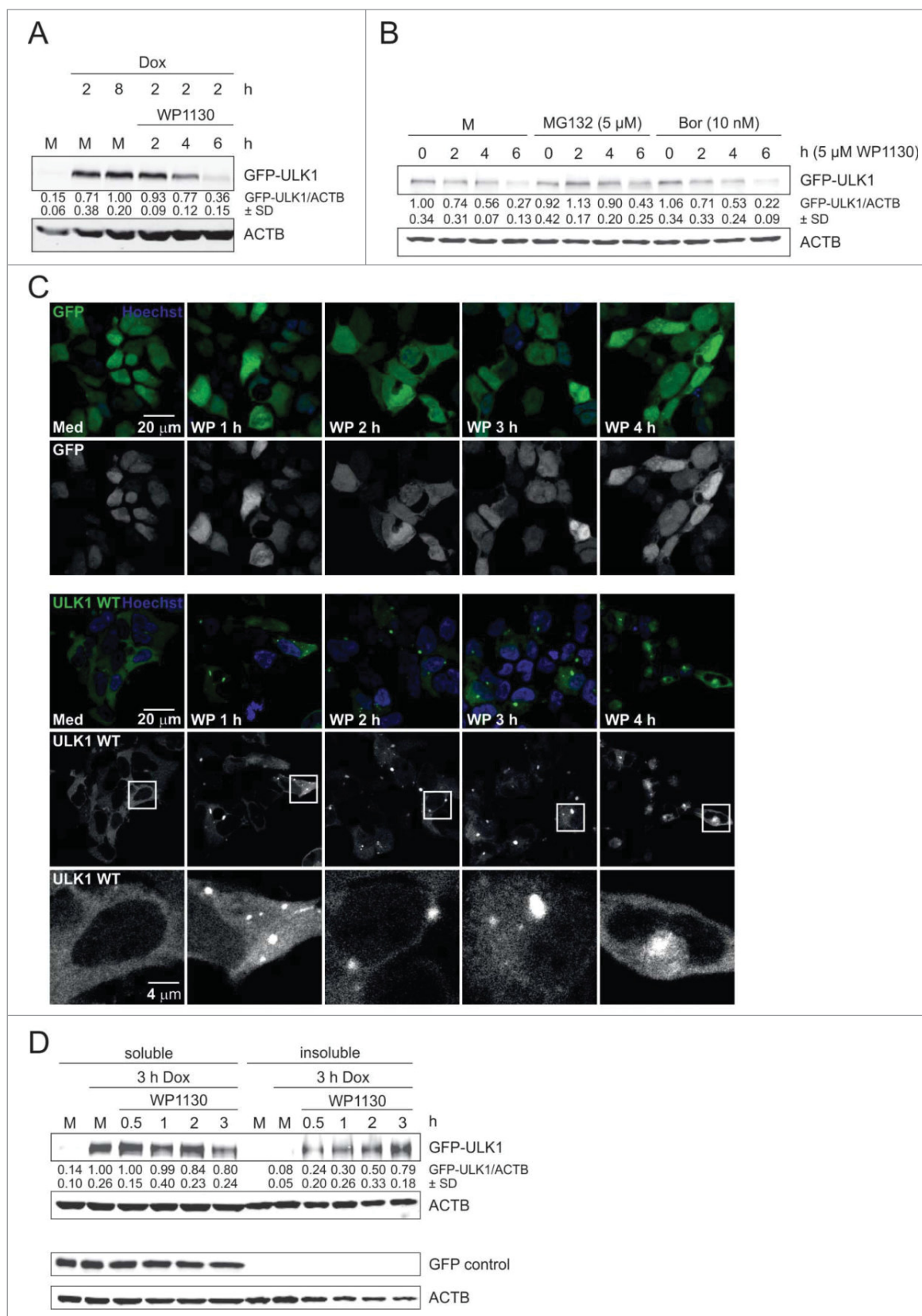


**Figure 1.** For figure legend, see page 1461.

lines, i.e., HEK293, HeLa, and U2OS cells (Fig. 2A). Again incubation with WP1130 apparently led to strongly reduced ULK1 protein levels in cleared cellular lysates of these cells. This effect could not be reversed by coincubation with different protease inhibitors or with bafilomycin A<sub>1</sub>, which raises the lysosomal pH by blocking the lysosomal proton pump and thus blocks autophagic degradation (Fig. S3). Additionally and like the GFP-tagged derivative, endogenous ULK1 redistributed from the Triton X-100-soluble to the -insoluble fraction in HEK293 cells (Fig. 2B, left panels), whereas overall cellular levels of endogenous ULK1 remained unaltered (Fig. 2B, right panels). We next addressed the question whether other components of the ULK1 complex (i.e., ATG13 and RB1CC1/FIP200) or components of the PIK3C3/VPS34-PIK3R4/VPS15-BECN1-ATG14 PtdIns3K complex (i.e., BECN1 and AMBRA1) are redistributed to aggresomes. However, these proteins were not present in the insoluble fraction following WP1130 treatment, (Fig. 2C) indicating a rather specific process for ULK1. Finally, we investigated whether ULK1 redistribution is a reversible process. For that, we treated HEK293 cells with WP1130 for 3 h, and then resuspended the cells in WP1130-free medium. We observed that the levels of Triton X-100 soluble ULK1 increased again, and that in turn the amount in the insoluble fraction decreased (Fig. S4) This indicates that WP1130-mediated relocalization of ULK1 to aggresomes is indeed a reversible process. Collectively, our results show that WP1130 treatment also results in the recruitment of endogenous ULK1 to aggresomes, but that this is not the case for other autophagy-relevant proteins.

#### WP1130 treatment increases ubiquitination of ULK1

Since WP1130 has been previously identified as deubiquitinase inhibitor<sup>26,27</sup> and since the juxtannuclear ULK1-aggresomes obviously contained ubiquitin (Fig. S2), we next asked the question whether the ubiquitination status of ULK1 is affected by this compound. In a first approach, we employed short-term incubation (0.5 h) with WP1130 and analyzed ubiquitination of immunopurified GFP-ULK1 by anti-mono- and poly-ubiquitin immunoblotting (Fig. 3A) Indeed, GFP-ULK1 ubiquitination increased with WP1130 treatment. In an alternative approach, we transfected Flp-In<sup>TM</sup> T-REx<sup>TM</sup> 293 cells expressing either GFP or GFP-ULK1 with cDNA encoding HA-ubiquitin and analyzed immunopurified GFP and GFP-ULK1 by anti-HA immunoblotting. Whereas we did not detect ubiquitinated

proteins from GFP-expressing cells, we again observed increased GFP-ULK1 ubiquitination following WP1130 treatment (Fig. 3B) In order to characterize the type of ubiquitin linkage, we transfected HEK293 cells with cDNAs encoding different HA-ubiquitin variants and incubated the cells with WP1130. Analysis of GFP-Trap<sup>®</sup>-purified GFP-ULK1 by anti-HA immunoblotting indicated that ubiquitination of ULK1 is mainly established by non-K48-, non-K63-linked ubiquitin chains (Fig. 3C) In order to confirm ULK1 ubiquitination by an alternative approach, we purified ubiquitinated proteins from cellular lysates using tandem ubiquitin binding entity (TUBE) technology. Treatment of HEK293 cells or Flp-In<sup>TM</sup> T-REx<sup>TM</sup> 293 cells with WP1130 increased the amount of purified ULK1 or GFP-ULK1 compared to untreated cells (Fig. 3D).

It has been previously reported that WP1130 targets the deubiquitinases (DUBs) USP5, USP9X, USP14, UCHL1 and UCHL5.<sup>27</sup> In order to test whether these DUBs are involved in the regulation of ULK1 expression levels, we transfected HEK293 cells simultaneously with the corresponding siRNAs and analyzed endogenous ULK1 expression after 48 and 72 h, respectively (Fig. S5A) However, we could not detect any alterations of ULK1 expression levels. Since USP9X is one major target of WP1130,<sup>27,28,31-33</sup> we also analyzed the effect of WP1130 on ULK1 expression levels in *USP9X*-/- HCT116 cells.<sup>34</sup> WP1130 reduced ULK1 levels in both *USP9X*+/- and *USP9X*-/- HCT116 cells to a similar extent (Fig. S5B) indicating that USP9X is not the major target of WP1130 with regard to ULK1 regulation. In order to identify the DUB(s) targeted by WP1130, we performed a DUB profiling assay with WP1130 using a library of 35 recombinant DUBs (DUB<sup>Profiler</sup><sup>TM</sup> Single Point Screening, Ubiquigent, Dundee, UK). However, none of the tested DUBs was significantly inhibited by 1 or 10  $\mu$ M WP1130 (Fig. S6) Notably, the 35 DUBs also contained the 5 enzymes previously reported to be inhibited by WP1130. Finally, we wanted to confirm that the effect caused by WP1130 is due to the inhibition of DUBs. For that, we employed the pan-DUB inhibitor PR619. This inhibitor transferred ULK1 from the soluble to the insoluble fraction similar to WP1130 (Fig. S7A and B) In contrast, the more selective DUB inhibitors LDN 57444 (targeting UCHL1) and Spautin-1 (targeting USP10 and USP13) did not result in a similar reduction of ULK1 in the soluble fraction (Fig. S7A) Importantly, all analyzed DUB inhibitors

**Figure 1 (See previous page).** WP1130 induces transfer of GFP-ULK1 to aggresomes. **(A)** After induction of GFP-ULK1 expression with doxycycline (Dox) for indicated times, Flp-In<sup>TM</sup> T-REx<sup>TM</sup> 293 GFP-ULK1 cells were left untreated (M) or treated with 5  $\mu$ M WP1130 for 2, 4 or 6 h. Equal protein amounts of cleared cellular lysates were subjected to anti-ULK1 and anti-ACTB/ $\beta$ -actin immunoblotting. **(B)** After induction of GFP-ULK1 expression with Dox for 3 h, cells were left untreated (M) or treated with 5  $\mu$ M MG132 or 10 nM bortezomib (Bor), respectively. After 30 min, cells were either lysed directly (0) or 5  $\mu$ M WP1130 was added for 2, 4, or 6 h. Subsequently cells were lysed and cleared cellular lysates were separated by SDS-PAGE and analyzed by immunoblotting using antibodies against ULK1 and ACTB/ $\beta$ -actin. **(C)** After induction of GFP-only (upper panels) or GFP-ULK1 (lower panels) expression with Dox for 3 h, Flp-In<sup>TM</sup> T-REx<sup>TM</sup> 293 cells were treated for indicated times with 5  $\mu$ M WP1130 and analyzed by confocal laser scanning microscopy. For GFP-ULK1 expressing cells, zoomed insets are displayed. The GFP-only or GFP-ULK1 signal is displayed in green and the Hoechst signal in blue in the merged images. **(D)** After induction of GFP-ULK1 or GFP-only expression with Dox for 3 h, Flp-In<sup>TM</sup> T-REx<sup>TM</sup> 293 cells were treated with 5  $\mu$ M WP1130 for the indicated intervals. Following WP1130 treatment, detergent-soluble and -insoluble fractions were prepared and analyzed for ULK1, GFP, and ACTB/ $\beta$ -actin levels by immunoblotting. **(A, B and D)** Data shown are representative of at least 3 independent experiments. Fold changes were calculated by dividing each normalized ratio (protein to loading control) by the average of the ratios of the control lane (control lane: fold change = 1.00, n  $\geq$  3). Results are mean  $\pm$  SD and are given below the corresponding blots.

did not induce caspase activity in the relevant time frame (Fig. S8) In summary, we showed that WP1130 increases ubiquitination of GFP-ULK1. Although this effect is likely caused by the inhibition of DUBs, the previously identified WP1130 targets are apparently not involved.

#### WP1130-induced recruitment to aggresomes reduces ULK1 kinase activity

Since we observed that WP1130 treatment leads to the transfer of ULK1 to aggresomes, we next analyzed whether this process also affects ULK1 kinase activity. We have previously identified PRKAB2/AMPK- $\beta$ 2 as direct ULK1 substrate.<sup>24</sup> Thus, we analyzed the phosphorylation status of PRKAB2/AMPK- $\beta$ 2 by immunoblotting. For GFP-ULK1, induction of ectopic over-expression is sufficient to increase ULK1 kinase activity (Fig. 4A) For endogenous ULK1, we starved HEK293 cells in EBSS in order to induce ULK1 kinase activity (Fig. 4B) WP1130 treatment reduced PRKAB2/AMPK- $\beta$ 2 phosphorylation as detected by a faster migration in SDS-PAGE (Fig. 4A and B) We also analyzed phosphorylation of PRKAA/AMPK- $\alpha$  at Thr172. Our group has previously shown that phosphorylation of this activating site is indirectly regulated by ULK1.<sup>24</sup> WP1130 treatment clearly reduced PRKAA/AMPK- $\alpha$  phosphorylation at Thr172 in GFP-ULK1-expressing (Fig. 4A) or wild-type HEK293 cells (Fig. 4B) without affecting total PRKAA/AMPK- $\alpha$  levels. Taken together, these observations suggest that the WP1130-mediated transfer of ULK1 to aggresomes negatively regulates ULK1 activity. In order to exclude the possibility that WP1130 functions as a direct ULK1 kinase inhibitor, we performed an *in vitro* kinase assay with recombinant GST-ULK1 and the substrate GST-myelin basic protein (MBP) in the absence and presence of WP1130. WP1130 did not influence ULK1-dependent phosphorylation of MBP (Fig. 4C) This observation is supported by a kinase screen with WP1130, which was performed by the MRC Protein Phosphorylation Unit in Dundee (UK). None of the 141 tested kinases (including ULK1 and ULK2)

were significantly inhibited by WP1130. The data can be found online at <http://www.kinase-screen.mrc.ac.uk/screening-compounds/591459>. Collectively, these results demonstrate that WP1130 negatively regulates ULK1 activity indirectly through ULK1 aggregation.

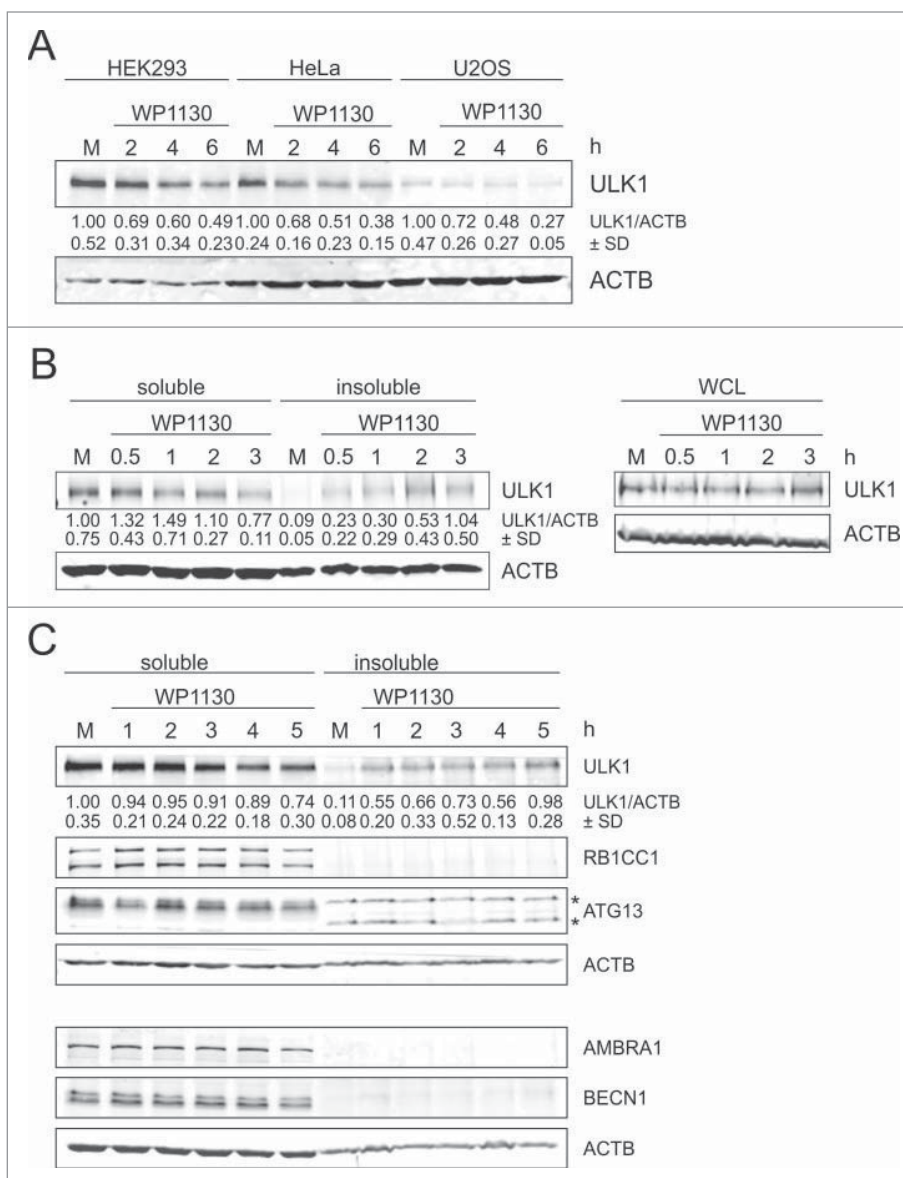


**Figure 2.** WP1130 induces aggregation of endogenous ULK1. **(A)** HEK293, HeLa, or U2OS cells were left untreated or were treated with 5  $\mu$ M WP1130 for 2, 4 or 6 h. Cleared cellular lysates were subjected to anti-ULK1 and anti-ACTB/ $\beta$ -actin immunoblotting. **(B)** HEK293 cells were left untreated or were treated with 5  $\mu$ M WP1130 for indicated intervals. Then detergent-soluble or -insoluble fractions, or whole-cell lysates (WCL) were prepared and analyzed by anti-ULK1 and anti-ACTB/ $\beta$ -actin immunoblotting. **(C)** HEK293 cells were left untreated or were treated with 5  $\mu$ M WP1130 for indicated intervals. Then detergent-soluble or -insoluble fractions were prepared and analyzed for ULK1, RB1CC1, ATG13, AMBRA1, BECN1 and ACTB/ $\beta$ -actin by immunoblotting. Asterisks indicate unspecific background bands. **(A–C)** Data shown are representative of at least 3 independent experiments. Fold changes were calculated by dividing each normalized ratio (protein to loading control) by the average of the ratios of the control lane (control lane: fold change = 1.00,  $n \geq 3$ ). Results are mean  $\pm$  SD and are given below the corresponding blots.

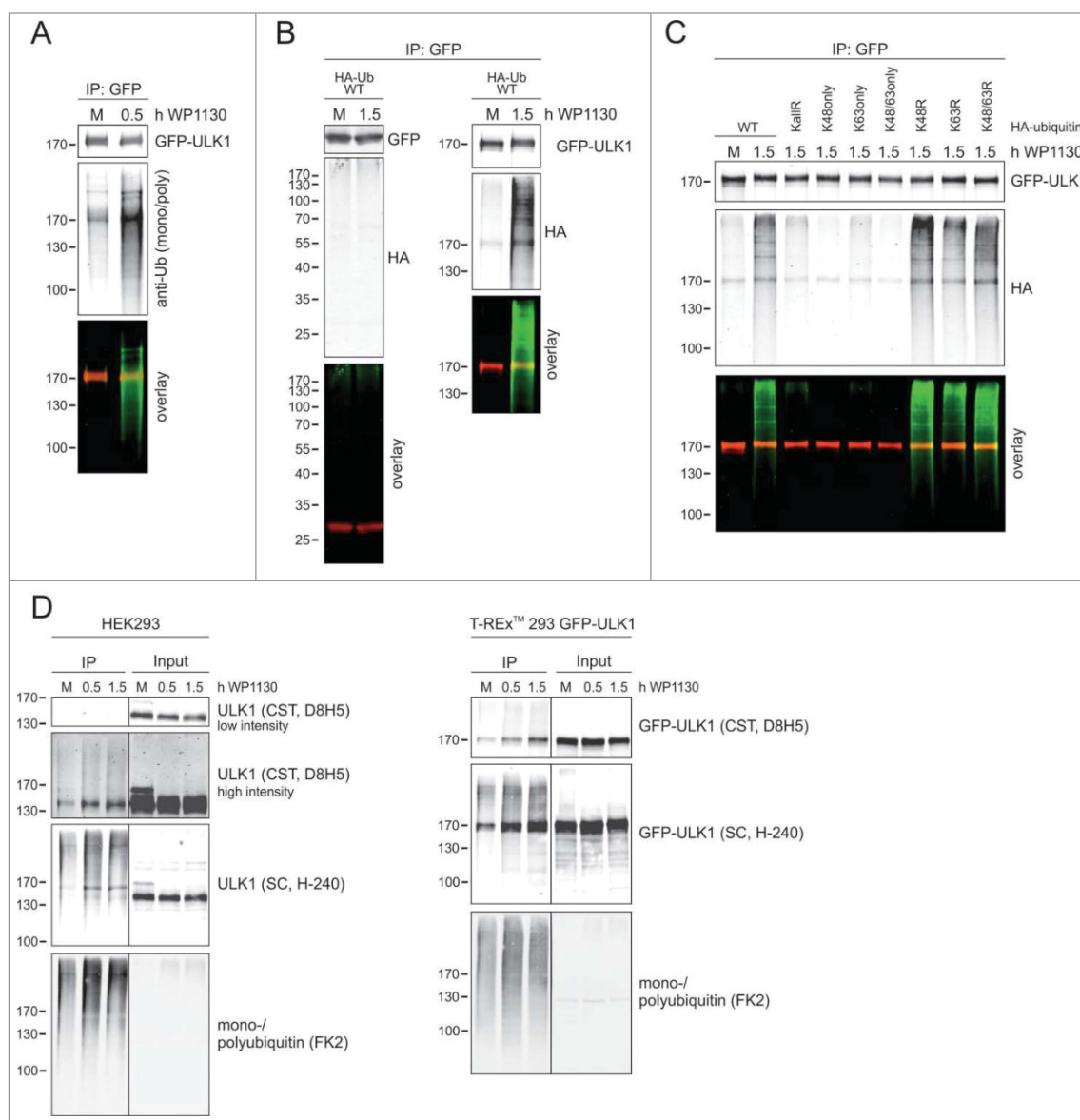


**Figure 3.** DUB inhibition leads to increased GFP-ULK1 ubiquitination. **(A)** After induction of GFP-ULK1 expression with Dox for 3 h, Flp-In™ T-REx™ 293 cells were incubated in full medium (M) with or without 5  $\mu$ M WP1130 for 0.5 h. Subsequently, cells were lysed and GFP-immunoprecipitation was performed. Purified GFP-ULK1 was analyzed by anti-ULK1 and anti-ubiquitin (P4D1) immunoblotting. ULK1 signal is red and ubiquitin signal is green in the merged image. **(B)** Flp-In™ T-REx™ 293 cells were transiently transfected with cDNA encoding HA-ubiquitin 24 h prior to WP1130 treatment. After induction of GFP or GFP-ULK1 expression with Dox for 3 h, cells were incubated in full medium (M) with or without 5  $\mu$ M WP1130 for 1.5 h. Subsequently, cells were lysed and GFP-immunoprecipitation was performed. Purified GFP (left panels) and GFP-ULK1 (right panels) were analyzed by anti-GFP, anti-ULK1 and anti-HA immunoblotting. GFP or GFP-ULK1 signal is red and HA signal is green in the merged images. **(C)** Flp-In™ T-REx™ 293 cells were transiently transfected with cDNAs encoding different HA-ubiquitin variants (WT, KallR, K48only, K63only, K48/63only, K48R, K63R, K48/63R) 24 h prior to WP1130 treatment. After induction of GFP-ULK1 expression with Dox for 3 h, cells were incubated in full medium (M) with or without 5  $\mu$ M WP1130 for 1.5 h. Subsequently, cells were lysed and GFP-immunoprecipitation was performed. Purified GFP-ULK1 was analyzed by anti-ULK1 and anti-HA immunoblotting. ULK1 signal is red and HA signal is green in the merged image. **(D)** HEK293 cells or GFP-ULK1-expressing Flp-In™ T-REx™ 293 cells were left untreated or were treated with 5  $\mu$ M WP1130 for indicated intervals. Subsequently, cells were lysed and immunoprecipitation of ubiquitinated proteins was performed using agarose-TUBE2. Purified ubiquitinated proteins were analyzed by anti-ULK1 (as indicated) or anti-ubiquitin (FK2) immunoblotting.

### WP1130 blocks the autophagic flux

It has been previously speculated that WP1130 might increase autophagy.<sup>27</sup> Since we observed reduced ULK1 activity upon WP1130 treatment, we next wanted to determine the effect of this compound on the autophagic flux. For that, we applied 3

independent readouts. First, we analyzed localization of endogenous LC3 in HEK293 cells by immunofluorescence. Starvation of the cells in EBSS resulted in an increase of LC3 puncta, which was further increased by treatment with bafilomycin A<sub>1</sub> (Fig. 5A). This effect was completely blocked by WP1130. All

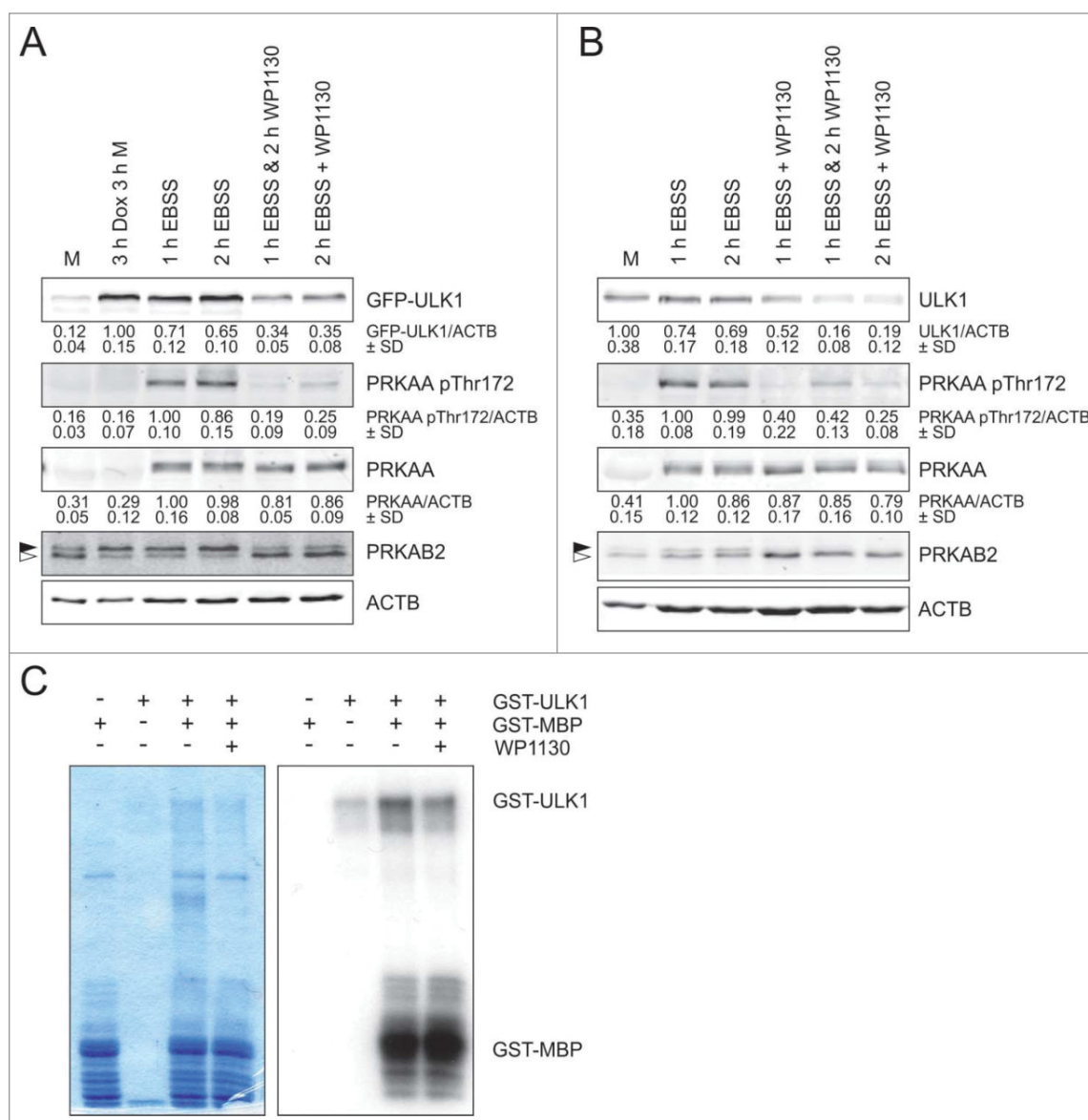


**Figure 4.** ULK1 activity is inhibited by WP1130. **(A)** After induction of GFP-ULK1 expression with Dox for 3 h, Fln<sup>TM</sup> T-REx<sup>TM</sup> 293 cells were incubated in full medium (M) or starvation medium (EBSS) for 1 or 2 h in the presence or absence of 5  $\mu$ M WP1130 for the indicated intervals. Subsequently, cells were lysed and cleared cellular lysates were separated by SDS-PAGE and analyzed by immunoblotting using antibodies against ULK1, PRKAA/AMPK- $\alpha$  (pThr172), PRKAA/AMPK- $\alpha$ , PRKAB1/2 (AMPK- $\beta$ 1/2) and ACTB/ $\beta$ -actin. **(B)** HEK293 cells were treated and analyzed as in **(A)**. **(C)** For an in vitro kinase assay, 1  $\mu$ g GST-myelin basic protein (MBP) was incubated with 0.5  $\mu$ g GST-ULK1 in the absence or presence of 5  $\mu$ M WP1130. As controls, GST-MBP or GST-ULK1 were incubated alone. After Coomassie staining of the gels (left panel), autoradiography was performed (right panel). **(A and B)** Solid arrowheads indicate the phosphorylated form of PRKAB2/AMPK- $\beta$ 2; open arrowheads indicate the unphosphorylated form. Data shown are representative of at least 3 independent experiments. Fold changes were calculated by dividing each normalized ratio (protein to loading control) by the average of the ratios of the control lane (control lane: fold change = 1.00,  $n \geq 3$ ). Results are mean  $\pm$  SD and are given below the corresponding blots.

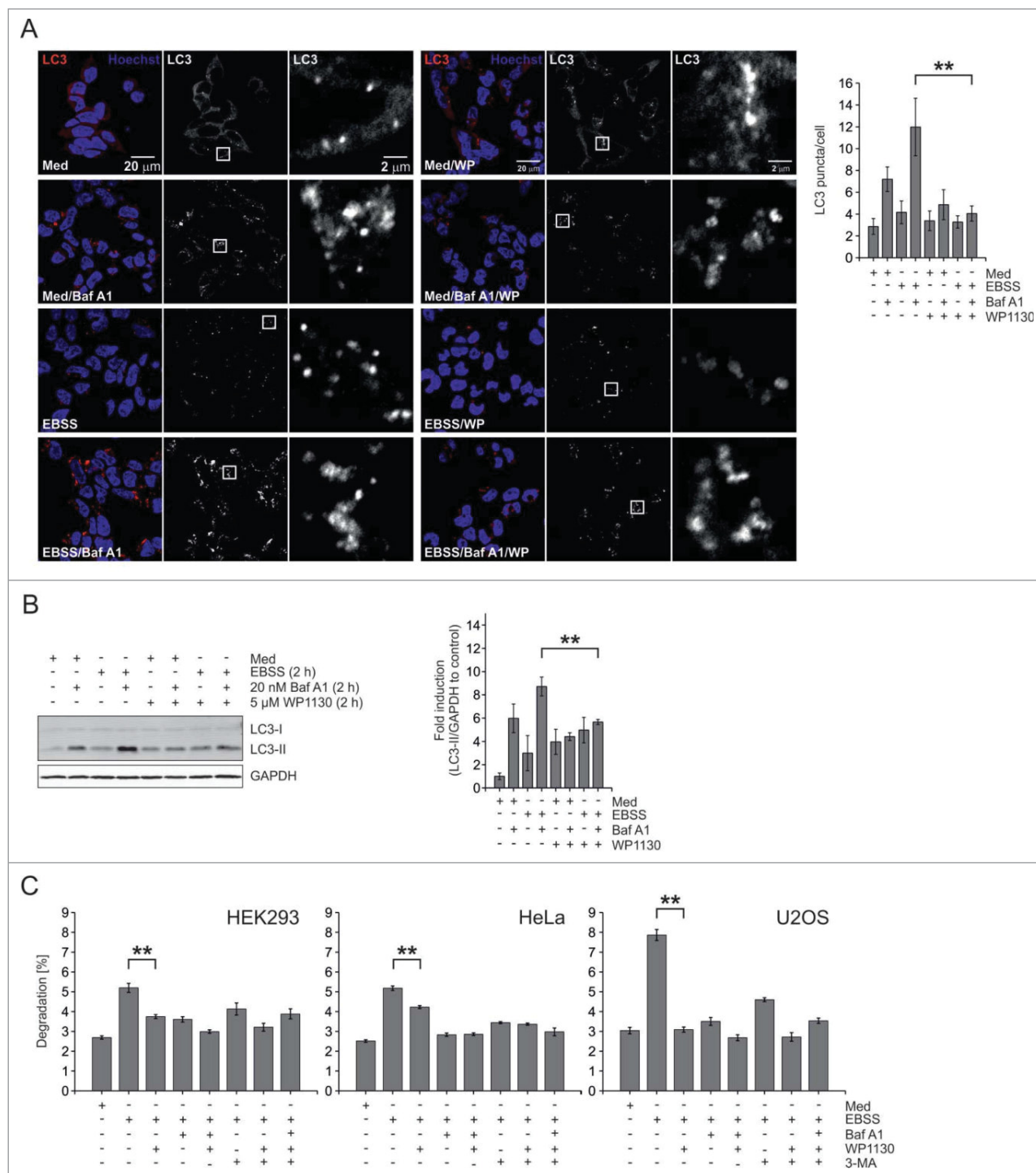
WP1130-treated cells showed similar LC3 puncta numbers, and there was no further increase with EBSS, indicating that autophagy is blocked at an early stage of the pathway. Second, we analyzed LC3 turnover in HEK293 cells by immunoblotting (Fig. 5B). This assay essentially confirmed the results obtained by LC3 immunofluorescence. All lysates derived from cells incubated with WP1130 showed similar LC3-II levels, and again there was no further increase with EBSS treatment. Of note, WP1130

treatment alone increased LC3-II levels. Third, we performed a long-lived protein degradation assay in HEK293, HeLa and U2OS cells (Fig. 5C). In all 3 cell lines, WP1130 significantly reduced the degradation of long-lived proteins. As a control we employed 3-methyladenine (3-MA), which is an inhibitor of the PtdIns3K complex and accordingly also blocks an initial step of the autophagic machinery. In summary, WP1130 efficiently blocks the autophagic flux in HEK293, HeLa, and U2OS cells.

Taken together, we showed that WP1130 targets ULK1/2 for ubiquitination and subsequent transfer to aggresomes, and thereby reduces the overall ULK1/2 enzymatic activity. Furthermore, the WP1130-mediated functional knockdown of ULK1/2 is accompanied with a reduced autophagic potential.

## Discussion

The mammalian ULK1-ATG13-RB1CC1-ATG101 complex is centrally involved in the initiating steps of autophagy. In recent years, the molecular regulation of this complex has been deciphered. Generally, major attention has been attributed to the



phosphorylation of the components of this complex. However, additional posttranslational modifications have been suggested to play an important role for ULK1 complex regulation, including acetylation and ubiquitination.<sup>18,19</sup> Here we report that the treatment of cells with the DUB inhibitor WP1130 leads to increased ULK1 ubiquitination and subsequent recruitment of ULK1 to aggresome-like structures. This ultimately results in reduced ULK1 activity. Furthermore, WP1130 treatment blocks the autophagic flux in HEK293, HeLa, and U2OS cells. Collectively, we hypothesize that the regulation of ULK1 ubiquitination might represent an efficient strategy to modulate autophagy in general and the ULK1 complex in particular.

The observed WP1130 effect might be caused by the fact that the proteasome cannot handle the increased abundance of ubiquitinated proteins in general and of ubiquitinated ULK1 in particular. Accordingly, ULK1 is transported to aggresomes due to proteasomal overload. An alternative possibility is that ULK1 is indeed regulated by a specific ubiquitin conjugation-deconjugation cycle, which becomes disrupted by WP1130-treatment. However, these 2 possibilities are not mutually exclusive and cannot be easily distinguished. Generally, non-K63 ubiquitin chains accumulate upon proteasome inhibition.<sup>35</sup> In turn, it has been previously reported that WP1130 treatment leads to the accumulation of JAK2-containing K63-linked ubiquitin chains or generally to the accumulation of cellular proteins containing both K48- and K63-linked polyubiquitin chains.<sup>26,27</sup> We observe that ULK1 is recruited to aggresome-like structures containing K63-linked ubiquitin. In addition, we found that immunopurified GFP-ULK1 apparently contains non-K48-, non-K63-linked ubiquitin chains. However, it has to be kept in mind that the "ubiquitin barcode" of ULK1 might vary during the trafficking from soluble fractions (which was analyzed in our experiments) to insoluble structures.

Recently, Nazio et al. have reported that MTOR controls ULK1 ubiquitination and function through the class III PtdIns3K complex component AMBRA1 and the associated E3-ligase TRAF6.<sup>19</sup> In their model, MTOR inhibits AMBRA1 under normal growth conditions through phosphorylation. Upon autophagy induction, AMBRA1 becomes dephosphorylated and supports TRAF6-mediated ULK1 ubiquitination. The authors show K63-linked ULK1 ubiquitination, but they do not comment on the lysine residues being ubiquitinated. Generally, Nazio et al. report ULK1 stabilization and self-association upon

ubiquitination. Whereas the latter observation might be in line with ours, we observe a prominent decline in ULK1 activity upon ubiquitination, which is in contrast to their results. Like Nazio et al., we were not able to identify the ubiquitinated lysine residues of ULK1 so far. In addition to TRAF6, it has been reported that the RFW2/COP1 E3 ligase (ring finger and WD repeat domain 2) interacts with the ULK1 complex.<sup>36</sup> Presumably this interaction is mediated via RB1CC1. However, the authors do not observe any alterations of ULK1 expression upon ectopic expression of RFW2.<sup>36</sup> It is likely that additional E3 ligases targeting ULK1 will be identified in the future.

The human genome encodes 79 DUBs which are predicted to be catalytically active, and they can be subdivided into 5 subfamilies.<sup>37</sup> Apparently, the reported WP1130 targets are not, or at least not only, involved in the regulation of ULK1. Especially USP9X has been established as target of WP1130.<sup>27,28,31-33</sup> However, ULK1 levels in the soluble fraction remained unaltered in cells which are deficient for USP9X or in which USP9X has been knocked down by siRNA. Furthermore, LC3 turnover occurred normally in USP9X-negative HCT116 cells, but was blocked by WP1130 treatment in both wild-type (WT) and USP9X-negative cells (data not shown). Taken together, it is well conceivable that additional DUBs or a combination of DUBs mediate the WP1130 effect on ULK1. Of note, the pan-DUB inhibitor PR619 phenocopied the effect of WP1130, indicating that ULK1 accumulation is indeed caused by the inhibition of DUBs. Accordingly, future studies need to reveal the exact positions of the post-translationally modified lysine residues of ULK1, the enzymes involved in ubiquitin conjugation/deconjugation, and the subtype of ubiquitin linkage in order to establish a more complete model of ubiquitin-dependent ULK1 regulation.

It is a difficult approach to determine whether the inhibitory effect of WP1130 on autophagy is solely mediated through the alteration of ULK1/2 ubiquitination, aggregation, and activity. The usage of genetic ULK1/2 knockout systems does not represent an entirely feasible approach since autophagy is largely blocked in these cell models. So far we can only say that putative ULK1/2-independent autophagy pathways are not equally affected by WP1130 (data not shown). Furthermore, of the analyzed proteins so far (i.e., ULK1, ATG13, RB1CC1, BECN1, and AMBRA1), only ULK1 is redistributed to aggresomes upon WP1130 treatment. Nevertheless, future studies will have to

**Figure 5 (See previous page).** The autophagic flux is inhibited by WP1130. **(A)** HEK293 cells were treated with full medium (Med) or starvation medium (EBSS) in the presence or absence of 20 nM bafilomycin A<sub>1</sub> (Baf A1) or 5 μM WP1130 for 2 h and were visualized by confocal laser scanning microscopy. The LC3 signal is displayed in red and the Hoechst signal in blue in the merged images. At least 168 cells were scored for each condition. The number of LC3 puncta and the number of cells per image were quantified using CellProfiler analysis software. Data represent mean ± SD; \*\**P* < 0.01 (Student *t* test, 2-sample assuming unequal variances). **(B)** HEK293 cells were incubated in full medium (Med) or starvation medium (EBSS) in the absence or presence of 20 nM bafilomycin A<sub>1</sub> (Baf A1) and/or 5 μM WP1130 for 2 h. Equal protein amounts from cleared cellular lysates were analyzed for LC3 and GAPDH by immunoblotting. Data shown are representative of at least 3 independent experiments. Fold changes were calculated by dividing each normalized ratio (protein to loading control) by the average of the ratios of the control lane (control lane: fold change = 1.00, *n* ≥ 3). Results are mean ± SD and are depicted in a bar diagram. \*\**P* < 0.01 (Student *t* test, 2-sample assuming unequal variances) **(C)** Cellular proteins of HEK293, HeLa and U2OS cells were labeled with L-[<sup>14</sup>C]valine as described in the Materials and Methods section. Cells were washed and treated with indicated medium (control or EBSS) and inhibitors (5 μM WP1130, 100 nM bafilomycin A<sub>1</sub>, 10 mM 3-methyladenine) for 4 h. For each sample, the radioactivity of the acid-soluble fraction of the medium and the radioactivity in the cells remaining in the well were measured. Percent degradation was assessed as the acid-soluble radioactivity of the medium divided by the total radioactivity. Data shown are mean of triplicates ± SD; \*\**P* < 0.01 (Student *t* test, 2-sample assuming unequal variances).

show whether additional components of the autophagic machinery are regulated by DUBs and thus are potentially involved in the WP1130-mediated inhibition of autophagy.

The ULK1 complex is tightly controlled by a network of upstream nutrient- or energy-sensing kinases, including AKT, MTOR, and AMPK. All these kinases directly phosphorylate ULK1 and thus act to regulate the ULK1 complex (reviewed in ref. 2, 7-11). Accordingly, different small compounds targeting these kinases modulate autophagy, e.g., rapamycin (inhibition of MTOR) or resveratrol (activation of AMPK). Notably, these substances generally induce autophagy. With regard to the inhibition of the autophagic flux, current compounds either target later steps of the autophagic machinery (e.g., bafilomycin A<sub>1</sub>, chloroquine), or the PIK3C3/VPS34-BECN1 complex (e.g., 3-methyladenine). As a serine/threonine kinase, ULK1 represents an appropriate target for pharmacological modulation, and recently the structure of the ULK1 kinase domain in complex with multiple inhibitors has been reported.<sup>38</sup> We propose that the development of more specific inhibitors of ULK1-deubiquitinating enzymes and thus the modulation of ULK1 ubiquitination might represent an alternative strategy to regulate ULK1 function, next to direct inhibition of the kinase activity. Generally, it has been proposed that MTOR inhibitors and other anticancer drugs induce cytoprotective autophagy, ultimately leading to a compromised efficacy of these compounds.<sup>11</sup> Therefore, combinatorial therapies employing these agents and parallel ULK1 inhibition might represent a promising anticancer strategy.

## Materials and Methods

### Cells

HEK293 cells, HeLa cells, U2OS cells, and Flp-In<sup>TM</sup> T-REx<sup>TM</sup> 293 cells (R780-07, Invitrogen, Life Technologies) inducibly expressing GFP-ULK1 WT, GFP-ULK1 kinase-dead (kd), GFP-ULK2 WT or GFP-only were cultured in DMEM (4.5 g/l D-glucose, L-glutamine [Gibco, Life Technologies, 41965-039]), supplemented with 10% fetal calf serum, 50 U/ml penicillin and 50 µg/ml streptomycin (full medium). Expression of the respective fusion protein was induced with 0.1 µg/ml doxycycline (Takara, Clontech, 631311). Wild-type and *USP9X*-/- HCT116 cells (previously described in ref. 34 and kindly provided by Fred Bunz, The Kimmel Cancer Center) were cultured in McCoy 5A medium (PromoCell, C-73220) supplemented with 10% fetal calf serum, 50 U/ml penicillin and 50 µg/ml streptomycin. For amino acid starvation, HEK293 cells and derivatives were washed once and incubated in EBSS (Gibco, Life Technologies, 14155-048) supplemented with 1.8 mM CaCl<sub>2</sub> and 0.813 mM MgSO<sub>4</sub> for the indicated times.

### Antibodies, recombinant proteins, and reagents

Anti-ACTB/β-actin (clone AC-74, A5316), anti-ATG101 (SAB4200175), anti-ATG13 (SAB4200100), and anti-TUBA4A/α-tubulin (clone B-5-1-2, T5168) were purchased from Sigma-Aldrich; anti-BECN1 (11427) and anti-ULK1 (H-240, sc-33182) from Santa Cruz Biotechnology; anti-RB1CC1/

FIP200 (A301-574A) from Bethyl Laboratories; anti-AMBRA1 (pab0224-P) from CovalAb S.A.S.; anti-GAPDH (clone 6C5, ab8245), anti-HA (clone 12CA5, ab16918), and anti-LMNB1/lamin B1 (ab16048) from Abcam; anti-PRKAA/AMPKα (2793), anti-phospho-PRKAA/AMPK-α Thr172 (2535), anti-PRKAB1/2 (AMPK-β1/2) (4150), anti-LC3B (2775), anti-ULK1 (clone D8H5, 8054), and anti-ubiquitin (clone P4D1, 3936) from Cell Signaling Technology; anti-ubiquitin (clone FK2, 04-263) and anti-ubiquitin K63-specific (clone Apu3, 05-1308) from Merck Millipore; anti-LC3 (PM036) and anti-SQSTM1/p62 (PM045) from MBL International; and anti-GFP (11814460001) from Roche Diagnostics. IRDye<sup>®</sup> 680- and IRDye<sup>®</sup> 800-conjugated secondary antibodies (926-68020/21 and 926-32210/11) were provided by LI-COR Biosciences. Alexa Fluor<sup>®</sup> 568-coupled donkey anti-rabbit IgG (H+L) (A10042) or donkey anti-mouse IgG (H+L) (A10037) and Alexa Fluor<sup>®</sup> 594-coupled goat anti-rabbit IgG (H+L) (A11037) were purchased from Molecular Probes, Life Technologies. Hoechst 33342 (H1399) was purchased from Life Technologies; bafilomycin A<sub>1</sub> (B1793), NEM (E3876), pepstatin A (77170), and 3-methyladenine from Sigma-Aldrich; puromycin (ant-pr-1) from InvivoGen (San Diego, CA, USA); Bortezomib (5.043.140.001), calpeptin (03-34-0051), cathepsin Inhibitor III (219419), MG132 (474790), Q-VD-OPh (551476), and Spautin-1 (567569) from Calbiochem, Merck Millipore; and PR619 (SI9619) and LDN 57444 (SI9639) from LifeSensors. WP1130 was purchased from Calbiochem, Merck Millipore (681685) or Axon Medchem BV (1779). GFP-Trap<sup>®</sup> coupled to agarose beads (gta-200) was purchased from ChromoTek. Agarose-TUBE2 was purchased from LifeSensors (UM402). Staurosporine (BML-E1156) was obtained from Enzo Life Sciences. [<sup>14</sup>C] Valine (NEC291EU050UC) was purchased from PerkinElmer. GST-ULK1 (SRP5205) and GST-MPB (SRP5096) were purchased from Sigma-Aldrich. [<sup>32</sup>P]Adenosine 5'-triphosphate (SRP-301) was provided by Hartmann Analytic.

### Expression constructs and transfections

Cloning of the cDNAs encoding human ULK1 or the kinase-dead mutant (D165A) of ULK1 into pcDNA5/FRT/TO-GFP and the generation of the corresponding Flp-In<sup>TM</sup> T-REx<sup>TM</sup> 293 cells has been previously described.<sup>24</sup> Human *ULK2* cDNA was amplified from Jurkat J16 cells and cloned into pcDNA5/FRT/TO-GFP. This vector was cotransfected with pOG44 into Flp-In<sup>TM</sup> TREx<sup>TM</sup> 293 cells (Invitrogen, Life Technologies, R780-07). Stable transfectants were selected with 200 µg/ml hygromycin B (Invitrogen, Life Technologies, 10687-010) and 5 µg/ml blasticidin (Invitrogen, Life Technologies, A11139-02). pCDNA3.1-based vectors encoding different HA-Ubiquitin variants (WT, KallR, K48R, K63R, K48/63R, K48only, K63only, and K48/63only) were obtained from <https://mrcppureagents.dundee.ac.uk> (generated by the MRC Protein Phosphorylation and Ubiquitylation Unit, University of Dundee, UK). For transient transfection, typically 10-cm diameter dishes of GFP-ULK1 Flp-In<sup>TM</sup> T-REx<sup>TM</sup> 293 cells were cultured, and were transfected with 14 µg DNA using FuGENE<sup>®</sup> HD transfection reagent (Roche Diagnostics, 04709713001)

### Immunoblotting and immunopurification

HEK293 cells or derivatives were incubated in full medium or EBSS supplemented with reagents and time points as indicated. Whole-cell lysates were prepared by heating cell pellets in 2x Laemmli reducing sample buffer for 5 min at 95°C. Detergent-soluble and detergent-insoluble fractions were obtained by lysing cells in lysis buffer (50 mM Tris-HCl, pH 7.5, 1 mM EDTA, 1% [v/v] Triton X-100 [Carl Roth GmbH + Co. KG, 3051.2], 1 mM Na<sub>3</sub>VO<sub>4</sub>, 50 mM NaF, 0.1% [v/v] DTT, 150 mM NaCl, Protease Inhibitor Cocktail [Sigma-Aldrich, P2714]) for 30 min on ice and centrifuged for 10 min at 20,000 g at 4°C. The supernatant fraction was used as the detergent-soluble fraction and the residual pellet fraction was heated in 2x Laemmli buffer for 5 min at 95°C and used as the detergent-insoluble fraction. In the case of the detergent-soluble fraction, equal protein amounts (as determined by Bradford assay) were separated on SDS-PAGE followed by standard immunoblot analysis. For the preparation of whole-cell lysates and detergent-insoluble fractions the cell number was adjusted. To immunopurify GFP-ULK1, cells were lysed in the above-mentioned lysis buffer for detergent-soluble fractions (additionally containing 2 mM NEM) for 30 min on ice and centrifuged for 10 min at 20,000 g at 4°C. Immunopurification was carried out for 16 h at 4°C with rotation after addition of GFP-Trap<sup>®</sup> beads. The agarose beads were washed 3 times with lysis buffer containing 2 mM NEM, heated for 5 min at 95°C in 2x Laemmli buffer and used for immunoblotting. Affinity purification of ubiquitinated proteins was carried out with Agarose-TUBE2 as described in the user's manual. The lysis buffer was supplemented with 2 mM NEM.

### In vitro kinase assay

For in vitro phosphorylation, 1 µg GST-MBP was incubated with 0.5 µg GST-ULK1 in 50 mM Tris-HCl, pH 7.5, 0.1 mM EGTA, 0.1 mM DTT, 5 mM Mg(CH<sub>3</sub>COO)<sub>2</sub> and 0.1 mM [<sup>32</sup>P]ATP in the absence or presence of 5 µM WP1130. The reaction was stopped by the addition of SDS sample buffer after 30 min at 30°C, and was then subjected to SDS-PAGE. After Coomassie staining of the gel, autoradiography was performed.

### Confocal laser scanning microscopy and LC3 puncta quantification

HEK293 cells or Flp-In<sup>TM</sup> T-REx<sup>TM</sup> 293 cells inducibly expressing GFP-ULK1 WT, GFP-ULK1 kd, GFP-ULK2 WT, or GFP-only were seeded on poly-L-lysine coated cover slips. Expression of the respective fusion protein was induced with 0.1 µg/ml doxycycline for 3 or 16 h. Incubation of cells was performed in media and for times as indicated. Cells were fixed with 4% paraformaldehyde in phosphate-buffered saline (PBS; Gibco, Life Technologies, 14190-094) buffer for 15 min. For analysis of GFP fusion proteins, cells were directly embedded in Mowiol 4-88 (Carl Roth GmbH + Co. KG, 0713.1) containing 1 µg/ml Hoechst. For immunofluorescent staining of endogenous LC3, ubiquitin, K63-linked ubiquitin and SQSTM1/p62, HEK293 cells were washed 3 times with PBS, incubated in 50 mM NH<sub>4</sub>Cl for 10 min and incubated in PBS for another 5 min. Cells were permeabilized with 0.05% saponin (Sigma-

Aldrich, 47036-50G-F) in PBS for 5 min and incubated for 1 h with the corresponding primary antibodies diluted in 0.05% saponin in PBS. Cells were washed 3 times with 0.05% saponin in PBS and incubated for 1 h with the appropriate secondary antibodies. After washing 2 times with 0.05% saponin in PBS and once with PBS, coverslips were embedded in Mowiol 4-88 containing 1 µg/ml Hoechst. For superresolution microscopy cover slips were embedded in VECTASHIELD mounting medium with DAPI (Vector Laboratories, H-1200). Cells were analyzed on a Zeiss LSM 710, Zeiss LSM 780 or Zeiss Elyra PS microscope (Oberkochen, Germany). Hoechst, DAPI, GFP, Alexa Fluor<sup>®</sup> 568 and Alexa Fluor<sup>®</sup> 594 were excited at 405 nm, 488 nm, 561 nm and 594 nm, respectively. The number of LC3 puncta and number of cells per image were quantified using CellProfiler analysis software.

### Long-lived protein degradation assay

Cells were incubated for 72 h with 0.125 µCi/ml L-[<sup>14</sup>C] valine-supplemented medium, followed by 2 washes and a 16-h chase in fresh medium containing 10 mM nonradioactive L-valine to allow degradation of short-lived proteins. Next, the cells were washed and treated with the indicated medium and inhibitors for 4 h. For each sample, the radioactivity of the acid-soluble fraction of the medium and the radioactivity in the cells remaining in the well were measured.

### Statistical analysis

For western blotting, fold changes were calculated by dividing each normalized density ratio (protein of interest to loading control) by the average of the density ratios of the control lane (control lane: fold change = 1.00, n ≥ 3). Results are mean ± SD and are given below the corresponding blots or are depicted in a bar diagram. For LC3 immunofluorescence, at least 168 cells were scored for each condition. The number of LC3 puncta and the number of cells per image were quantified using CellProfiler analysis software. Data represent mean ± SD and are depicted in a bar diagram. For the long-lived protein degradation assay, the radioactivity of the acid-soluble fraction of the medium and the radioactivity in the cells remaining in the well were measured for each sample. Percent degradation was assessed as the acid-soluble radioactivity of the medium divided by the total radioactivity. Data shown are mean of triplicates ± SD and are depicted in a bar diagram. For all analyses, *P* values were determined by the Student *t* test (2-samples, unequal variances) and the significance levels were set as follows: \* indicates *P* < 0.05, \*\* indicates *P* < 0.01, \*\*\* indicates *P* < 0.001.

### Disclosure of Potential Conflicts of Interest

No potential conflicts of interest were disclosed.

### Acknowledgments

We thank Fred Bunz for providing *USP9X*<sup>+/o</sup> and *USP9X*<sup>-/o</sup> HCT116 cells, and the MRC Protein Phosphorylation and Ubiquitylation Unit (University of Dundee, UK) for providing

anti-USP9X antibodies and cDNAs encoding HA-ubiquitin variants. We thank Stefanie Weidtkamp-Peters and the Center for Advanced Imaging (CAi) of the Heinrich-Heine University Düsseldorf for their support with confocal laser scanning microscopy. We would like to thank Trond Lamark, Terje Johansen, Ian Ganley, and Philip Cohen for helpful discussions.

### Funding

This work was supported by the Deutsche Forschungsgemeinschaft STO 864/3-1 and STO 864/4-1 (to B.S.), the Research

Committee of the Medical Faculty of the Heinrich-Heine-University Düsseldorf 58/2013 (to B.S.), and the Düsseldorf School of Oncology (to S.W. and B.S.; funded by the Comprehensive Cancer Center Düsseldorf/Deutsche Krebshilfe and the Medical Faculty of the Heinrich-Heine-University Düsseldorf).

### Supplemental Material

Supplemental data for this article can be accessed on the publisher's website.

### References

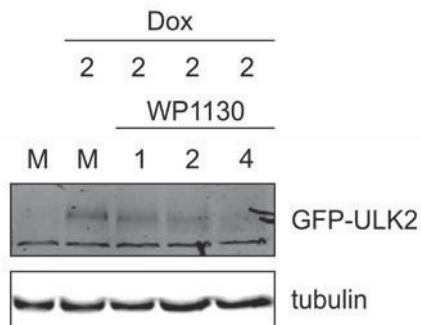
- Mizushima N, Yoshimori T, Ohsumi Y. The role of Atg proteins in autophagosome formation. *Annu Rev Cell Dev Biol* 2011; 27:107-32; PMID:21801009; <http://dx.doi.org/10.1146/annurev-cellbio-092910-154005>
- Alers S, Löffler AS, Wesselborg S, Stork B. Role of AMPK-mTOR-Ulk1/2 in the regulation of autophagy: cross talk, shortcuts, and feedbacks. *Mol Cell Biol* 2012; 32:2-11; PMID:22025673; <http://dx.doi.org/10.1128/MCB.06159-11>
- Chan EY, Longatti A, McKnight NC, Tooze SA. Kinase-inactivated ULK proteins inhibit autophagy via their conserved C-terminal domains using an Atg13-independent mechanism. *Mol Cell Biol* 2009; 29:157-71; PMID:18936157; <http://dx.doi.org/10.1128/MCB.01082-08>
- Ganley IG, Lam du H, Wang J, Ding X, Chen S, Jiang X. ULK1-ATG13-FIP200 complex mediates mTOR signaling and is essential for autophagy. *J Biol Chem* 2009; 284:12297-305; PMID:19258318
- Hosokawa N, Hara T, Kaizuka T, Kishi C, Takamura A, Miura Y, Iemura S, Natsume T, Takehana K, Yamada N, et al. Nutrient-dependent mTORC1 association with the ULK1-Atg13-FIP200 complex required for autophagy. *Mol Biol Cell* 2009; 20:1981-91; PMID:19211835; <http://dx.doi.org/10.1091/mbc.E08-12-1248>
- Jung CH, Jun CB, Ro SH, Kim YM, Otto NM, Cao J, Kundu M, Kim DH. ULK-Atg13-FIP200 complexes mediate mTOR signaling to the autophagy machinery. *Mol Biol Cell* 2009; 20:1992-2003; PMID:19225151; <http://dx.doi.org/10.1091/mbc.E08-12-1249>
- Alers S, Löffler AS, Wesselborg S, Stork B. The incredible ULKs. *Cell Commun Signal* 2012; 10:7; PMID:22413737; <http://dx.doi.org/10.1186/1478-811X-10-7>
- Chan EY. mTORC1 phosphorylates the ULK1-mAtg13-FIP200 autophagy regulatory complex. *Sci Signal* 2009; 2:pe51; PMID:19690328; <http://dx.doi.org/10.1126/scisignal.284pe51>
- Chan EY, Tooze SA. Evolution of Atg1 function and regulation. *Autophagy* 2009; 5:758-65; PMID:19411825; <http://dx.doi.org/10.4161/auto.8709>
- Mizushima N. The role of the Atg1/ULK1 complex in autophagy regulation. *Curr Opin Cell Biol* 2010; 22:132-9; PMID:20056399; <http://dx.doi.org/10.1016/j.ccb.2009.12.004>
- Wong PM, Puente C, Ganley IG, Jiang X. The ULK1 complex: sensing nutrient signals for autophagy activation. *Autophagy* 2013; 9:124-37; PMID:23295650; <http://dx.doi.org/10.4161/auto.23323>
- Alers S, Löffler AS, Paasch F, Dieterle AM, Keppeler H, Lauber K, Campbell DG, Fehrenbacher B, Schaller M, Wesselborg S, et al. Atg13 and FIP200 act independently of Ulk1 and Ulk2 in autophagy induction. *Autophagy* 2011; 7:1423-33; PMID:22024743; <http://dx.doi.org/10.4161/auto.7.12.18027>
- Bach M, Larance M, James DE, Ramm G. The serine/threonine kinase ULK1 is a target of multiple phosphorylation events. *Biochem J* 2011; 440:283-91; PMID:21819378; <http://dx.doi.org/10.1042/BJ20101894>
- Egan DF, Shackelford DB, Mihaylova MM, Gelino S, Kohnz RA, Mair W, Vasquez DS, Joshi A, Gwinn DM, Taylor R, et al. Phosphorylation of ULK1 (hATG1) by AMP-activated protein kinase connects energy sensing to mitophagy. *Sci* 2011; 331:456-61; PMID:21205641; <http://dx.doi.org/10.1126/science.1196371>
- Kim J, Kundu M, Viollet B, Guan KL. AMPK and mTOR regulate autophagy through direct phosphorylation of Ulk1. *Nat Cell Biol* 2011; 13:132-41; PMID:21258367; <http://dx.doi.org/10.1038/ncb2152>
- Mack HI, Zheng B, Asara JM, Thomas SM. AMPK-dependent phosphorylation of ULK1 regulates ATG9 localization. *Autophagy* 2012; 8:1197-214; PMID:22932492; <http://dx.doi.org/10.4161/auto.20586>
- Shang L, Chen S, Du F, Li S, Zhao L, Wang X. Nutrient starvation elicits an acute autophagic response mediated by Ulk1 dephosphorylation and its subsequent dissociation from AMPK. *Proc Natl Acad Sci U S A* 2011; 108:4788-93; PMID:21383122; <http://dx.doi.org/10.1073/pnas.1100844108>
- Lin SY, Li TY, Liu Q, Zhang C, Li X, Chen Y, Zhang SM, Lian G, Ruan K, Wang Z, et al. GSK3-TIP60-ULK1 signaling pathway links growth factor deprivation to autophagy. *Sci* 2012; 336:477-81; PMID:22539723; <http://dx.doi.org/10.1126/science.1217032>
- Nazio F, Strappazzon F, Antonioli M, Bielli P, Cianfanelli V, Bordini M, Grotzmeier C, Dengjel J, Piacentini M, Fimia GM, et al. mTOR inhibits autophagy by controlling ULK1 ubiquitylation, self-association and function through AMBRA1 and TRAF6. *Nat Cell Biol* 2013; 15:406-16; PMID:23524951; <http://dx.doi.org/10.1038/ncb2708>
- Di Bartolomeo S, Corazzari M, Nazio F, Oliverio S, Lisi G, Antonioli M, Pagliarini V, Matteoni S, Fuoco C, Giunta L, et al. The dynamic interaction of AMBRA1 with the dynein motor complex regulates mammalian autophagy. *J Cell Biol* 2010; 191:155-68; PMID:20921139; <http://dx.doi.org/10.1083/jcb.201002100>
- Russell RC, Tian Y, Yuan H, Park HW, Chang YY, Kim J, Kim H, Neufeld TP, Dillin A, Guan KL. ULK1 induces autophagy by phosphorylating Beclin-1 and activating VPS34 lipid kinase. *Nat Cell Biol* 2013; 15:741-50; PMID:23685627; <http://dx.doi.org/10.1038/ncb2757>
- Tang HW, Wang YB, Wang SL, Wu MH, Lin SY, Chen GC. Atg1-mediated myosin II activation regulates autophagosome formation during starvation-induced autophagy. *EMBO J* 2011; 30:636-51; PMID:21169990; <http://dx.doi.org/10.1038/emboj.2010.338>
- Papinski D, Schuschnig M, Reiter W, Wilhelm L, Barnes CA, Maiolica A, Hansmann I, Pfaffenwimmer T, Kijanska M, Stoffel I, et al. Early steps in autophagy depend on direct phosphorylation of atg9 by the atg1 kinase. *Mole Cell* 2014; 53:471-83; PMID:24440502; <http://dx.doi.org/10.1016/j.molcel.2013.12.011>
- Löffler AS, Alers S, Dieterle AM, Keppeler H, Franz-Wachtel M, Kundu M, Campbell DG, Wesselborg S, Alessi DR, Stork B. Ulk1-mediated phosphorylation of AMPK constitutes a negative regulatory feedback loop. *Autophagy* 2011; 7:696-706; PMID:21460634; <http://dx.doi.org/10.4161/auto.7.7.15451>
- Bartholomeusz GA, Talpaz M, Kapuria V, Kong LY, Wang S, Estrov Z, Priebe W, Wu J, Donato NJ. Activation of a novel Bcr/Abl destruction pathway by WP1130 induces apoptosis of chronic myelogenous leukemia cells. *Blood* 2007; 109:3470-8; PMID:17202319; <http://dx.doi.org/10.1182/blood-2006-02-005579>
- Kapur V, Levitzki A, Bornmann WG, Maxwell D, Priebe W, Sorenson RJ, Showalter HD, Talpaz M, Donato NJ. A novel small molecule deubiquitinase inhibitor blocks Jak2 signaling through Jak2 ubiquitination. *Cell Signal* 2011; 23:2076-85; PMID:21855629; <http://dx.doi.org/10.1016/j.celsig.2011.08.002>
- Kapur V, Peterson LF, Fang D, Bornmann WG, Talpaz M, Donato NJ. Deubiquitinase inhibition by small-molecule WP1130 triggers aggresome formation and tumor cell apoptosis. *Cancer Res* 2010; 70:9265-76; PMID:21045142; <http://dx.doi.org/10.1158/0008-5472.CAN-10-1530>
- Sun H, Kapuria V, Peterson LF, Fang D, Bornmann WG, Bartholomeusz G, Talpaz M, Donato NJ. Bcr-Abl ubiquitination and Usp9x inhibition block kinase signaling and promote CML cell apoptosis. *Blood* 2011; 117:3151-62; PMID:21248063; <http://dx.doi.org/10.1182/blood-2010-03-276477>
- Johnston JA, Ward CL, Kopito RR. Aggresomes: a cellular response to misfolded proteins. *J Cell Biol* 1998; 143:1883-98; PMID:9864362; <http://dx.doi.org/10.1083/jcb.143.7.1883>
- Alemu EA, Lamark T, Torgersen KM, Birgisdotir AB, Larsen KB, Jain A, Olsvik H, Overvatn A, Kirkin V, Johansen T. ATG8 family proteins act as scaffolds for assembly of the ULK complex: sequence requirements for LC3-interacting region (LIR) motifs. *J Biol Chem* 2012; 287:39275-90; PMID:23043107; <http://dx.doi.org/10.1074/jbc.M112.378109>
- Peddaboina C, Jupiter D, Fletcher S, Yap JL, Rai A, Tobin RP, Jiang W, Rascoe P, Rogers MK, Smythe WR, et al. The downregulation of Mcl1 via USP9X inhibition sensitizes solid tumors to Bclxl inhibition. *BMC Cancer* 2012; 12:541; PMID:23171055; <http://dx.doi.org/10.1186/1471-2407-12-541>
- Peng Z, Maxwell DS, Sun D, Bhanu Prasad BA, Schuber PT, Jr., Pal A, Ying Y, Han D, Gao L, Wang S, et al. Degrasyn-like symmetrical compounds: Possible therapeutic agents for multiple myeloma (MM-1). *Bioorg Med Chem* 2014; 22:1450-8; PMID:24457091; <http://dx.doi.org/10.1016/j.bmc.2013.12.048>
- Wang S, Kollipara RK, Srivastava N, Li R, Ravindranathan P, Hernandez E, Freeman E, Humphries CG, Kapur P, Lotan Y, et al. Ablation of the oncogenic transcription factor ERG by deubiquitinase inhibition in prostate cancer. *Proc Natl Acad Sci U S A* 2014; 111(11):4251-6; PMID:24591637; <http://dx.doi.org/10.1073/pnas.1322198111>
- Harris DR, Mims A, Bunz F. Genetic disruption of USP9X sensitizes colorectal cancer cells to 5-fluorouracil.

- Cancer Biol Therapy 2012; 13:1319-24; PMID:22895071; <http://dx.doi.org/10.4161/cbt.21792>
35. Xu P, Duong DM, Seyfried NT, Cheng D, Xie Y, Robert J, Rush J, Hochstrasser M, Finley D, Peng J. Quantitative proteomics reveals the function of unconventional ubiquitin chains in proteasomal degradation. *Cell* 2009; 137:133-45; PMID:19345192; <http://dx.doi.org/10.1016/j.cell.2009.01.041>
36. Kobayashi S, Yoneda-Kato N, Itahara N, Yoshida A, Kato JY. The COP1 E3-ligase interacts with FIP200, a key regulator of mammalian autophagy. *BMC Biochem* 2013; 14:1; PMID:23289756; <http://dx.doi.org/10.1186/1471-2091-14-1>
37. Komander D, Clague MJ, Urbe S. Breaking the chains: structure and function of the deubiquitinases. *Nat Rev Mol Cell Biol* 2009; 10:550-63; PMID:19626045; <http://dx.doi.org/10.1038/nrm2731>
38. Lazarus MB, Novotny CJ, Shokat KM. Structure of the Human Autophagy Initiating Kinase ULK1 in Complex with Potent Inhibitors. *ACS Chem Biol* 2015; 10(1):257-61; PMID:25551253; <http://dx.doi.org/10.1021/cb500835z>

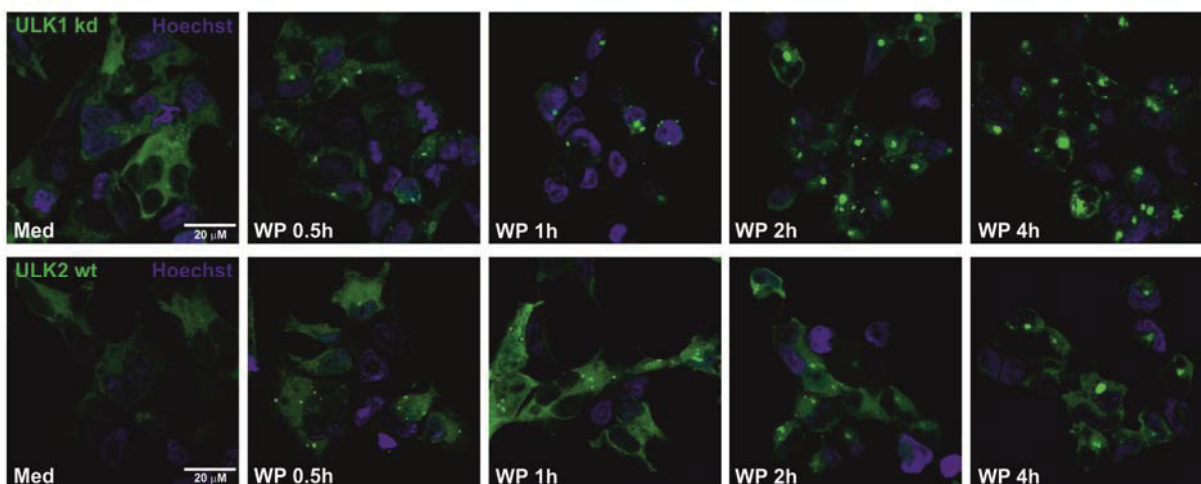
## Supplementary Figures

### Supplementary Figure 1

A

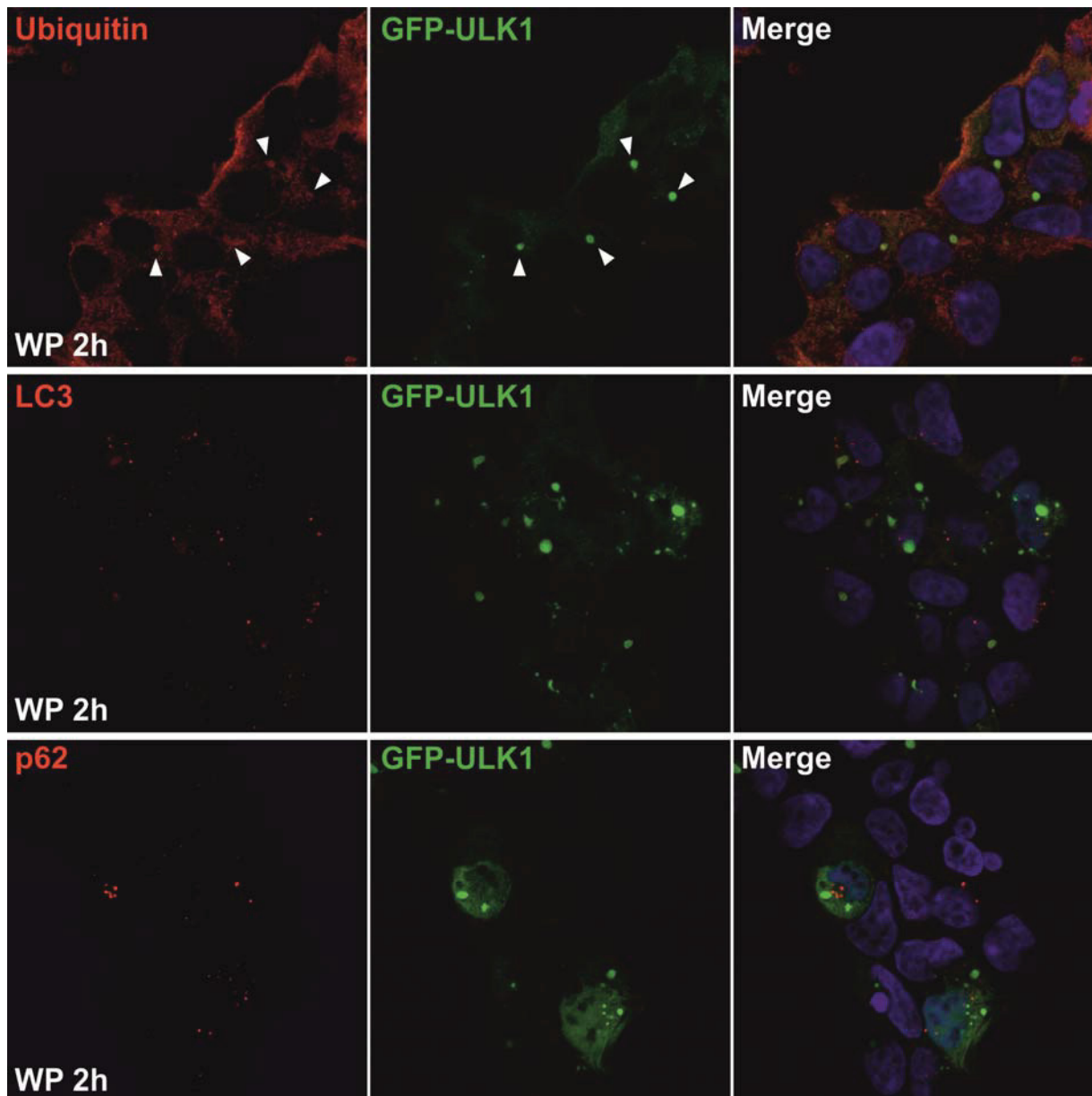


B



**WP1130 induces aggregation of GFP-ULK2 and kinase-dead GFP-ULK1.** (A) After induction of GFP-ULK2 expression with doxycycline (Dox) for indicated times, Flp-In<sup>TM</sup> T-REX<sup>TM</sup> 293 GFP-ULK2 cells were treated with 5 μM WP1130 for 1, 2 or 4 h. Equal protein amounts of cleared cellular lysates were subjected to anti-GFP and anti-tubulin immunoblotting. (B) After induction of GFP-ULK1 kinase-dead (kd) or GFP-ULK2 expression with Dox for 3 h, Flp-In<sup>TM</sup> T-REX<sup>TM</sup> 293 cells were treated for indicated times with 5 μM WP1130 and analyzed by confocal laser scanning microscopy. The GFP-ULK1 kd or GFP-ULK2 signal is displayed in green and the Hoechst signal in blue.

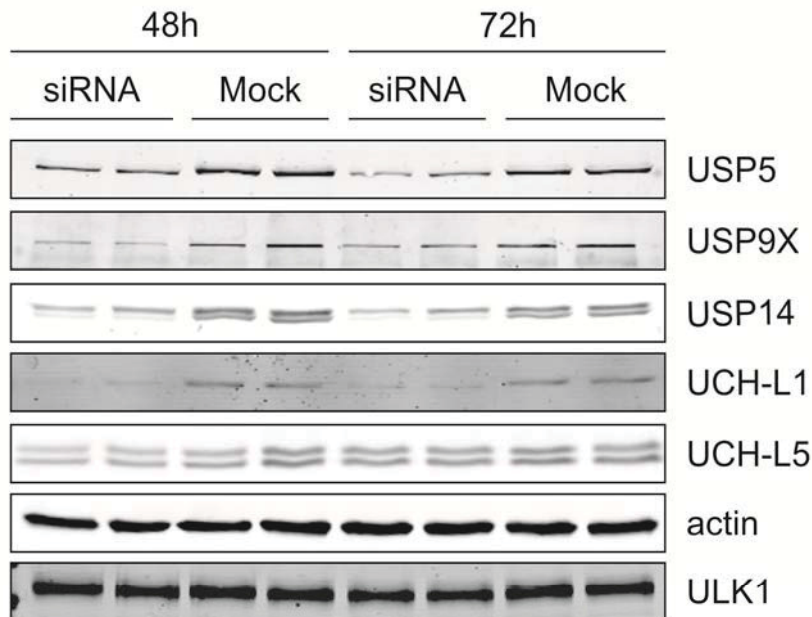
Supplementary Figure 2



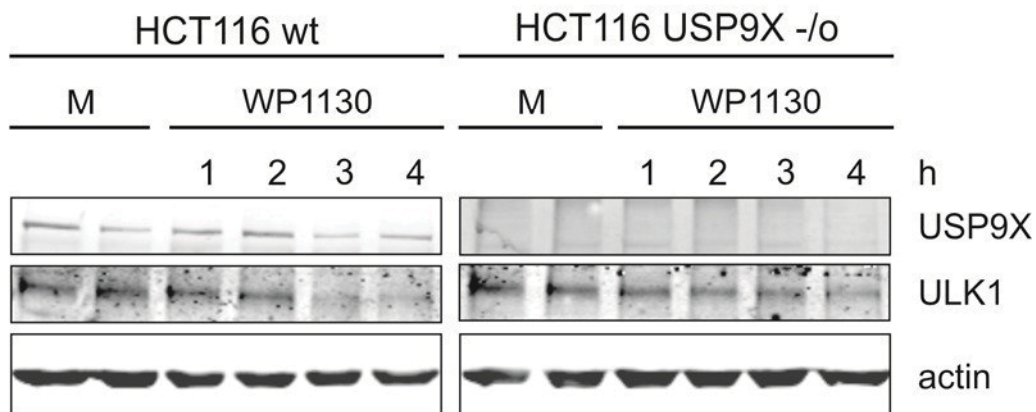
**WP1130 induced aggresomes comprise ubiquitin but do apparently not contain p62 or LC3.** After induction of GFP-ULK1 expression with doxycycline (Dox) for 3 h, Flp-In<sup>TM</sup> T-REX<sup>TM</sup> 293 GFP-ULK1 cells were treated with 5  $\mu$ M WP1130 for 2 h, immunostained for ubiquitin, LC3 and p62, and analyzed by confocal laser scanning microscopy. In the upper panels, aggresomes stained for ubiquitin and GFP-ULK1 are indicated by white arrowheads.

Supplementary Figure 3

**A**



**B**



**Knockdown or knockout of various deubiquitinases targeted by WP1130 does not result in aggregation of endogenous ULK1.** (A) HEK293 cells were simultaneously transfected with 20 nM ON-TARGETplus SMARTpool® siRNA for USP5, USP9X, USP14, UCH-L1 and UCH-L5. Cells were incubated for 48 or 72 h. Equal protein amounts of cleared cellular lysates were analyzed by immunoblotting for USP5, USP9X, USP14, UCH-L1, UCH-L5, actin and ULK1. (B) HCT116 wt cells and HCT116 USP9X knockout cells were treated with 5  $\mu$ M WP1130 for indicated times. Cleared cellular lysates were subjected to anti-USP9X, anti-ULK1 and anti-actin immunoblotting.

Supplementary Figure 4

DUB <sup>profiler</sup> ™ Single Point Screening (Ubiquigent Ltd, Dundee, Scotland, UK)							
Activity [% Control]*							
	WP1130 concentration [μM]	1	10		WP1130 concentration [μM]	1	10
Compound control	Product Signal Modulation**	-3	-5	Compound control	Product Signal Modulation**	-3	-5
USPs	USP1	91	94	UCHs	UCHL1	99	78
	USP2	100	111		UCHL3	97	88
	USP4	91	95		UCHL5	89	86
	USP5	98	93		BAP1	87	82
	USP6	97	109	OTUs	OTU1	97	99
	USP7	91	96		OTUB2	88	80
	USP9X	93	85		OTUD3	101	102
	USP11	105	98		OTUD6A	88	97
	USP15	99	96		OTUD6B	96	87
	USP19	126	109		Cezanne	89	87
	USP20	91	96	JAMMs	AMSH-LP	96	93
	USP21	88	89		AMSH-LP (+Zinc)	94	99
	USP25	102	92	Josephins	Ataxin3	97	80
	USP28	97	105		Ataxin3L	108	105
	USP30	102	102		JOSD1	126	116
	USP35	105	88		JOSD2	110	93
	USP36	90	96				
	USP45	106	100				
	CYLD	84	91				

\* % Control = ((sample - mean no enzyme)/(mean plus enzyme - mean no enzyme))\*100

\*\* Product Signal Modulation = ((sample - mean modulator control)/(mean modulator control))\*100

**WP1130 does not significantly inhibit 35 members of the DUB family.** The DUB<sup>profiler</sup>™ Single Point Screening was performed by Ubiquigent Ltd (Dundee, Scotland, UK). WP1130 was tested at two different concentrations (1 or 10 μM) in a ubiquitin-rhodamine(110)-glycine substrate-based assay. Data given represent activity [% control].

## Supplementary Movies 1-3

Movie 1: GFP-ULK1\_Medium.avi

Movie 2: GFP-ULK1\_WP1130.avi

Movie 3: GFP-ULK1\_WP1130 + nocodazole.avi

**WP1130 induces transfer of GFP-ULK1 to aggresomes.** After induction of GFP-ULK1 expression with doxycycline (Dox) for 3 h, Flp-In<sup>TM</sup> T-REx<sup>TM</sup> 293 GFP-ULK1 cells were treated with 5  $\mu$ M WP1130 with and without 10  $\mu$ M nocodazole over a time period of 4 h. GFP-ULK1 was visualized by live-cell-imaging.

## Supplementary Materials and Methods

### *Generation of Flp-In<sup>TM</sup> T-REx<sup>TM</sup> 293 cells inducible expressing GFP-ULK1 kd or GFP-ULK2*

Cloning of the cDNA encoding the kinase-dead mutant (D165A) of human ULK1 into pcDNA5/FRT/TO-GFP and the generation of the corresponding Flp-In<sup>TM</sup> T-REx<sup>TM</sup> 293 cells has been previously described.<sup>24</sup> Human *ULK2* cDNA was amplified from Jurkat J16 cells and cloned into pcDNA5/FRT/TO-GFP. This vector was co-transfected with pOG44 into Flp-In<sup>TM</sup> T-REx<sup>TM</sup> 293 cells (R780-07, Invitrogen, Life Technologies, Carlsbad, CA, USA). Stable transfectants were selected with 200 µg/ml hygromycin B (10687-010, Invitrogen, Life Technologies) and 5 µg/ml blasticidin (A11139-02, Invitrogen, Life Technologies).

### *Immunofluorescence of ubiquitin, LC3, and p62*

Flp-In<sup>TM</sup> T-REx<sup>TM</sup> 293 GFP-ULK1 cells were seeded overnight on poly-L-lysine coated cover slips. After induction of GFP-ULK1 expression with doxycycline for 3 h, cells were washed with PBS and fixed in 4% PFA for 15 min. Hereafter cells were washed three times with PBS, incubated in 50 mM NH<sub>4</sub>Cl for 10 min and incubated in PBS for another 5 min. Cells were permeabilized with 0.05% Saponin (47036-50G-F, Sigma-Aldrich, St. Louis, MO, USA) in PBS for 5 min and incubated for 1 h with anti-ubiquitin (04-263, clone FK2, Upstate, Merck Millipore, Darmstadt, Germany), anti-LC3 (PM036, MBL International, Woburn, MA, USA) or anti-p62 (PM045, MBL International, Woburn, MA, USA), respectively. Antibodies were diluted in 0.05% Saponin in PBS. Cells were washed three times with 0.05% Saponin in PBS and incubated for 1 h with Alexa Fluor®647-coupled anti-rabbit IgG (H+L) (111-605-003, Jackson ImmunoResearch Laboratories, West Grove, PA, USA) or anti-mouse IgG (H+L) (115-605-003, Jackson ImmunoResearch Laboratories, West Grove, PA, USA), respectively. After washing two times with 0.05% Saponin in PBS and once with PBS, cover slips were embedded in Mowiol 4-88 containing 1 µg/ml Hoechst on an object slide.

### *siRNA-mediated knockdown of DUBs*

HEK293 cells were seeded on a 24-well plate overnight. Cells were transfected according to manufacturer's instructions with 20 nM ON-TARGETplus SMARTpool® siRNA (Dharmacon, Thermo Scientific, Waltham, MA, USA) of USP5 (L-006095-00-0005), USP9X (L-006099-00-0005), USP14 (L-006065-00-0005), UCH-L1 (L-004309-00-0005) and UCH-L5 (L-006060-00-

0005). Knockdown efficiency was analyzed by immunoblotting for USP5 (A301-542A, Bethyl Laboratories Inc., MO, USA), USP9X (kindly provided by the Division of Signal Transduction Therapy, College of Life Sciences, University of Dundee, Scotland, UK), USP14 (8159, Cell Signaling Technology), UCH-L1 (3524, Cell Signaling Technology), UCH-L5 (ab124931, Abcam), actin and ULK1.

#### *Live-cell imaging*

Flp-In<sup>TM</sup> T-REx<sup>TM</sup> 293 GFP-ULK1 cells were seeded overnight onto Nunc<sup>TM</sup> Lab-Tek<sup>TM</sup> Chambered Coverglasses (155411, Thermo Scientific, Waltham, MA, USA). After induction of GFP-ULK1 expression with doxycycline for 3 h, media was replaced with DMEM-GFP medium (Evrogen) and treated with 5  $\mu$ M WP1130 with or without 10  $\mu$ M nocodazole (Sigma Aldrich). Life cell imaging of GFP-Ulk1 was performed on a Deltavision Deconvolution microscope (GE Healthcare, Issaquah, WA) equipped with a solid-state light source, a 60x NA 1.42 objective and a Coolsnap HQ2 CCD camera. The cells were kept at 37°C and 5% CO<sub>2</sub> using a CO<sub>2</sub>- and temperature-controlled incubator (Okolabs).

# Paper 3



# Systematic analysis of ATG13 domain requirements for autophagy induction

## AUTHORS/AFFILIATIONS

Nora Wallot-Hieke<sup>1</sup>, Neha Verma<sup>2</sup>, David Schlütermann<sup>1</sup>, Niklas Berleth<sup>1</sup>, Jana Deitersen<sup>1</sup>, Philip Böhrer<sup>1</sup>, Fabian Stuhldreier<sup>1</sup>, Wenxian Wu<sup>1</sup>, Sabine Seggewiß<sup>1</sup>, Christoph Peter<sup>1</sup>, Holger Gohlke<sup>2</sup>, Noboru Mizushima<sup>3</sup>, Björn Stork<sup>1,\*</sup>

<sup>1</sup>*Institute of Molecular Medicine I, Medical Faculty, Heinrich Heine University Düsseldorf, 40225 Düsseldorf, Germany*

<sup>2</sup>*Institute for Pharmaceutical and Medicinal Chemistry, Faculty of Mathematics and Natural Sciences, Heinrich Heine University Düsseldorf, 40225 Düsseldorf, Germany*

<sup>3</sup>*Department of Biochemistry and Molecular Biology, Graduate School and Faculty of Medicine, The University of Tokyo, Tokyo 113-0033, Japan*

## CONTACT

\*Corresponding author:

Björn Stork, Universitätsstr. 1, Building 23.12, 40225 Düsseldorf, Germany,

Tel.: +49 (0)211 81 11954, Fax: +49 (0)211 81 14103, E-mail: bjoern.stork@uni-duesseldorf.de

**KEYWORDS:** ATG13, ATG101, autophagy, RB1CC1, ULK1

**ABBREVIATIONS:** AMPK, AMP-activated protein kinase; ATG, autophagy-related; BafA1, bafilomycin A1; EBSS, Earle's Balanced Salt Solution; GABARAP, Gamma-aminobutyric acid A receptor-associated protein; HORMA, Hsp1, Rev7 and MAD2; KO, knockout; LIR, LC3-interacting region; MAP1LC3/LC3, microtubule-associated protein 1 light chain 3; MEF, mouse embryonic fibroblast; MM-GB/SA, molecular mechanics Generalized Born solvent-accessible surface area; MTORC1/2, mechanistic target of rapamycin (serine/threonine kinase) complex 1/2; PAS, phagophore assembly site; PLPD, phospholipid-binding domain; RB1CC1/FIP200, RB1-inducible coiled-coil 1; RPS6KB1, ribosomal protein S6 kinase, polypeptide 1; SQSTM1/p62, sequestosome 1; ULK1/2, unc-51 like kinase 1/2; WIP2, WD repeat domain, phosphoinositide interacting 2; WT, wild-type

## ABSTRACT

Macroautophagy/autophagy is an evolutionarily conserved cellular process whose induction is regulated by the ULK1 protein kinase complex. The subunit ATG13 functions as an adaptor protein by recruiting ULK1, RB1CC1 and ATG101 to a core ULK1 complex. Furthermore, ATG13 directly binds both phospholipids and members of the Atg8 family. The central involvement of ATG13 in complex formation makes it an attractive target for autophagy regulation. Here, we analyzed known interactions of ATG13 with proteins and lipids for their potential modulation of ULK1 complex formation and autophagy induction. Targeting the ATG101-ATG13 interaction showed the strongest autophagy-inhibitory effect, whereas the inhibition of binding to ULK1 or RB1CC1 had only minor effects, emphasizing that mutations interfering with ULK1 complex assembly do not necessarily result in a blockade of autophagy. Furthermore, inhibition of ATG13 binding to phospholipids or ATG8 proteins had only mild effects on autophagy. Generally, the observed phenotypes were more severe when autophagy was induced by MTORC1/2 inhibition compared to amino acid starvation. Collectively, these data establish the interaction between ATG13 and ATG101 as a promising target in disease-settings where the inhibition of autophagy is desired.

## INTRODUCTION

Autophagy is an intracellular degradation process mediating the clearance of misfolded or damaged proteins, protein aggregates, or entire organelles. During the course of autophagy, a phagophore forms from microdomains of the ER. This phagophore further engulfs the cargo to be removed. By addition of membrane compartments originating from different cellular sources, the phagophore closes into a mature autophagosome. This double-membraned vesicle then fuses with lysosomes, giving rise to an autolysosome in which the cargo becomes degraded by lysosomal hydrolases. This process is conserved from yeast to higher eukaryotes including mammals, and autophagy is essential for functional metabolism and cell integrity. Accordingly, the dysregulation of autophagy is implicated in various human diseases such as cancer, neurodegenerative diseases such as Alzheimer and Parkinson, myopathies, and heart and liver diseases.<sup>1-4</sup>

Autophagy is executed on a basal level in most cell types, but can be actively induced by nutrient deprivation or other stress conditions. Autophagy activating pathways all converge on the induction of the ULK1 complex, a central regulation node within the autophagy network. This protein complex comprises the Ser/Thr protein kinase ULK1 (unc-51 like kinase 1) and the interacting proteins ATG13, ATG101 and RB1CC1/FIP200 (RB1-inducible coiled-coil 1).<sup>5,8</sup> Knockdown and knockout experiments revealed essential roles for each of these proteins in autophagy. Knockout of either *Atg13* or *Rb1ccc1* leads to embryonic lethality,<sup>9, 10</sup> whereas *ulk1<sup>-/-</sup>* or *ulk2<sup>-/-</sup>* mice have rather mild autophagy phenotypes and *ulk1/2<sup>-/-</sup>* mice are alive but die shortly after birth.<sup>11-13</sup> Fibroblasts isolated from these *ulk1/2* double-knockout mice are responsive to glucose deprivation but do not display autophagy induction by amino acid withdrawal.<sup>11</sup> The ULK1 complex itself is regulated by upstream nutrient- and energy-sensing kinases, such as mTOR (mechanistic target of rapamycin [serine/threonine kinase]), AMPK (AMP-activated protein kinase), and AKT1 (reviewed in ref. 14-17). The individual subunits of the ULK1 complex have been investigated in detail over the past years, but still information about the relevance of the single protein-protein interactions within the complex is missing. Most reports suggest that ATG13 is the central subunit of this complex and recruits the

remaining components,<sup>6, 18-20</sup> though one report indicates a direct interaction of ULK1 and RB1CC1 independent of ATG13.<sup>5</sup> Along these lines, the modulation of protein-protein interactions involving ATG13 might be a valuable approach to regulate autophagy signaling pathways.

The N terminus of ATG13 comprises a HORMA domain functioning as an ATG101-interaction platform. This domain was first identified in the *Saccharomyces cerevisiae* proteins HoRmA<sub>1</sub>, Rev7, and Mad2, which display sequence similarities but no functional overlaps.<sup>21</sup> Jao et al. are the first to identify a HORMA domain in ATG13.<sup>22</sup> Mad2 can switch between an open (O-Mad2) and a closed (C-Mad2) conformation, and the ATG13 HORMA structure corresponds to the C-Mad2 state.<sup>22</sup> This finding has been complemented by 3 other groups reporting the structure of ATG101 as O-Mad2-like and the HORMA-mediated dimerization of ATG13 and ATG101, respectively.<sup>20, 23, 24</sup> Suzuki et al. show that an ATG101 version which cannot dimerize with ATG13 is not incorporated into the ULK1 complex, ultimately leading to impaired autophagy induction. The recruitment of the other subunits into the complex is unaffected.<sup>20</sup> Of note, additional binding partners of the Atg13/ATG13 HORMA domain have been reported, including ATG14 and yeast Atg9.<sup>22, 25</sup> Next to the HORMA domain, ATG13 contains a phospholipid binding motif at its extreme N terminus.<sup>26</sup> Four amino acid residues conserved across species mediate its interaction with phosphatic acid (PA), phosphatidylinositol 3-phosphate (PtdIns3P), phosphatidylinositol 4-phosphate (PtdIns4P) and to a lesser extent with phosphatidylinositol 3,4,5-trisphosphate (PtdIns(3,4,5)P<sub>3</sub>). Mutation of these 4 key residues severely decreases phospholipid binding, inhibits translocation of ATG13 to the autophagosome formation site and impedes autophagic flux upon starvation.<sup>26</sup>

In contrast to the structured N terminus, the C-terminal part of ATG13 is intrinsically disordered.<sup>27, 28</sup> In yeast Atg13, the intrinsically disordered region (IDR) harbors the interaction sites for Atg1 and Atg17, representing the yeast orthologs for ULK1 and RB1CC1, respectively.<sup>29, 30</sup> In agreement with these data for yeast, Jung et al. have mapped the ULK1 and RB1CC1 interaction sites to the C terminus of human ATG13.<sup>19</sup> Our group has fine-mapped these sites. We have observed an ATG13 isoform in the DT40 chicken B-lymphocyte cell line missing a 26 amino acid stretch encoded

by exon12. This isoform cannot bind to RB1CC1.<sup>31</sup> With regard to ULK1, we have previously identified the last 3 amino acids of ATG13 to be indispensable for ULK1 binding.<sup>18</sup> Notably, the deletion of this short peptide and correspondingly the disruption of the ATG13-ULK1 interaction had only minor effects on autophagy induction.<sup>18</sup>

Finally, a MAP1LC3/LC3-interacting region (LIR) motif was identified in ATG13. The LIR mediates interaction with members of the Atg8 family, and Alemu et al. have observed that the ATG13 LIR preferentially associates with the GABARAP subfamily of Atg8 proteins.<sup>32</sup> Suzuki et al. have determined the crystal structures of 3 MAP1LC3/LC3 isoforms in complex with a peptide containing the residues 436 to 447 of ATG13.<sup>33</sup> They also have performed mutational analysis of LC3A with either increased or decreased LIR-binding affinity and observe a defect in autophagosome formation.<sup>33</sup> However, since this defect might be caused by altered binding to other LIR-containing proteins and not necessarily to ATG13, the specific function of the ATG13 LIR remains elusive so far.

In the present work, we aimed at systematically investigating the individual importance of the ATG13 interaction sites for ULK1 complex formation, recruitment to the autophagosome formation site, and autophagy induction. For this, we made use of different proautophagic stimuli (i.e., amino acid starvation and MTOR inhibition) and different autophagy readouts (LC3 turnover; LC3, WIPI2, and ATG16L1 puncta formation). It appears that the association of ATG101 with ATG13 is central for autophagy induction. In contrast, binding of both ULK1 and RB1CC1 is not mandatory for this process. Generally, the observed effects were more pronounced upon MTOR inhibition, confirming the accepted model of MTOR-mediated regulation of the ULK1 complex and indicating that crude EBSS treatment might induce autophagy independently of the MTOR-ULK1 axis. We suggest that—next to the direct inhibition of ULK1 kinase activity—interference with the ATG13-ATG101 interaction might represent a promising approach to regulate autophagy induction.

## RESULTS

In order to comprehensively analyze the ATG13 domain requirements for autophagy, we performed a systematic analysis using specific ATG13 variants incapable of binding to phospholipids, ATG101, RB1CC1, ATG8 family members, or ULK1, respectively (Fig. 1A, B).

### **The amino acid sequence V348-M373 of ATG13 comprises the RB1CC1 interaction site**

The ATG13-RB1CC1 interaction site was reported to be located at the C terminus of ATG13.<sup>19</sup> We have previously identified an ATG13 isoform in the chicken B-lymphocyte cell line DT40, in which deletion of the amino acids encoded by exon 12 lead to inhibited interaction of ATG13 with RB1CC1.<sup>31</sup> The amino acid sequence encoded by avian exon 12 corresponds to the amino acid sequence V348 to M373 of human ATG13 isoform 2, which is encoded by human exon 14. Deletion of this sequence disrupted the ATG13-RB1CC1 interaction, while binding of ATG13 to ULK1 and ATG101 was not affected. This was evident from immunopurification experiments and from increased protein levels of ATG101 and ULK1 following the expression of ATG13 variants in *atg13* KO MEFs (Fig. 2A). In order to exclude the possibility that the deletion of V348-M373 only results in a weakened interaction that is not detectable by immunopurification, we performed 2 additional assays to monitor protein interaction *in vivo*. First, we employed a proximity ligation assay that allows detection of single protein-protein interactions using antibody-recognition combined with exponential signal amplification by PCR. Visualization is mediated by fluorescent nucleotides. HA-tagged ATG13 variants were stained with mouse anti-HA antibodies and RB1CC1 with rabbit anti-RB1CC1 antibodies. As negative controls *Atg13* WT MEFs expressing untagged ATG13 and *atg13* KO MEFs expressing ATG13 lacking the entire C terminus ( $\Delta$ C) were used. Cells reconstituted with full-length ATG13 displayed strong signals with significant difference to control cells (Fig. 2B). In contrast, MEFs expressing ATG13( $\Delta$ V348-M373) revealed a signal count similar to control cells, indicating the disruption of the interaction with RB1CC1. Second, we used the *in vivo* biotin labelling assay developed by Ting and colleagues.<sup>34,36</sup> In this assay, ATG13 variants were tagged with the ascorbate

peroxidase derivative APEX2 and expressed in *atg13* KO MEFs. Upon activation of the peroxidase, the provided biotin-phenol is converted to biotin-phenoxyl radicals, which covalently react with nearby electron-rich amino acids and thereby label proteins with biotin. Since phenoxyl radicals are short-lived and have a small labelling radius, only proteins proximal to the APEX2 fusion protein become biotinylated.<sup>34,36</sup> Subsequent cell lysis and enrichment of biotinylated proteins by streptavidine beads allow detection of interacting proteins. Immunoblotting revealed that RB1CC1 was only purified from cells expressing full-length ATG13 but was absent in all other samples (Fig. 2C). On the contrary, ATG101 was purified with all ATG13 variants. Note that ATG13 itself is biotinylated and purified; therefore, proteins might be purified due to biotinylation or interaction with ATG13. Nevertheless, both assays confirm that the ATG13 sequence V348-M373 mediates the interaction with RB1CC1.

Next we questioned if and how the assembly of the ULK1 complex might be affected by the inhibition of the ATG13-RB1CC1 interaction. For this, size-exclusion chromatography experiments were conducted. As has been reported previously,<sup>10</sup> *atg13* KO MEFs do not assemble the ULK1 complex (Fig. 2D, upper panels and black curve in diagrams). Whereas RB1CC1 is present in high-molecular mass fractions corresponding to complexes of approximately 3 MDa (Fig. 2D, fractions 18 to 21), ULK1 only distributes in lower-molecular mass fractions. ATG101 exists mainly as a monomer in fractions containing molecules lower than 43 kDa. Re-expression of wild-type ATG13 in these KO cells restores the assembly of the ULK1 complex, with all analyzed proteins being present in the high-molecular mass fractions (Fig. 2D, middle panels and blue curve in diagrams). Additionally, ATG101 and ATG13 display high protein amounts in fractions corresponding to a molecular mass of 400 to 200 kDa (Fig. 2D, middle panels, fractions 29 to 36). Finally, disruption of the RB1CC1 interaction with ATG13 by deleting the V348-M373 sequence resulted in a disassembled ULK1 complex and a shift of ATG13, ULK1 and ATG101 to lower-molecular mass fractions (Fig. 2D, lower panels and red curve in diagrams). Of note, ULK1 distribution resembles the *atg13* KO phenotype, whereas ATG101 accumulates in fractions corresponding to 400 to 200 kDa protein complexes, which is different from KO cells (Fig. 2D, compare black and red curve in diagrams). Similarly, ATG13 protein levels are

almost completely depleted in high-molecular mass fractions and are mainly present in later fractions. These data indicate that ATG13-containing subcomplexes are formed in cells expressing the ATG13( $\Delta$ V348-M373) variant rather than the entire RB1CC1-dependent ULK1 complex. Besides ATG13, these complexes might harbor ULK1, ATG101, or both (Fig. 2A).

Because the ULK1 complex is not formed when the interaction of ATG13 and RB1CC1 is inhibited, we next asked if this has an effect on the recruitment of both proteins to the autophagosome formation site. Immunofluorescence experiments showed diffuse distribution for both proteins under growing conditions in *atg13* KO MEFs reconstituted with full-length ATG13 with a perinuclear accumulation of RB1CC1 (Fig. 3, ATG13 DMEM). Following autophagy induction by amino acid starvation, ATG13 and RB1CC1 exhibited colocalizing dots that likely represent the autophagosome formation site (Fig. 3, ATG13 EBSS, see inset). In contrast, expression of the ATG13( $\Delta$ V348-M373) variant did not promote the recruitment of either ATG13 or RB1CC1 to the PAS, and distribution of both proteins was unaffected by autophagy induction (Fig. 3, right panels).

Taken together, the sequence V348-M373 represents the RB1CC1 interaction site in ATG13, and this protein-protein interaction can be abolished by the deletion of this peptide. This in turn provokes disassembly of the ULK1 complex and inhibited recruitment to the phagophore.

#### **The amino acids I131, R133, V134 and Y138 of ATG13 are mandatory for the interaction with ATG101**

In addition to the RB1CC1 interaction, we were also interested in the binding of ATG13 to ATG101. We conducted a computational alanine scanning of the ATG13-ATG101 interface on the structure of the human ATG13-ATG101 HORMA heterodimer (PDB ID: 5C50; ref. 24) using the DrugScore<sup>PI</sup> webserver.<sup>37</sup> Interface residues resulting in a binding free energy change  $\Delta\Delta G > 1$  kcal mol<sup>-1</sup> when mutated to alanine were considered binding hot spots (I131, R133, V134, Y138; Fig. 4A, upper panel). Isoleucine, arginine, and tyrosine are enriched in hot spot residues.<sup>38</sup> To independently validate the

predicted hotspots, we performed MM-GB/SA calculations combined with a decomposition of the effective binding energy on a per-residue level.<sup>39, 40</sup> The MM-GB/SA calculations confirmed that R133, V134, Y138, and to a lesser extent I131, contribute most to the effective binding energy (Fig. 4A, middle panel). In addition, R139 and R142 were identified by MM-GB/SA but not by DrugScore<sup>PI</sup>, and Y115 *vice versa*. Furthermore, a cluster of potential binding hot spots located in the connector loop (residues 33 to 58) of ATG13 was identified by MM-GB/SA but not by DrugScore<sup>PI</sup> (Fig. S1). The consensus hot spot residues in the ATG13 interface (Fig. 4A, lower panel) were then changed to alanine, and binding of ATG101 to these ATG13 variants was analyzed by a bimolecular fluorescence complementation assay.

For this analysis, ATG13 and ATG101 were fused to the N- or C-terminal part of the YFP variant Venus, respectively. Upon expression of VenusN-ATG13 and VenusC-ATG101 fusion proteins in *atg13* KO MEFs, Venus fluorescence was complemented by the interaction of wild-type ATG13 and ATG101. Mutations of single amino acids did not influence the interaction between ATG13 and ATG101 (data not shown). However, exchange of the 4 amino acids I131, R133, V134 and Y138 to alanine led to the disruption of the ATG13-ATG101 interaction as detected by decreased Venus fluorescence (Fig. 4B). When performing immunoblotting of ATG101, we detected low protein levels in cells transfected with the mutant ATG13 that were similar to the ones observed for *atg13* KO MEFs (Fig. 4B). This is due to the absence of the stabilizing effect of the ATG13-ATG101 protein-protein interaction on ATG101; the stabilizing effect is evident in cells expressing full-length ATG13 (Fig. 4B). We also performed immunopurification experiments of ATG101. Only wild-type ATG13 was copurified, while the 4 amino acid ATG13 variant (I131, R133, V134, Y138A; named HORMA domain mutant, HD<sup>mut</sup>) was not capable of interacting with ATG101 (Fig. 4C). Furthermore, due to the missing ATG13 interaction, copurification of the other ULK1 complex members ULK1 and RB1CC1 was not possible. We also analyzed ATG13 harboring a mutated phospholipid binding domain (PLBD<sup>mut</sup>). This motif is very proximal to the HORMA domain, and mutation might unintentionally affect the HORMA domain function. In our purification experiments, the ATG13(PLBD<sup>mut</sup>) variant was copurified with

ATG101 indicating an intact HORMA domain (Fig. 4C, PLBD<sup>mut</sup>). By combining the HD mutation with the PLBD variant (Fig. 4C, PLBD<sup>mut</sup>, HD<sup>mut</sup>) the interaction with ATG101 was again inhibited. Importantly, the interaction with ATG14, which has recently been reported to bind to the HORMA domain of ATG13,<sup>41</sup> was neither affected by the HD nor the PLBD mutation (Fig. S2). The interaction of ATG13 with ULK1 or RB1CC1, respectively, was not affected either (Fig. S2).

As described above for the RB1CC1-binding interface, we next investigated the ULK1 complex assembly by size-exclusion chromatography and recruitment to the phagophore by immunofluorescence. Mutation of the phospholipid binding site did not affect the ULK1 complex assembly (Fig. 5A, PLBD<sup>mut</sup>, red curve in diagrams). In contrast, mutation of the ATG101 interaction site severely altered complex assembly (Fig. 5B, HD<sup>mut</sup>, red curve in diagrams). Distribution of ATG101 resembles the *atg13* KO phenotype as it is only present as a monomer in the low-molecular mass fractions, while it is completely absent from both the 3 MDa and 400 to 200 kDa protein complexes. ATG13 was present in low amounts in the early molecular mass fractions and concentrated in later fractions. Additional mutation of the phospholipid-binding domain did not exhibit an additive effect on the distribution of the ULK1 components (Fig. 5C, PLBD<sup>mut</sup>, HD<sup>mut</sup>, red curve in diagrams). The described ATG13 variants were further analyzed in combination with a disrupted RB1CC1 interaction. Double mutation of the phospholipid- and RB1CC1-binding site (Fig. 5A, PLBD<sup>mut</sup>, ΔV348-M373; green curve in diagrams) induced a redistribution of ATG13, ATG101 and ULK1 into later fractions as was detected for the single ΔV348-M373 variant (see Fig. 2D). Combination of the RB1CC1 binding-deficient with the ATG101 binding-deficient mutant did not further impact ATG101 but promoted an additional reduction of ULK1 and ATG13 protein levels in early molecular mass fractions (Fig. 5B, HD<sup>mut</sup>, ΔV348-M373; green curve in diagrams). Finally, complex formation did not change in the triple mutant compared to the double mutant PLBD<sup>mut</sup>, HD<sup>mut</sup> (Fig. 5C, PLBD<sup>mut</sup>, HD<sup>mut</sup>, ΔV348-M373; compare red and green curves in diagrams).

The immunofluorescence experiments revealed that most ATG13 variants that are not capable of a proper ULK1 complex formation do not support ATG13 and RB1CC1 colocalization upon

autophagy induction either (Fig. 4D, PLBD<sup>mut</sup>, ΔV348-M373; HD<sup>mut</sup>, ΔV348-M373; PLBD<sup>mut</sup>, HD<sup>mut</sup>, ΔV348-M373). The corresponding single mutations lacking either intact ATG101- or phospholipid-binding properties supported formation of ATG13- and RB1CC1-positive puncta, though their number appeared to be independent of autophagy induction by starvation (Fig. 4D, PLBD<sup>mut</sup>; HD<sup>mut</sup>). However, in cells expressing the ATG13 variant lacking both the ATG101 and phospholipid interaction site, a permanent accumulation of ATG13 and RB1CC1 was detected, which was even increased upon autophagy induction (Fig. 4D and S3, PLBD<sup>mut</sup>, HD<sup>mut</sup>). This notable phenotype was reversed by additionally mutating the RB1CC1 interaction site (Fig. 4D, PLBD<sup>mut</sup>, HD<sup>mut</sup>, ΔV348-M373). Based on this observation, we hypothesize that the accumulation of ATG13 and RB1CC1 is potentially caused by inhibited signaling progression downstream of the recruitment of these proteins to the phagophore or a very early formation site. Since deletion of the RB1CC1 binding site abolished this accumulation, we suspect that the recruitment of ATG13 and RB1CC1 is dependent on their interaction and might occur earlier within the temporal hierarchy. In turn, ATG13-dependent binding to ATG101 and phospholipids are both important for the release of ATG13 and RB1CC1 from the phagophore. It is noteworthy that the disruption of one of the 2 interaction interfaces (PLBD<sup>mut</sup> or HD<sup>mut</sup>) does not affect signaling progression, indicating that interactions mediated by these interfaces might somehow compensate each other.

**The ATG13-ULK1 interaction is required for ULK1 complex formation and recruitment to the autophagosome formation site while the LIR motif is dispensable**

Two additional interaction interfaces have been reported for ATG13 proteins. The LC3-interacting region (LIR) domain mediates direct interaction of ATG13 with members of the Atg8 family. In agreement with the report on the LIR motif in ATG13 by Alemu et al.,<sup>32</sup> we exchanged F407 and I410 to alanine (Fig. 1B) to effectively inhibit interaction with LC3s and GABARAPs. These mutations did not have an effect on ULK1 complex formation as shown by size-exclusion chromatography (Fig. 6A,

LIR<sup>mut</sup>; upper panels and red curve in diagrams), whereas a double mutant lacking both the LIR and the RB1CC1 interaction site showed disruption of the complex (**Fig. 6A**, LIR<sup>mut</sup><sub>ΔV348-M373</sub>; green curve in diagrams). Furthermore, we observed proper recruitment of ATG13 and RB1CC1 to the PAS after autophagy induction (**Fig. 6B**, LIR<sup>mut</sup>), which again was abolished by additional deletion of the RB1CC1 binding site (**Fig. 6B**, LIR<sup>mut</sup><sub>ΔV348-M373</sub>). Interestingly, mutation of the LIR motif did not affect the colocalization of ATG13 with LC3 after autophagy induction by EBSS treatment (**Fig. 6C**, LIR<sup>mut</sup>), which was also inhibited by deletion of the RB1CC1 interaction (**Fig. 6C**, LIR<sup>mut</sup><sub>ΔV348-M373</sub>). Of note, expression of this ATG13 double mutant led to increased localization of ATG13 to the nucleus despite autophagy induction.

Finally, we applied the ΔTLQ mutation, which has previously been validated for the inhibition of the ULK1-ATG13 interaction (**Fig. 1B**).<sup>18</sup> Deletion of the minimal ULK1 interaction site in ATG13 resulted in a shift of ULK1 to later fractions in size-exclusion chromatography, while both ATG101 and ATG13 were still present in high-molecular mass fractions (ref. 18 and **Fig. 6A**, ΔTLQ; lower panels and red curve in diagrams). Deletion of both the ULK1 and RB1CC1 interaction sites in ATG13 resulted in the depletion of ATG101 from early fractions (**Fig. 6A**, ΔV348-M373,ΔTLQ; green curve in diagrams). Despite the fact that the ATG13(ΔTLQ) variant still interacts with RB1CC1, recruitment of both proteins to the autophagosome formation site was inhibited (**Fig. 6B**, ΔTLQ).

#### **Mutations of interaction sites in ATG13 partly affect amino acid starvation-induced autophagy**

After mapping the interaction sites between ATG13 and its binding partners, we were next interested in their relevance for autophagy regulation. First, we investigated the requirement of the ATG13-RB1CC1 interaction, since this interaction is apparently essential for the formation of the 3 MDA ULK1 complex. In a first approach, we analyzed amino acid starvation-induced mCitrine-LC3B degradation by flow cytometry. Cells with an intact autophagy signaling machinery display low fluorescence after autophagy induction, and this effect can be reversed by adding bafilomycin A<sub>1</sub>, as can be seen in

Atg13 WT MEFs as well as in atg13 KO MEFs reconstituted with full-length ATG13 (**Fig. 7A**). Unexpectedly, expression of the ATG13 mutant ΔV348-M373 did not influence autophagy activity, since LC3B degradation as detected by a reduced fluorescence intensity was observed after treatment with EBSS (**Fig. 7A**). To further confirm this result, we performed immunofluorescence of endogenous LC3. This assay supported our previous observation, since the number of LC3-positive puncta increased in cells expressing either wild-type or ATG13(ΔV348-M373) upon bafilomycin A<sub>1</sub> treatment, and this effect was enhanced by inducing autophagy with EBSS (**Fig. 7B**). Finally, we performed an LC3 turnover assay by immunoblotting. Again Atg13 WT MEFs and atg13 KO MEFs reconstituted with either full-length ATG13 or the ΔV348-M373 variant displayed similar LC3-II levels in cells treated with bafilomycin A<sub>1</sub> alone (basal autophagy) or in combination with EBSS (induced autophagy) (**Fig. 7C**). Similar to the atg13 KO MEFs, an ATG13 version lacking the entire C terminus (ΔC) did not reveal any detectable autophagic flux (**Fig. 7C**). Since the autophagy readouts employed so far rely on LC3 lipidation and/or degradation, we decided to check another autophagic marker. We chose the early autophagy protein WIPI2, which is recruited to the phagophore shortly after ULK1 complex activation. Immunofluorescence of WIPI2 in atg13 KO MEFs expressing full-length ATG13 or the ΔV348-M373 mutant showed diffuse distribution in the cytoplasm under growing conditions, while WIPI2 puncta formation was induced by autophagy induction (**Fig. 8**, ATG13; and ΔV348-M373). Collectively, these data suggest that the interaction between ATG13 with RB1CC1 is not mandatory for autophagy induction.

As these findings were rather surprising, we further analyzed the other interaction motifs of ATG13. Mutation of the phospholipid-binding domain did not influence autophagy induction by amino acid starvation with EBSS either. LC3-II protein levels were similar in cells reconstituted with wild-type ATG13 or the PLBD mutant (**Fig. 7D**, PLBD<sup>mut</sup>). Likewise, mutation of both the phospholipid- and the RB1CC1-binding site did not significantly affect autophagic activity (**Fig. 7D**, PLBD<sup>mut</sup><sub>ΔV348-M373</sub>). In contrast, mutation of the ATG101 interaction site resulted in significantly reduced autophagic flux (**Fig. 7D**, HD<sup>mut</sup>). Concomitant deletion of the RB1CC1 interaction site did not have an

additional effect (**Fig. 7D**, HD<sup>mut</sup>, $\Delta$ V348-M373). However, interference with both the phospholipid binding as well as the ATG101 interaction could further reduce the autophagic activity (**Fig. 7D**, PLBD<sup>mut</sup>,HD<sup>mut</sup>). This was also evident from the analysis of SQSTM1/p62 levels, which are highly accumulated in *atg13* KO MEFs and in cells expressing the double mutant PLBD<sup>mut</sup>,HD<sup>mut</sup> (**Fig. 7E**). These results were further supported by WIPI2 immunofluorescence. While we detected WIPI2 puncta formation upon autophagy induction in cells expressing the ATG13 variants PLBD<sup>mut</sup>, and PLBD<sup>mut</sup>, $\Delta$ V348-M373 (**Fig. 8**, PLBD<sup>mut</sup>, and PLBD<sup>mut</sup>, $\Delta$ V348-M373), inhibition of ATG101 binding to ATG13 severely inhibited WIPI2 puncta formation after autophagy induction (**Fig. 8**, HD<sup>mut</sup>, HD<sup>mut</sup>, $\Delta$ V348-M373; PLBD<sup>mut</sup>,HD<sup>mut</sup>, and PLBD<sup>mut</sup>,HD<sup>mut</sup>, $\Delta$ V348-M373). Notably, these cells displayed very small WIPI2-positive structures, which were not regulated by autophagy induction.

As in our MEF cell lines the signal for LC3-II appeared to be very similar between full medium and EBSS in the presence of bafilomycin A<sub>1</sub>, we hypothesized that the induction of autophagy is masked by high levels of basal autophagy. We therefore repeated the starvation experiments for cell lines displaying reduced autophagic activity (HD<sup>mut</sup>, HD<sup>mut</sup>, $\Delta$ V348-M373; PLBD<sup>mut</sup>,HD<sup>mut</sup>, and PLBD<sup>mut</sup>,HD<sup>mut</sup>, $\Delta$ V348-M373) with a shortened incubation time of 1 h (**Fig. S4**). In this setup, differences in autophagic flux caused by ATG13 mutations were even more obvious and further confirmed our result that inhibition of the ATG13-ATG101 interaction has a tremendous impact on autophagy induction.

Next, mutation of the LIR motif was analyzed. Interestingly, we detected a slight increase of LC3-II levels in samples treated with starvation medium and bafilomycin A<sub>1</sub> compared to cells expressing wild-type ATG13 (**Fig. 7F**, LIR<sup>mut</sup> and ATG13; **Fig. S5**). This effect was reversed when both the interaction with LC3s or GABARAPs, and RB1CC1 were inhibited, since cells expressing this ATG13 double mutant displayed autophagic activity similar to wild-type ATG13 expressing cells (**Fig. 7F**, LIR<sup>mut</sup>, $\Delta$ V348-M373). WIPI2 staining also showed puncta formation upon autophagy induction (**Fig. 8**). However, with this readout, we did not observe significant differences between wild-type and LIR<sup>mut</sup>, and/or LIR<sup>mut</sup>, $\Delta$ V348-M373-expressing cells.

Finally, we investigated the mutation of both the ULK1 and the RB1CC1 interaction site. Our group has previously reported that inhibition of ATG13-ULK1 binding resulted in slightly but not significantly decreased autophagic activity.<sup>38</sup> This reduced autophagic activity was further decreased by additional mutation of the RB1CC1 interaction site (**Fig. 7F**,  $\Delta$ V348-M373, $\Delta$ TLQ). Consistently, WIPI2 puncta formation upon autophagy induction is present in cells expressing the ATG13( $\Delta$ TLQ) mutant; however, it appears severely decreased by further mutation of the RB1CC1 interaction site (**Fig. 8**,  $\Delta$ TLQ; and  $\Delta$ V348-M373, $\Delta$ TLQ).

### **Mutations of interaction sites in ATG13 have severe effects on autophagy induction by MTORC1/2 inhibition**

Because amino acid starvation by EBSS incubation is a rather crude treatment and ULK1/2-independent autophagy pathways have been described by several groups,<sup>31, 31, 42-44</sup> we next wanted to selectively target ULK1 signaling by the modulation of MTOR activity. To do so, we used torin2, a member of the Tor kinase domain inhibitor family (TORKinibs), which inhibits both MTOR complex 1 and 2 (MTORC1/2). Furthermore, rapamycin was used, which interacts with FKBP1A and thereby inhibits interaction of MTOR with RPTOR and MTORC1 formation.

First, we analyzed the ability of the inhibitors to induce the autophagy signaling pathway via MTOR inhibition. We found that torin2, similar to EBSS treatment, inhibits ULK1 phosphorylation at T758 as well as RPS6KB1 phosphorylation at T389, both of which are well known MTOR phosphorylation sites (**Fig. S6A to C**). Rapamycin-induced effects on RPS6KB1 phosphorylation at T389 were similar, but the inhibition of ULK1 T758 phosphorylation appeared much weaker (**Fig. S6B and S6C**). Nevertheless, this site was not absolutely “rapamycin-resistant”.<sup>45</sup> Consistently, ULK1 kinase activity as monitored by immunoblotting for phospho-S318 in ATG13 was more prominently induced by torin2 than by rapamycin (**Fig. S6B and S6C**). Furthermore, torin2 induced the recruitment of the ULK1 complex to the phagophore similarly as starvation with EBSS (**Fig. S7**).

In *atg13* KO MEFs reconstituted with full-length ATG13 autophagy was induced following treatment with these inhibitors (**Fig. 9A**, ATG13). Interference with the RB1CC1-ATG13 interaction had only minor effects on autophagic activity (**Fig. 9A**,  $\Delta V348$ -M373) as we have already detected for EBSS treatment.

Mutation of either the phospholipid-binding domain or the ATG101-interacting HORMA domain inhibited autophagy induction by torin2 and rapamycin (**Fig. 9B**, HD<sup>mut</sup>; and PLBD<sup>mut</sup>). Although this has been observed for the HD<sup>mut</sup> variant upon EBSS treatment, the effect for the PLBD<sup>mut</sup> is much more obvious for torin2 and rapamycin. It appears that cells expressing these ATG13 variants retain some autophagic activity, since we detected a slight increase of LC3-II levels in samples treated with bafilomycin A<sub>1</sub>. This was totally erased by mutating both the phospholipid- and the ATG101-binding domain (**Fig. 9C**, PLBD<sup>mut</sup>, HD<sup>mut</sup>). In these cells, the addition of bafilomycin A<sub>1</sub> did not stimulate an accumulation of LC3-II compared to control cells. The subsequent deletion of the RB1CC1-binding domain did not have an additional effect (**Fig. 9C**, PLBD<sup>mut</sup>, HD<sup>mut</sup>,  $\Delta V348$ -M373).

Next, the mutated LIR motif was investigated. In contrast to EBSS treatment, autophagy induction with torin2 or rapamycin neither increased nor inhibited autophagic activity in cells expressing the ATG13 variant (**Fig. 9D**, LIR<sup>mut</sup>). We detected an additive effect for the ATG13 double mutant additionally lacking the RB1CC1 interaction site (**Fig. 9D**, LIR<sup>mut</sup>,  $\Delta V348$ -M373). In these cells, autophagic activity was significantly decreased when treated with torin2. These cells show increased levels when treated with bafilomycin A<sub>1</sub> but this effect was not further increased by torin2. These results indicate that basal autophagy is still active but autophagy induction by torin2 is not possible. This was not the case for rapamycin stimulation, since we detected only minor effects on autophagy induction.

At last, we studied the ATG13( $\Delta$ TLQ) mutant lacking ULK1 interaction. Similar to the LIR mutant, autophagy was not induced by torin2 treatment although basal activity was still detectable (**Fig. 9E**,  $\Delta$ TLQ). Additional mutation of the RB1CC1 interaction site did not have any further effect

(**Fig. 9E**,  $\Delta V348$ -M373,  $\Delta$ TLQ). Rapamycin induced autophagy in cells expressing the ATG13( $\Delta$ TLQ) variant (**Fig. 9E**,  $\Delta$ TLQ) although this was significantly reduced compared to control cells. Again autophagy was not induced in cells expressing the double mutant  $\Delta V348$ -M373,  $\Delta$ TLQ (**Fig. 9E**,  $\Delta V348$ -M373,  $\Delta$ TLQ).

As has been done for EBSS experiments, we verified our results obtained for torin2-induced autophagy by immunofluorescence. Since we could not detect significant WIPI2 puncta formation upon torin2 treatment (**Fig. 5B**), we monitored ATG16L1 puncta formation, another well-characterized marker for autophagosomes (**Fig. 5B**). We observed a significant increase in puncta formation upon both EBSS and torin2 treatment for cells expressing wild-type ATG13 as well as ATG13 with a mutated LIR domain (**Fig. 5B**, ATG13; LIR<sup>mut</sup>). Cells expressing ATG13 with disrupted RB1CC1- or ULK1-binding sites depicted inducible ATG16L1 puncta formation as well (**Fig. 5B**,  $\Delta V348$ -M373;  $\Delta$ TLQ). For all other cell lines, ATG16L1 puncta were not detectable. Taking all our observations together, it appears that targeting the interaction between ATG101 and ATG13 has the most severe effects on autophagy induction with regard to all applied stimuli and readouts (**Fig. 10**, HD<sup>mut</sup>). LC3-II accumulation was blocked at least to ~50%, while WIPI2 dot formation was reduced to less than 20% and ATG16L1 to ~30%. These effects were even more pronounced when binding to both ATG101 and phospholipids was blocked (**Fig. 10**, PLBD<sup>mut</sup>, HD<sup>mut</sup>). In contrast, single interference with the binding to the other 2 ULK1 complex components, ULK1 and RB1CC1, respectively, did not or only weakly affect autophagy induction. However, the combination of these 2 mutations clearly inhibited autophagy induction upon MTOR inhibition (**Fig. 10**,  $\Delta V348$ -M373,  $\Delta$ TLQ).

## DISCUSSION

In this study, we have systematically evaluated the relevance of the individual ATG13 interaction sites for the autophagic function of ATG13. In recent years, it became evident that the ULK1 protein kinase complex is an essential signaling node for the induction of autophagy. The core ULK1 complex consists of ULK1, ATG13, RB1CC1 and ATG101. Our analysis showed that targeting the ATG101-ATG13 protein interaction has the strongest effect on autophagy regulation. Though the remaining ATG13 interaction sites partially displayed functions during autophagy induction mediated by MTOR inhibition, mutations within the ATG13 HORMA domain clearly affected autophagy induced by amino acid starvation. In contrast, the interactions of ATG13 with ULK1 or RB1CC1 appeared to be rather dispensable for this type of autophagy induction.

The possibility to induce autophagy independently of ULK1/2 has been suggested by different groups. One might speculate that interference with the ATG13-ATG101 interaction targets both the ULK1 complex during canonical autophagy and potential ULK1-independent complexes that still rely on ATG13 and ATG101. These latter complexes might play a role in autophagy induction and/or during autophagy progression. Congruent to our observations, Suzuki et al. have reported that autophagy is defective in *atg101* KO MEFs expressing an ATG101 version that can no longer bind ATG13.<sup>20</sup> The authors have already suggested that ATG101 fulfills 2 proautophagic functions: i) the stabilization of ATG13 and ii) the recruitment of downstream factors via a protruding loop termed WF finger.<sup>20</sup> Mutation of either the ATG13 interaction interface or the WF finger inhibited autophagy.<sup>20</sup> Future studies will have to reveal possible interacting molecules of the WF finger, and it remains to be shown that this motif is important for both ULK1-dependent and -independent processes.

Although the described observations suggest a central role for the ATG13-ATG101 interaction, we cannot entirely exclude that our ATG13 HORMA domain mutations simultaneously affect the binding to other reported interacting partners, i.e. ATG14 in higher eukaryotes and Atg9 in

yeast.<sup>25, 41</sup> Recently, Park et al. report that ATG14 is bound to a region between residues 1 to 198 in ATG13, which represents the HORMA domain.<sup>41</sup> They show that this interaction enables ULK1-dependent phosphorylation of ATG14, which in turn stimulates the kinase activity of the class III phosphatidylinositol 3-kinase (PtdIns3K) complex.<sup>41</sup> The observations by Park et al. are consistent with data obtained by Jao et al., who report that the HORMA domain of yeast Atg13 is important for the recruitment of the Atg14-containing class III PtdIns3K complex.<sup>22</sup> However, at least our immunopurification experiments indicate that binding to ATG14 is not altered for our ATG13 HORMA domain variants. In *S. cerevisiae*, a second binding partner of the Atg13 HORMA domain has been identified: Suzuki et al. show that Atg9 vesicles are recruited to the PAS via the interaction with the ATG13 HORMA domain.<sup>25</sup> This model has been recently refined by Yamamoto et al. Apparently, Atg13 links Atg17-Atg29-Atg31 complexes with each other via 2 distinct regions, ultimately resulting in the self-assembly of the Atg1 complexes.<sup>30</sup> The supra-molecular self-assembly of the Atg1 complexes then leads to the recruitment of Atg9 vesicles.<sup>30</sup> Ohsumi and colleagues have been able to generate an Atg9 binding-deficient Atg13 variant, and the residues of Atg13 mediating this interaction are located to  $\beta$ -strands 4 to 6 and the hinge loop.<sup>25</sup> In contrast, human ATG13 binds to human ATG101 via the  $\alpha$ C and the  $\alpha$ A- $\alpha$ B connector, including  $\beta$ 2'.<sup>24</sup> Furthermore, the interface between Atg101/ATG101 and Atg13/ATG13 is mostly conserved between fission yeast and human.<sup>20, 24, 46</sup> In all, there are 2 aspects that arise from these observations. First, there is certainly crosstalk between the Atg1/ULK1 complex and Atg9/ATG9, both in yeast and mammalian model systems. In 2004, Reggiori et al. report that Atg9 cycles through the PAS in an Atg1-Atg13-dependent manner.<sup>47</sup> Sekito et al. have found that Atg9 interacts with Atg17 in *S. cerevisiae*.<sup>48</sup> This interaction appears to be essential for the recruitment of Atg9 to the PAS and requires Atg1.<sup>48</sup> Rao et al. also report the direct interaction of Atg9 with Atg17.<sup>49</sup> They observe that the Atg9-Atg17 interaction is inhibited by the regulatory Atg31-Atg29 subcomplex but restored by the association of the Atg1-Atg13 subcomplex.<sup>49</sup> Finally, Papinski et al. have characterized Atg1-dependent phosphorylation of Atg9.<sup>50</sup> With regards to higher eukaryotes, Young et al. observe that ULK1 regulates the starvation-induced redistribution of ATG9

from the trans-Golgi network to endosomes.<sup>51</sup> Mack et al. report that the AMPK-dependent phosphorylation of ULK1 regulates ATG9 localization,<sup>52</sup> and Weerasekara et al. observe that these 2 kinases mediate the phosphorylation of ATG9.<sup>53</sup> Recently, Karanasios et al. report that the nucleation of autophagosomes is initiated by the ULK1 complex on ER tubulovesicular regions marked by ATG9 vesicles.<sup>54</sup> Second, to our knowledge, there is no evidence so far that Atg13/ATG13 directly interacts with Atg9/ATG9 in Atg101/ATG101-positive cells, i.e. fission yeast or higher eukaryotes. Along these lines, a simultaneous interaction of ATG101 and ATG9 with the HORMA domain of ATG13 has not been described. Further studies are necessary to characterize the mutual influence of the known and potentially additional ATG13 HORMA domain interaction partners in mammalian model systems.

The phospholipid-binding motif is located proximal to the HORMA domain and has been shown to be important for the translocation of ATG13 to early autophagosomal structures.<sup>26</sup> The lipid-binding capabilities of yeast Atg13 were addressed by Rao et al. They observe that Atg13 does not bind to small unilamellar vesicles containing either 40 mol% phosphatidylserine or 30 mol% phosphatidylinositol or 25 mol% phosphatidylinositol supplemented with 2.5 mol% phosphatidylinositol-3-phosphate.<sup>49</sup> However, Atg13 is still recruited to small unilamellar vesicles composed of yeast polar lipids, indicating that other lipids than the mentioned ones are required for Atg13 binding.<sup>49</sup> In our experimental setup, mutation of the phospholipid-binding motif clearly inhibited autophagy induction by rapamycin or torin2 treatment but not by amino acid starvation. These data are partially similar to the findings reported by Karanasios et al. Notably, the inhibition of both binding to phospholipids and ATG101 enhanced the phenotypes of both individual mutations and resulted in accumulation of ATG13 and RB1CC1 within puncta independent of autophagy induction. We speculate that the components of the ULK1 complex can be recruited to early autophagosomal structures possibly prior to phagophore formation, but that the subsequent release from this site is inhibited by blocked binding of phospholipids and ATG101. The observed accumulation of ATG13 and RB1CC1 was entirely abrogated by further inhibiting the ATG13-RB1CC1 interaction, hinting towards a hierarchical order of protein interactions. Nevertheless, neither the

occurrence of these ATG13/RB1CC1 puncta nor their inhibition had implications for autophagy execution.

Generally, the data obtained for the RB1CC1-binding site are rather unexpected. Interference with the ATG13-RB1CC1 interaction resulted in disassembled ULK1 complexes and inhibited recruitment of ATG13 and RB1CC1 to the phagophore. However, we did not see any effect on autophagic activity. Our group has previously observed that deletion of the RB1CC1 interaction site in ATG13 results in inhibited autophagy in chicken DT40 B-lymphocytes.<sup>31</sup> Furthermore, Chen et al. have identified the corresponding amino acids in RB1CC1 mediating the interaction with ATG13.<sup>55</sup> The ATG13-binding site in RB1CC1 is established by amino acids 582 to 585 (LQFL) in human RB1CC1.<sup>55</sup> The authors employ a knock-in mouse model expressing a RB1CC1 variant that cannot bind ATG13, and they observe that autophagy is completely blocked but that the nonautophagic functions of RB1CC1 fully support embryogenesis.<sup>55</sup> These observations are contradictory to our results. The usage of different model systems and/or autophagy readouts might contribute to this discrepancy. We suggest that the components of the ULK1 complex become recruited to the phagophore independently of a fully assembled ULK1 complex, ultimately resulting in regular autophagy progression. Since we observe that the interaction between ATG13 and RB1CC1 is important for their recruitment to the autophagosomal formation site but not mandatory for autophagy induction, it also appears possible that they support autophagy execution remotely from the autophagosomal formation site. Still, we cannot exclude that ATG13- and RB1CC1-positive puncta might still form but are not detectable due to reduced size or shortened half-life. Alternatively, other ULK1 complex components than ATG13 might directly interact with RB1CC1, or mammalian ATG13 possesses multiple RB1CC1-binding sites, as has been reported for yeast Atg13.<sup>30</sup> However, all these possibilities are clearly not supported by our immunoprecipitations, proximity ligation assays, biotinylation labelling experiments, or size-exclusion chromatographies.

The interaction of ATG13 and ULK1 is relevant for proper autophagy induction by EBSS stimulation as reported by our group,<sup>18</sup> although the  $\Delta$ TLQ-mutation-dependent reduction of the

autophagic flux was not significant. In contrast, autophagic flux induced by rapamycin or torin2 was significantly decreased in cells expressing the ULK1 binding-deficient ATG13 variant, albeit basal autophagy levels were present. This is in accordance with the accepted model that autophagy induction by direct MTOR inhibition unequivocally relies on the ULK1 complex. At this point, we note that torin2 has a much stronger effect on ULK1 S758 and ATG13 S318 phosphorylation than rapamycin. Although we would not state that ULK1 S758 phosphorylation is rapamycin resistant as previously suggested,<sup>45</sup> the rapamycin-induced reduction of ULK1 phosphorylation is weaker than the one observed for torin2.

We also investigated the relevance of the LIR motif in ATG13. To date LIR motifs (alternatively termed Atg8-family interacting motif, AIM) have been identified for several components of the Atg1/ULK1 complexes, e.g. for yeast Atg1 or mammalian ULK1, ATG13, and RB1CC1.<sup>32, 33, 56-58</sup> Kraft et al. report that mutation of the Atg1 LIR motif sensitizes cells for autophagy defects,<sup>56</sup> and Nakatogawa et al. observe that mutations in the Atg1 LIR cause a significant defect in autophagy, without affecting the functions of Atg1 during autophagosome formation.<sup>57</sup> With regard to mammalian ULK1, Kraft et al. show that the number of ULK1-positive structures upon starvation is significantly reduced for the LIR-mutated ULK1, whereas the total number of WIPI2 puncta is increased.<sup>56</sup> These data indicate that the ULK1 LIR motif is required for efficient recruitment to phagophores or autophagosomes and that WIPI2-positive autophagosomes or autophagosome precursors are stalled at an early stage during autophagy in cells expressing the ULK1 LIR mutant.<sup>56</sup> Similarly, Alemu et al. show that ULK1 needs the LIR motif to get recruited to WIPI2- and LC3-positive structures, again supporting the conclusion that ULK1 is located on phagophores and/or autophagosomes and might participate in later steps of autophagy.<sup>32</sup> Two groups have identified a LIR motif within ATG13.<sup>32, 33</sup> Suzuki et al. have determined the crystal structures of 3 LC3 isoforms in complex with the Atg13 LIR.<sup>33</sup> However, so far an investigation of the ATG13-specific relevance of the LIR motif has not been reported. We did not observe any alterations of the recruitment of ATG13 or RB1CC1 to puncta upon mutation of the ATG13 LIR motif. Furthermore, WIPI2 puncta formation was

not significantly affected by LIR mutation. However, LC3 turnover appeared to be rather increased than repressed. Notably, mutation of both the LIR motif and the RB1CC1 interaction site resulted in an enhanced nuclear localization of both ATG13 and LC3 following autophagy induction.

Huang et al. report that nuclear LC3 becomes deacetylated by SIRT1 and then traffics to the cytoplasm and enables autophagosome formation.<sup>59</sup> The association of deacetylated LC3 with autophagy factors shifts its distribution from the nucleus toward the cytoplasm.<sup>59</sup> Although a nuclear function of ATG13 has not been reported yet, it is tempting to speculate that ATG13 (possibly in combination with RB1CC1) participates in the regulation of the subcellular LC3 distribution. When ATG13 is released from the ULK1 complex by deletion of the RB1CC1 interaction site, LC3 is retained in the nucleus. Notably, nuclear functions and/or localization have been reported for ULK1, ULK2 and RB1CC1.<sup>60-62</sup>

In summary, we suggest that the ATG13-ATG101 interaction represents one Achilles heel of autophagy induction and, accordingly, is an attractive target for therapeutic interventions in disease settings where the inhibition of autophagy is desired. Several ULK1 kinase inhibitors have been identified and characterized.<sup>63-66</sup> However, these compounds neglect ULK1/2-independent autophagy pathways, which might still depend on the ATG13-ATG101 interaction. It is tempting to speculate that small-molecule compounds interfering with this protein-protein interaction might be therapeutically valuable drugs.

## MATERIALS & METHODS

### **Antibodies and reagents**

Antibodies against ACTB/ $\beta$ -actin (clone AC-74, Sigma-Aldrich, A5316), ATG101 (Sigma-Aldrich, SAB4200175), ATG13 (Sigma-Aldrich, SAB4200100), ATG13 phospho (p)-S318 (Rockland Immunochemicals, 600-401-C49), ATG14 (MBL, PD026), ATG16L1 (MBL, PM040), HA (Covance, MMS-101R, now BioLegend, 901501), LC3 (for immunoblotting: Cell Signaling Technology, 2775 [detects endogenous levels of total LC3B protein; cross-reactivity may exist with other LC3 isoforms according to manufacturer specification]; for immunofluorescence: MBL International, PM036 [reacts with LC3A/LC3B/LC3C according to manufacturer specification]), RPS6KB1 phospho (p)-T389 (clone 1A5, Cell Signaling Technology, 9206), RB1CC1 (for immunoblotting: Bethyl Laboratories, A301-536A; for immunofluorescence: Proteintech, 17250-1-AP), SQSTM1/p62 (PROGEN Biotechnik, GP62-C), ULK1 (clone D8H5, Cell Signaling Technology, 8054), ULK1 phospho (p)-S757 (Cell Signaling Technology, 6888), VCL/Vinculin (Sigma-Aldrich, V9131), and WIP1 (Serotec, MCA5780GA) were used. IRDye 800- or IRDye 680-conjugated secondary antibodies were purchased from LI-COR Biosciences (926-32210/11, 926-68070/71, 926-68024 and 926-32214), Alexa Fluor<sup>®</sup> 488-conjugated goat anti-mouse IgG and Alexa Fluor<sup>®</sup> 647-conjugated goat anti-rabbit or anti-mouse IgG antibodies from Jackson ImmunoResearch Laboratories (111-605-003 and 111-605-003). Other reagents used were bafilomycin A<sub>1</sub> (Sigma-Aldrich, B1793 and Alfa Aesar, J61835), torin2 (Selleckchem, S2817), rapamycin (Calbiochem, 553210), protein A/G Sepharose (GE Healthcare, 17-5280-01 and 17-0618-01) and HA-agarose (Sigma-Aldrich, A2095).

### **Cell lines and cell culture**

Wild-type and *atg13* KO MEFs containing an insertion of a gene-trap cassette in the *Atg13* gene have previously been described.<sup>10</sup> Cells were cultured in high glucose (4.5 g/l) DMEM supplemented with 10% FCS at 37°C in a 5% CO<sub>2</sub> humidified atmosphere. For amino acid starvation, cells were washed

25

once with DPBS (Dulbecco's Phosphate-Buffered Saline, Gibco, 14190-094) and incubated for the indicated time points in EBSS (Earle's Balanced Salt Solution, Gibco, 24010-043).

### **Immunopurification, immunoblotting and size-exclusion chromatography**

Immunopurification and immunoblotting were done as described previously.<sup>18</sup> For size-exclusion chromatography, S100 extracts were prepared by resuspending cell pellets in RoederA buffer (10 mM HEPES, pH 7, 10 mM KCl, 1.5 mM MgCl<sub>2</sub>, 0.5 mM DTT and protease inhibitor cocktail [Roche, 04693132001]), incubating at room temperature for 10 min and disruption with 10 strokes in a 1 ml tight Wheaton-dounce homogenizer (Wheaton, 357538). NaCl concentration was adjusted to 150 mM and lysates were centrifuged at 17,000 x g for 30 min. Supernatants were filtered through a 45-nm PVDF filter unit and applied onto a Superose 6 increase 10/300 GL column (GE Healthcare, 29-0915-96). The column was calibrated with a Gel Filtration Calibration Kit (GE Healthcare, 28-4038-42, dextran blue (2 MDa), TG/thyroglobulin (669 kDa), ferritin (440 kDa), ALDO/aldolase (158 kDa) and RNaseA (14 kDa)). For quantification of protein levels in each fraction, immunoblotting was performed and densitometry was done using Image Studio Light Version 4 (LI-COR Biosciences). Protein ratios (fraction to input) were normalized to the fraction with highest signal intensity.

### **Immunofluorescence**

Cells were grown on glass cover slips one day prior to stimulation, fixation with 4% formaldehyde-PBS for 15 min on ice, quenching with 50 mM NH<sub>4</sub>Cl for 15 min and permeabilization with 50  $\mu$ g/ml digitonin (Roth, 4005) for 5 min. Samples were blocked with 3% BSA (Roth, 8076)-PBS and incubated with primary antibodies for 1 h. After secondary antibody incubation, samples were washed 2 times with 0.2 % Tween-20 (Sigma-Aldrich, P1379) in PBS. Cells were embedded in Mowiol-488 (Sigma-Aldrich, 81381) containing DAPI. Imaging was performed with a Zeiss LSM 710 or 780 confocal laser

26

scanning microscope (Zeiss, Köln, Germany) with a Plan Achromat 63x/1.4 oil objective (Zeiss, Köln, Germany). Quantification of images was performed with Fiji.<sup>67</sup> For that, signals and nuclei were counted per image and a signal-to-nuclei ratio was calculated.

### Flow cytometry

Cells stably expressing mCitrine-LC3B were incubated in EBSS starvation medium for 8 h. Cells were trypsinized and analyzed for mCitrine fluorescence using an EC800 cell analyser (Sony, Tokyo, Japan).

### Retroviral transfection

Generation of pMSCVpuro-HA-ATG13 based vectors has previously been described.<sup>18</sup> Briefly, for the generation of cDNAs encoding *ATG13* mutants mutagenesis PCRs were performed using the following primers:  $\Delta V348$ -M373: CAACCCATTAAACCAGGTGAATCTCCAGATTC,  $\Delta$ CT: GTAATATACCGTCTGTAGAATAAGCGGCCGCTCGAAAC, phospholipid binding domain (PLBD<sup>mut</sup>): CTGATCTCAATCCAGGACGCGGACTGGACGGTTATTGCAATTTTGGCCCTCAAGACTG, HORMA domain (HD<sup>mut</sup>): CTGAAGTCCCTTCTTGCTGCAACTGGGGGACACACAGCCGTAGGCTCTCCAGGAAAC, LIR domain (LIR<sup>mut</sup>): CCATGATGAGCCGCTTATGGCAGACTTTAAAC,  $\Delta$ TLD: CCTTTGTGGAATAAGCGGCCGCTCGAAAC. Reverse complement sequences of forward primers were used as reverse primers. Plat-E cells (kindly provided by Toshio Kitamura, Institute of Medical Science, University of Tokyo, Japan) were used as packaging cell line. Transfection with retroviral expression vectors was performed with FUGENE® 6 (Roche, 11988387001). *atg13* KO MEF cells were incubated with retroviral supernatant fractions containing 3 mg/ml polybrene (Sigma-Aldrich, H9268-106) and selected in medium containing 2.5 mg/ml puromycin (InvivoGen, ant-pr-1). Generation of MEFs stably expressing mCitrine-LC3B was performed as previously described.<sup>18</sup>

### Bimolecular fluorescence complementation assay

Vectors containing the N- and C-terminal sequence of Venus were kindly provided by Michael Engelke.<sup>68</sup> Sequences encoding VAMP7 or  $\Delta$ N-BLNK (also known as SLP-65) were excised by *Bam*HI and *Eco*RI or *Bgl*II and *Not*I digestion, respectively. Vector backbones were blunted and ligated generating pMSCVbleo-VenusC and pMSCVpuro-VenusN. VenusC cDNA was then cloned into the pBABEhygro vector (Addgene, 1765; deposited by Hartmut Land & Jay Morgenstern & Bob Weinberg). *ATG13* and *ATG101* cDNAs were inserted by sequence and ligation-independent cloning (SLIC; ref. 69) using the following primers: *ATG13* fwd: CAACTTCAAGATCCGCCACACATCGAAGATCGGCCCGAAATTCGGTGCATAAATTCGAAATGATCTGAAACAG AAAGTGATG, *ATG13* rev: GACTGCCTTGGGAAAAGCGCCTCCCTACCCGGTAGAATTTTACTGCAGGGTTTCCACAAAGGC, *ATG101* fwd:

GCGTGCATAAATTCGAAATGATCTCGAGCAGAAAAGTGTGATGAACCACTAAGTGTGCTGGAGGTGCTGGAG, and *ATG101* rev: GACACACATTCCACAGGTGCTGACTCAGAGGGCAAGGGTGTCTTTGATG. As templates pMSCV-HA-ATG13 and CMV-FLAG-ATG101 (Addgene, 22877; deposited by Noboru Mizushima) were used, thereby generating pMSCVpuro-VenusN-ATG13 and pBABEhygro-VenusC-ATG101. The SLIC protocol (ref. 69) was performed with slight alterations, i.e., single strands were generated using the Klenow fragment at 37°C for 30 min, followed by heat inactivation at 75°C for 15 min. *atg13* KO MEFs stably expressing VenusC-ATG101 were generated by retroviral transfection. These cells were further incubated with VenusN-ATG13 viroid supernatant for 24 h. Cells were trypsinized and used for flow cytometric analysis or cleared cellular lysates were obtained for immunoblotting.

### Biotin-phenol labelling in live cells

For the generation of pMSCV-HA-APEX2-ATG13 SLIC was performed with the primers ACGATGTCCAGATTACGCCGGATCCGGAAAGTCTTACCCAACCTGTGAGTG and

AGCCCGAGGTCGAGCCCGAGCCCTTGGCGGCATCAGCAAACCCAAAGCTCGGAAAG using pcDNA3  
Connexin43-GFP-APEX2 (Addgene, 49385; deposited by Alice Ting) as a template for APEX2  
amplification and GGGCTCGGGCTGACCTCGGGCTCGGGCGAAACTGATCTCAATCCACAGGACAG and  
CCGGTAGAATTCTGTTCCGAGCGCCGCTTACTGCAGGG for ATG13 amplification. pMSCV-HA-ATG13 was  
digested with *Bam*HI and *Not*I. Subsequently mutagenesis PCR was performed for ATG13 mutants  
and stable cell lines were generated by retroviral transfection. The biotinylation protocol was  
performed as previously described.<sup>35</sup> For enrichment of biotinylated proteins, cells were lysed in RIPA  
buffer containing protease quenchers, and streptavidin agarose (Sigma-Aldrich, S1638) was used for  
protein purification.

#### **Proximity-ligation assay**

In situ analysis of protein interaction was performed with the DuoLink<sup>®</sup> system from Sigma-Aldrich  
(Sigma-Aldrich, DUO92101). Cells were plated on glass cover slips 1 day prior to fixation with 4%  
formaldehyde-PBS for 15 min on ice, quenching with 50 mM NH<sub>4</sub>Cl for 15 min and permeabilization  
with 50 µg/ml digitonin for 5 min. Samples were blocked with 3% BSA-PBS and incubated with  
primary antibodies for 1 h. Secondary antibody probing, ligation and amplification were performed  
according to the manufacturer's protocol. Imaging was performed on an inverse laser scanning  
confocal microscope in z stacks. Stacks were merged with average intensities. Signals and nuclei were  
counted per image and the signal-to-nuclei ratio was calculated.

#### **Computational alanine scanning and MM-GB/SA calculations**

The structure of the human ATG13-ATG101 HORMA heterodimer (PDB ID: 5C50, ref. 24) was  
prepared with the protein preparation wizard in Maestro.<sup>70</sup> A conformational ensemble was  
generated from 3 explicit solvent MD simulations of 250 ns length, performed with the Amber14

software package. All MD simulations and subsequent MM-GB/SA calculations were carried out as  
described previously.<sup>71</sup> The same structure was used as input structure for the DrugScore<sup>PPH</sup>  
webservice to perform computational alanine scanning.<sup>37</sup>

## ACKNOWLEDGMENTS

We thank Toshio Kitamura for providing Plat-E cells and Michael Engelke for providing vectors containing the N- and C-terminal sequence of Venus. This work was supported by the Deutsche Forschungsgemeinschaft STO 864/3-1, STO 864/4-1, STO 864/5-1 (to B.S.) and GRK 2158 (to H.G. and to B.S.), and the Research Committee of the Medical Faculty of the Heinrich Heine University Düsseldorf 22/2015 (to B.S.).

## CONFLICT OF INTEREST STATEMENT

The authors declare that there are no competing financial interests in relation to the work described.

## REFERENCES

1. Dikic I, Johansen T, Kirkin V. Selective autophagy in cancer development and therapy. *Cancer Res* 2010; 70:3431-4.
2. Levine B, Kroemer G. Autophagy in the pathogenesis of disease. *Cell* 2008; 132:27-42.
3. Mizushima N, Levine B, Cuervo AM, Klionsky DJ. Autophagy fights disease through cellular self-digestion. *Nature* 2008; 451:1069-75.
4. Mowers EE, Sharifi MN, Macleod KF. Autophagy in cancer metastasis. *Oncogene* 2016.
5. Ganley IG, Lam du H, Wang J, Ding X, Chen S, Jiang X. ULK1-ATG13-FIP200 complex mediates mTOR signaling and is essential for autophagy. *J Biol Chem* 2009; 284:12297-305.
6. Hosokawa N, Hara T, Kaizuka T, Kishi C, Takamura A, Miura Y, Iemura S, Natsume T, Takehana K, Yamada N, et al. Nutrient-dependent mTORC1 association with the ULK1-Atg13-FIP200 complex required for autophagy. *Mol Biol Cell* 2009; 20:1981-91.
7. Hosokawa N, Sasaki T, Iemura S, Natsume T, Hara T, Mizushima N. Atg101, a novel mammalian autophagy protein interacting with Atg13. *Autophagy* 2009; 5:973-9.
8. Mercer CA, Kaliappan A, Dennis PB. A novel, human Atg13 binding protein, Atg101, interacts with ULK1 and is essential for macroautophagy. *Autophagy* 2009; 5:649-62.
9. Gan B, Peng X, Nagy T, Alcaraz A, Gu H, Guan JL. Role of FIP200 in cardiac and liver development and its regulation of TNFalpha and TSC-mTOR signaling pathways. *The Journal of cell biology* 2006; 175:121-33.
10. Kaizuka T, Mizushima N. Atg13 is Essential for Autophagy and Cardiac Development in Mice. *Mol Cell Biol* 2015; 36:585-95.
11. Cheong H, Lindsten T, Wu J, Lu C, Thompson CB. Ammonia-induced autophagy is independent of ULK1/ULK2 kinases. *Proc Natl Acad Sci U S A* 2011; 108:11121-6.
12. Kundu M, Lindsten T, Yang CY, Wu J, Zhao F, Zhang J, Selak MA, Ney PA, Thompson CB. Ulk1 plays a critical role in the autophagic clearance of mitochondria and ribosomes during reticulocyte maturation. *Blood* 2008; 112:1493-502.

13. Lee EJ, Tournier C. The requirement of uncoordinated 51-like kinase 1 (ULK1) and ULK2 in the regulation of autophagy. *Autophagy* 2011; 7:689-95.
14. Alers S, Löffler AS, Wesselborg S, Stork B. Role of AMPK-mTOR-ULK1/2 in the regulation of autophagy: cross talk, shortcuts, and feedbacks. *Mol Cell Biol* 2012; 32:2-11.
15. Papinski D, Kraft C. Regulation of Autophagy By Signaling Through the Atg1/ULK1 Complex. *J Mol Biol* 2016; 428:1725-41.
16. Wesselborg S, Stork B. Autophagy signal transduction by ATG proteins: from hierarchies to networks. *Cellular and molecular life sciences : CMLS* 2015.
17. Wong PM, Puente C, Ganley IG, Jiang X. The ULK1 complex: sensing nutrient signals for autophagy activation. *Autophagy* 2013; 9:124-37.
18. Hieke N, Löffler AS, Kaizuka T, Berleth N, Böhrer P, Driessen S, Stuhldreier F, Friessen O, Assani K, Schmitz K, et al. Expression of a ULK1/2 binding-deficient ATG13 variant can partially restore autophagic activity in ATG13-deficient cells. *Autophagy* 2015; 11:1471-83.
19. Jung CH, Jun CB, Ro SH, Kim YM, Otto NM, Cao J, Kundu M, Kim DH. ULK-Atg13-FIP200 complexes mediate mTOR signaling to the autophagy machinery. *Mol Biol Cell* 2009; 20:1992-2003.
20. Suzuki H, Kaizuka T, Mizushima N, Noda NN. Structure of the Atg101-Atg13 complex reveals essential roles of Atg101 in autophagy initiation. *Nat Struct Mol Biol* 2015; 22:572-80.
21. Aravind L, Koonin EV. The HORMA domain: a common structural denominator in mitotic checkpoints, chromosome synapsis and DNA repair. *Trends Biochem Sci* 1998; 23:284-6.
22. Jao CC, Ragusa MJ, Stanley RE, Hurley JH. A HORMA domain in Atg13 mediates PI 3-kinase recruitment in autophagy. *Proc Natl Acad Sci U S A* 2013; 110:5486-91.
23. Michel M, Schwarten M, Decker C, Nagel-Steger L, Willbold D, Weiergraber OH. The mammalian autophagy initiator complex contains two HORMA domain proteins. *Autophagy* 2015:0.
24. Qi S, Kim do J, Stjepanovic G, Hurley JH. Structure of the Human Atg13-Atg101 HORMA Heterodimer: an Interaction Hub within the ULK1 Complex. *Structure* 2015; 23:1848-57.
25. Suzuki SW, Yamamoto H, Oikawa Y, Kondo-Kakuta C, Kimura Y, Hirano H, Ohsumi Y. Atg13 HORMA domain recruits Atg9 vesicles during autophagosome formation. *Proceedings of the National Academy of Sciences of the United States of America* 2015; 112:3350-5.
26. Karanasios E, Stapleton E, Manifava M, Kaizuka T, Mizushima N, Walker SA, Ktistakis NT. Dynamic association of the ULK1 complex with omegasomes during autophagy induction. *J Cell Sci* 2013; 126:5224-38.
27. Fujioka Y, Suzuki SW, Yamamoto H, Kondo-Kakuta C, Kimura Y, Hirano H, Akada R, Inagaki F, Ohsumi Y, Noda NN. Structural basis of starvation-induced assembly of the autophagy initiation complex. *Nature structural & molecular biology* 2014; 21:513-21.
28. Mei Y, Su M, Soni G, Salem S, Colbert CL, Sinha SC. Intrinsically disordered regions in autophagy proteins. *Proteins* 2014; 82:565-78.
29. Chew LH, Lu S, Liu X, Li FK, Yu AY, Klionsky DJ, Dong MQ, Yip CK. Molecular interactions of the Saccharomyces cerevisiae Atg1 complex provide insights into assembly and regulatory mechanisms. *Autophagy* 2015; 11:891-905.
30. Yamamoto H, Fujioka Y, Suzuki SW, Noshiro D, Suzuki H, Kondo-Kakuta C, Kimura Y, Hirano H, Ando T, Noda NN, et al. The Intrinsically Disordered Protein Atg13 Mediates Supramolecular Assembly of Autophagy Initiation Complexes. *Dev Cell* 2016; 38:86-99.
31. Alers S, Löffler AS, Paasch F, Dieterle AM, Keppeler H, Lauber K, Campbell DG, Fehrenbacher B, Schaller M, Wesselborg S, et al. Atg13 and FIP200 act independently of Ulk1 and Ulk2 in autophagy induction. *Autophagy* 2011; 7:1423-33.
32. Alemu EA, Lemark T, Torgersen KM, Birgisdottir AB, Larsen KB, Jain A, Olsvik H, Overvatn A, Kirkin V, Johansen T. ATG8 family proteins act as scaffolds for assembly of the ULK complex: sequence requirements for LC3-interacting region (LIR) motifs. *J Biol Chem* 2012; 287:39275-90.
33. Suzuki H, Tabata K, Morita E, Kawasaki M, Kato R, Dobson RC, Yoshimori T, Wakatsuki S. Structural basis of the autophagy-related LC3/Atg13 LIR complex: recognition and interaction mechanism. *Structure* 2014; 22:47-58.

34. Hung V, Zou P, Rhee HW, Udeshi ND, Cracan V, Svinikina T, Carr SA, Mootha VK, Ting AY. Proteomic mapping of the human mitochondrial intermembrane space in live cells via ratiometric APEX tagging. *Mol Cell* 2014; 55:332-41.
35. Lam SS, Martell JD, Kamer KJ, Deerinck TJ, Ellisman MH, Mootha VK, Ting AY. Directed evolution of APEX2 for electron microscopy and proximity labeling. *Nat Methods* 2015; 12:51-4.
36. Rhee HW, Zou P, Udeshi ND, Martell JD, Mootha VK, Carr SA, Ting AY. Proteomic mapping of mitochondria in living cells via spatially restricted enzymatic tagging. *Science* 2013; 339:1328-31.
37. Krüger DM, Gohlke H. DrugScorePPI webserver: fast and accurate in silico alanine scanning for scoring protein-protein interactions. *Nucleic Acids Res* 2010; 38:W480-6.
38. Moreira IS, Fernandes PA, Ramos MJ. Hot spots—a review of the protein-protein interface determinant amino-acid residues. *Proteins* 2007; 68:803-12.
39. Gohlke H, Kiel C, Case DA. Insights into protein-protein binding by binding free energy calculation and free energy decomposition for the Ras-Raf and Ras-RalGDS complexes. *J Mol Biol* 2003; 330:891-913.
40. Homeyer N, Gohlke H. Free Energy Calculations by the Molecular Mechanics Poisson-Boltzmann Surface Area Method. *Mol Inform* 2012; 31:114-22.
41. Park JM, Jung CH, Seo M, Otto NM, Grunwald D, Kim KH, Moriarity B, Kim YM, Starker C, Nho RS, et al. The ULK1 complex mediates MTORC1 signaling to the autophagy initiation machinery via binding and phosphorylating ATG14. *Autophagy* 2016; 12:547-64.
42. Choi H, Merceron C, Mangiavini L, Seifert EL, Schipani E, Shapiro IM, Risbud MV. Hypoxia promotes noncanonical autophagy in nucleus pulposus cells independent of MTOR and HIF1A signaling. *Autophagy* 2016; 12:1631-46.
43. Gao Y, Liu Y, Hong L, Yang Z, Cai X, Chen X, Fu Y, Lin Y, Wen W, Li S, et al. Golgi-associated LC3 lipidation requires V-ATPase in noncanonical autophagy. *Cell Death Dis* 2016; 7:e2330.
44. Manzoni C, Mamais A, Roosen DA, Dihanich S, Soutar MP, Plun-Favreau H, Bandopadhyay R, Hardy J, Tooze SA, Cookson MR, et al. mTOR independent regulation of macroautophagy by Leucine Rich Repeat Kinase 2 via Beclin-1. *Sci Rep* 2016; 6:35106.
45. Kang SA, Pacold ME, Cervantes CL, Lim D, Lou HJ, Ottina K, Gray NS, Turk BE, Yaffe MB, Sabatini DM. mTORC1 phosphorylation sites encode their sensitivity to starvation and rapamycin. *Science* 2013; 341:1236566.
46. Noda NN, Mizushima N. Atg101: Not Just an Accessory Subunit in the Autophagy-initiation Complex. *Cell Struct Funct* 2016; 41:13-20.
47. Reggiori F, Tucker KA, Stromhaug PE, Klionsky DJ. The Atg1-Atg13 complex regulates Atg9 and Atg23 retrieval transport from the pre-autophagosomal structure. *Dev Cell* 2004; 6:79-90.
48. Sekito T, Kawamata T, Ichikawa R, Suzuki K, Ohsumi Y. Atg17 recruits Atg9 to organize the pre-autophagosomal structure. *Genes Cells* 2009; 14:525-38.
49. Rao Y, Perna MG, Hofmann B, Beier V, Wollert T. The Atg1-kinase complex tethers Atg9-vesicles to initiate autophagy. *Nat Commun* 2016; 7:10338.
50. Papinski D, Schuschnig M, Reiter W, Wilhelm L, Barnes CA, Maiolica A, Hansmann I, Pfaffenwimmer T, Kijanska M, Stoffel I, et al. Early steps in autophagy depend on direct phosphorylation of Atg9 by the Atg1 kinase. *Molecular cell* 2014; 53:471-83.
51. Young AR, Chan EY, Hu XW, Kochi R, Crawshaw SG, High S, Hailey DW, Lippincott-Schwartz J, Tooze SA. Starvation and ULK1-dependent cycling of mammalian Atg9 between the TGN and endosomes. *J Cell Sci* 2006; 119:3888-900.
52. Mack HJ, Zheng B, Asara JM, Thomas SM. AMPK-dependent phosphorylation of ULK1 regulates ATG9 localization. *Autophagy* 2012; 8:1197-214.
53. Weerasekara VK, Panek DJ, Broadbent DG, Mortenson JB, Mathis AD, Logan GN, Prince JT, Thomson DM, Thompson JW, Andersen JL. Metabolic-stress-induced rearrangement of the 14-3-3zeta interactome promotes autophagy via a ULK1- and AMPK-regulated 14-3-3zeta interaction with phosphorylated Atg9. *Molecular and cellular biology* 2014; 34:4379-88.

54. Karanasios E, Walker SA, Okkenhaug H, Manifava M, Hummel E, Zimmermann H, Ahmed Q, Domart MC, Collinson L, Ktistakis NT. Autophagy initiation by ULK complex assembly on ER tubulovesicular regions marked by ATG9 vesicles. *Nat Commun* 2016; 7:12420.
55. Chen S, Wang C, Yeo S, Liang CC, Okamoto T, Sun S, Wen J, Guan JL. Distinct roles of autophagy-dependent and -independent functions of FIP200 revealed by generation and analysis of a mutant knock-in mouse model. *Genes Dev* 2016; 30:856-69.
56. Kraft C, Kijanska M, Kalte E, Siergiejuk E, Lee SS, Semplicio G, Stoffel I, Brezovich A, Verma M, Hansmann I, et al. Binding of the Atg1/ULK1 kinase to the ubiquitin-like protein Atg8 regulates autophagy. *EMBO J* 2012; 31:3691-703.
57. Nakatogawa H, Ohbayashi S, Sakoh-Nakatogawa M, Kakuta S, Suzuki SW, Kirisako H, Kondou Kakuta C, Noda NN, Yamamoto H, Ohsumi Y. The autophagy-related protein kinase Atg1 interacts with the ubiquitin-like protein Atg8 via the Atg8 family interacting motif to facilitate autophagosome formation. *J Biol Chem* 2012; 287:28503-7.
58. Okazaki N, Yan J, Yuasa S, Ueno T, Kominami E, Masuho Y, Koga H, Muramatsu M. Interaction of the Unc-51-like kinase and microtubule-associated protein light chain 3 related proteins in the brain: possible role of vesicular transport in axonal elongation. *Brain Res Mol Brain Res* 2000; 85:1-12.
59. Huang R, Xu Y, Wan W, Shou X, Qian J, You Z, Liu B, Chang C, Zhou T, Lippincott-Schwartz J, et al. Deacetylation of nuclear LC3 drives autophagy initiation under starvation. *Mol Cell* 2015; 57:456-66.
60. Chano T, Ikegawa S, Kontani K, Okabe H, Baldini N, Saeki Y. Identification of RB1CC1, a novel human gene that can induce RB1 in various human cells. *Oncogene* 2002; 21:1295-8.
61. Joshi A, Iyengar R, Joo JH, Li-Harms XJ, Wright C, Marino R, Winborn BJ, Phillips A, Temirov J, Sciarretta S, et al. Nuclear ULK1 promotes cell death in response to oxidative stress through PARP1. *Cell Death Differ* 2015.
62. Shin SH, Lee EJ, Chun J, Hyun S, Kang SS. ULK2 Ser 1027 Phosphorylation by PKA Regulates Its Nuclear Localization Occurring through Karyopherin Beta 2 Recognition of a PY-NLS Motif. *PLoS One* 2015; 10:e0127784.
63. Egan DF, Chun MG, Vamos M, Zou H, Rong J, Miller CJ, Lou HJ, Raveendra-Panickar D, Yang CC, Sheffler DJ, et al. Small Molecule Inhibition of the Autophagy Kinase ULK1 and Identification of ULK1 Substrates. *Mol Cell* 2015; 59:285-97.
64. Lazarus MB, Novotny CJ, Shokat KM. Structure of the human autophagy initiating kinase ULK1 in complex with potent inhibitors. *ACS chemical biology* 2015; 10:257-61.
65. Lazarus MB, Shokat KM. Discovery and structure of a new inhibitor scaffold of the autophagy initiating kinase ULK1. *Bioorganic & medicinal chemistry* 2015; 23:5483-8.
66. Petherick KJ, Conway OJ, Mpamhanga C, Osborne SA, Kamal A, Saxty B, Ganley IG. Pharmacological Inhibition of ULK1 Kinase Blocks Mammalian Target of Rapamycin (mTOR)-dependent Autophagy. *J Biol Chem* 2015; 290:11376-83.
67. Schindelin J, Arganda-Carreras I, Frise E, Kaynig V, Longair M, Pietzsch T, Preibisch S, Rueden C, Saalfeld S, Schmid B, et al. Fiji: an open-source platform for biological-image analysis. *Nat Methods* 2012; 9:676-82.
68. Engelke M, Pirkuliyeva S, Kuhn J, Wong L, Boyken J, Herrmann N, Becker S, Griesinger C, Wienands J. Macromolecular assembly of the adaptor SLP-65 at intracellular vesicles in resting B cells. *Sci Signal* 2014; 7:ra79.
69. Li MZ, Elledge SJ. Harnessing homologous recombination in vitro to generate recombinant DNA via SLIC. *Nat Methods* 2007; 4:251-6.
70. Sastry GM, Adzhigirey M, Day T, Annabhimoju R, Sherman W. Protein and ligand preparation: parameters, protocols, and influence on virtual screening enrichments. *J Comput Aided Mol Des* 2013; 27:221-34.

71. Ciglia E, Vergin J, Reimann S, Smits SH, Schmitt L, Groth G, Gohlke H. Resolving hot spots in the C-terminal dimerization domain that determine the stability of the molecular chaperone Hsp90. *PLoS One* 2014; 9:e96031.

## FIGURE LEGENDS

**Figure 1.** Interaction interfaces of human ATG13. **(A)** Schematic representation of human ATG13 (isoform 2; Uniprot identifier O75143-2). Amino acid sequences involved in binding to proteins and phospholipids are indicated.<sup>18, 20, 23, 24, 26, 31-33, 56</sup> **(B)** List of ATG13 mutations investigated in this paper. Targeted domains, interaction partners, applied mutations and labelling used for this manuscript are given.

**Figure 2.** The amino acid sequence V348-M373 comprises the RB1CC1 binding region in ATG13. **(A)** *atg13* KO MEFs retrovirally transfected with empty vector or cDNA encoding either HA-ATG13 or HA-ATG13( $\Delta$ V348-M373) were lysed and cleared cellular lysates were subjected to immunopurifications with anti-HA-agarose or protein A/G beads in combination with anti-RB1CC1 or anti-ATG101 antibodies, respectively. Purified proteins were subjected to SDS-PAGE and analyzed by immunoblotting for RB1CC1, ULK1, ATG13, HA, or ATG101. **(B)** *atg13* KO MEFs stably expressing HA-ATG13 or the indicated mutants were seeded onto glass cover slips. Next day cells were used for proximity ligation assay as described in the material and methods section (anti-HA antibody: covance MMS-101P). Nuclei were stained with DAPI. Signals and nuclei per image were counted and the signal:nuclei ratio was calculated. Data are represented as mean  $\pm$  SEM. Samples without significant difference display identical letter (Student t test, 2-sample assuming unequal variances; minimum of 24 images was analyzed). **(C)** *atg13* KO MEFs stably expressing HA-APEX2 alone or fused to either wild-type ATG13 or the indicated mutants were pre-incubated with phenol-biotin for 30 min and peroxidase was activated by adding H<sub>2</sub>O<sub>2</sub> for 1 min. Cells were washed 3 times with quenching solution and lysed. Biotinylated proteins were purified using streptavidin agarose. Purified proteins were analyzed by immunoblotting for RB1CC1, HA, or ATG101. **(D)** S100 extracts of cells described in **(A)** were separated by size-exclusion chromatography on a Superose 6 increase column. Fractions were analyzed by immunoblotting for the indicated proteins. Diagrams show protein levels for each

fraction at a ratio of the input and normalized to the fraction containing the highest concentration of the analyzed protein. Curves for controls (KO and ATG13) are reused in figures 5 and 6.

**Figure 3.** Disruption of the RB1CC1-binding region in ATG13 inhibits mutual recruitment to the phagophore. *atg13* KO MEFs retrovirally transfected with cDNA encoding either HA-ATG13 or HA-ATG13( $\Delta$ V348-M373) were seeded onto glass cover slips one day prior to stimulation with full medium (DMEM) or starvation medium (EBSS) for 1 h. Cells were fixed, permeabilized and stained for HA (covance MMS-101P) and RB1CC1. An inverse confocal laser scanning microscope was used for imaging. Puncta and colocalization per cell quantification was done using fiji software. Data represent mean + SEM. A minimum of 168 cells per stimulation was analyzed. Statistical analysis using the Student t test, 2-sample assuming unequal variances was performed comparing EBSS to DMEM for each individual cell line. No statistical significance with  $P < 0.05$  was obtained. Columns for control (ATG13) are reused in figures 4, 6, and supplementary figure S9. Scale bar: 20  $\mu$ m.

**Figure 4.** Mutation of residues I131, R133, V134 and Y138 in ATG13 is sufficient to inhibit its interaction with ATG101. (A) Computational alanine scanning of the ATG13-ATG101 interface was performed using the structure of the human ATG13-ATG101 HORMA heterodimer (PDB ID: 5C50, ref. 24) and the DrugScore<sup>PPI</sup> webserver (ref. 37) (upper panel).  $\Delta\Delta G$  denotes binding free energy differences for wild-type residue-to-Ala mutations; residues yielding  $\Delta\Delta G > 1$  kcal mol<sup>-1</sup> are considered binding hot spots. In the middle panel, per-residue effective binding energies ( $\Delta G_{\text{binding}}$ ) computed by the MM-GB/SA approach (ref. 39, 40) are shown. Residues considered hot spots according to both methods are colored in red. In the lower panel, the localization of these residues in the ATG13 interface is shown. (B) *atg13* KO MEFs stably expressing VenusC-ATG101 and Venus-ATG13 (wild-type or the indicated mutants) were trypsinized and analyzed for Venus fluorescence using a flow cytometer. The median of fluorescence intensity for each sample was normalized to

control cells lacking Venus-ATG13 expression (“none”) and was plotted in a bar diagram representing mean  $\pm$  SEM. Samples without significant difference display identical letters (Student t test, 2-sample assuming unequal variances). Representative data are plotted in a histogram. Cell lysates were examined for expression of the indicated proteins by immunoblotting. (C) *atg13* KO MEFs retrovirally transfected with empty vector or cDNA encoding either HA-ATG13 or the indicated variants were lysed and cleared cellular lysates were subjected to immunopurification with anti-ATG101 antibodies and a protein A/G-Sepharose mix. Purified proteins were subjected to SDS-PAGE and analyzed by immunoblotting for RB1CC1, ULK1, or HA. (D) *atg13* KO MEFs stably expressing the indicated HA-tagged ATG13 variants were grown on glass cover slips one day prior to incubation with starvation medium (EBSS) for 2 h, fixation and permeabilization. Immunofluorescence for HA (covance MMS-101P) and RB1CC1 was performed. An inverse confocal laser scanning microscope was used for imaging. Please note that we detected a high number of HA-positive puncta varying in size and intensity, of which only a minor portion colocalized with RB1CC1 puncta. This might be due to the exogenous expression of HA-ATG13 variants. Puncta and colocalization per cell quantification was done using fiji software. A minimum of 89 cells per stimulation was analyzed. Data represent mean + SEM. Statistical analysis using the Student t test, 2-sample assuming unequal variances was performed comparing EBSS to DMEM for each individual cell line.  $**P < 0.01$ ,  $***P < 0.001$ . Scale bar: 20  $\mu$ m.

**Figure 5.** Mutation of the HORMA domain, but not of the phospholipid-binding domain leads to disintegration of the ULK1 complex. (A to C) S100 extracts of *atg13* KO MEFs stably expressing HA-ATG13 or the indicated mutants were separated by size-exclusion chromatography on a Superose 6 increase column. Fractions were analyzed by immunoblotting for the indicated proteins. Diagrams show protein levels for each fraction at a ratio of the input and normalized to the fraction containing the highest concentration of the analyzed protein. Curves for controls (KO and ATG13) are reused in figures 2 and 6.

test, 2-sample assuming unequal variances). **(B)** Untransfected *Atg13* wild-type (WT) MEFs or *atg13* KO MEFs retrovirally transfected with empty vector (KO) or cDNA encoding the indicated ATG13 variants were grown on glass cover slips overnight and incubated for 2 h in growth medium or starvation medium (EBSS) in the presence or absence of 40 nM bafilomycin A<sub>1</sub> (BafA<sub>1</sub>). Cells were fixed, permeabilized and stained for LC3. Imaging was performed using an inverse confocal laser scanning microscope and puncta per cell quantification was done using Fiji software. Data represent mean + SEM. Statistical analysis using the Student t test, 2-sample assuming unequal variances was performed comparing LC3 puncta accumulation during EBSS + BafA<sub>1</sub> treatment for depicted cell lines. **\*\*P < 0.01, \*\*\*P < 0.001** (Student t test, 2-sample assuming unequal variances). **(C, D, F)** Untransfected *Atg13* wild-type MEFs (WT) or *atg13* KO MEFs retrovirally transfected with empty vector (KO) or cDNA encoding the indicated ATG13 variants were incubated as described in **(B)**. Cleared cellular lysates were analyzed by immunoblotting for HA, LC3, ACTB, and VCL. Fold changes were calculated by dividing each normalized ratio (protein to loading control) by the average of the ratios of the control lane (ATG13 in medium). Results are mean + SEM **\*P < 0.05, \*\*P < 0.01, n.s., not significant** (Student t test, 2-sample assuming unequal variances). **(E)** *atg13* KO MEFs retrovirally transfected with empty vector (KO) or cDNA encoding the indicated ATG13 variants were incubated in growth medium or starvation medium (EBSS) for 2 h. Cleared cellular lysates were analyzed by immunoblotting for SQSTM1 or VCL.

**Figure 8.** Differential requirement of ATG13 interaction interfaces for amino acid starvation-induced WIPI2 puncta formation. **(A)** *atg13* KO MEFs retrovirally transfected with cDNA encoding the indicated ATG13 variants were grown on glass cover slips overnight and incubated in growth medium (DMEM) or starvation medium (EBSS) for 2 h. Cells were fixed, permeabilized and stained for WIPI2. Imaging was performed using an inverse confocal laser scanning microscope. Puncta per cell quantification was done using Fiji software. Data represent mean + SEM. Statistical analysis using the

**Figure 6.** Composition of the ULK1 complex is influenced by the ATG13-ULK1 interaction but not by the LIR motif of ATG13. **(A)** S100 extracts of *atg13* KO MEFs stably expressing the indicated HA-ATG13 variants were separated by size-exclusion chromatography on a Superose 6 increase column. Fractions were analyzed by immunoblotting for the indicated proteins. Diagrams show protein levels for each fraction at a ratio of the input and normalized to the fraction containing the highest concentration of the analyzed protein. Curves for controls (KO and ATG13) are reused in figures 2 and 5. **(B)** Cells described in **(A)** were seeded onto glass cover slips one day prior to stimulation with full medium (DMEM) or starvation medium (EBSS) for 1 h. Cells were fixed, permeabilized and stained for HA (covance MMS-101P) and RB1CC1. An inverse confocal laser scanning microscope was used for imaging. Puncta and colocalization per cell quantification was done using Fiji software. A minimum of 127 cells per stimulation was analyzed. Data represent mean + SEM. Statistical analysis using the Student t test, 2-sample assuming unequal variances was performed comparing EBSS to DMEM for each individual cell line. **\*P < 0.05, \*\*P < 0.01, \*\*\*P < 0.001**. Scale bar: 20 μm. **(C)** *atg13* KO MEFs stably expressing HA-ATG13 or the indicated mutants were seeded onto glass cover slips one day prior to stimulation with starvation medium (EBSS) for 2 h. Cells were fixed, permeabilized and stained for HA (covance MMS-101P) and LC3. An inverse confocal laser scanning microscope was used for imaging. Scale bar: 20 μm.

**Figure 7.** Differential requirement of ATG13 interaction interfaces for amino acid starvation-induced LC3 turnover. **(A)** *Atg13* wild-type MEFs (WT) or *atg13* KO MEFs stably expressing mChitrine-LC3B and the indicated ATG13 variants were cultured in growth medium or starvation medium (EBSS) with or without 40 nM bafilomycin A<sub>1</sub> (BafA<sub>1</sub>) for 8 h. Total cellular mChitrine-LC3B signals were analyzed by flow cytometry. The median of fluorescence intensity for each sample was normalized to wild-type cells incubated in growth medium. Data represent mean + SEM. **\*\*P < 0.01, \*\*\*P < 0.001** (Student t

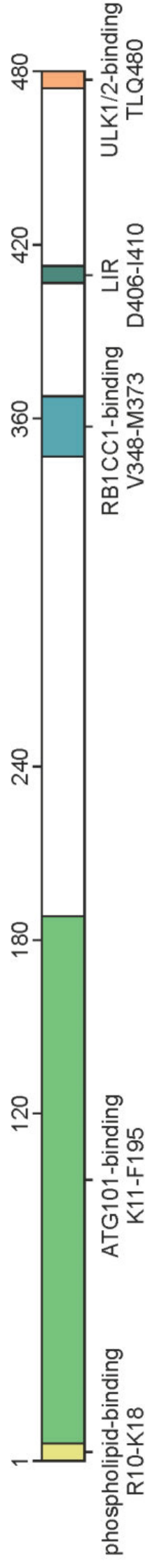
Student t test, 2-sample assuming unequal variances was performed comparing EBSS to DMEM for each individual cell line. \* $P < 0.05$ , \*\* $P < 0.01$ , \*\*\* $P < 0.001$ . Scale bar: 20  $\mu\text{m}$ .

**Figure 9.** Differential requirement of ATG13 interaction interfaces for autophagy induced by MTOR inhibition. **(A to E)** *atg13* KO MEFs retrovirally transfected with empty vector (KO) or cDNA encoding the indicated ATG13 variants were incubated for 2 h in growth medium in the presence or absence of 250 nM torin2 (left panels) or 500 nM rapamycin (right panels) and 40 nM bafilomycin A<sub>1</sub> (BafA<sub>1</sub>). Cleared cellular lysates were analyzed by immunoblotting for LC3 and ACTB. Fold changes were calculated by dividing each normalized ratio (protein to loading control) by the average of the ratios of the control lane (ATG13 in the medium). Results are mean  $\pm$  SEM \* $P < 0.05$ , \*\* $P < 0.01$ , \*\*\* $P < 0.001$  (Student t test, 2-sample assuming unequal variances).

**Figure 10.** Summary of the effects of mutations in ATG13 interaction interfaces on autophagy induction by amino acid starvation or MTOR inhibition. The heat map shows i) the percentage of LC3-II signal detected by immunoblotting for the indicated stimuli in the presence of bafilomycin A<sub>1</sub> (columns 1 to 3), ii) the increase of WIPI2 and ATG16L1 puncta formation after autophagy induction by the indicated stimuli (columns 4 to 6), or iii) the percentage of colocalization events of HA-ATG13 variants and RB1CC1 after treatment with the indicated stimuli (columns 7 and 8). All values were normalized to the control, which was set to 100% (ATG13, first row). The range for mapping was defined from 5.7 to 159. The value for LIR<sup>mut</sup> under EBSS stimulation (267.6%) was set to out of range, and the color code dark red was manually assigned (n.d., not determined).

# Figure 1

## A

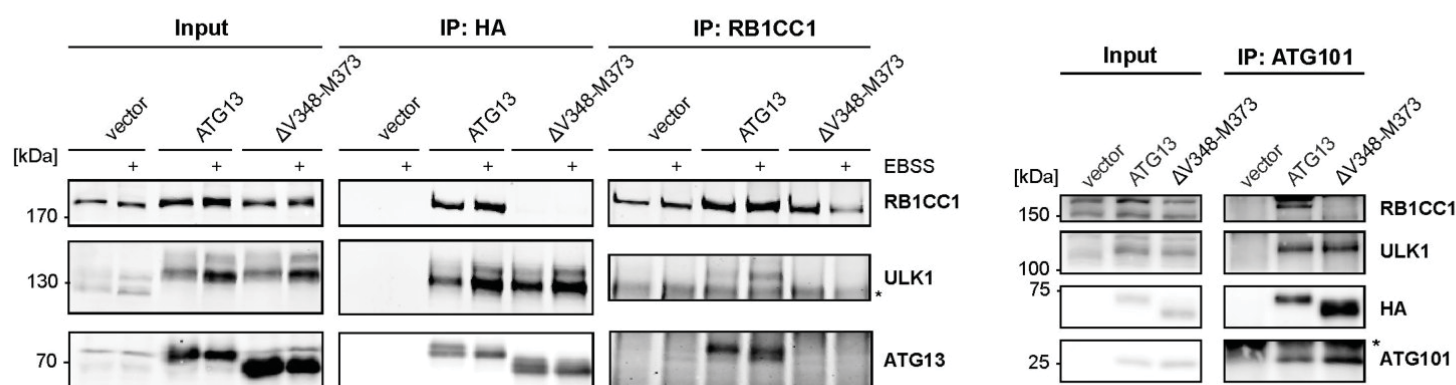


## B

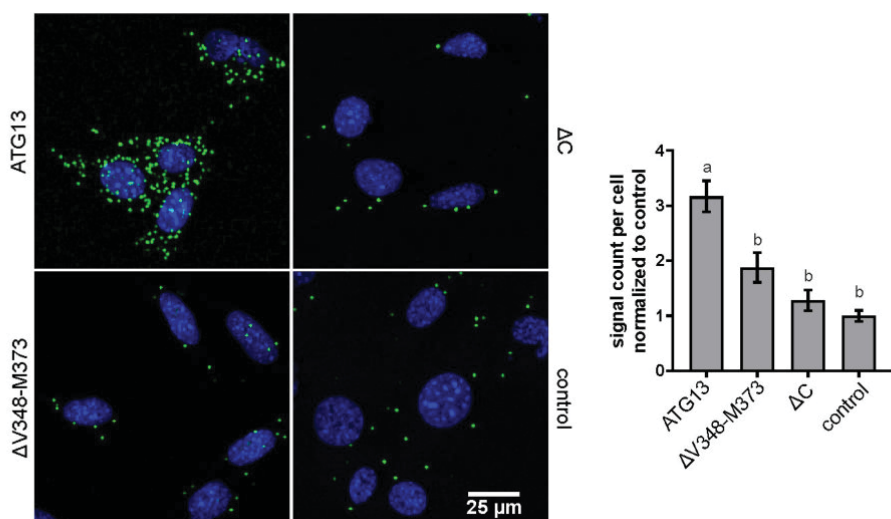
domain	interaction	mutation	labeling	Ref
phospholipid-binding domain	phospholipids: PA, PtdIns3P, PtdIns4P, PtdIns(3,4,5)P <sub>3</sub>	R10,K11,K15,K18A	PLBD <sup>mut</sup>	26
HORMA domain	ATG101	I131,R133,V134,Y138A	HD <sup>mut</sup>	this study
RB1CC1-binding motif	RB1CC1	ΔV348-M373	ΔV348-M373	31
LIR domain	Atg8 family members	F407,I410A	LIR <sup>mut</sup>	32
ULK1/2-binding motif	ULK1/2	ΔTLQ480	ΔTLQ	18

Figure 2

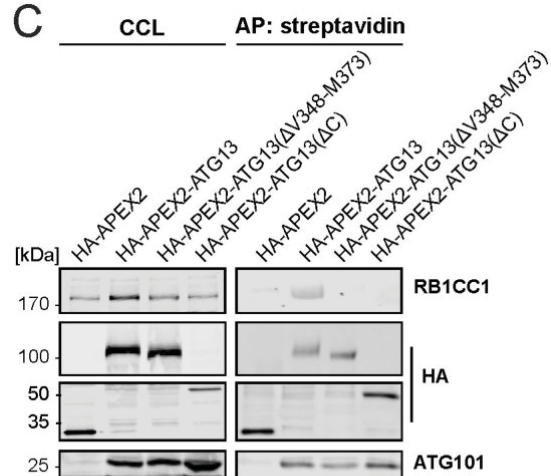
A



B



C



D

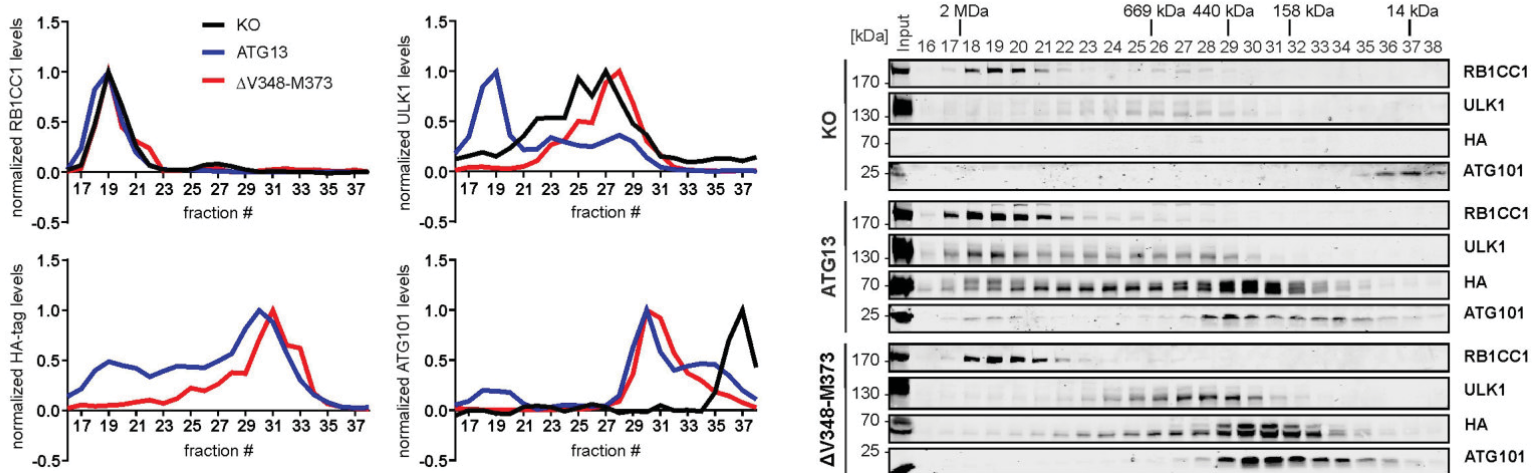
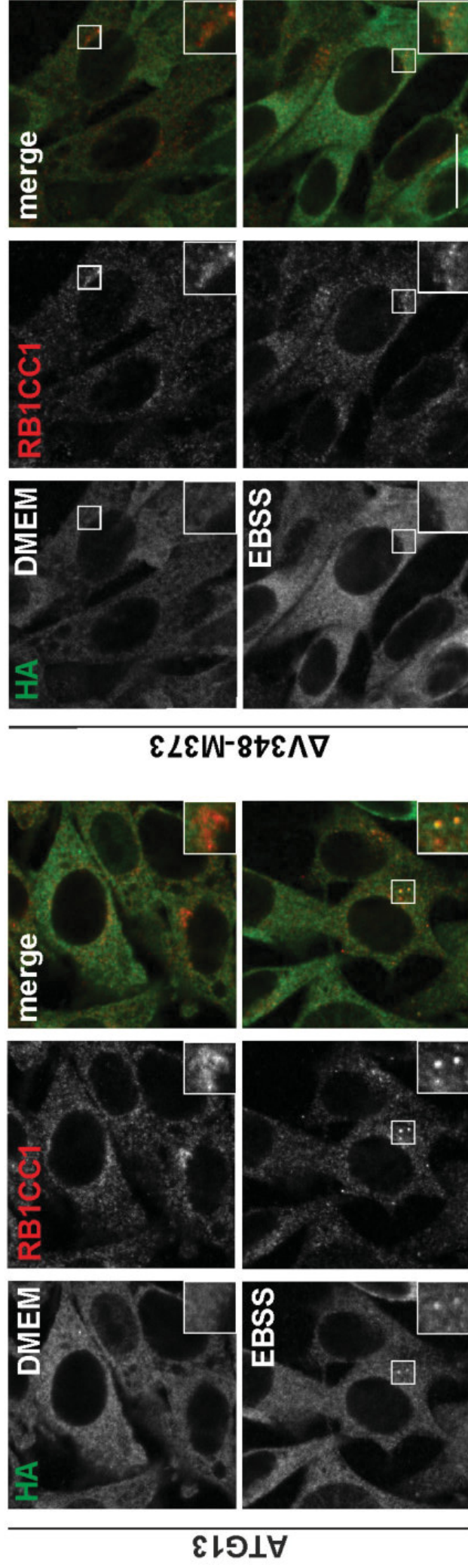


Figure 3



Medium  
EBSS

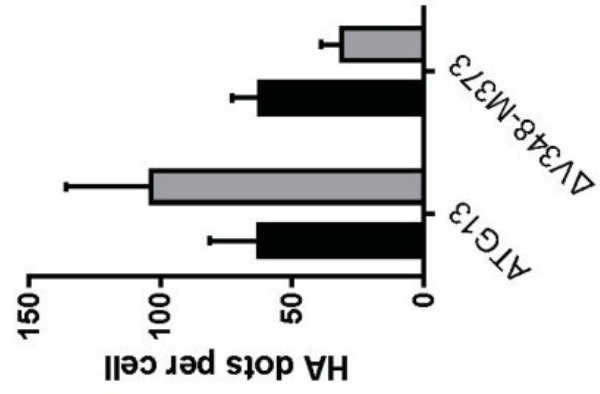
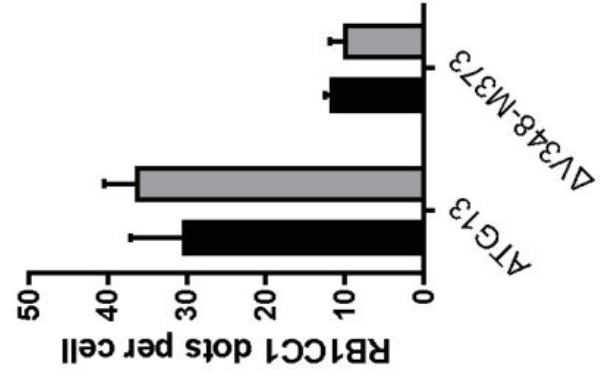
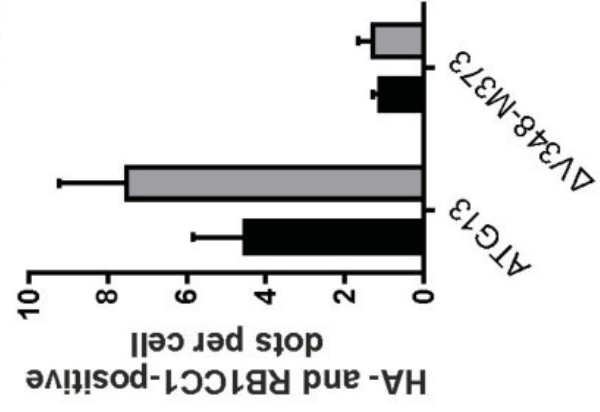




Figure 5

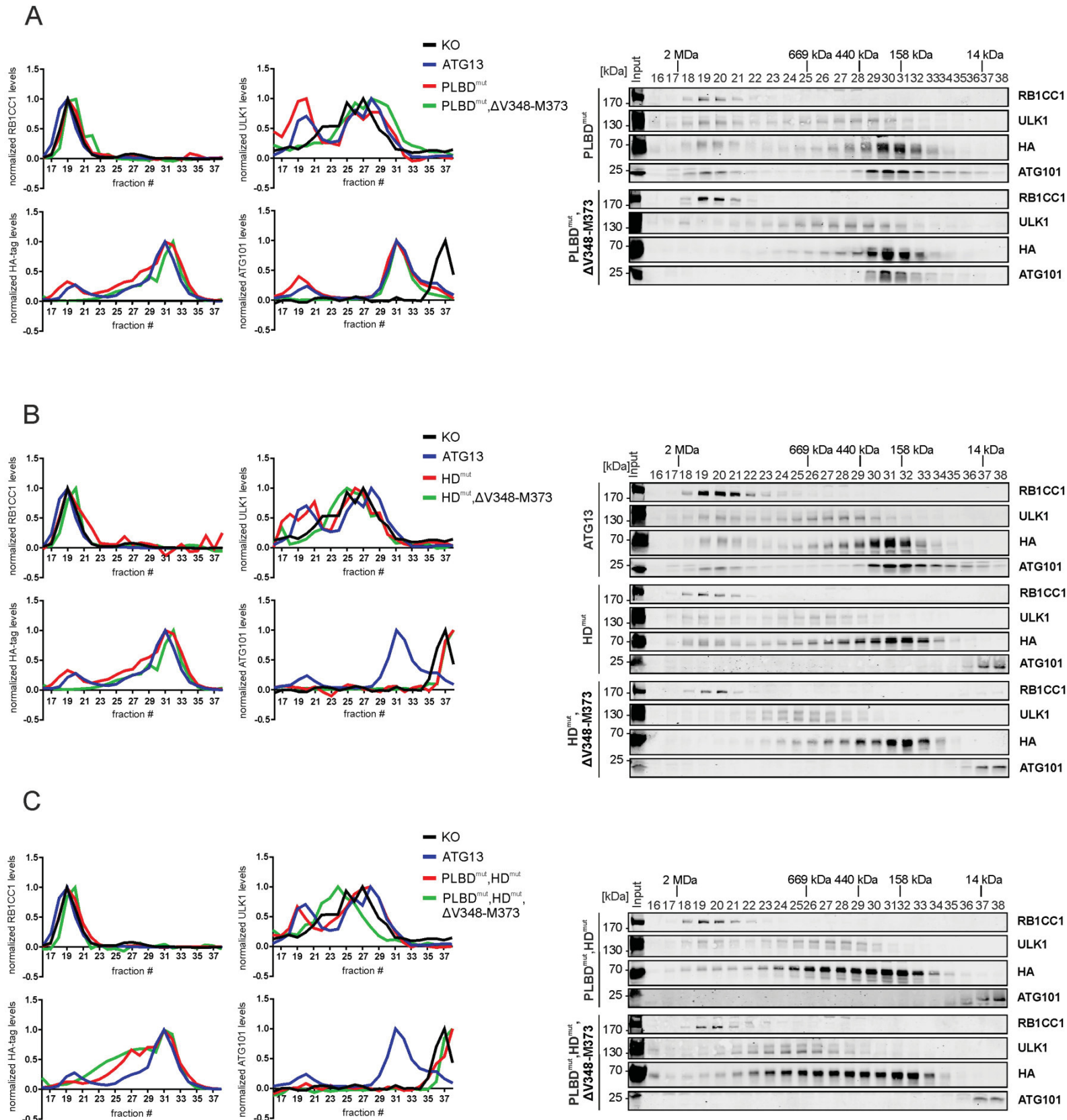
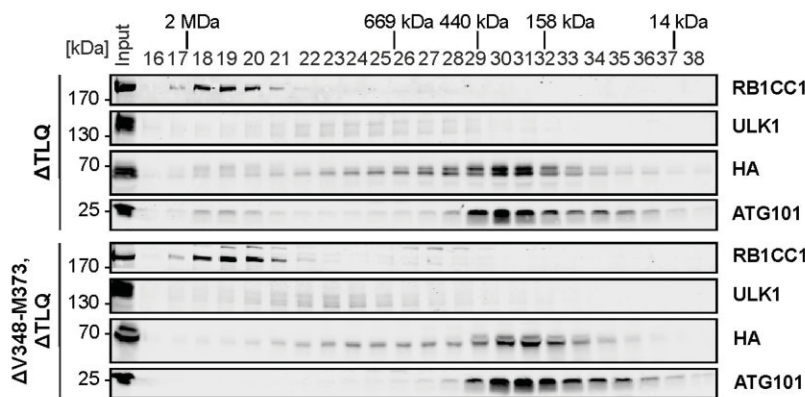
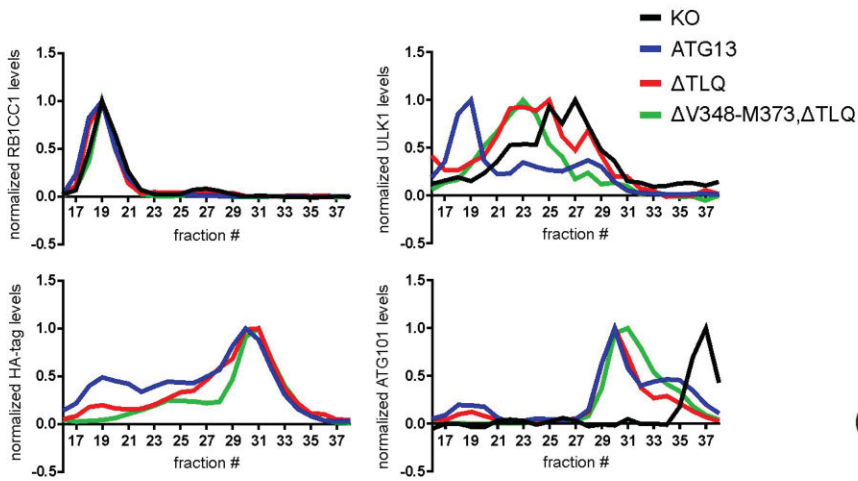
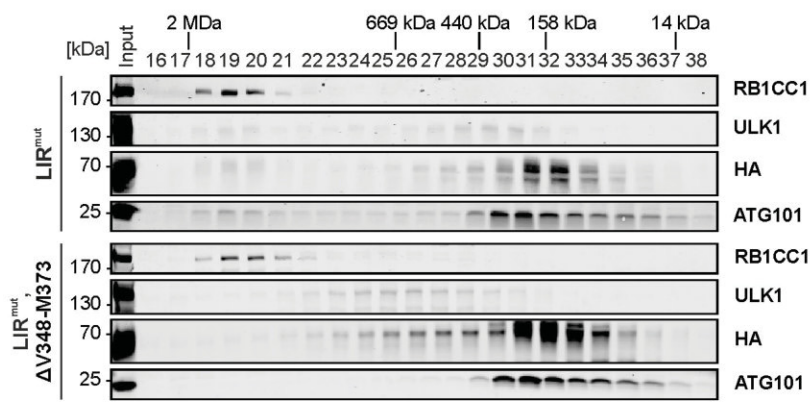
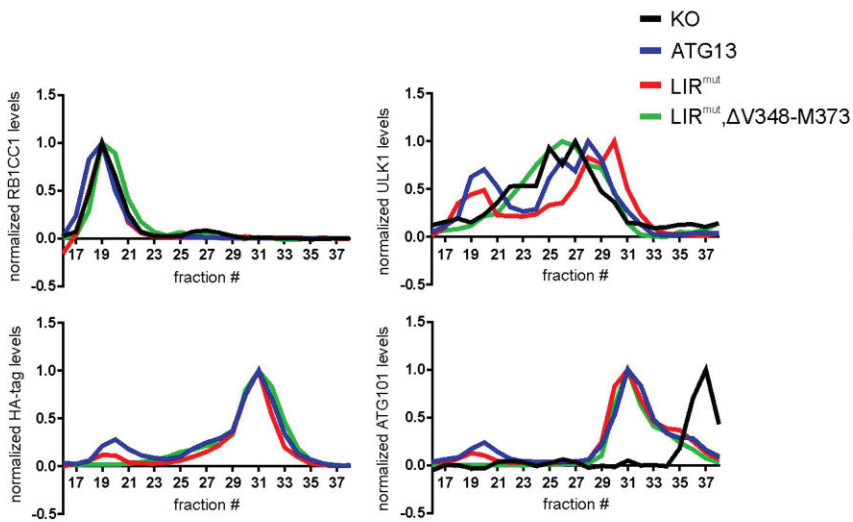
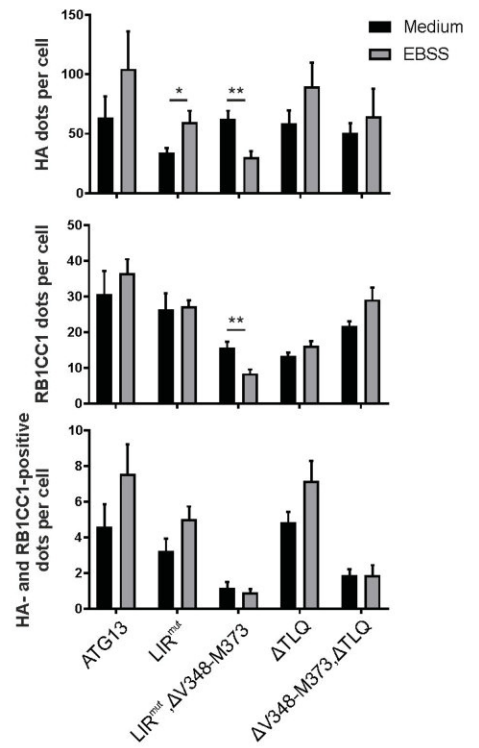
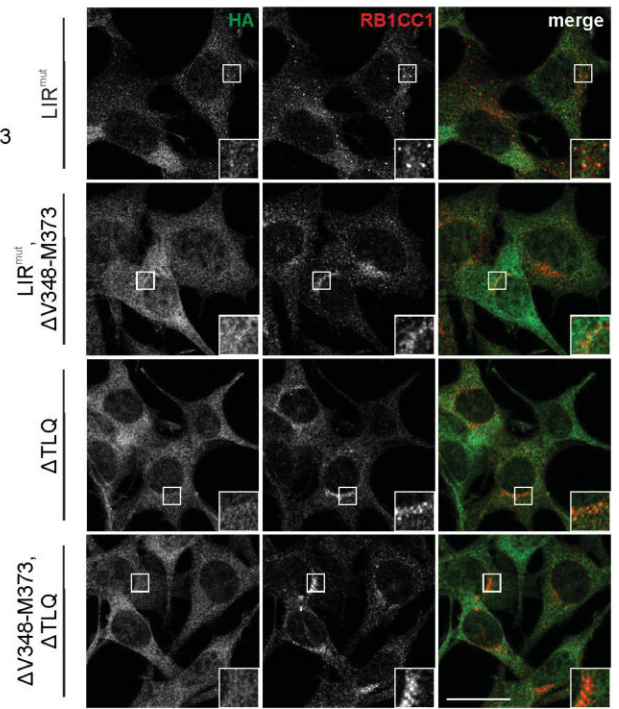


Figure 6

A



B



C

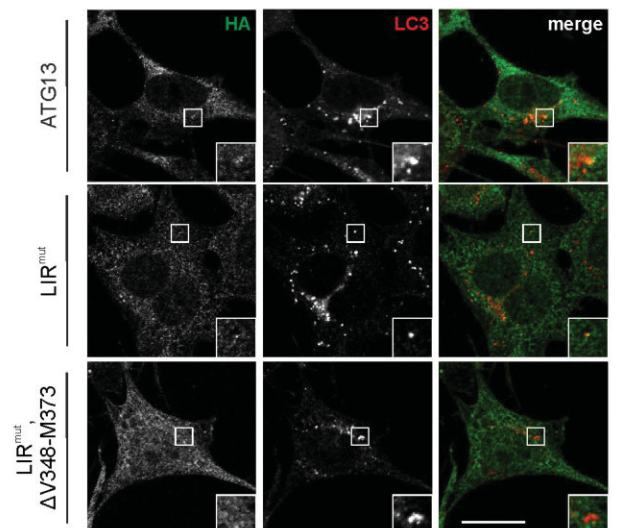
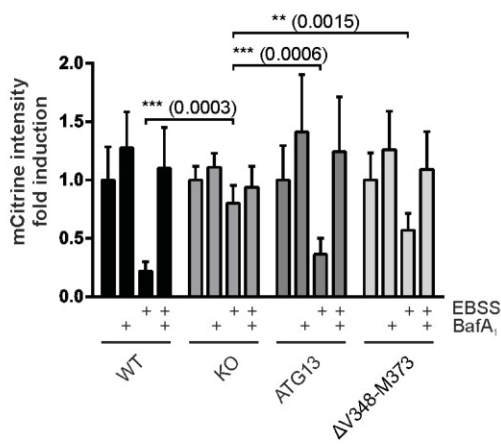
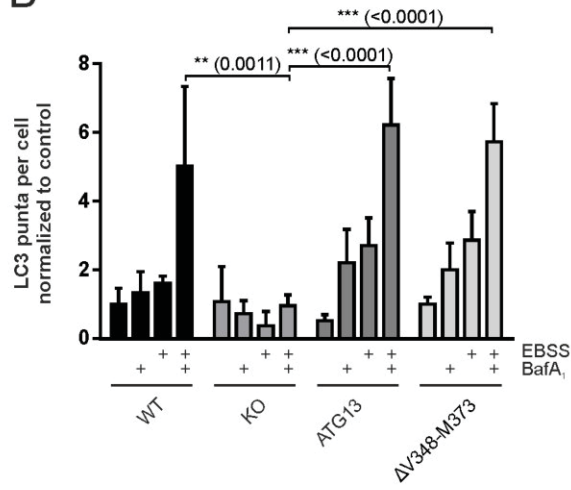


Figure 7

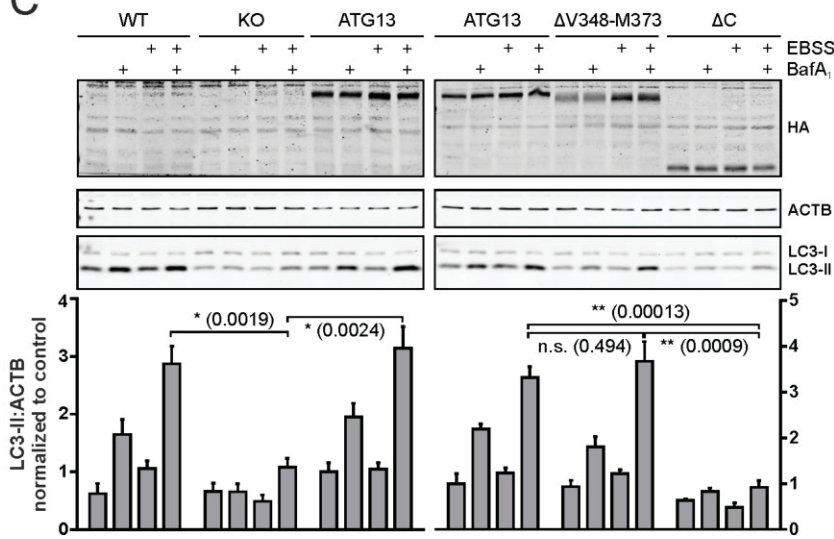
A



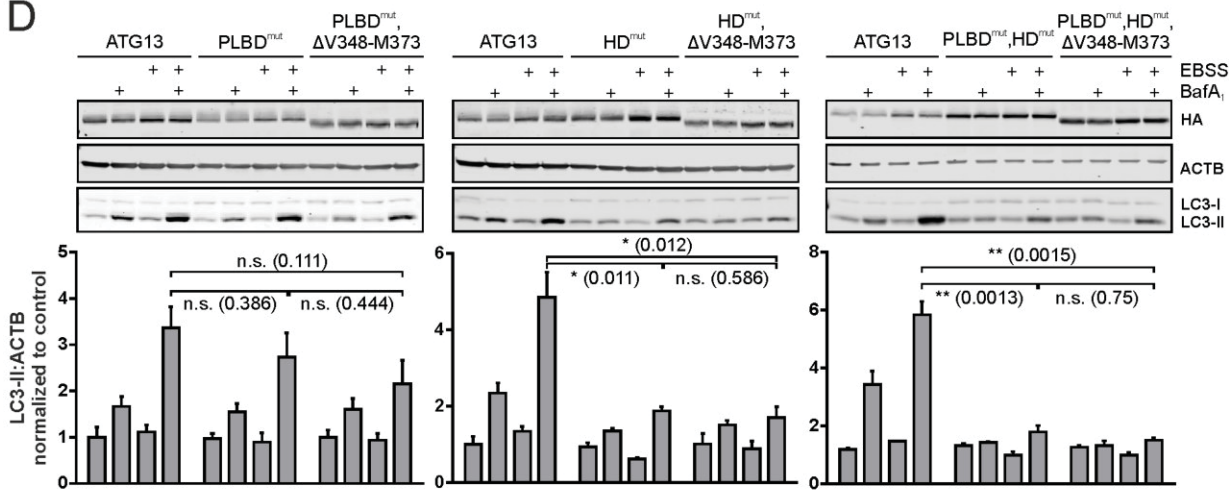
B



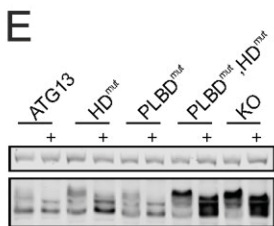
C



D



E



F

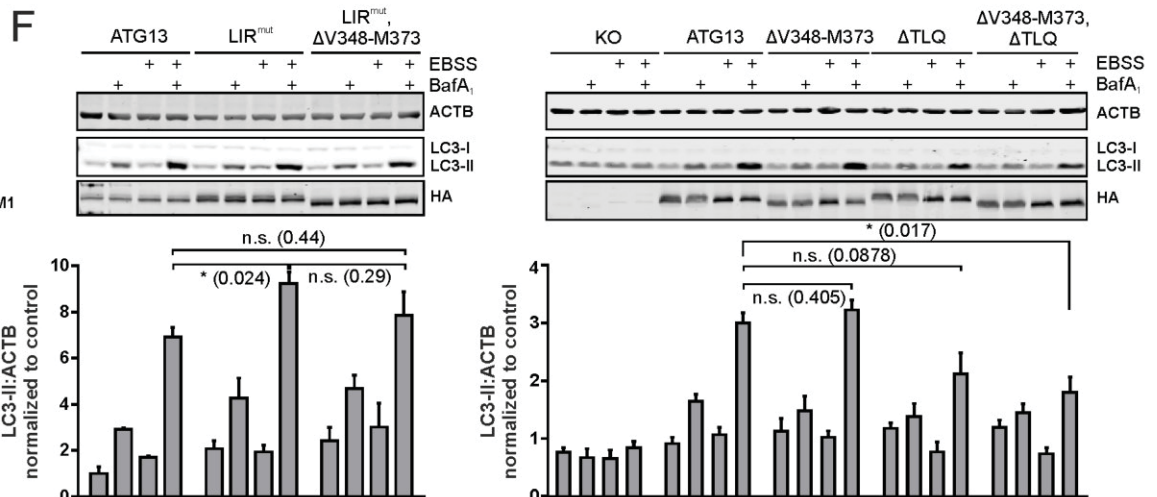


Figure 8

IF: WIP12

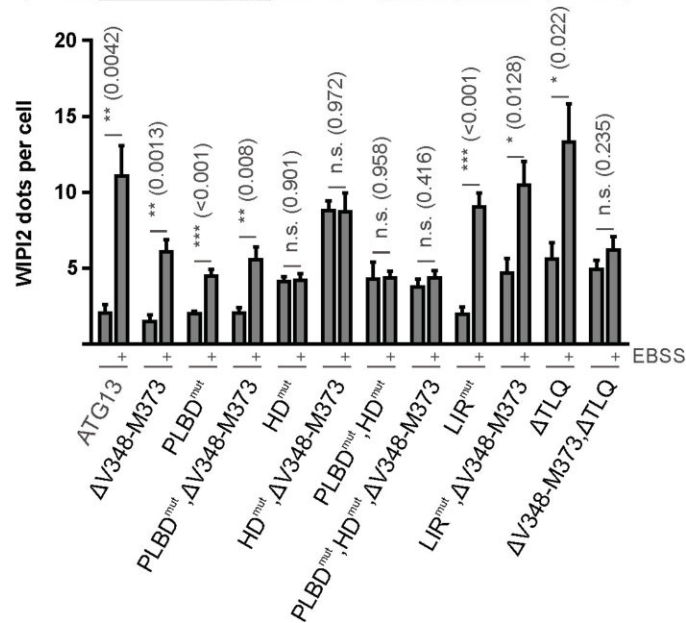
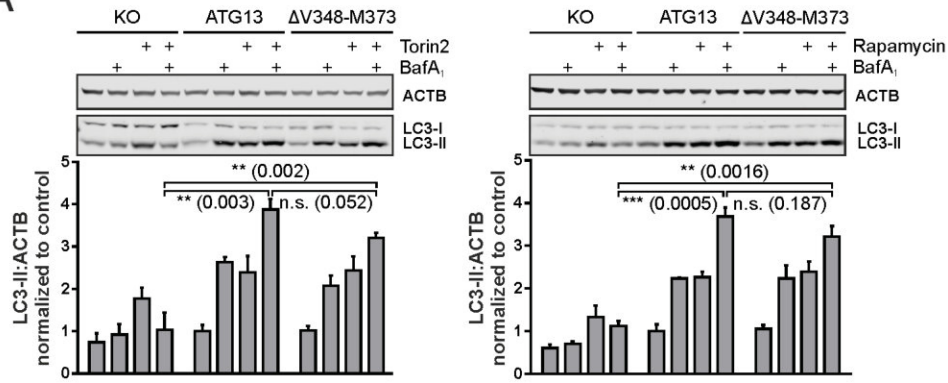
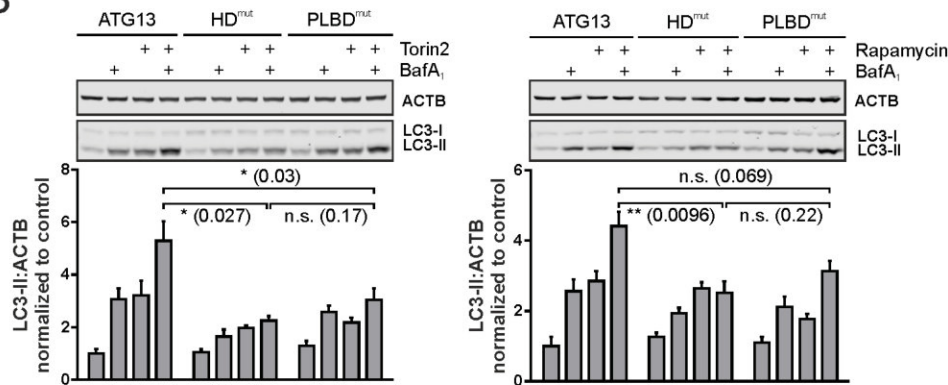


Figure 9

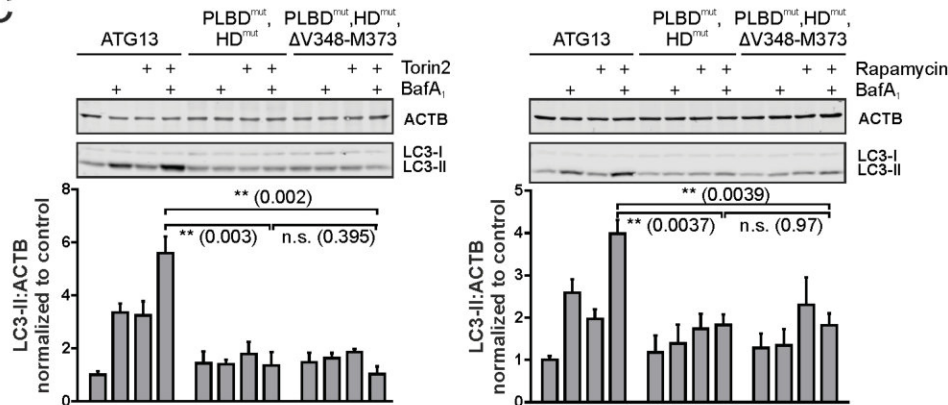
A



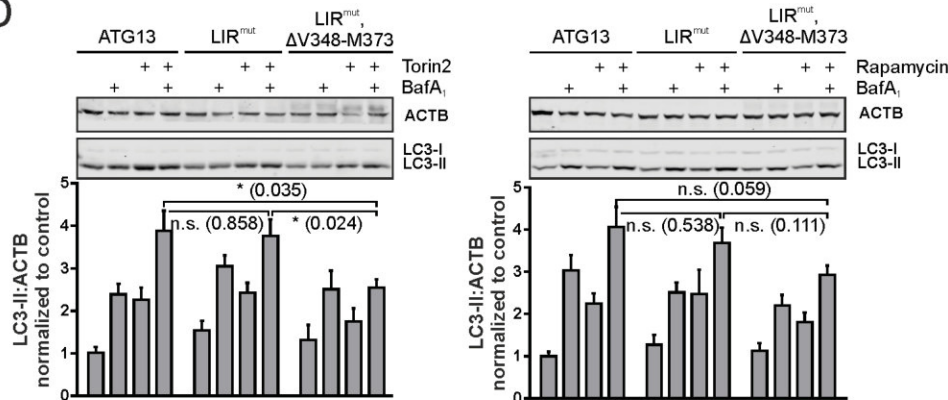
B



C



D



E

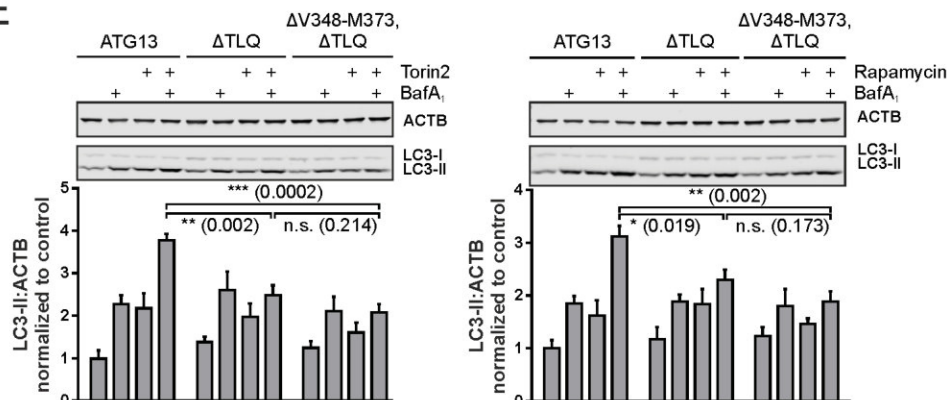
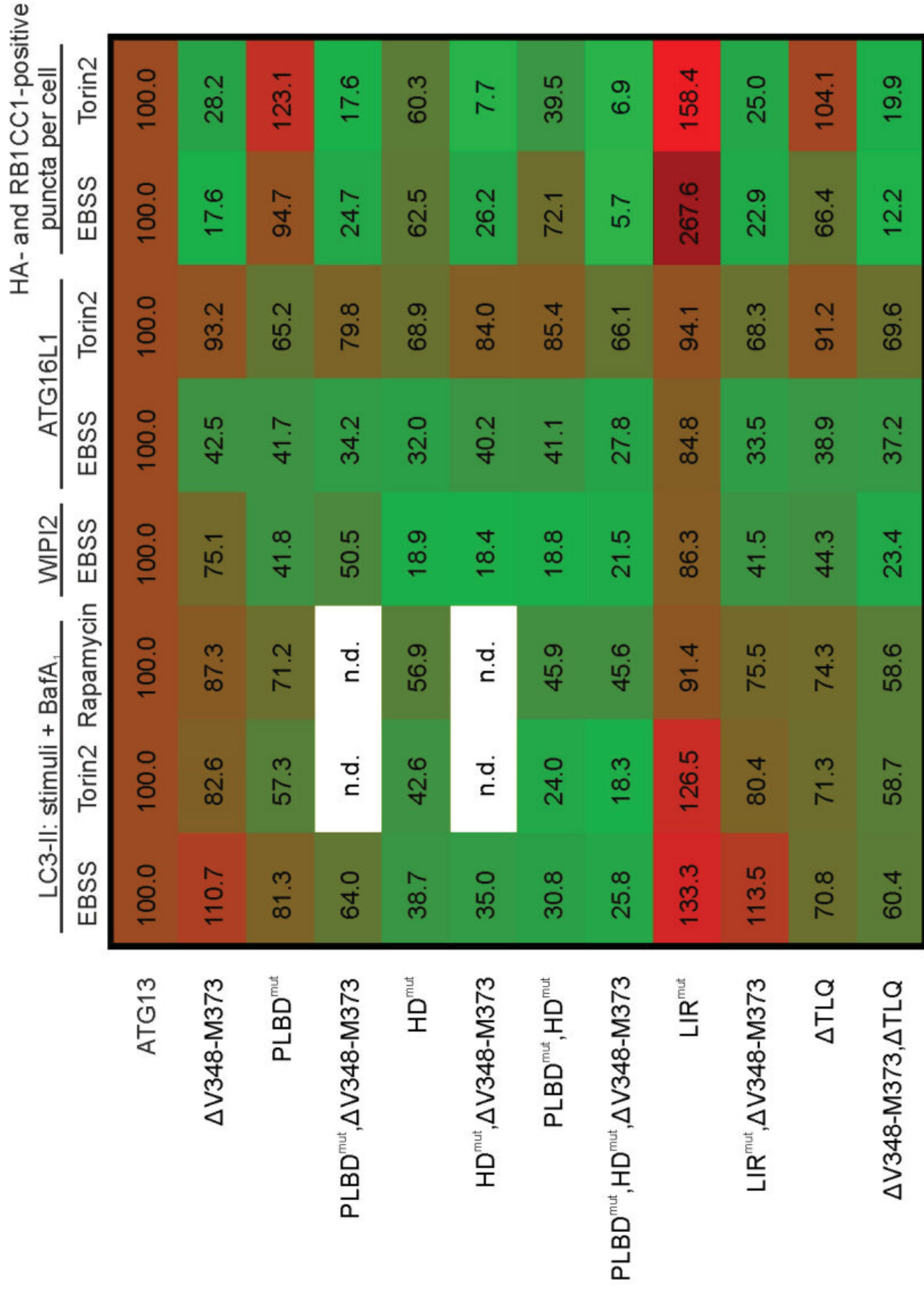


# Figure 10



## Supplementary Figures

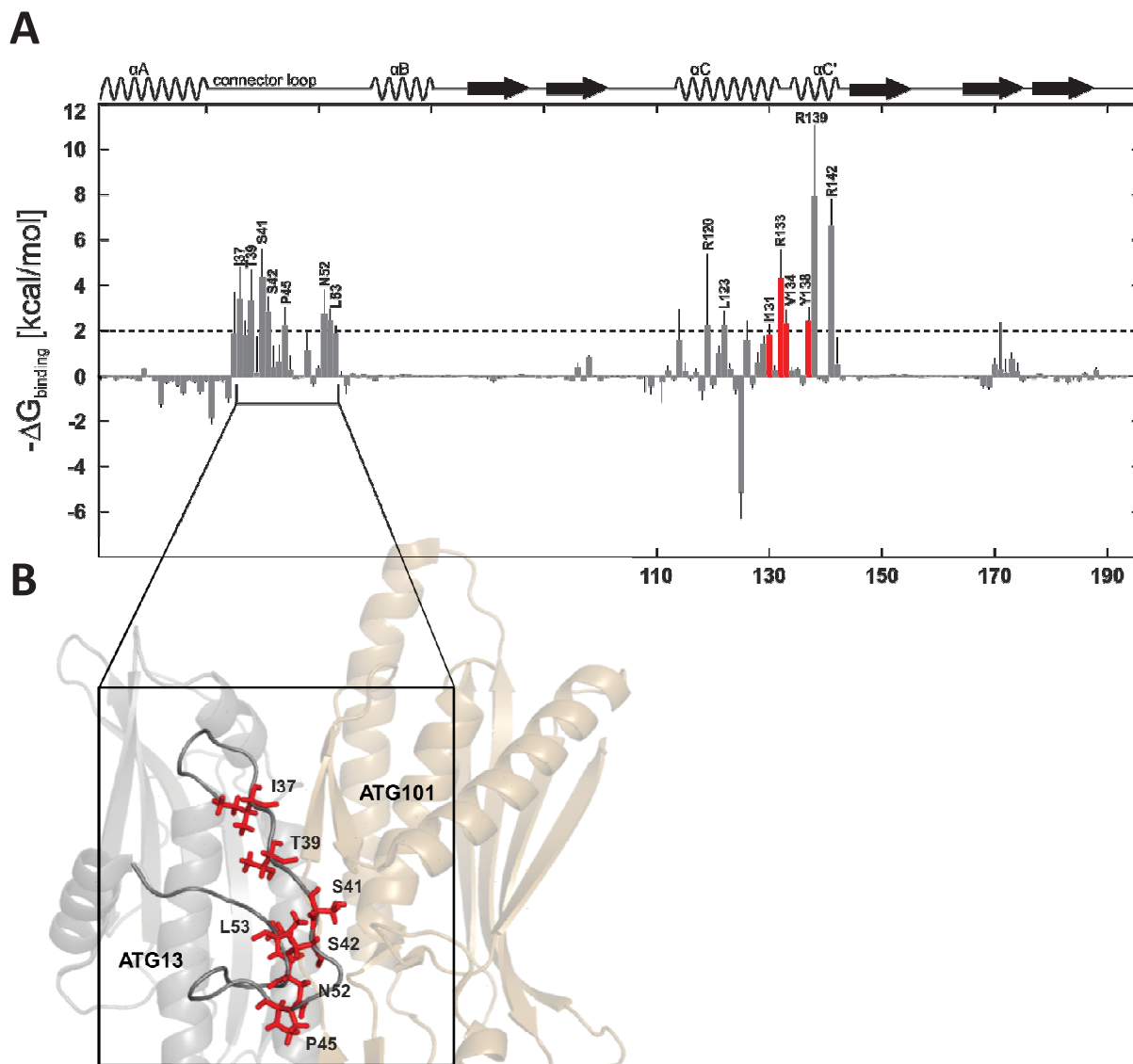


**Figure S1.** A second hot spot region located in the connector loop was identified by MM-GB/SA calculations. **(A)** Contribution of all amino acids of the HORMA domain of ATG13 to the heterodimer stability.  $\Delta G$  values denote the effective energy of binding on a per-residue level calculated by the MM-GB/SA approach.<sup>39,40</sup> Amino acids considered as hot spots by the computational alanine scanning (**Fig. 3A**) and here are colored in red. The standard error in the mean is shown by black bars. In the upper part of the panel, the secondary structure of the human ATG13 HORMA domain is shown. **(B)** Cluster of hot spot residues localized on the connector loop of the HORMA domain of ATG13.

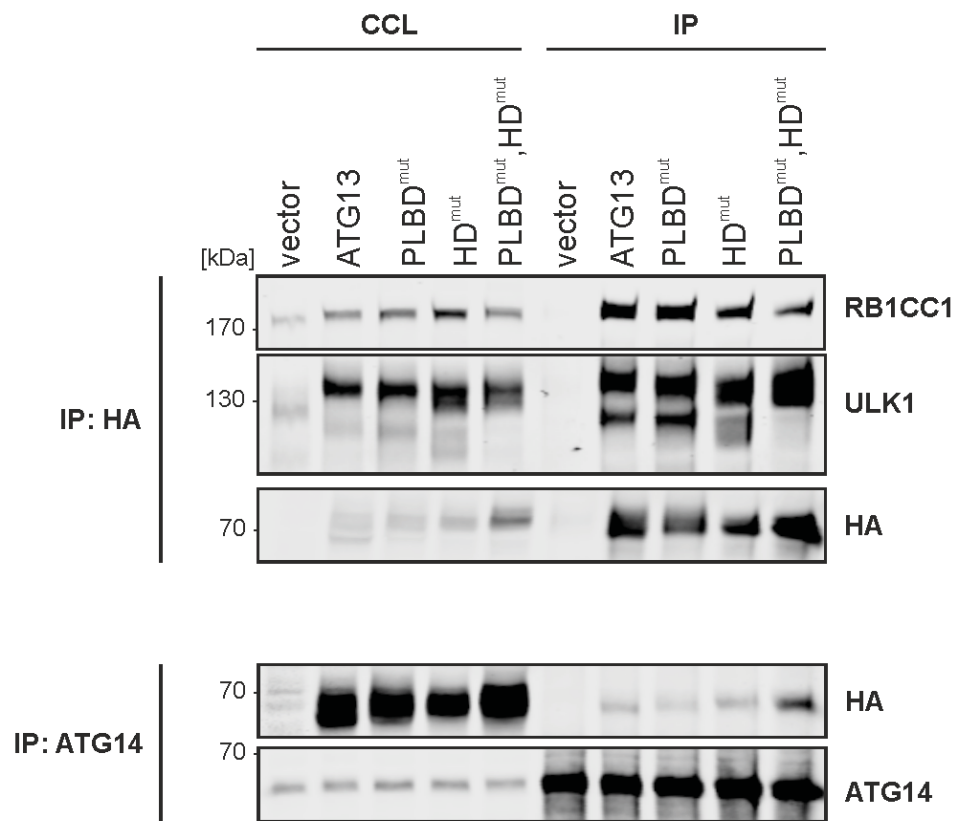


**Figure S2.** Exchange of ATG13 residues I131, R133, V134 and Y138 to alanines does not disturb interaction with ATG14. Lysates of *atg13* KO MEFs stably expressing HA-ATG13 or the indicated variants were subjected to anti-HA or anti-ATG14 immunopurification and interacting proteins were detected by immunoblotting.

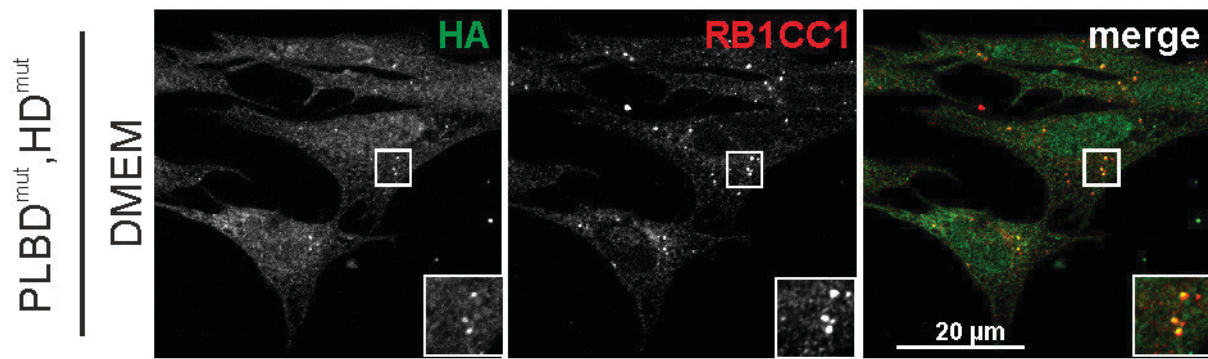


**Figure S3.** A permanent accumulation of ATG13 and RB1CC1 can be observed in cells expressing the ATG13 variant lacking both the ATG101 and phospholipid interaction site even under full medium conditions. *atg13* KO MEFs stably expressing HA-ATG13(PLBD<sup>mut</sup>,HD<sup>mut</sup>) were seeded onto glass cover slips 1 day prior to fixation and immunofluorescence staining for the indicated antibodies (anti-HA antibody: covance MMS-101P).

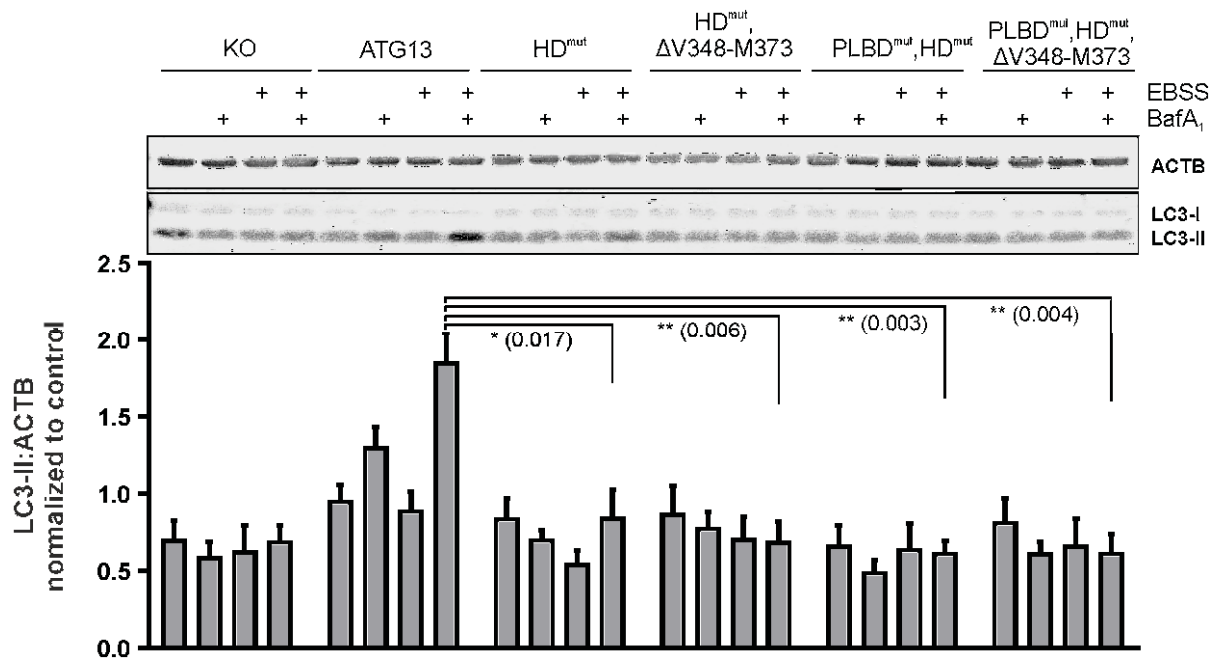


**Figure S4.** Inhibition of the ATG13-ATG101 interaction blocks autophagic flux. *atg13* KO MEFs retrovirally transfected with empty vector (KO) or cDNA encoding the indicated ATG13 variants were incubated in growth medium or EBSS starvation medium in the absence or presence of 40 nM bafilomycin A<sub>1</sub> (BafA<sub>1</sub>) for 1 h. Cell lysates were analyzed by immunoblotting for the indicated antibodies. Fold changes were calculated by dividing each normalized ratio (protein to loading control) by the average of the ratios of the control lane (ATG13 in medium). Results are mean + SEM \**P* < 0.05, \*\**P* < 0.01 (Student t test, 2-sample assuming unequal variances).

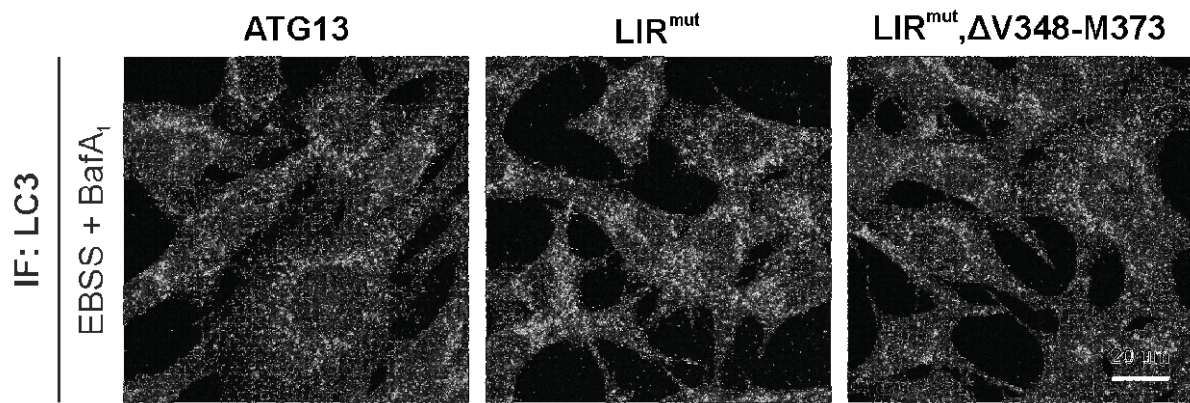


**Figure S5.** The number of LC3 puncta is slightly increased in cells expressing an ATG13 variant with mutated LIR domain. *atg13* KO MEFs stably expressing the indicated ATG13 variants were grown on glass cover slips overnight and incubated in starvation medium (EBSS) with 40 nM bafilomycin A<sub>1</sub> (BafA<sub>1</sub>) for 2 h. Cells were fixed, permeabilized and stained for LC3. Imaging was performed using an inverse confocal laser scanning microscope.

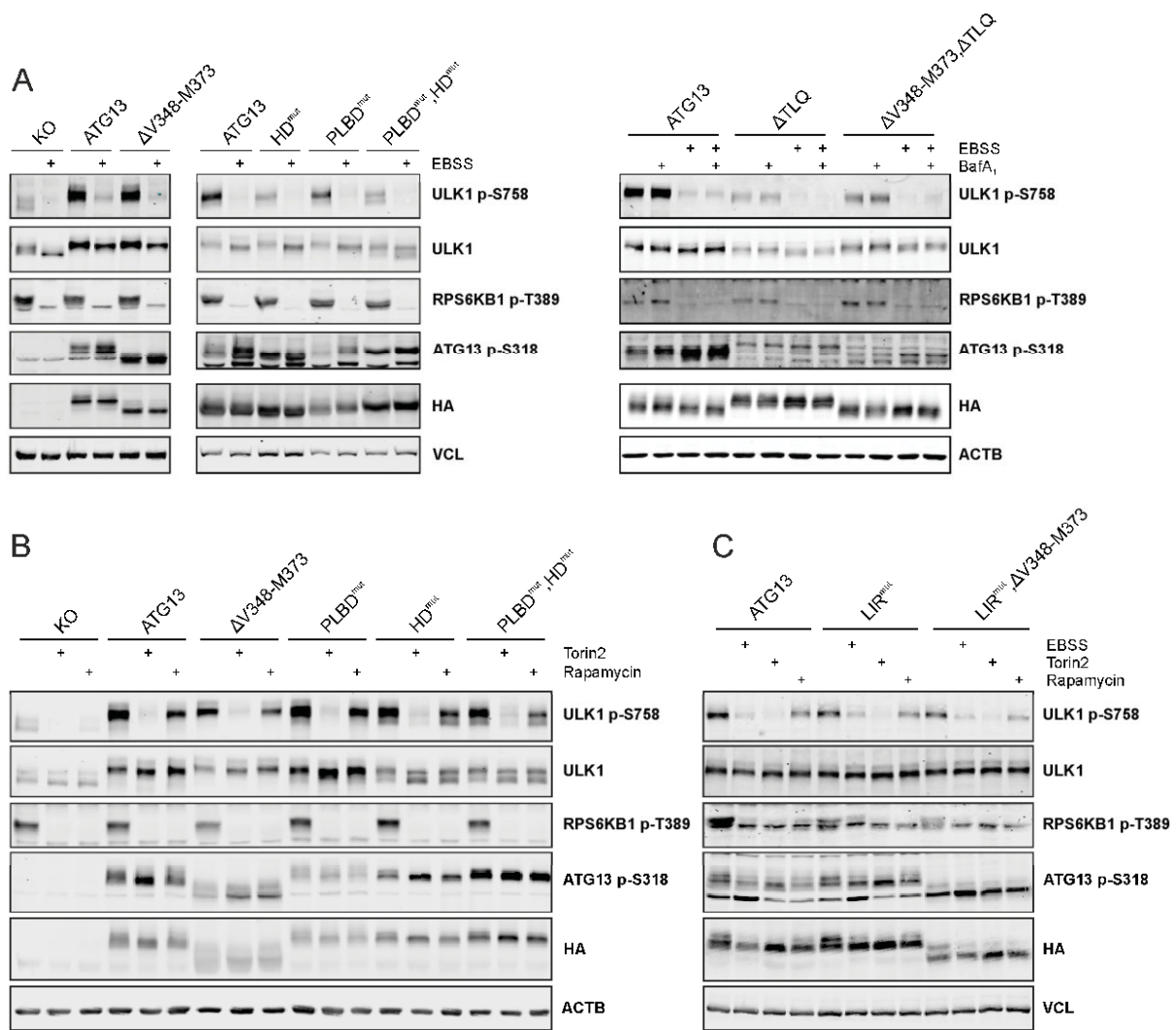


**Figure S6.** Effect of ATG13 variants on MTORC1 and ULK1 kinase activity during autophagy induction by various stimuli. **(A to C)** *atg13* KO MEFs retrovirally transfected with empty vector (KO) or cDNA encoding the indicated ATG13 variants were incubated in growth medium in the presence or absence of 250 nM torin2 or 500 nM rapamycin or in EBSS starvation medium for 2 h. Cell lysates were analyzed by immunoblotting for the indicated antibodies.

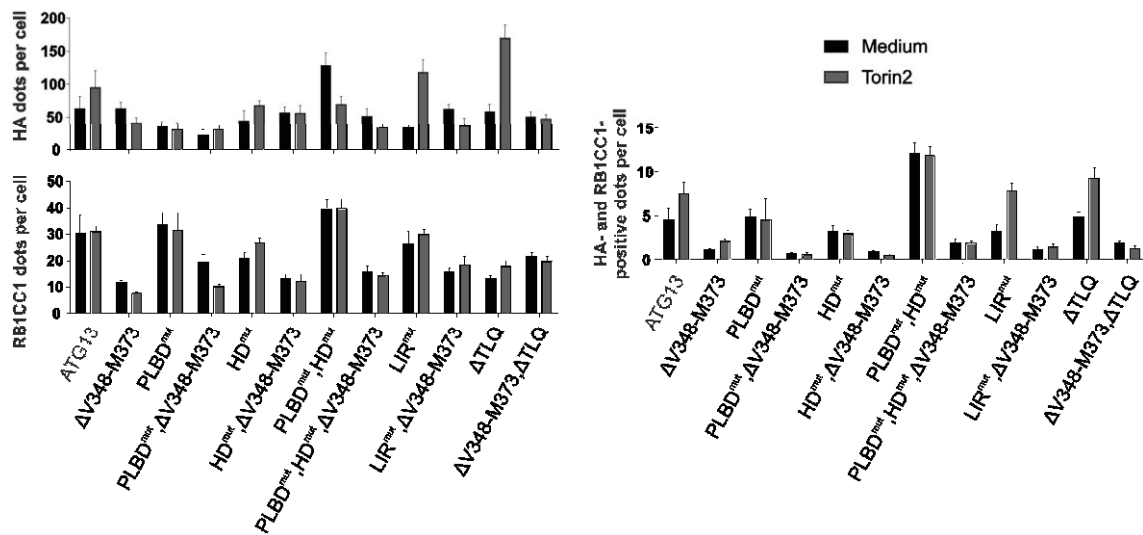
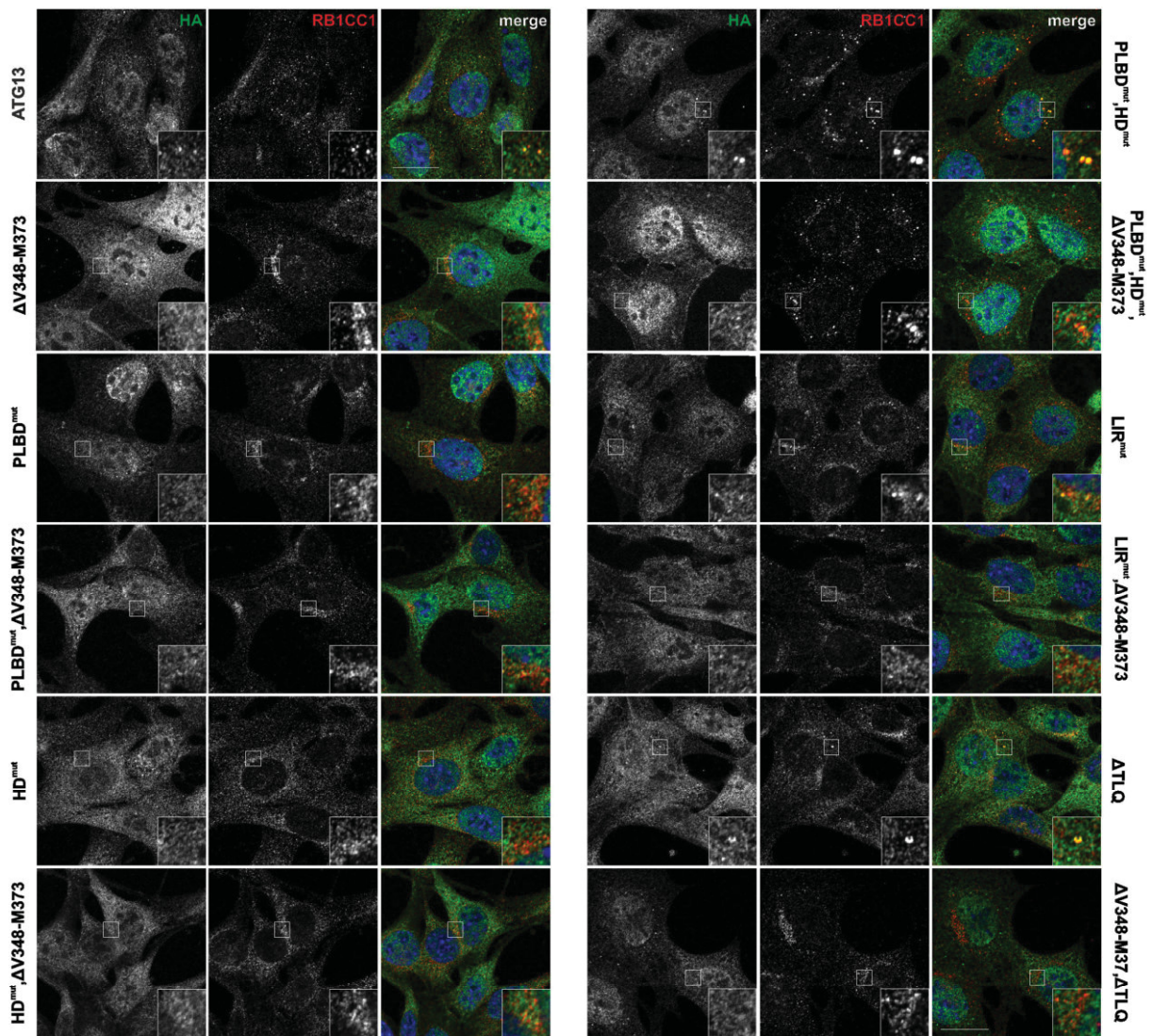


**Figure S7.** Analysis of HA-ATG13- and RB1CC1-positive dots upon treatment with torin2. *atg13* KO MEFs retrovirally transfected with empty vector (KO) or cDNA encoding the indicated ATG13 variants were seeded onto glass cover slips one day prior to incubation with

growth medium in the presence or absence of 250 nM torin2 for 1 h. Cells were fixed, permeabilized, and stained for the indicated antibodies. Imaging was done using an inverse laser scanning microscope. Puncta and colocalization per cell quantification was done using fiji software. Data represent mean + SEM. Scale bar: 20  $\mu$ m. Please note that during revision of this manuscript we were provided with a new lot of anti-HA antibody (covance MMS-101P was replaced by BioLegend 901501), which now shows nuclear localization in every cell line as compared to previous results, e.g., shown in Fig. 6C.

IF: WIPI2

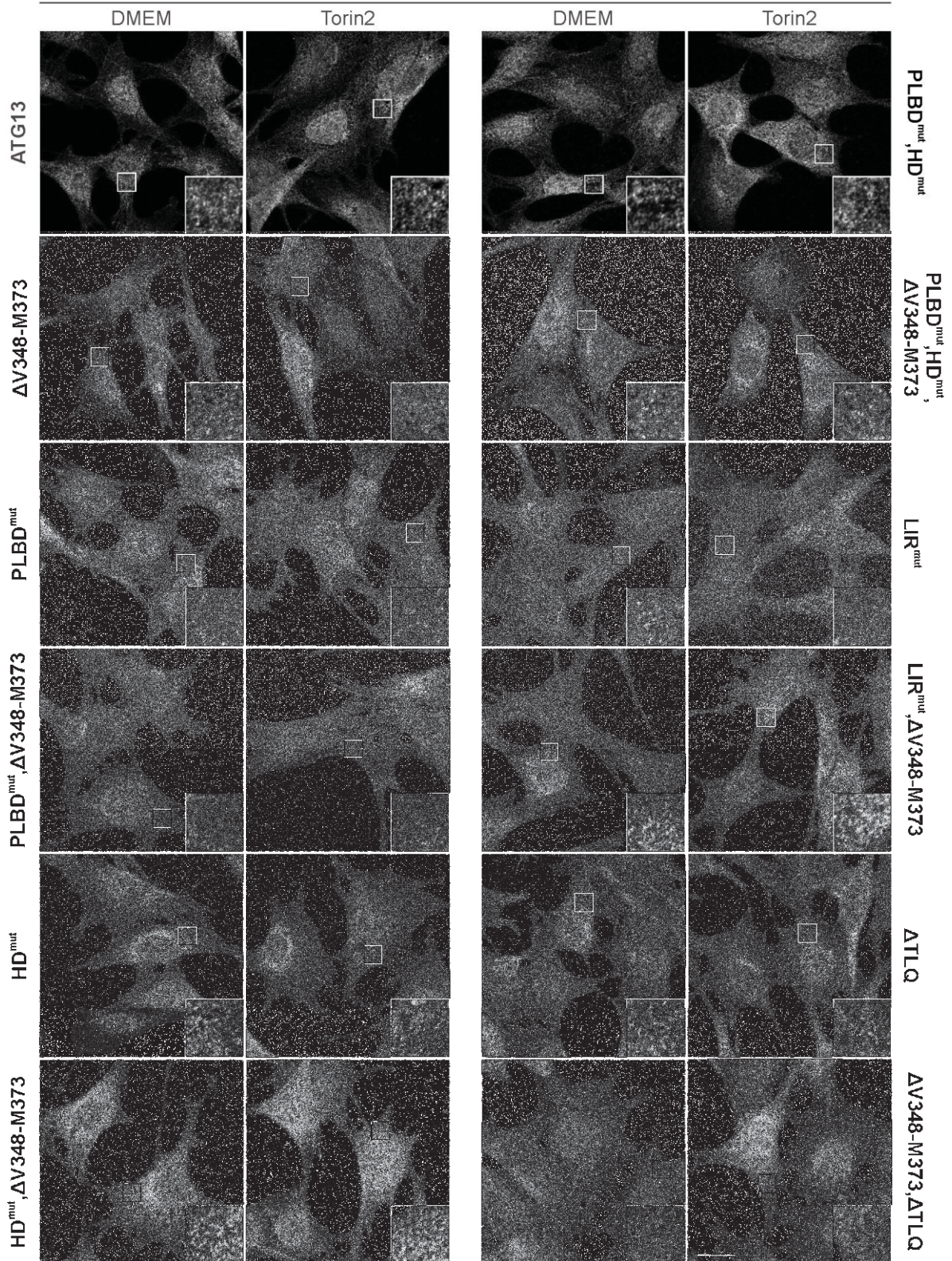


**Figure S8.** WIPI2 puncta formation is not detectable upon torin2 treatment. *atg13* KO MEFs retrovirally transfected with empty vector (KO) or cDNA encoding the indicated ATG13 variants were seeded onto glass cover slips one day prior to incubation with growth medium

in the presence or absence of 250 nM torin2 for 1 h. Cells were fixed, permeabilized, and stained for the indicated antibodies. Imaging was done using an inverse laser scanning microscope. Scale bar: 20  $\mu\text{m}$ .

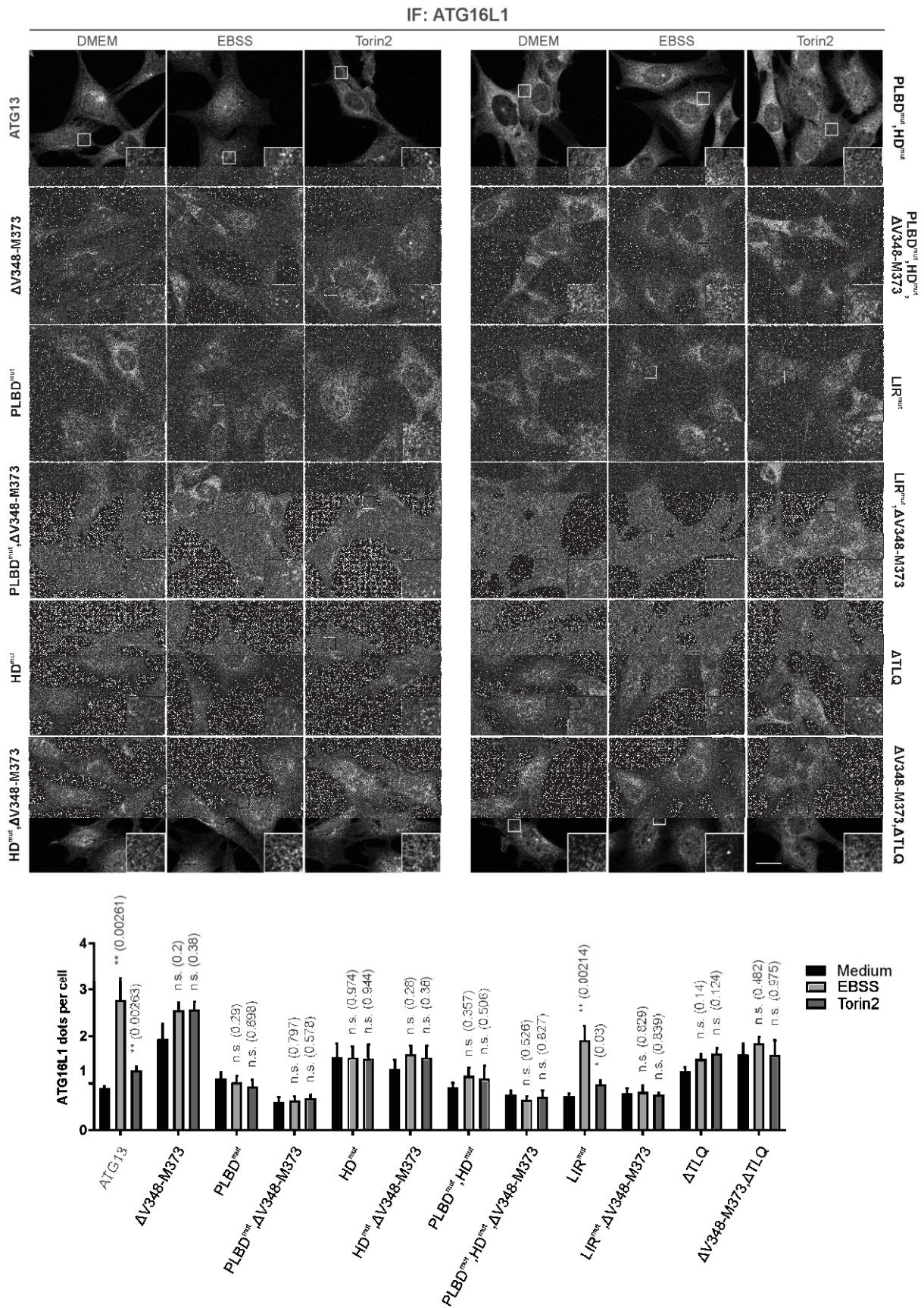


**Figure S9.** Analysis of ATG16L1 puncta formation in cells expressing different ATG13 variants upon EBSS or torin2 treatment. *atg13* KO MEFs retrovirally transfected with empty vector

(KO) or cDNA encoding the indicated ATG13 variants were seeded onto glass cover slips one day prior to incubation with growth medium in the presence or absence of 250 nM torin2 or EBSS starvation medium for 1 h. Cells were fixed, permeabilized, and stained for the indicated antibodies. Imaging was done using an inverse laser scanning microscope. Puncta per cell quantification was done using fiji software. Data represent mean + SEM. Statistical analysis using the Student t test, 2-sample assuming unequal variances was performed comparing EBSS or torin2 to DMEM for each individual cell line. \* $P < 0.05$ , \*\* $P < 0.01$ , n.s., not significant. Scale bar: 20  $\mu\text{m}$ .

# Supplementary Methods

## Macro for quantification of WIPI2 puncta and DAPI-stained nuclei

- dir1 directory to original images, dir2 directory to processed images

-d0: channel AlexaFluor647: WIPI2 staining

-d1: channel DAPI: nuclei staining

```
dir1 = getDirectory("Choose a Directory ");
dir2 = getDirectory("Choose a Directory ");
setBatchMode(true);
list = getFileList(dir1);
for (i=0; i<list.length; i++)
{
    open(dir1+list[i]);
    title = File.nameWithoutExtension ;
        run("Split Channels");
        saveAs("Tiff", dir2+title+"d0.tif");
        close();
        saveAs("Tiff", dir2+title+"d1.tif");
        close();
        open(dir2+title+"d1.tif");
        run("Unsharp Mask...", "radius=500 mask=0.90");
        run("Median...", "radius=10");
        run("Unsharp Mask...", "radius=500 mask=0.90");
        run("Make Binary");
        run("Fill Holes");
        run("Analyze Particles...", "size=10-1000 summarize");
        saveAs("Tiff", dir2+title+"d1_binary.tif");
        open(dir2+title+"d0.tif");
        run("Gaussian Blur...", "sigma=3");
        run("Subtract Background...", "rolling=6");
        saveAs("Tiff", dir2+title+"d0_processed.tif");
        setThreshold(40, 255);
        run("Convert to Mask");
        run("Analyze Particles...", " summarize");
        saveAs("Tiff", dir2+title+"d0_binary.tif");
        close();
}
setBatchMode(false);
selectWindow("Summary");
saveAs("Text", dir2+"Summary.txt");
showMessage("Macro is finished");
exit();
```

### Macro for quantification of LC3 puncta and DAPI-stained nuclei

- dir1 directory to original images, dir2 directory to processed images
- d0: channel AlexaFluor488: LC3 staining
- d1: channel DAPI: nuclei staining

```
dir1 = getDirectory("Choose a Directory ");
dir2 = getDirectory("Choose a Directory ");
setBatchMode(true);
list = getFileList(dir1);
for (i=0; i<list.length; i++)
{
    open(dir1+list[i]);
    title = File.nameWithoutExtension ;
        run("Split Channels");
        saveAs("Tiff", dir2+title+"d0.tif");
        close();
        saveAs("Tiff", dir2+title+"d1.tif");
        close();
        open(dir2+title+"d1.tif");
        run("Unsharp Mask...", "radius=500 mask=0.90");
        run("Median...", "radius=10");
        run("Unsharp Mask...", "radius=500 mask=0.90");
        run("Make Binary");
        run("Fill Holes");
        run("Analyze Particles...", "size=10-1000 summarize");
        saveAs("Tiff", dir2+title+"d1_binary.tif");
        open(dir2+title+"d0.tif");
        run("Enhance Contrast...", "saturated=0.01 normalize");
        run("Subtract Background...", "rolling=1.5");
        saveAs("Tiff", dir2+title+"d0_processed.tif");
        setThreshold(69, 255);
        run("Convert to Mask");
        run("Analyze Particles...", " summarize");
        saveAs("Tiff", dir2+title+"d0_binary.tif");
        close();
}
setBatchMode(false);
selectWindow("Summary");
saveAs("Text", dir2+"Summary.txt");
showMessage("Macro is finished");
exit();
```

## Macro for quantification of ATG16L1 puncta and DAPI-stained nuclei

- dir1 directory to original images, dir2 directory to processed images
- d0: channel AlexaFluor647: ATG16L1 staining
- d1: channel DAPI: nuclei staining

```
dir1 = getDirectory("Choose a Directory ");
dir2 = getDirectory("Choose a Directory ");
setBatchMode(true);
list = getFileList(dir1);
for (i=0; i<list.length; i++)
{
    open(dir1+list[i]);
    title = File.nameWithoutExtension ;
        run("Split Channels");
        saveAs("Tiff", dir2+title+"d0.tif");
        close();
        saveAs("Tiff", dir2+title+"d1.tif");
        close();
        open(dir2+title+"d1.tif");
        run("Unsharp Mask...", "radius=500 mask=0.90");
        run("Median...", "radius=10");
        run("Unsharp Mask...", "radius=500 mask=0.90");
        run("Make Binary");
        run("Fill Holes");
        run("Analyze Particles...", "size=10-1000 summarize");
        saveAs("Tiff", dir2+title+"d1_binary.tif");
            open(dir2+title+"d0.tif");
            run("Gaussian Blur...", "sigma=3");
            run("Subtract Background...", "rolling=6");
            saveAs("Tiff", dir2+title+"d0_processed.tif");
            setThreshold(65, 255);
        run("Convert to Mask");
        run("Analyze Particles...", " summarize");
            saveAs("Tiff", dir2+title+"d0_binary.tif");
            close();
    }
setBatchMode(false);
selectWindow("Summary");
saveAs("Text", dir2+"Summary.txt");
showMessage("Macro is finished");
exit();
```

## Macro for quantification of HA and RB1CC1 puncta and DAPI-stained nuclei

- dir1 directory to original images, dir2 directory to processed images
- d0: channel AlexaFluor488: HA staining
- d1: channel AlexaFluor647: RB1CC1 staining
- d2: channel DAPI: nuclei staining

```
dir1 = getDirectory("Choose a Directory ");
dir2 = getDirectory("Choose a Directory ");
setBatchMode(true);
list = getFileList(dir1);
for (i=0; i<list.length; i++)
{
    open(dir1+list[i]);
    title = File.nameWithoutExtension ;
        run("Split Channels");
        saveAs("Tiff", dir2+title+"d0.tif");
        close();
        saveAs("Tiff", dir2+title+"d1.tif");
        close();
        saveAs("Tiff", dir2+title+"d2.tif");
        close();
        open(dir2+title+"d2.tif");
        run("Unsharp Mask...", "radius=500 mask=0.90");
        run("Median...", "radius=10");
        run("Unsharp Mask...", "radius=500 mask=0.90");
        run("Make Binary");
        run("Fill Holes");
        run("Analyze Particles...", "size=10-1000 summarize");
        saveAs("Tiff", dir2+title+"d2_binary.tif");
        open(dir2+title+"d0.tif");
        run("Subtract...", "value=25");
        run("Subtract Background...", "rolling=3");
        saveAs("Tiff", dir2+title+"d0_processed.tif");
        setThreshold(75, 255);
        run("Convert to Mask");
        saveAs("Tiff", dir2+title+"d0_binary.tif");
        run("Analyze Particles...", "size=0.00-0.50 summarize");
        close();
        open(dir2+title+"d1.tif");
        run("Subtract...", "value=25");
        run("Gaussian Blur...", "sigma=2");
        run("Subtract Background...", "rolling=3");
        saveAs("Tiff", dir2+title+"d1_processed.tif");
        setThreshold(25, 255);
        run("Convert to Mask");
        saveAs("Tiff", dir2+title+"d1_binary.tif");
        run("Analyze Particles...", "summarize");
        close();
        open(dir2+title+"d0_binary.tif");
        setPasteMode("AND");
```

```
        run("Copy");
        open(dir2+title+"d1_binary.tif");
        run("Paste");
        saveAs("Tiff", dir2+title+"d0_1_features.tif");
        run("Analyze Particles...", " summarize");
        close();
    }
    setBatchMode(false);
    selectWindow("Summary");
    saveAs("Text", dir2+"Summary.txt");
    showMessage("Macro is finished");
    exit();
```